

AD-A114 305

WOODWARD-CLYDE CONSULTANTS HOUSTON TX

F/S 8/13

STUDY TO INVESTIGATE THE EFFECTS OF SKIN FRICTION ON THE PERFOR--ETC(U)

MAR 82 J AUDIBERT, D AGGARWAL, W GARDNER

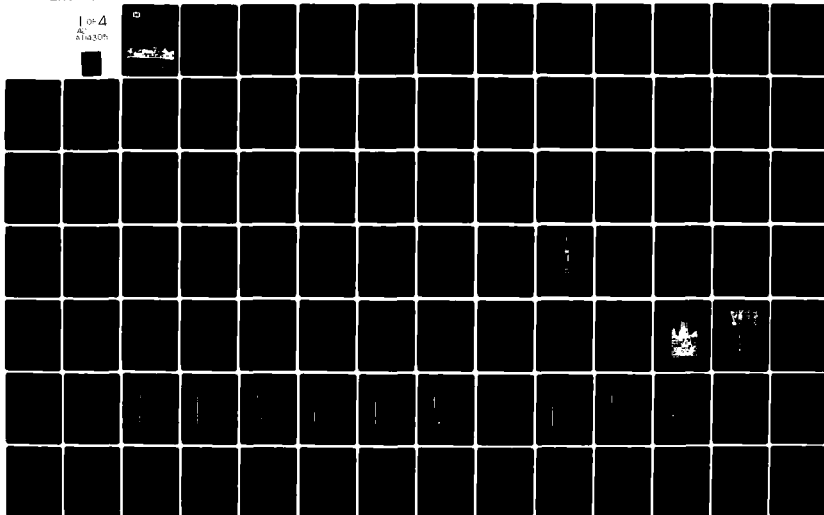
DACA39-80-C-0001

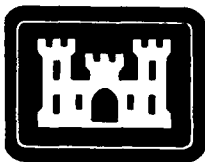
UNCLASSIFIED

TR-8L-82-1

NL

1 of 4  
A114305





TECHNICAL REPORT GL-82-1

STUDY TO INVESTIGATE THE EFFECTS OF  
SKIN FRICTION ON THE PERFORMANCE OF  
DRILLED SHAFTS IN COHESIVE SOILS

Volumes I, II, and III.

by

Woodward-Clyde Consultants  
7330 Westview Drive  
Houston, Tex. 77055

March 1982  
Final Report

Approved For Public Release; Distribution Unlimited



Prepared for Office, Chief of Engineers, U. S. Army  
Washington, D. C. 20314

Under Work Unit AT40/E0/006

Monitored by Geotechnical Laboratory  
U. S. Army Engineer Waterways Experiment Station  
P. O. Box 631, Vicksburg, Miss. 39180

DTIC  
ELECTE  
MAY 5 1982

A

82 05 05 010

DTIC FILE COPY

Do not destroy this report when no longer needed.  
Return it to the originator.

The findings in this report are not to be construed as an official  
Department of the Army position unless so designated,  
by other authorized documents.

The contents of this report are not to be used for  
advertising, publication, or promotional purposes.  
Citation of trade names does not constitute an  
official endorsement or approval of the use of  
such commercial products.

Unclassified

SECURITY CLASSIFICATION OF THIS PAGE (When Data Entered)

REPORT DOCUMENTATION PAGE		READ INSTRUCTIONS BEFORE COMPLETING FORM
1. REPORT NUMBER Technical Report GL-82-1	2. GOVT ACCESSION NO.	3. RECIPIENT'S CATALOG NUMBER
4. TITLE (and Subtitle) STUDY TO INVESTIGATE THE EFFECTS OF SKIN FRICTION ON THE PERFORMANCE OF DRILLED SHAFTS IN COHESIVE SOILS; Volumes I, II, and III		5. TYPE OF REPORT & PERIOD COVERED Final report
7. AUTHOR(s)		6. PERFORMING ORG. REPORT NUMBER
9. PERFORMING ORGANIZATION NAME AND ADDRESS Woodward-Clyde Consultants 7330 Westview Drive Houston, Tex. 77055		8. CONTRACT OR GRANT NUMBER(s) DACA39-80-C-0001
11. CONTROLLING OFFICE NAME AND ADDRESS Office, Chief of Engineers, U. S. Army Washington, D. C. 20314		10. PROGRAM ELEMENT, PROJECT, TASK AREA & WORK UNIT NUMBERS Work Unit AT40/E0/006
14. MONITORING AGENCY NAME & ADDRESS (if different from Controlling Office) U. S. Army Engineer Waterways Experiment Station Geotechnical Laboratory P. O. Box 631, Vicksburg, Miss. 39180		12. REPORT DATE March 1982
		13. NUMBER OF PAGES 359
		15. SECURITY CLASS. (of this report) Unclassified
16. DISTRIBUTION STATEMENT (of this Report)  Approved for public release; distribution unlimited.		15a. DECLASSIFICATION/DOWNGRADING SCHEDULE
17. DISTRIBUTION STATEMENT (of the abstract entered in Block 20, if different from Report)		
18. SUPPLEMENTARY NOTES Available from National Technical Information Service, 5285 Port Royal Road, Springfield, Va. 22151.		
19. KEY WORDS (Continue on reverse side if necessary and identify by block number)		
20. ABSTRACT (Continue on reverse side if necessary and identify by block number)  The general objective of this study was to investigate the effects of skin friction on performance of drilled shafts in cohesive soils. The inves- tigation was conducted and discussed here in three stages: field, laboratory, and theoretical analyses.  Four test shafts were constructed in 1969 at a test site located in southeastern Houston, Texas, where detailed subsurface exploration and soil characterizations had been made. Load tests on the carefully instrumented (Continued)		

DD FORM 1 JAN 73 1473 EDITION OF 1 NOV 65 IS OBSOLETE

Unclassified  
SECURITY CLASSIFICATION OF THIS PAGE (When Data Entered)



Unclassified

SECURITY CLASSIFICATION OF THIS PAGE(When Data Entered)

20. ABSTRACT (Continued).

test shafts produced high-quality data documented in a series of reports made available to the public.

For this study, a thorough subsurface investigation was performed to provide a detailed evaluation of the soil and groundwater conditions existing at the test site. Representative samples of the subsoils were obtained for laboratory analyses. Pressuremeter tests, borehole shear tests and static cone penetrometer soundings were also conducted.

The geotechnical laboratory investigation was conducted to provide a characterization of the in-situ soil properties and parameters as well as their state-of-stress. Tests to investigate the pertinent physical and index properties of representative soil samples were conducted. Direct shear, triaxial compression, and one-dimensional consolidation tests were conducted to evaluate the strength and deformation characteristics of the in-situ soils. Both consolidated isotropic undrained triaxial compression (CIU) tests with pore pressure measurements and unconsolidated undrained (UU) tests were performed. The coefficient of earth pressure at rest ( $K_0$ ) was evaluated. Special direct shear tests were run to assess the residual strength of the soil. Tests were conducted to investigate mortar-soil interface shear characteristics as a simulation of shaft-soil interaction under load. The effect of soil property changing with time was also investigated.

Various methods of evaluating the ultimate shaft friction of drilled shafts in cohesive soils were described and assessed. Evaluation of ultimate shaft friction was first made by theoretically based techniques, such as Alpha ( $\alpha$ ), Beta ( $\beta$ ), and effective stress methods, which utilized basic soil properties to predict shaft friction. Subsequently, other techniques were investigated including application of laboratory soil-mortar interface shear measurement and in-situ borehole shear test. The application of moisture migration concepts to the prediction of shaft friction was also investigated. The load-settlement analysis selected for this study focused on a numerical load-transfer technique. This work included derivation of load-transfer curves from load test results, prediction of the load-settlement response of these shafts, and the comparison of these data to the actual measured data.

Accession No.	
NTIS GPO	<input checked="" type="checkbox"/>
DTIC TAB	<input type="checkbox"/>
Unannounced	<input type="checkbox"/>
Justification	
By	
Distribution/	
Availability Codes	
Avail and/or	
Dis	<input checked="" type="checkbox"/>

DTIC  
COPY  
INSPECTED  
2

Unclassified

SECURITY CLASSIFICATION OF THIS PAGE(When Data Entered)

## PREFACE

The work described in this report was performed under Contract No. DACA39-80-C-0001 (Neg), "Study to Investigate the Effects of Skin Friction on the Performance of Drilled Shafts in Cohesive Soils," between the U. S. Army Engineer Waterways Experiment Station and Woodward-Clyde Consultants (WCC) during the period from December 1978 to August 1981. This work is part of an effort to develop improved design and construction procedures in support of Work Unit AT40/E0/006, "Development of Methodology for Design of Drilled Piers in Cohesive Soils," sponsored by the Office, Chief of Engineers, U. S. Army.

The general objective of this work is to provide improved understanding of the effects of skin friction on the performance of drilled shafts in cohesive soils. This was accomplished by completing field and laboratory soil tests in Beaumont clay of Houston, Texas, and conducting analyses to predict the performance of drilled shafts that had been constructed and load tested in 1969 and to determine any changes as a result of time effects. Mr. W. S. Gardner, Executive Vice President of Woodward-Clyde Consultants, was Principal Investigator, and Mr. G. L. Baker, Vice President, was Project Manager.

The investigation was conducted in three stages: field, laboratory and theoretical analyses. Thus, the report is issued in three separate volumes (all contained herein) as follows:

Volume I - "Field Investigation" describes the field investigation phase of this study, presents the background information, site selection criteria, and scope of the work, describes the vertical and horizontal soil sampling programs, and the in-situ testing program.

Volume II - "Laboratory Testing" presents a description of the laboratory testing program, the laboratory test

results and a characterization of pertinent soil properties and parameters from both the field and laboratory test data.

Volume III - "Assessment and Prediction of Skin Friction of Shafts in Beaumont Clay" presents a description of the assessment of techniques relevant to the prediction of the ultimate skin friction of shafts drilled in cohesive soils as well as a prediction of the load-settlement relationship of such shafts.

The field investigation of this study (Volume I) was performed under the direction of Mr. W. S. Gardner and Mr. G. L. Baker by Dr. J. Audibert and Mr. D. Aggarwal. The laboratory investigation (Volume II) was performed under the direction of Mr. Gardner by Dr. R. Singh, with the assistance of Mr. J. Kim. The theoretical analysis (Volume III) was performed by Mr. Gardner and Dr. Sircar (Load-Deformation Prediction) with assistance from Dr. Singh and Mr. W. Ping. The report was finalized under the direction of Mr. Baker and Mr. Gardner.

The contract was monitored by Dr. Lawrence D. Johnson, Research Group, Soil Mechanics Division (SMD), Geotechnical Laboratory (GL), under the supervision of Mr. G. B. Mitchell, SMD, Mr. C. L. McAnear, Chief, SMD, GL, and Dr. William F. Marcuson III, Chief, GL. Directors of WES during the conduct of this study were COL Nelson P. Conover, CE, and COL Tilford C. Creel, CE. The Technical Director was Mr. F. R. Brown.

## CONTENTS

	<u>Page</u>
PREFACE . . . . .	i
CONVERSION FACTORS, U. S. CUSTOMARY TO METRIC (SI)	
UNITS OF MEASUREMENT . . . . .	iv
VOLUME I: FIELD INVESTIGATION	
VOLUME II: LABORATORY TESTING	
VOLUME III: ASSESSMENT AND PREDICTION OF SKIN	
FRICTION OF SHAFTS IN BEAUMONT CLAY	

CONVERSION FACTORS, U. S. CUSTOMARY TO METRIC (SI)  
UNITS OF MEASUREMENT

U. S. customary units of measurement can be converted to metric (SI) units as follows:

<u>Multiply</u>	<u>By</u>	<u>To Obtain</u>
feet	0.3048	metres
inches	2.54	centimetres
kips (force)	4448.222	newtons
kips (force) per square foot	47.88026	kilopascals
miles (U. S. statute)	1.609347	kilometres
pounds (force)	4.448222	newtons
pounds (force) per square foot	47.88026	pascals
pounds (force) per square inch	6894.757	pascals
pounds (mass) per cubic foot	16.01846	kilograms per cubic metre
tons (2000 lb, mass)	907.1847	kilograms
tons (mass) per square foot	9764.856	kilograms per square metre

VOLUME I

FIELD INVESTIGATION

By  
J. Audibert and D. Aggarwal

## TABLE OF CONTENTS

	Page
PART I: INTRODUCTION .....	2
PART II: SCOPE OF WORK .....	4
PART III: SUBSURFACE SITE INVESTIGATION .....	6
Conventional Vertical Soil Borings .....	6
Horizontal Sampling .....	7
Denison Sampling .....	10
PART IV: IN-SITU TESTING .....	11
Pressuremeter Test Program .....	11
Borehole Shear Test Program .....	17
Piezometric Measurements .....	22
Static Cone Penetrometer Tests (CPT) .....	22
PART V: CONCLUSIONS .....	26
PART VI: LITERATURE CITED .....	28
4 TABLES	
22 FIGURES	
APPENDIX A: FIELD LOG OF VERTICAL SOIL BORINGS .....	A1
APPENDIX B: PRESSUREMETER TEST CURVES FOR BORINGS B-1 AND B-3....	B1
APPENDIX C: CONCRETE-COATED SHEAR PLATE DETAILS FOR BOREHOLE SHEAR TESTS .....	C1
APPENDIX D: CALIBRATION CHARTS, BOREHOLE SHEAR TESTS .....	D1
APPENDIX E: PIEZOMETER READINGS .....	E1

STUDY TO INVESTIGATE THE EFFECTS OF SKIN FRICTION ON THE

PERFORMANCE OF DRILLED SHAFTS IN COHESIVE SOILS

VOLUME I - FIELD INVESTIGATION

PART I: INTRODUCTION

A drilled shaft is formed by boring an open cylindrical hole into the soil and subsequently filling the hole with concrete. Excavation is accomplished usually by a mobile drilling rig equipped with a large helical auger or a cylindrical drilling bucket. Once in place, a drilled shaft acts essentially like a driven pile, except that its behavior under load may differ because of the dissimilar geometries and installation techniques.

A typical drilled shaft is shown in Figure 1. Other terminology commonly used to describe a drilled shaft includes: drilled pier, drilled caisson, and bored pile.

The prediction of shaft performance and design of drilled shafts in cohesive soils involve complex interrelationships that include numerous factors such as method of installation, stress-strain behavior and heterogeneity of foundation soils, dragdown from consolidation and uplift from swell of surrounding cohesive soils, vertical and lateral loads applied to the shaft, effects of adjacent shafts, changes in soil strength and adhesion between soil and shaft due to changes in moisture, and geometry and orientation of the shaft.

Existing theories and empirical procedures are often overly conservative and do not lead to optimum efficiency. Field tests are commonly needed to check the design of shaft foundations.

The U. S. Army Engineer Waterways Experiment Station (WES), Vicksburg, Mississippi, is conducting work to develop improved methodology for design of drilled concrete shafts in cohesive soils. One important aspect of this work is to evaluate the effects of skin friction on the



performance of drilled shafts from results of laboratory tests on soil samples and field load tests.

Woodward-Clyde Consultants (WCC) conducted this study for WES in three stages including (1) field investigation, (2) laboratory testing, and (3) geotechnical engineering analyses.

An appropriate site was identified by WCC prior to commencing the study. The site selection criteria were as follows:

- a. Soil conditions are well documented and characterized.
- b. Drilled shafts were installed on site some years ago (5 to 10 years ago).
- c. Drilled shafts were load tested shortly after construction, and are still accessible today.
- d. Present site and shaft conditions are such as to allow assessment of effect of time on load transfer and soil properties evolution in shaft vicinity.

Four test shafts were constructed at a test site located on Texas State Department of Highways and Public Transportation (THD) right-of-way at the intersection of State Highway 225 and Interstate Highway 610 in southeastern Houston, Texas (Fig. 2a). The detailed subsurface exploration and soil characterizations had been made in 1969, and load tests on four carefully instrumented test shafts produced high-quality data documented in a series of reports published by the Center for Highway Research of the University of Texas at Austin (O'Neill and Reese, 1970).

The load tests had been performed on all four test shafts at this location and three of these shafts (S-2, S-3 and S-4) still exist beneath a shallow (3 to 4 ft)\* fill. The locations of the test shafts and the previous borings are shown on Figure 2b. Profiles of soil composition and test shafts are shown on Figure 2c.

---

\* A table of factors for converting U. S. customary units of measurement to metric (SI) units is presented on page iv.

## PART II: SCOPE OF WORK

The scope of work of the field investigation consists of the following items:

- a. Select a test site that had the characteristics necessary for the prescribed study.
- b. Perform a thorough subsurface investigation to provide a detailed evaluation of the soil and groundwater conditions existing at the test site and to obtain representative samples of the subsoils suitable for laboratory analyses.
- c. Obtain block samples (approximately 1-ft cube) to be excavated from the access shaft at depths 7, 11, 15, 19, and 23 ft to check for disturbance in the boring samples.
- d. Conduct pressuremeter tests in a boring close to the drilled shaft to establish the in-situ state of horizontal stress near the drilled shaft so as to improve the hindcasting analysis using the results of special laboratory and/or in-situ interface shear tests to predict the load transfer along the drilled shafts.

Borehole shear tests and static cone penetrometer soundings were internally funded by the Professional Development Committee of Woodward-Clyde Consultants and the results made available to this study.

The scope of the geotechnical laboratory investigation is to provide a characterization of the in-situ soil properties and parameters as well as their state-of-stress. The laboratory testing program consists of the following:

- a. handling and testing of representative soil samples;
- b. physical and index property tests;
- c. triaxial compression and one-dimensional consolidation tests;
- d. direct shear and residual strength tests;
- e. mortar-soil interface tests; and
- f. earth pressure-at-rest tests.

The laboratory test results were characterized in terms of:

- a. stratigraphy;
- b. stress state;
- c. undrained, drained and residual shear strengths;
- d. deformation characteristics;
- e. interface shear; and
- f. soil property changes with time.

The scope of the analytic investigation is subdivided into (1) a detailed interpretation of the load test results, (2) an evaluation of the ultimate shaft resistance in comparison with the existing load test data, and (3) evaluation of the conformance of load-settlement predictions with the observed behavior of the test shafts.

Evaluation of the ultimate shaft friction was first made by theoretically based techniques which utilized basic soil property to predict shaft friction. Subsequently, other techniques were investigated including application of laboratory soil-mortar interface shear measurement, and in-situ borehole shear test. In addition, the application of moisture migration concepts to the prediction of shaft friction was also investigated. Evaluation of the load-settlement analyses was focused on a numerical load-transfer technique. This work included derivation of load-transfer curves from load test results and prediction of the load-settlement behavior of the test shafts.

### PART III: ANALYSIS OF LOAD TEST RESULTS

The shaft load transfer reflecting the mean deformation of the shaft versus total shaft load was first analyzed using the interpretation of the instrumented load tests provided by O'Neill and Reese for each of the four shaft types employed. An interpretation of the Shaft S-1 load distribution data provided by O'Neill and Reese was subsequently used to conduct an independent interpretation of the load-transfer curves at each level of instrumentation. The results of these analyses are summarized in the following sections.

#### Shaft and Load-Test Data

Test Shaft S-1 was selected for detailed analysis. For interpretation of the load-transfer curves, the diameter of S-1 was assumed to be 2.5 ft and the shaft length 23.1 ft. Note that upon a subsequent removal of the shaft, an average diameter of 2.56 ft was measured.

The first loading of the shaft was conducted by applying loads in increments of 5 or 10 tons every 2.5 minutes. Loading continued until plunging of the shaft was observed. Subsequent to unloading, a second load test was immediately conducted to investigate reloading effects. Finally, 3.5 months after the initial testing, a third load test was conducted to investigate the effects of setup on the shaft capacity.

#### Top Deformation-Total Shaft Load Behavior

The total shaft (skin friction) and base load curve versus top deformation curves reported by O'Neill and Reese for each of the test shafts are reproduced in Appendix B as Figures B1 through B4. The peak and minimum post-peak ultimate shaft load and the associated mean deformation shaft at the top of the shaft are tabulated in Table 1 for the four shafts tested.

A piezometer was installed in Boring B-1 and is shown in Figure 3 as P-1.

A Shelby tube could not be retrieved at 14-ft depth in Boring B-2. A new boring (Boring B-2A) was made 6 in. further away from Shaft S-3. This second location is shown in Figure 3 and identified as P-2, indicating that a piezometer was installed in this boring. Boring B-3 also had to be relocated when bad weather prevented drilling the boring beyond 10-ft depth and the hole caved in. The new location (Boring B-3A) was drilled 14 ft 6 in. away from Shaft S-3 and is identified in Figure 3 as P-3, indicating that a piezometer was installed at this location. The field logs for each of the borings are presented in Appendix A.

The Sinco diaphragm-type piezometers installed in each boring had their tips at different elevations so as to enable an evaluation of any peculiarity in the piezometric profile. The method of installation of the piezometers, the depths of the tips and the measurement results are discussed later in this report in the section on in-situ tests.

Five pressuremeter tests were conducted in Boring B-1 and one pressuremeter test was conducted in Boring B-3. The pressuremeter tests and their results are discussed in the section on in-situ tests.

Five other vertical borings (BHS-1 through BHS-5) were drilled at the site (see Fig. 3) to make borehole shear tests at various depths. The test procedures and results are discussed later in this report in the section on in-situ tests.

#### Horizontal Sampling

Horizontal-oriented samples were obtained at depths of 7, 11, 15, 19 and 23 ft adjacent to Shaft S-3. The purpose of these samples was to obtain detailed information relative to the change in soil properties outward from the face of the shaft and to permit direct shear tests with a failure plane parallel to the vertical movement of the shaft.

The samples were obtained by drilling and casing a large (5-ft) diameter access shaft in which a man could work. Before drilling the access shaft, the exact location of Shaft S-3 was determined and the top of the shaft uncovered. Inspection of the top of Shaft S-3 indicated that the instrumentation cable appeared to be intact and could perhaps be reused if load tests on this shaft are to be performed in the future. With the location of Shaft S-3 known, the access shaft could be located approximately 4 ft away so as to allow two successive 2-ft-long samples to be obtained between the access shaft and Shaft S-3 at the desired depths.

The first 5-ft-diameter access shaft, shown as location #1 in Figure 3, was augered with its center 8.3 ft away from the center of Shaft S-3 so as to result in a distance of 52 in. between the near edge offset of the access shaft and the concrete shaft face of Shaft S-3. This hole caved in below 13 ft due to a 48-hr delay in the delivery of the corrugated metal pipe (CMP) casing by the supplier. The location was abandoned and the hole backfilled to within about 4 ft of the ground surface. The shallow pit was later used to check out the horizontal sampling system and procedures specially developed for this project. A second exploratory shaft (location #2 in Fig. 3) was then augered and cased as planned.

The horizontally oriented Shelby tube samples were obtained using 30-in.-long by 4-1/2-in.-diameter steel thin-walled tubes. Six-inch holes had been burnt in the casing, before installation, at the desired sampling depths of 7, 11, 15, 19 and 23 ft. The Shelby tubes were jacked into the soil using a double acting center hole jack with a 6-in. stroke (Fig. 4).

A specially designed and machined solid aluminum head with a 1-in. threaded hole was attached to the top of the Shelby tubes. A 1-in. threaded rod was screwed into the head and passed through the hollow piston of the center hole jack.

During insertion of the Shelby tube into the soil the jack reacted against the opposite wall of the casing (Fig. 4a). The full penetration

of the Shelby tube was obtained by several consecutive travels of the piston and by a combination of blocking of the jack and threading of the nut on the 1-in. threaded rod.

To retrieve the samples, the jack was turned around and used in a pulling mode (Fig. 4b). Consecutive travels of the piston were required to complete the extraction of the tube from the soil.

Two successive samples were obtained at each depth in order to sample the 51 in. of soil separating the access shaft wall from the face of Shaft S-3. The pushing of the second tube was terminated when there was no further movement of the Shelby tube indicating that the tube had hit the concrete face of Shaft S-3.

The bottom of the access shaft (location #2) was not stable due to seepage filling the bottom three feet of the casing. Horizontal sampling operations thus could not be carried out at the 23-ft depth. The access shaft was backfilled 4 ft and sampling operations began at a depth of 19 ft. However, once the first sample had been obtained at the 19-ft depth, at a distance of 2 to 4 ft away from Shaft S-3, water started seeping in very steadily, causing temporary suspension of the sampling operation.

When the sampling operations were resumed, the water which had filled the access shaft to a depth of 12 ft, approximately to the depth of the groundwater level (Appendix E) was pumped out using a sump pump and a wooden platform placed on the soft bottom. The second sample (closest to Shaft S-3) at the 19-ft depth was then obtained.

The access shaft was then backfilled to a depth of 15 ft and the horizontal Shelby tube samples obtained. Similarly, samples were obtained at depths of 11 and 7 ft.

Once all the horizontal Shelby tube samples had been obtained, the access hole was backfilled to a depth of 2 ft, the CMP casing torch cut at that level and the rest of the access shaft backfilled.

### Denison Sampling

Because it would not have been practical and safe (no casing could have been installed while augering down the access shaft) to obtain block samples as originally planned, large diameter Denison samples were obtained in the "free field", southwest of Shaft S-3, at a distance of 36 ft from the center of Shaft S-3. The Denison samples were obtained at depths of 5, 7, 11, 15, 19 and 23 ft. Each sample was 5-1/2-in. nominal diameter and 2 ft in length.

The Denison core barrel (Fig. 5) recovers a relatively large sample in the inner, non-rotating barrel. The inner barrel is lined with a thin sheet metal liner so that the samples can be recovered and preserved in the same manner as when using thin-wall Shelby tube samplers.

In a Denison core barrel, the inner tube and cutter bit precede the rotating outer tube into the formation, thus improving the chances of retrieving an undisturbed and uncontaminated (by the drilling fluid) sample. The sheet metal liner further helps in preventing contamination or physical disturbance of the soil sample during removal from the sampler.

After the liner was removed, the sample was identified and logged and the ends of the liner were sealed using a non-shrink wax.



## PART IV: IN-SITU TESTING

### Pressuremeter Test Program

#### Pressuremeter Testing

Six pressuremeter tests were performed in Boring B-1 and one test in Boring B-3 using the WCC Menard Type GA pressuremeter system.

As shown in Figure 6, the pressuremeter apparatus consists of a probe, a volume measurement and pressure-control instrument, and a gas-supply tank. The cylindrical probe contains an expandable rubber membrane (measuring cell) and two contiguous independently expandable guard cells. The measurement system and the measurement cell are filled with water and the volume change induced in the measuring cell is measured by the sight tube volumeter. Expansion of the measuring cell is controlled by applying gas pressure from the gas-supply tank to the fluid column through a pressure regulator system. The pressure-control system contains a fluid regulator and a differential pressure regulator. This regulator maintains a constant differential pressure of one bar between the fluid pressure in the measuring cell and the gas pressure in the guard cell at all times during the test. Pressure gages measure the pressure in both the guard cell and in the measuring cell.

The key to obtaining good quality results is careful hole preparation. The borings were advanced by taking a 24-in.-long, 3-in.-diameter Shelby tube sample. A 34-in.-long, 2.5-in.-diameter Shelby tube sample was taken at the level of the pressuremeter test and then immediately inserting the pressuremeter probe into this smaller diameter sampling hole. The pressuremeter tests were conducted in pre-drilled holes by expanding both the measuring and guard cells against the walls of the soil boring. This process was repeated to a depth of 34 ft utilizing a flight auger or rotary wash drilling under the water table to clean out the hole after testing and large diameter sampling. Undrained pressuremeter tests were performed utilizing a standard one minute stress interval duration with an unload-reload cycle midway through the test. Fur-

ther information on the pressuremeter apparatus and test procedure is presented by Baguelin, et al. (1978).

#### Testing Results

Pressuremeter test curves for Borings B-1 and B-3 are presented in Appendix B. Soil properties have been interpreted from the test curves and are summarized in Table 1.

In-situ Stresses. The in-situ horizontal effective stress was determined from the configuration of the initial portion of the pressuremeter test curve. An independent check of the interpreted horizontal stress by a relationship proposed by Marsland and Randolph (1977) was also utilized. According to their suggested relationship, the peak pressure below which the pressuremeter stress-strain response is linear should correspond to a pressure  $P_f$ :

$$P_f = P_o + S_u \quad (1)$$

where:  $P_o$  = total horizontal ground stress measured by the pressuremeter; and  
 $S_u$  = undrained shear strength.

The undrained shear strength is determined as discussed later in this section. Values of  $P_o$  are iterated until the Marsland and Randolph relationship is satisfied. A typical pressuremeter test curve showing an interpretation of  $P_o$  and  $P_f$  is shown in Figure 7. Values of the in-situ horizontal effective stress are plotted on Figure 8. Also plotted on this figure are lines of horizontal effective stress which correspond to specific values of the coefficient of earth pressure at rest,  $K_o$ , which relates the horizontal effective stress  $\bar{\sigma}_h$  to vertical effective stress  $\bar{\sigma}_v$  by:

$$\bar{\sigma}_h = K_o \bar{\sigma}_v \quad (2)$$

Brooker and Ireland (1965) presented data on stiff clays which suggested that a relationship between  $K_o$ , overconsolidation ratio (OCR), and angle of internal friction ( $\phi$ ), exists for each type of clay:

$$K_o = (1 - \sin \phi) OCR^m \quad (3)$$

where:  $m = 0.58 (PI)^{-0.12}$

with:  $PI =$  plasticity index of the soil.

O'Neill and Reese (1972) suggest that  $OCR = 4$ ,  $\phi = 20$  degrees, and  $PI = 20$  percent may be representative for the Beaumont clay formation found at this site. Using these data, a  $K_o$  value of 1.1 would be calculated by Equation 3.

Since the pressuremeter-derived  $K_o$  values are significantly higher than 1.1, the pressuremeter curves were reinterpreted to obtain lower limit values of  $\bar{\sigma}_h$  which are also plotted on Figure 8. These lower limit values represent an absolute minimum using the Davidson (1979) procedure which was not subject to the Marsland and Randolph check. These minimum horizontal stress values are much closer to the  $K_o$  suggested by Brooker and Ireland, but they still are over 20 percent higher. The higher pressuremeter-derived  $K_o$  values may be explained by the fact that overconsolidation of the Beaumont clay was caused by desiccation and not previous overburden loading. The Brooker and Ireland relationships were developed for preloaded clays and may not be strictly valid for desiccated clays.

A horizontal OCR can also be interpreted from the pressuremeter curve as:

$$OCR = \frac{P_f - u}{P_o - u} = \frac{\bar{\sigma}_{h \max}}{\bar{\sigma}_h} \quad (4)$$

where:  $u =$  ambient pore pressure

$\bar{\sigma}_{h \max} =$  maximum past horizontal effective stress

Values of pressuremeter OCR ranging from 2.2 to 4.7, with an average of 3.6, were obtained and appear to be in agreement with O'Neill's data.

Elastic Modulus. An elastic modulus  $E$  can be calculated from the linear portion, or "pseudo elastic" portion, of the pressuremeter test curve (see Fig. 7).

$$E = 2(1 + \nu)V_o \frac{\Delta P}{\Delta V} \quad (5)$$

$$V_o = V_i + \Delta V_o \quad (6)$$

where:  $\nu$  = Poisson's ratio,  
 $\Delta V_o$  = volume change corresponding to  $p_o$ ,  
 $\Delta P/\Delta V$  = linear slope of test curve, and  
 $V_i$  = initial volume of probe.

Initial pressuremeter modulus values are plotted in Figure 9. An unload-reload modulus can also be determined from the linear portion of the unload-reload cycle of the pressuremeter curve. Unload-reload pressuremeter moduli are also plotted in Figure 9.

Pressuremeter test results obtained during other projects on the stiff clays in Houston (Merritt, Davidson and Baker, 1979), Chicago (Davidson and Perez, 1979) and Seattle (Davidson and Perez, 1980) have indicated that the initial pressuremeter modulus is not the initial tangent modulus of the soil, but a modulus which is influenced by the level of stress relief or unloading of the soil during hole preparation. This modulus typically equals or exceeds the initial tangent modulus from unconfined compression (UC) or unconsolidated-undrained triaxial (UU) tests on fissured clay. However, compared to good quality laboratory tests such as anisotropically-consolidated-undrained (CU) triaxial testing, the initial pressuremeter modulus falls somewhere between the secant modulus at 50 percent of the peak stress and secant modulus at failure. These trends are in apparent agreement with the

data on this project based on the laboratory test results reported by O'Neill and Reese (1972).

Comparisons of Menard pressuremeter test results with self-boring pressuremeter, CU triaxial and plane strain triaxial test results on the Seattle stiff clay (Davidson and Perez, 1980) revealed that the unload-reload modulus was approximately equal to the "true" initial tangent modulus of the soil. This "true" modulus was back-calculated from measured performance of a tied-back excavation which was modeled using the finite element method. Therefore, the significantly higher unload-reload pressuremeter moduli may, in fact, be a more realistic measure of the actual in-situ initial tangent modulus of the Beaumont clay.

Undrained Shear Strength. The undrained shear strength,  $S_u$ , was determined from the failure portion of the pressuremeter test curves using the Gibson and Anderson (1961) procedure:

$$S_u = \frac{P_L - P_o}{\beta} \quad (7)$$

where:  $P_L$  = pressuremeter limit pressure  
 $\beta$  = pressuremeter bearing capacity factor (similar to the bearing capacity factor  $N_c$  for long footings, Calhoun, 1970)  
 $\beta$  = 5.1 for stiff clay.

Pressuremeter derived undrained shear strengths are plotted in Figure 10. Alternatively, the undrained shear strength can be determined as the peak of a shear stress-strain curve developed from the pressuremeter curve following a theoretical equation presented by Palmer (1972), Ladanyi (1972), and Baguelin, et al. (1972).

$$(\sigma_r - \sigma_\theta)/2 = (dP/d\epsilon)_r \epsilon_r \quad (8)$$

where:  $(\sigma_r - \sigma_\theta)/2$  = shear stress

$(dP/d\epsilon)_r$  = slope of pressuremeter pressure radial strain curve

$\epsilon_r$  = radial strain.

Using a simplified procedure developed by Wroth and Hughes (1973) and modified by Marsland and Randolph (1977), undrained shear strength values were calculated and plotted on Figure 10. Note that the Marsland and Randolph (1977) procedure always yields higher shear strengths because these strengths are peak strengths at a small strain and may be influenced by hole disturbance. The Gibson and Anderson (1961) shear strength may reflect residual strengths which are measured at larger strains.

WCC's experience in Houston, Chicago and Seattle indicates that the Gibson and Anderson (1961) undrained shear strength generally agrees with the shear strengths determined from good quality laboratory tests. The Marsland and Randolph (1977) shear strengths are usually 15 to 40 percent higher than the Gibson and Anderson (1961) shear strengths. The higher disparities are encountered in soils which experience a higher level of hole preparation disturbance which is controlled by the strength of the soil and the type of hole preparation method.

Also plotted in Figure 10 is the shear strength profile from UU tests performed at this site as reported by O'Neill and Reese (1972). Near the surface the pressuremeter and laboratory strengths agree, but the deeper pressuremeter tests indicate strengths which are 50 to 100 percent larger than the laboratory tests. The wide disparity at 30 ft may be due to a change in material; the coarser grained saturated silt can be easily tested by the pressuremeter, but may be disturbed in sampling and sample preparation for laboratory testing.

#### Conclusions

The Menard pressuremeter tests have indicated that:

- a. Higher horizontal stresses may exist near the pier than would be anticipated based on relationships for stiff clays presented by Brooker and Ireland (1965).

- b. Higher initial tangent modulus values were measured by the pressuremeter than were indicated from the results of UU triaxial testing reported by O'Neill and Reese (1972).
- c. Undrained shear strengths determined from the pressuremeter were in agreement with UU triaxial test shear strength in the upper 10 ft of the soil profile. Below 10 ft of depth, the pressuremeter shear strengths were 50 to 100 percent higher than the laboratory test strengths reported by O'Neill and Reese (1972). No significant decrease in strength for the silt layer at 30 ft was revealed by the pressuremeter in contrast with that indicated by the laboratory testing.

### Borehole Shear Test Program

#### Introduction

This section contains the results of a field testing program consisting of a series of borehole shear tests using a specially modified device to simulate a concrete-soil interface. The field testing program is part of an applied research project funded by the Professional Development Committee of Woodward-Clyde Consultants and was conducted in conjunction with the WES project described in this report.

#### The Bore Hole Shear Device

The borehole shear test was developed by Handy and Fox (1967) at Iowa State University (ISU) in 1964 as an in-situ test method that would provide the soil shear strength parameters  $C$  and  $\phi$ . The borehole shear test equipment is a portable hand-operated kit, sized for use in a 3-in.-diameter test hole and with sufficient rods and pneumatic tubing to permit testing to a depth of about 24 ft. The test is similar to the direct shear test in that normal and shearing forces are applied to a thin shear zone of predetermined orientation and size. As in the direct shear test, drainage can be controlled only by varying the consolidation time and the shear strain rate.

The conventional borehole shear test apparatus consists of two grooved steel plates, each comprising about 90 degrees of a cylindrical surface, that are pressed against the walls of the borehole by a pneumatic cylinder actuated by pressurized  $CO_2$  (see Fig. 11). The normal

pressure between the plates and the soil is controlled and measured by a regulator and Bourdon tube gage in the CO<sub>2</sub> system. After the normal pressure has been applied for a preselected consolidation time, the plates are pulled axially up the hole by a small work gear jack, and the pulling force is measured using a load cell that consists of two hydraulic cylinders and a Bourdon tube gage. Axial displacement during shear is monitored by marking the gears of the pulling jack, and the pulling force is read at predetermined displacement intervals. When the pulling force reaches an ultimate value, indicating shear of the soil along a surface parallel to the face of the plates, the pulling force is relaxed. The normal pressure is increased and after a similar consolidation period shear is again induced. This process is repeated several times, resulting in a shear strength versus normal pressure relationship similar to the results of a series of direct shear tests. Normally, stage testing appears to give the same results as relocating the shear plates on a fresh surface for each new normal pressure increment. Presumably, a new failure surface develops in fresh soil a slight distance further from the plates during each increment.

Published results (Lohnes and Handy, 1968; Wineland, 1976; Nickel, 1976) have been based largely on tests on partially saturated silty clays, saturated silts, and soft clays. For such soils the "normal" consolidation time of 5 minutes and shear displacement rate of .002 in./sec. appear to give consolidated-drained strength parameters. For overconsolidated highly plastic clays these procedures appear to give undrained or intermediate results. A set of smaller shear plates with more widely spaced teeth was recently developed for use in very stiff clays (Lutenegger, et al., 1978).

#### Description of Test Equipment

For this project the standard borehole shear test equipment manufactured by Handy Geotechnical Instruments, Inc., Ames, Iowa, was used. The only modification was the substitution of specially constructed concrete shear plates in place of the grooved steel plates.



The normal steel shear plates are 2 in. wide by 2.5 in. high. The gages limit the maximum stress measurement range to about 7 ksf using the standard shear plates.

The concrete shear plates were about 1.5 in. wide by 2.8 in. high and had a cylindrical radius of 1.5 in. The plates were cast in a smooth brass mold using Type III cement, water and sand passing a #10 sieve. Mix proportions and a gradation curve for the sand are contained in Appendix C. After curing under water for several days the concrete plates were air-dried and glued to steel backing plates using epoxy cement. The plates were then roughened by sanding with sandpaper and brushing lightly with a wire brush.

The test equipment was calibrated in the Houston WCC laboratory. Calibration procedures and results are presented in Appendix D.

#### Test Procedures and Results

The tests were performed at five general depths. To facilitate coordination with use of the drilling rig for other operations on the site, a separate boring was drilled for each test depth. Each boring was drilled with a 4-in.-diameter flight auger to a depth about 1 ft above the desired test depth. The test section itself was formed by sampling with a standard 3-in.-OD Shelby tube pushed 24 in. Because the concrete shear plates were slightly thicker than the original steel plates, there was insufficient clearance to insert the test unit into the hole formed by the Shelby tube, and it was necessary to ream each hole using the special reamer provided with the test kit. The reamer is a slotted length of 3-in.-OD Shelby tube with a scalloped sharpened cutting edge. The reamer was attached to a handle of 1/2-in. pipe and pushed and turned into the hole by hand. Very thin shavings of the clay were obtained. It was not possible to observe the final condition of the test surface.

During the course of the testing program, several of the test procedures were varied so as to determine their effects on the results. Test 1 was conducted as a staged test; that is, without relocating the shear plates to a fresh soil surface for each normal pressure

increment, using the recommended 5 minute consolidation time and .002 in./sec shear displacement rate. One point of the test was then rerun with the test head rotated 90 degrees to relocate the shear plates on a fresh soil surface.

Test 2 was then run 6 in. lower in the same boring with a consolidation time of 30 minutes and a displacement rate of .0002 in./sec. The second point of Test 2 gave a much lower strength than those obtained in Test 1, but when the shear plates were relocated to the fresh surface and the second point rerun, the results were similar to those of Test 1. It was concluded that consolidation times and shear rates were not critical, and thereafter the tests were generally conducted with a consolidation time of 10 minutes and a displacement rate of .0005 in./sec.

The fourth point of Test 8 was repeated twice, resetting the plates to their original position each time, to check the effects of remolding. The effect on the peak shear stress was found to be slight.

A free subsurface water table was indicated at a depth of about 13 ft from observations in a boring that stood open overnight. Free water entered Borings 1 and 2, and Tests 6 and 7 were conducted beneath the water surface. A trace of water was observed below the level of Test 8 in Boring 5. Test 5 was conducted well above the water table, but water was added to the boring one-half hour before testing. The fifth point of Test 5, conducted in an inundated hole, was repeated using a consolidation time of 30 minutes and a displacement rate of .0001 in./sec. Again, the effect on the results was small.

The concrete shear plates were not used for Test 4. Instead, the 1-in.-square shear plates with two teeth, recently developed at ISU for use in very stiff clays, were used. The device was removed from the boring after each test increment, inspected, and relocated to fresh soil for each new increment as recommended. It was observed that after each of the first two shear increments, the plates were not fully covered with soil, but contained a small wedge of clay ahead of each tooth. After the third and fourth points, the shear plates were fully covered with a cake of soil about 0.1 to 0.15 in. thick.

### Discussion of Results

The strength envelopes and stress-displacement curves obtained for the eight tests are presented in Figures 12 through 20. During calibration it was discovered that significant compression of the load cell occurred, and the measured displacements have been corrected for compression. Because it is difficult to begin a shear increment at exactly zero shear stress, the curves have also been adjusted visually to begin at the origin.

The strength envelopes were drawn through the data points using linear regression. In general, the data points closely fit the linear strength envelopes. The cohesion intercept and angle of shearing resistance determined in this manner for each test are listed in Table 2.

Because the test is essentially an interface friction test rather than a soil shear test, the terms "cohesion" and "angle of internal friction" do not strictly apply. It was observed after each test that very little soil clung to the face of the shear plates. The shear plates were slightly dirty, but the aggregate was always visible. This would appear to indicate that the movement took place at the interface rather than within the soil. The very low values of shear displacement at peak shear stress would also appear to indicate an interface failure.

### Conclusions

- a. The borehole shear tests have indicated that the tests gave consistent results with linear relationships between peak shear stress and applied normal stress.
- b. The test results were insensitive to consolidation time and shear displacement rate within practical ranges.
- c. The tests conducted below the water table or in inundated holes produced significantly different results than the tests conducted above the water table.
- d. The one test conducted in an inundated hole is similar to those run below the water table.

### Piezometric Measurements

Sinco diaphragm-type piezometers were installed at each of the three vertical boring locations and shown as P-1, P-2, and P-3 on the plot plan showing the location of the soil borings on Figure 3.

The tips of the three piezometers were installed at different depths. Piezometer P-1, in Boring B-1, was installed at a depth of 26 ft. Piezometer P-2, in Boring B-2A, was installed at a depth of 29.5 ft below ground surface. Piezometer P-3, in Boring B-3A, was installed at a depth of 15.5 ft.

#### Installation Procedure

The piezometers tips were soaked in water for a few hours prior to installation in the hole. The holes were backfilled with sand to the depth where the piezometer was to be installed. The piezometers were held vertically at that depth and about 4 ft of sand poured over the piezometer tip. The piezometers were then sealed at the top using a 4-ft-thick layer of bentonite pellets seals. A sketch of the piezometer installation in each boring is shown on the boring logs in Appendix A.

#### Piezometer Readings

The piezometers were read using a Sinco pneumatic pore pressure indicator model 51421-A. The pressure measurements were made in accordance with the instructions supplied with the piezometer instruction manual by Sinco.

The piezometer readings are presented in Appendix E and summarized in Table 3. The water table is seen to be located approximately 11 ft beneath the existing ground level.

### Static Cone Penetrometer Tests (CPT)

#### Introduction

Two static cone penetrometer tests (CPT) were performed at locations CPT-1 and CPT-2, located as shown in Figure 3, using a mechanical Dutch cone penetrometer rig shown in Figure 21. The Dutch cone penetrom-

meter is a jacking device which measures penetration resistances of a specially designed cone as it is pushed into the soil. The magnitude of the measured resistances is an indication of certain soil properties in situ.

The CPT's were funded by Woodward-Clyde Consultants' Professional Development Committee and the data are made available to this project for enhancing the data on site subsurface conditions.

In the following paragraphs the methods for reducing test data to cone resistances (also called cone bearing values) and for deducing soil properties from the cone bearing values will only be briefly described. A detailed description of the cone, test methods and interpretation of the data is given by Sanglerat (1972). In the United States, the test methods have been tentatively standardized by ASTM designation D 3441-75 T.

#### Reducing the CPT Data

The hydraulic jack, anchored into the soil at the ground surface, pushes a string of rods into the ground. The lower end of the rods is equipped with a specially designed cone. The design is such that the penetration resistance forces acting on the cone are measured at the surface by means of a manometer.

Two resistances are measured while the cone is being advanced at a rate of 2 cm/sec. The first is the tip resistance acting on the horizontal cross-sectional area of the cone ( $10 \text{ cm}^2$ ). The second resistance is the sum of the tip resistance and the local friction resistance acting on the side of the local friction sleeve. The local friction force acts on the friction sleeve which has a peripheral surface area of  $150 \text{ cm}^2$ . Since during testing there are no moving parts other than the cone tip, no other forces are measured. During a cone sounding, tests are made at intervals of 20 cm in the vertical direction. The first test is usually made at 40 cm below grade to insure that the cone tip is fully embedded into the soil.

Each test consists of advancing the cone a total distance of 8 cm in two increments of 4 cm each. This is done in one continuous stroke, without stopping. The first stroke advances only the cone tip itself, which gives the tip resistance,  $R_q$ . As soon as the friction sleeve is dragged down along with the cone tip, which occurs after the cone tip has moved 4 cm, the observed resistance increases by the amount of the friction,  $R_f$ , of the soil acting on the side of the friction sleeve and the reading is that of the sum of the cone tip and the friction resistance,  $R_q + R_f$ . The readings are then transformed into cone resistance values, or cone bearing values,  $q_c$ , and local friction,  $f_c$ . Both are expressed in  $\text{kg/cm}^2$ .

The friction ratio is also usually calculated from the test data; it is not a measured value. It is defined as  $\text{F.R.} = f_c \times 100 / q_c$  expressed in percent.

The friction ratio is strictly an empirical correlation between the test results and soil type classification. Without it, it is never possible to classify the soils being penetrated. With it, most of the time the classification is satisfactory.

#### Soil Classification From the CPT Data

Before determining what the cone bearing values and the local friction mean in terms of physical and mechanical quantities for soils, it is first necessary to determine to which type of soil these values apply, since the interpretation of one specific reading for a clay is quite different than that for a sand.

This is done using the friction ratio data. It has been observed through many years of practice and through tens of thousands of tests that the friction ratio can be accurately correlated with the type of soil. The correlation between F.R. and soil type has its limitations, however; the most important one being in the case of peats. This is because the structure of peats may vary so radically from the micro-structure to that of matted vegetation. Table 4 summarizes the correlation between soil types and friction ratio.

Some special cases require more than the F.R. for adequate identification. For example, clays of moderate to high sensitivity have an F.R. of 2 or less together with a  $q_c$  of 14 or less. Similarly, the F.R. alone is not sufficient to distinguish between silts and sandy clays and clayey sands. However, silts will always have a friction ratio of between 2 and 5 with cone values varying between about 20 for loose silts and 60 for dense ones. A sandy clay will exhibit a cone bearing value of less than 15 if the clay is very stiff and less as the clay consistency decreases.

#### Determination of Mechanical and Physical Properties of Soils From CPT Data

The cone bearing value,  $q_c$ , is an indication of the in-situ, undrained shear strength of cohesive soils and of the state of compactness of cohesionless soils.

If the friction ratio is 5 or more, the soils are basically clayey and their undrained shear strength can be estimated from the  $q_c$  values from the following equivalence:

$$q_c/20 \leq S_u \leq q_c/8 \quad \text{in kg/cm}^2 \text{ or tsf} \quad (9)$$

For a particular clay, a correlation much higher than the general correlation given above can be obtained. The variations are due to different proportions of soil type constituents in different clay soils. When little to no previous data are available, a reasonable correlation to start from is  $S_u = q_c/15$ .

#### CPT Test Results

As previously mentioned, two CPT soundings were made at the site (Figs. 22a, 22b). The interpreted shear strength profiles are presented in Figure 22c.

The excellent resolution of the stratigraphy by means of the Dutch cone can be easily recognized in Figure 22c. In particular, the silty layers reflected around 15- and 30-ft depths by the sharp variations in the Atterberg Limits and natural water content profiles presented by O'Neill and Reese (1970) are easily identifiable in both the F.R. and  $S_u$  profiles shown in Fig. 22c.

## PART V: CONCLUSIONS

The field testing program enabled soil samples to be obtained for the extensive laboratory testing program. The field testing program also exposed the drilled shaft which enabled the inspection of the exposed shaft, revealing that the instrumentation cable still seemed to be intact and could perhaps be reused if load tests on this shaft were to be performed in the future.

The borehole shear interface test gave consistent results with linear relationships between peak shear stress and applied normal stress. The test results were insensitive to consolidation time and shear displacement rate within practical ranges. The tests conducted below the water table or in inundated holes produced significantly different results than the tests conducted in the dry. The one test conducted in an inundated hole gave similar results to those run below the water table.

The piezometers installed showed that the water table was almost constant at the site and to be located approximately 11 ft beneath the existing ground level.

It is recommended that a load test be carried out on drilled shaft S-3 in order to determine the present long-term capacity of the shaft.

The pressuremeter tests conducted close to the drilled shaft showed that higher horizontal stresses may exist near the pile than would be anticipated based on relationships for stiff clays presented by Brooker and Ireland (1965). Also, higher initial tangent modulus values were measured by the pressuremeter than were indicated from the results of UU triaxial testing reported by O'Neill and Reese (1972). Finally, undrained shear strengths determined from the pressuremeter were in agreement with UU triaxial tests shear strength in the upper 10 ft of the soil profile. Below the 10-ft depth, pressuremeter shear strengths were 50 to 100 percent higher than the laboratory test strengths reported by O'Neill and Reese (1972). No significant decrease in strength for the silt layer at 30 ft was revealed by the pressuremeter in contrast



with that indicated by the laboratory test results reported by O'Neill and Reese (1972).

## PART VI: LITERATURE CITED

- Baguelin, F., Jezequel, J. F., LeMee, E. and LeMehaute, A. 1972. Expansion of cylindrical probes in cohesive soils. *Journal of Soil Mechanics and Foundation Engineering*, ASCE. Vol 98 (SM11).
- Baguelin, F., Jezequel, J. F. and Shields, D. H. 1978. The pressuremeter and foundation engineering. Series in Rock and Soil Mechanics, (214), Trans Tech Publications, Germany.
- Brooker, E. W. and Ireland, H. O. 1965. Earth pressures at rest related to stress history. *Canadian Geotechnical Journal*. Vol 2 (1):1-15.
- Calhoun, J. L. 1970. "Field Load Testing with the Pressuremeter," Proceedings of the 19th Annual SMF Conference, University of Kansas, March 1970.
- Davidson, R. R. 1979. Interpretation of the pressuremeter test, Woodward-Clyde Consultants Technical Memorandum No. 104-78.
- Davidson, R. R. and Perez, J-Y. 1979. Geotechnical investigations and recommendations, Michigan/Oak project, Woodward-Clyde Consultants report prepared for Skidmore, Owings and Merrill.
- Davidson, R. R. and Perez, J-Y. 1980. Pressuremeter research, I-90 project, Seattle, Washington, Report to WCC Professional Development Committee, February, 11 pp.
- Gibson, R. E. and Anderson, W. F. 1961. In-situ measurement of soil properties with the pressuremeter. *Civil Engineering and Public Works Review*, London. Vol 56 (658):615-618.
- Handy, R. L. and Fox, N. S. 1967. A soil bore-hole direct-shear test device. *Highway Research News*. (27):42-51.
- Ladanyi, B. 1972. In-situ determination of undrained stress-strain behavior of sensitive clays with the pressuremeter - Technical Note. *Canadian Geotechnical Journal*. Vol 9 (3):313-319.
- Lohnes, R. P. and Handy, R. L. 1968. Slope angles in friable loess. *Journal of Geology*. Vol 76 (3).
- Lutenegger, A. J., Reames, B. D. and Handy, R. L. 1978. Bore-hole shear test for stiff soil - Technical Note. *Journal of the Geotechnical Engineering Division*, ASCE. Vol 104 (GT11):1403-1407.

Marsland, A. and Randolph, M. E. 1977. Comparison of the results from pressuremeter tests and large in situ plate tests in London clay. *Geotechnique*. Vol 27 (2):217-243.

Merritt, B. K., Davidson, R. R. and Baker, G. L. 1979. Menard pressuremeter experience in Beaumont clay, presented at Spring Texas Section ASCE Meeting, Austin, Texas.

O'Neill, M. W. and Reese, L. C. 1970. Behavior of axially loaded drilled shafts in Beaumont clay, Research Report 89-8, Center for Highway Research, The University of Texas at Austin, Texas.

O'Neill, M. W. and Reese, L. C. 1972. Behavior of bored piles in Beaumont clay. *Journal of the Soil Mechanics and Foundation Engineering Division, ASCE*. Vol 98 (SM2).

Nickel, Stephen H. 1976. Discussion of "Borehole Shear Device," by John Wineland, *In-Situ Measurement of Soil Properties, ASCE*. Vol II, pp 172-174.

Palmer, A. C. 1972. Undrained plane-strain expansion of a cylindrical cavity in clay: a simple interpretation of the pressuremeter test. *Geotechnique*. Vol 22 (3):451-457.

Reese, L. C., and Wright, S. J. 1977. Drilled shaft manual, Implementation Package 77-21, Department of Transportation, Offices of Research and Development, Washington, D.C.

Sanglerat, G. 1972. *The penetrometer and soil exploration*. Elsevier, New York.

Wineland, J. D. 1976. "Borehole Shear Device," Proceedings of the Conference on In Situ Measurement of Soil Properties, American Society of Civil Engineers, Vol I, pp. 511-522.

Wroth, C. P. and Hughes, J. M. O. 1973. Discussion, *Geotechnique*. Vol 23 (2):284-287

Table 1  
Summary of Pressuremeter Test Results  
Boring B-1 (B-3)

Depth ft	$\sigma_{ho}$ $t/ft^2$	$u$ $t/ft^2$	$\bar{\sigma}_{ho}$ $t/ft^2$	$\bar{\sigma}_v$ $t/ft^2$	$K_o$	$\sigma_{hmax}$ $t/ft^2$	$\bar{\sigma}_{hmax}$ $t/ft^2$	OCR	$E$ $t/ft^2$	$E^+$ $t/ft^2$	$S_u^*$ $t/ft^2$	$S_u^{**}$ $t/ft^2$	$P_L$ $t/ft^2$	Comments
5.58	.45	-	.45	.37	1.22	2.1	2.1	4.7	144	289	1.25	1.70	7.0	
10.83	1.40	-	1.40	.68	2.06	4.0	4.0	2.9	128	396	1.29	1.48	8.0	
15.83	1.56	.03	1.53	.96	1.59	5.9	5.9	3.9	188	864	1.85	2.15	11.0	
20.83	1.51	.18	1.33	1.12	1.19	5.4	5.2	3.9	166	441	2.31	2.90	13.3	
25.83	2.36	.34	2.02	1.28	1.58	8.1	7.8	3.9	149	792	2.28	4.0	14.0	Insufficient failure por- tion of test for $S_u^{**}$ in- terpretation
30.50	2.50	.48	2.02	1.42	1.42	5.0	4.5	2.2	197	636	1.89	2.3	12.5	
(9.50)	1.05	-	1.05	.59	1.78	3.7	3.7	3.5	151	438	1.17	1.4	7.0	

\*Gibson and Anderson (1961) procedure

\*\*Marsland and Randolph (1977) procedure

Table 2  
Summary of Bore Hole Shear Test Results

Test Number	Boring Number	Depth ft	Water Conditions	Cohesion Intercept ksf	Angle of Shear Resistance degrees	Remarks
1 & 1A	BHS-4	10.8-11.0	None	.21	22.3	1-in.-square grooved steel plates
2 & 2A	BHS-4	11.3-11.7	None	.08	24.4	
3	BHS-3	7.2-7.5	None	.17	24.1	
4	BHS-3	7.6-7.7	None	3.09	6.0	
5	BHS-3	6.7-7.0	Added	.11	13.3	
6	BHS-1	22.0-22.2	Standing at 20.0'	.16	10.4	
7	BHS-2	18.8-19.0	Standing at 17.0'	.12	10.8	
8	BHS-5A	15.2-15.4	Trace at 16.0'	.21	10.7	

Table 3  
Summary of Piezometer Readings

Date	Piezometer Readings (psi)			Water Table Depth (ft)		
	P1	P2	P3	P1	P2	P3
4/3/80	6.47	8.2	--	11.08	10.58	--
4/7/80	6.4	7.8	--	11.23	11.50	--
4/26/80	6.3	7.9	1.9	11.46	11.27	11.12
4/27/80	6.3	7.9	1.8	11.46	11.27	11.35
4/28/80	6.3	7.9	1.9	11.46	11.27	11.12
4/29/80	6.4	8.0	1.9	11.23	11.04	11.12
5/1/80	6.4	8.0	1.9	11.23	11.04	11.12
5/3/80	6.4	8.0	1.9	11.23	11.04	11.12
5/5/80	6.4	8.0	1.9	11.23	11.04	11.12

Note: Sensor Elevation: P1 = 26.0 ft; P2 = 29.5 ft; P3 = 15.5 ft.

Table 4  
Identification of Soil Type Using CPT Data

SOIL TYPE	FRICTION RATIO
pure clay of low sensitivity	8 or more
silty clay to clayey silt	5 to 8
sandy clay to clayey sand	2 to 5
silts	2 to 5
silty sand, fine to medium coarse	1 to 2
coarse clean sands	1 or less
peats	varies widely

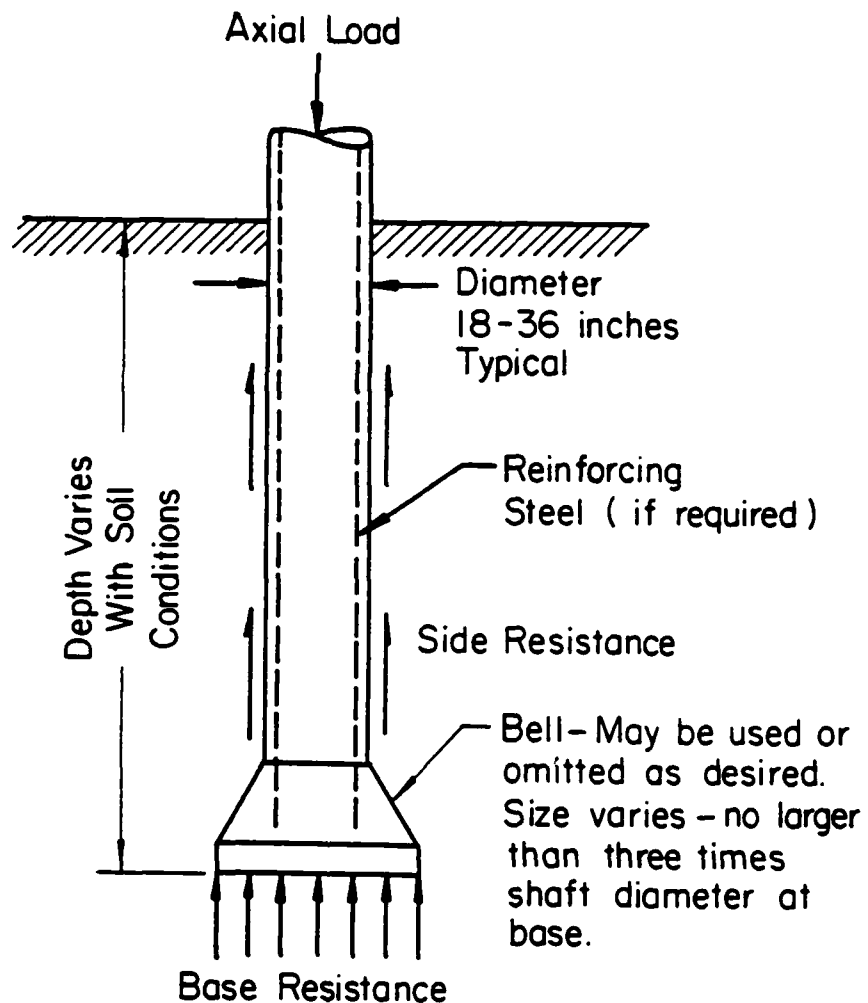


FIGURE 1. TYPICAL DRILLED SHAFT  
(after Reese and Wright, 1977)



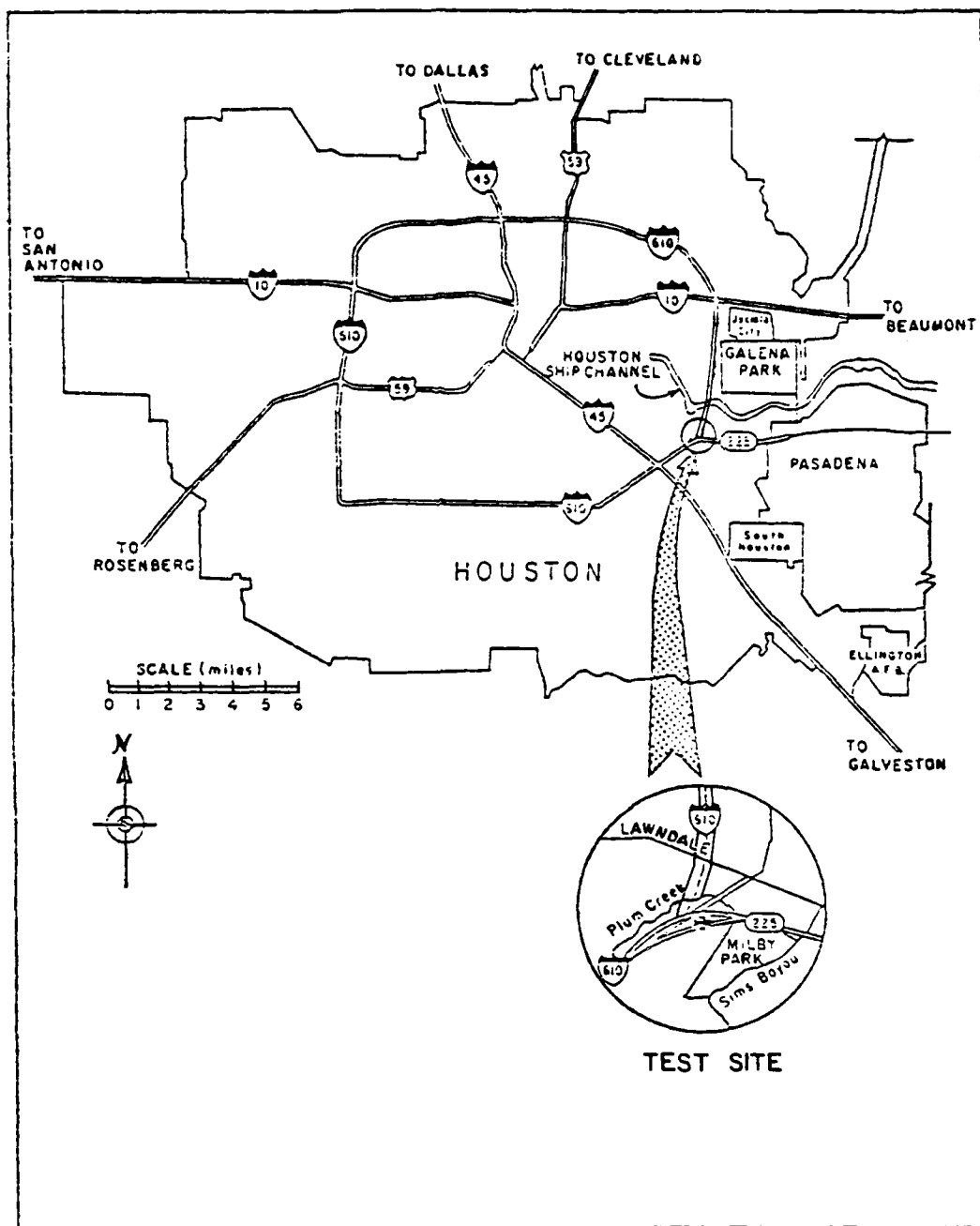


FIGURE 2(a). LOCATION MAP FOR SELECTED TEST SITE

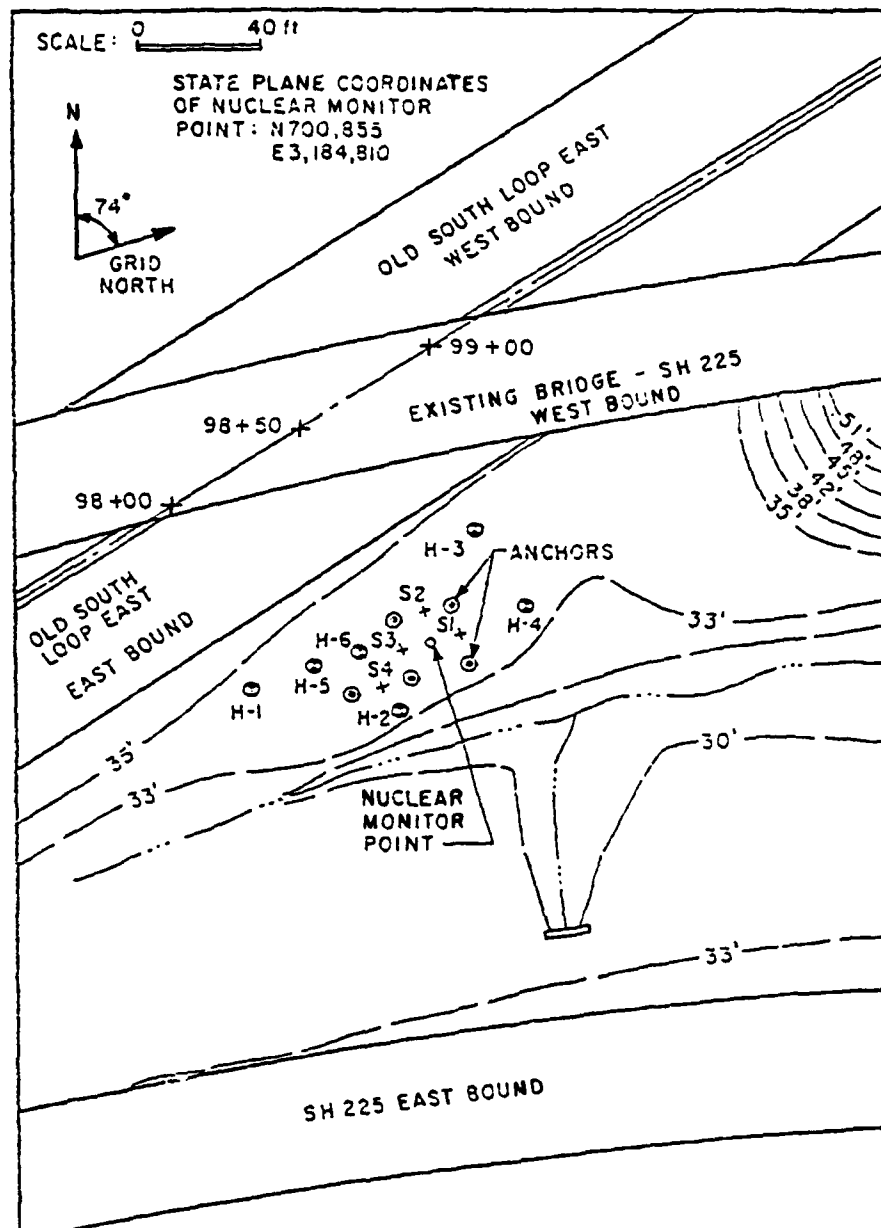


FIGURE 2(b). DETAILED MAP OF THE SELECTED TEST SITE,  
SHOWING LOCATION OF TEST SHAFTS AND SOIL BORINGS  
(After O'Neill and Reese, 1970)

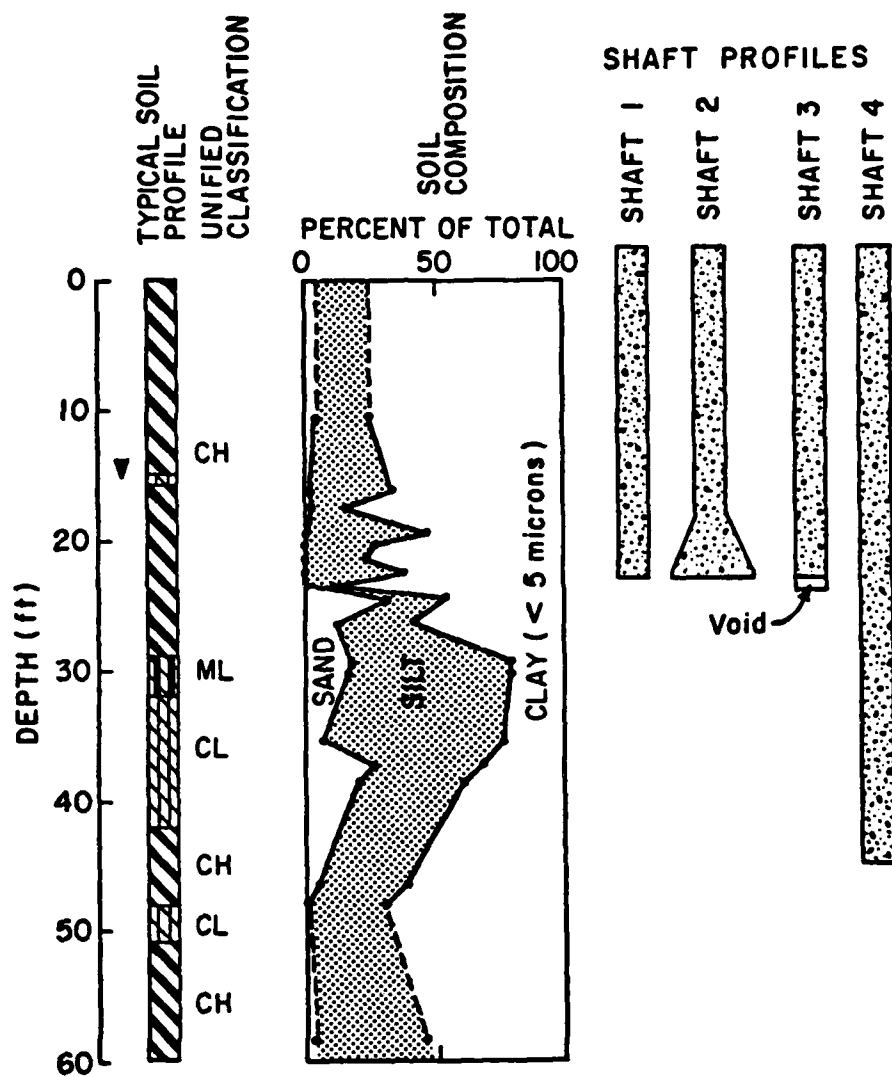


FIGURE 2(c). PROFILES OF SOIL COMPOSITION AND TEST SHAFTS, SH225 TEST SITE. (After O'Neill and Reese, 1970)

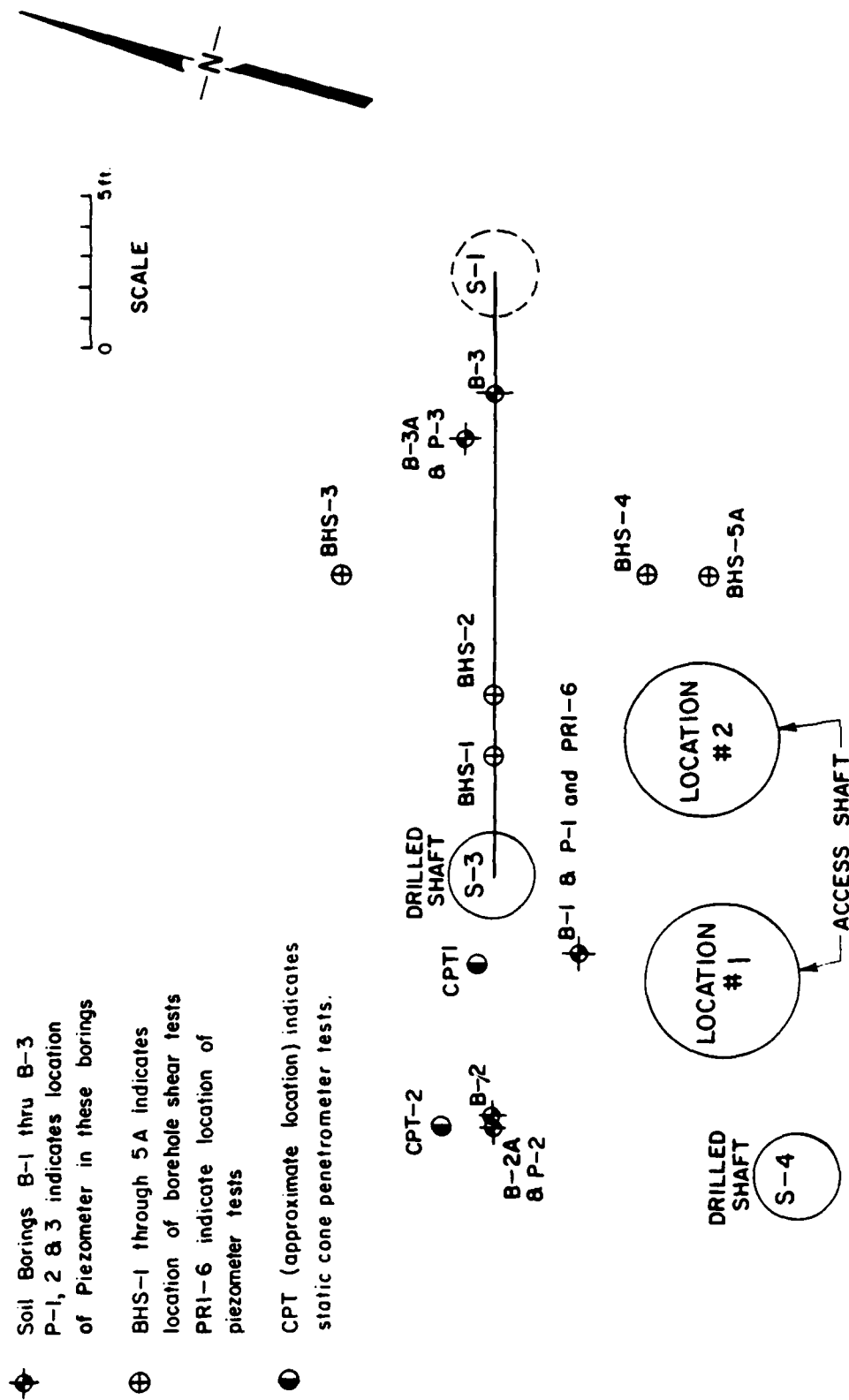


FIGURE 3. PLOT PLAN OF SOIL BORING LOCATION AT TEST SITE, HOUSTON, TEXAS

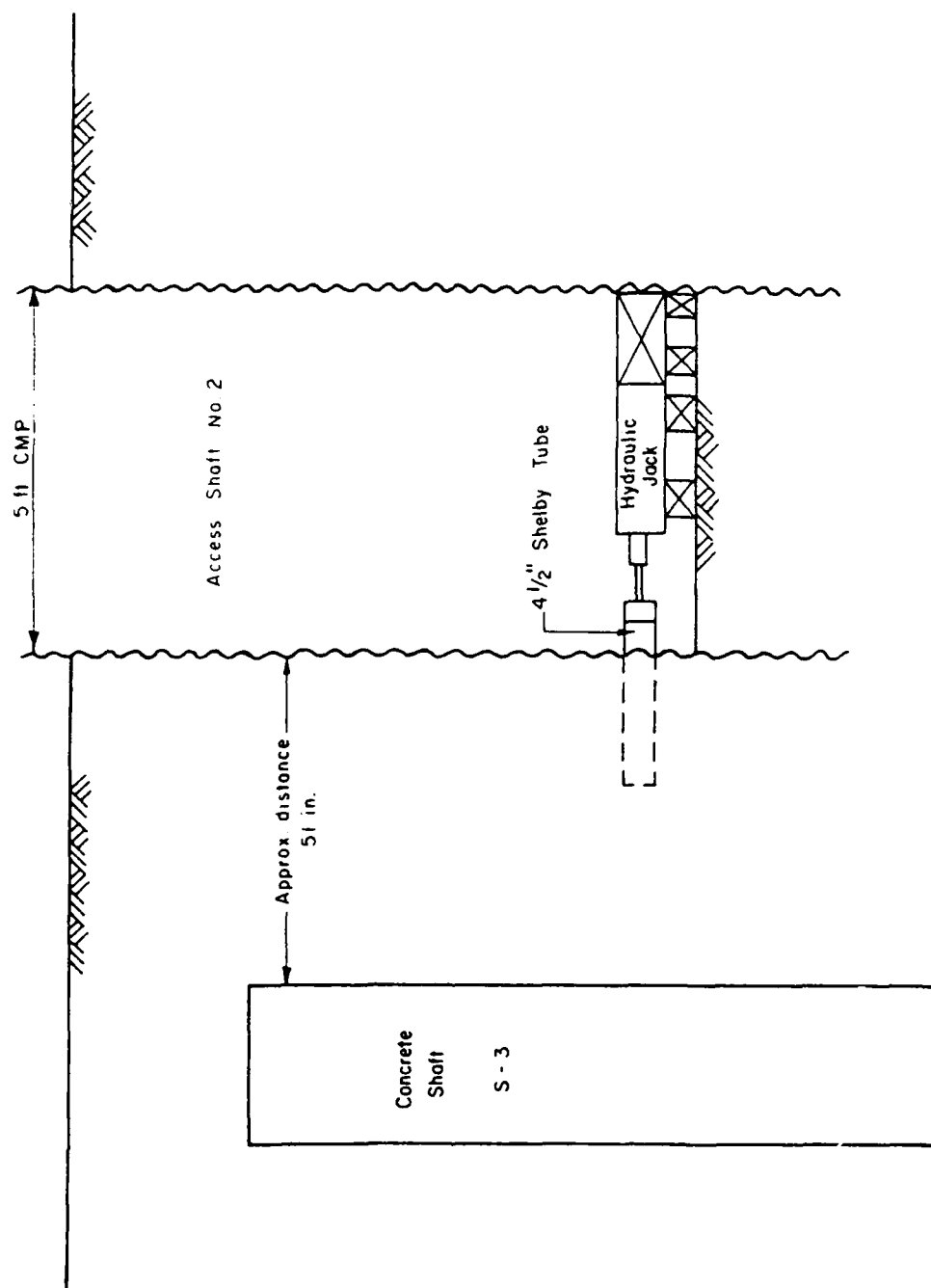


FIGURE 4(a). OBTAINING HORIZONTAL SAMPLES - PUSHING THE 4-1/2-IN. SHELBY TUBE INTO THE SOIL

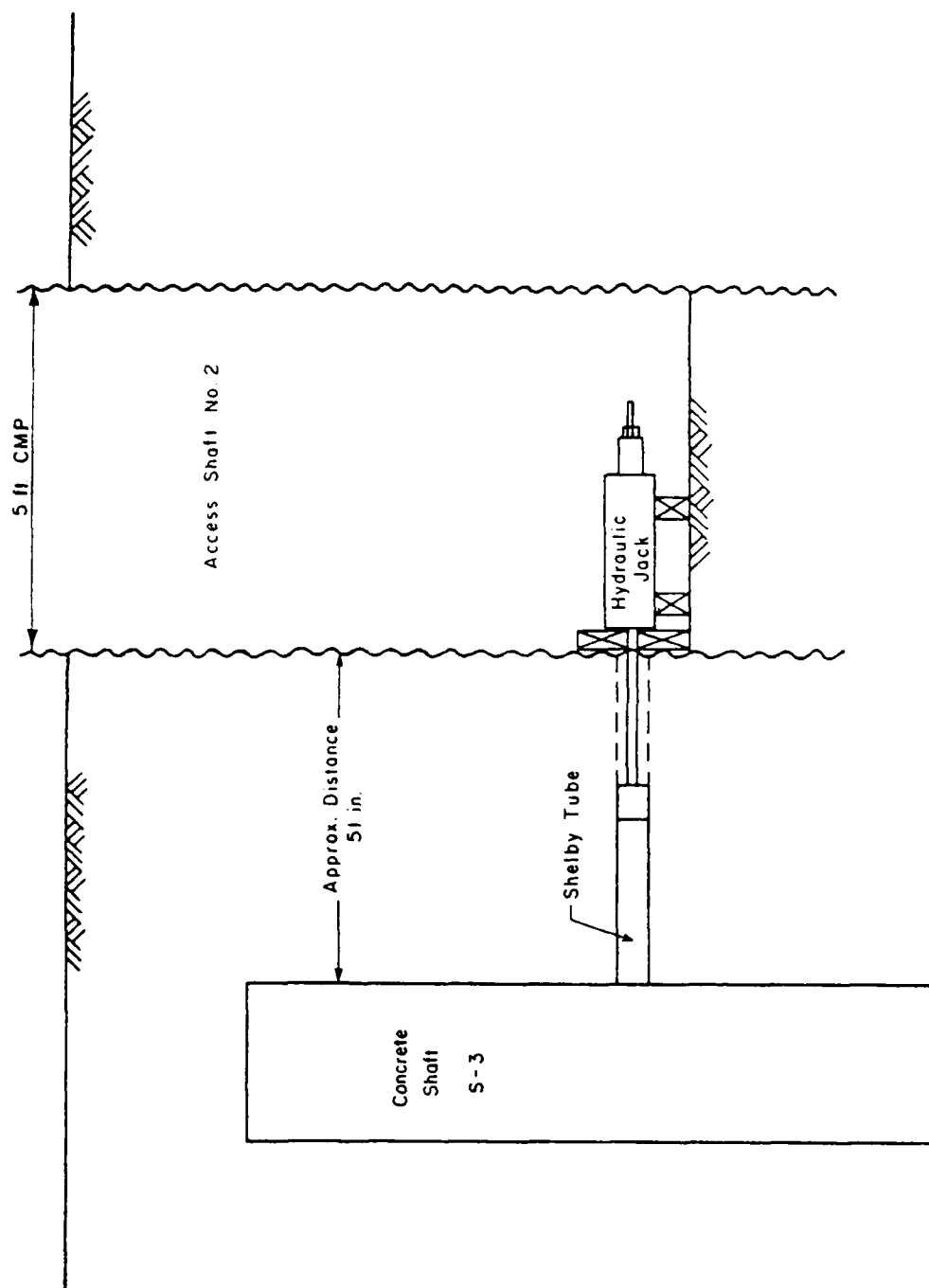


FIGURE 4(b). OBTAINING HORIZONTAL SAMPLES - PULLING OUT THE SHELBY TUBE



FIGURE 5. THE DENISON CORE BARREL

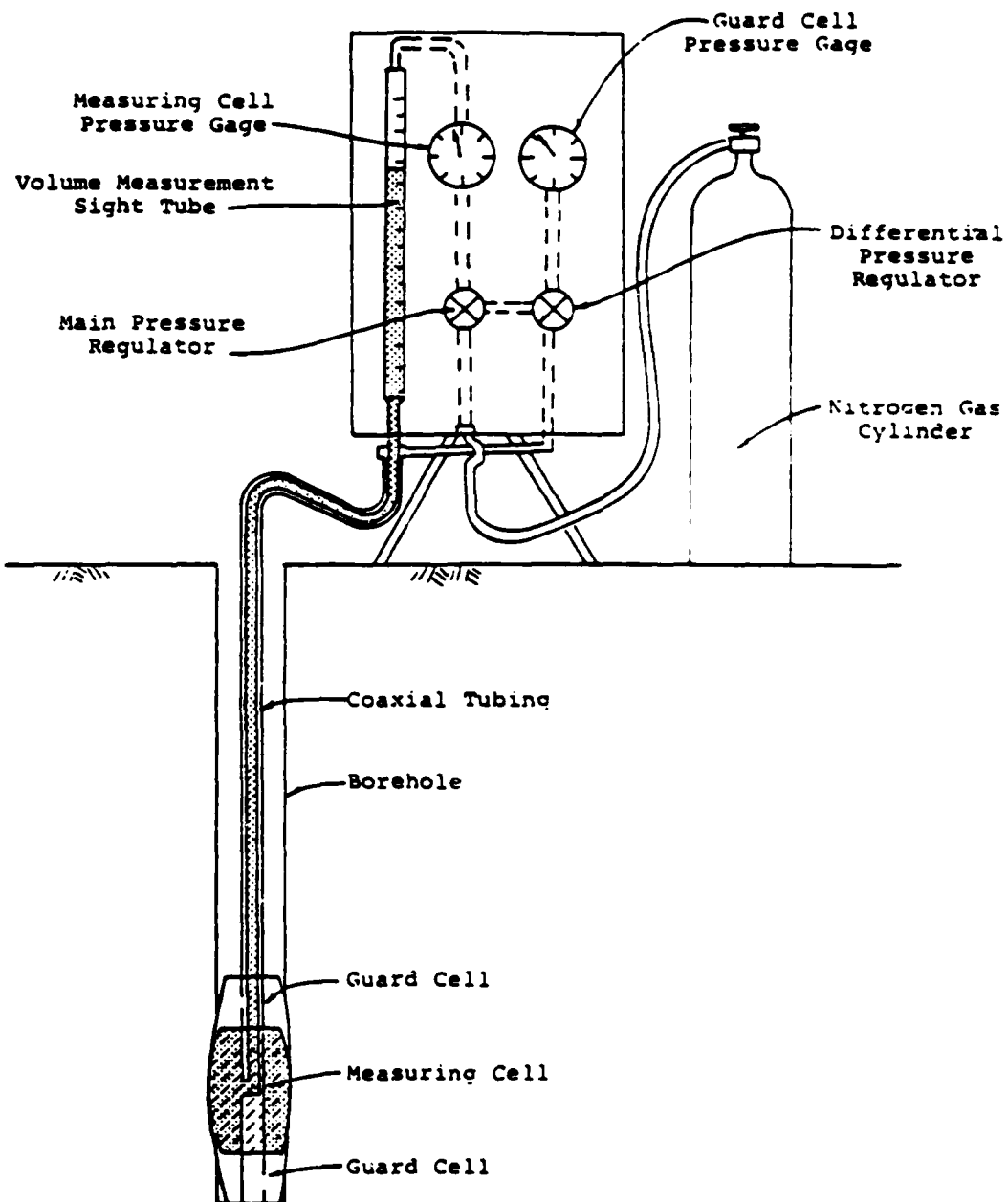


FIGURE 6. MENARD GA PRESSUREMETER TEST APPARATUS SCHEMATIC



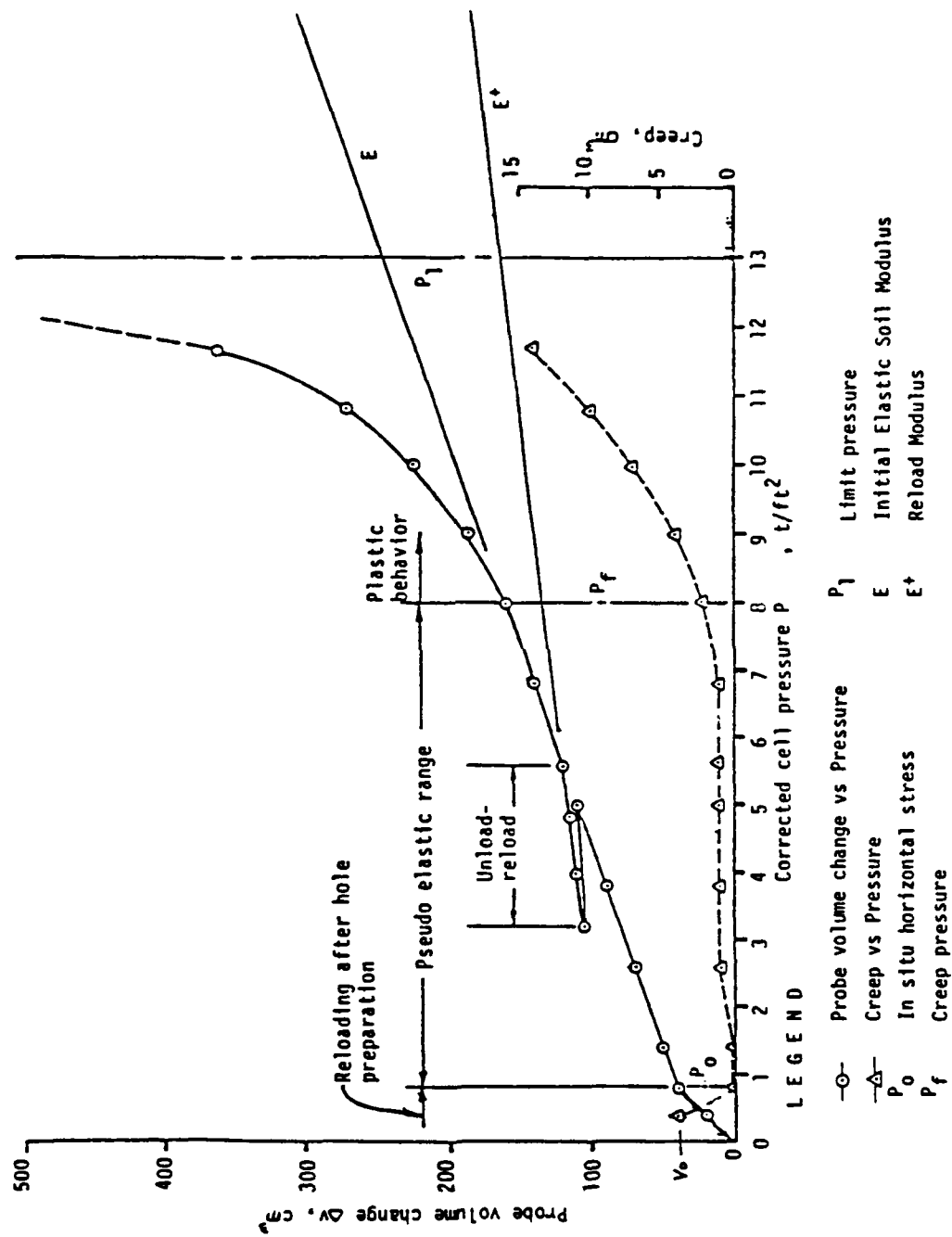


FIGURE 7. TYPICAL PRESSUREMETER TEST PLOT

# IN SITU HORIZONTAL EFFECTIVE STRESS $\bar{\sigma}_h, \text{t/ft.}^2$

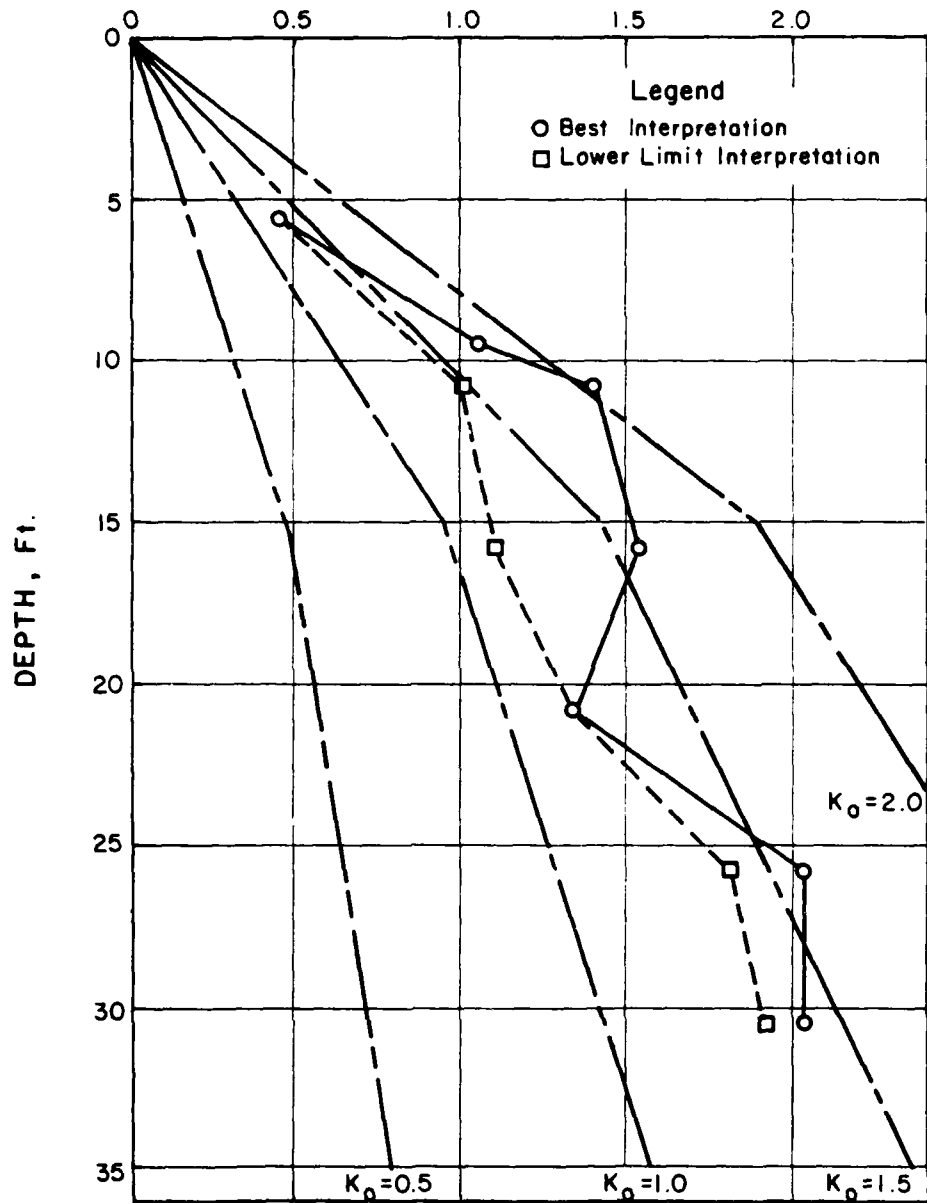


FIGURE 8. IN-SITU HORIZONTAL EFFECTIVE STRESS

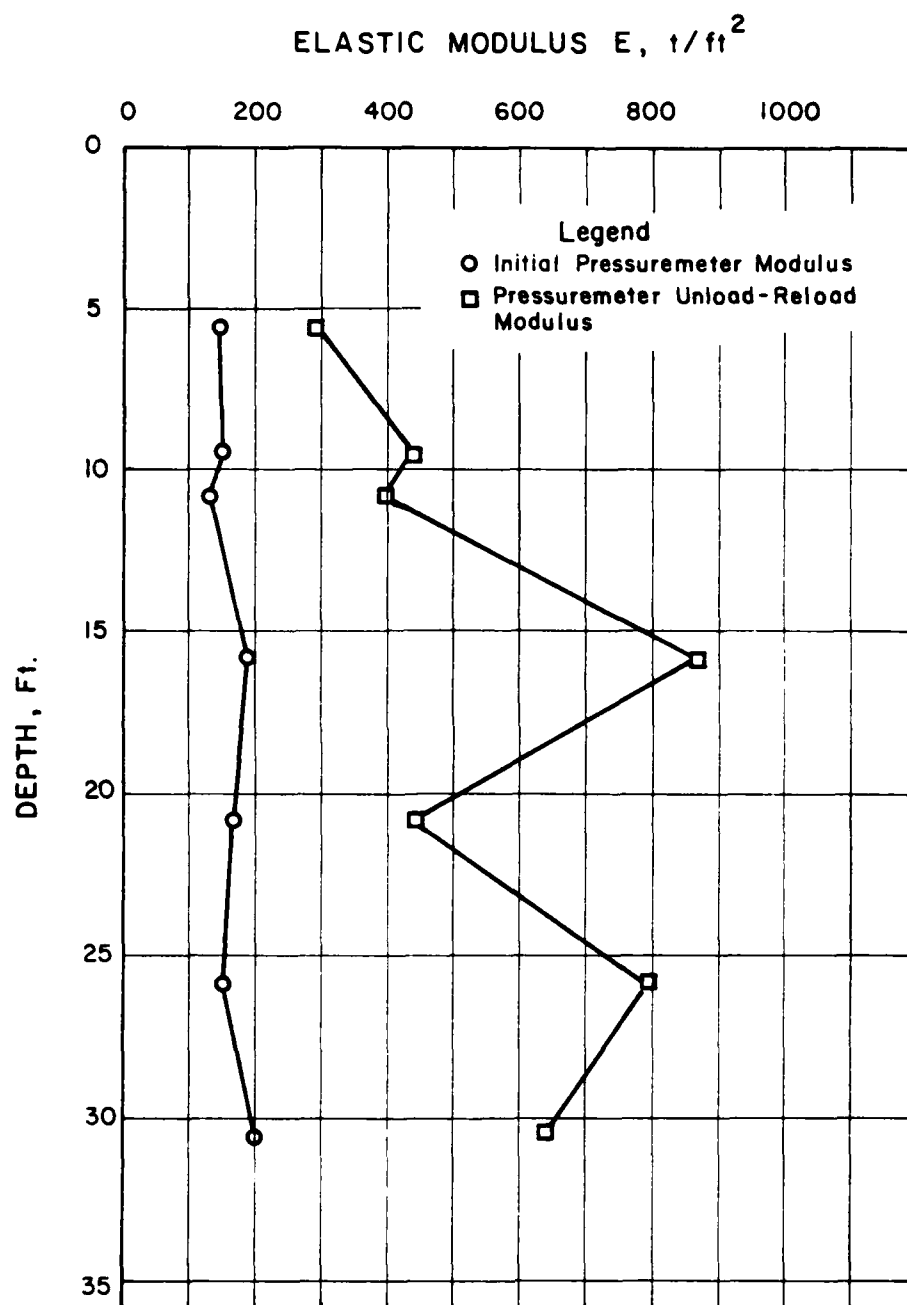


FIGURE 9. PRESSUREMETER ELASTIC MODULUS

# UNDRAINED SHEAR STRENGTH $S_u$ , t/ft.<sup>2</sup>

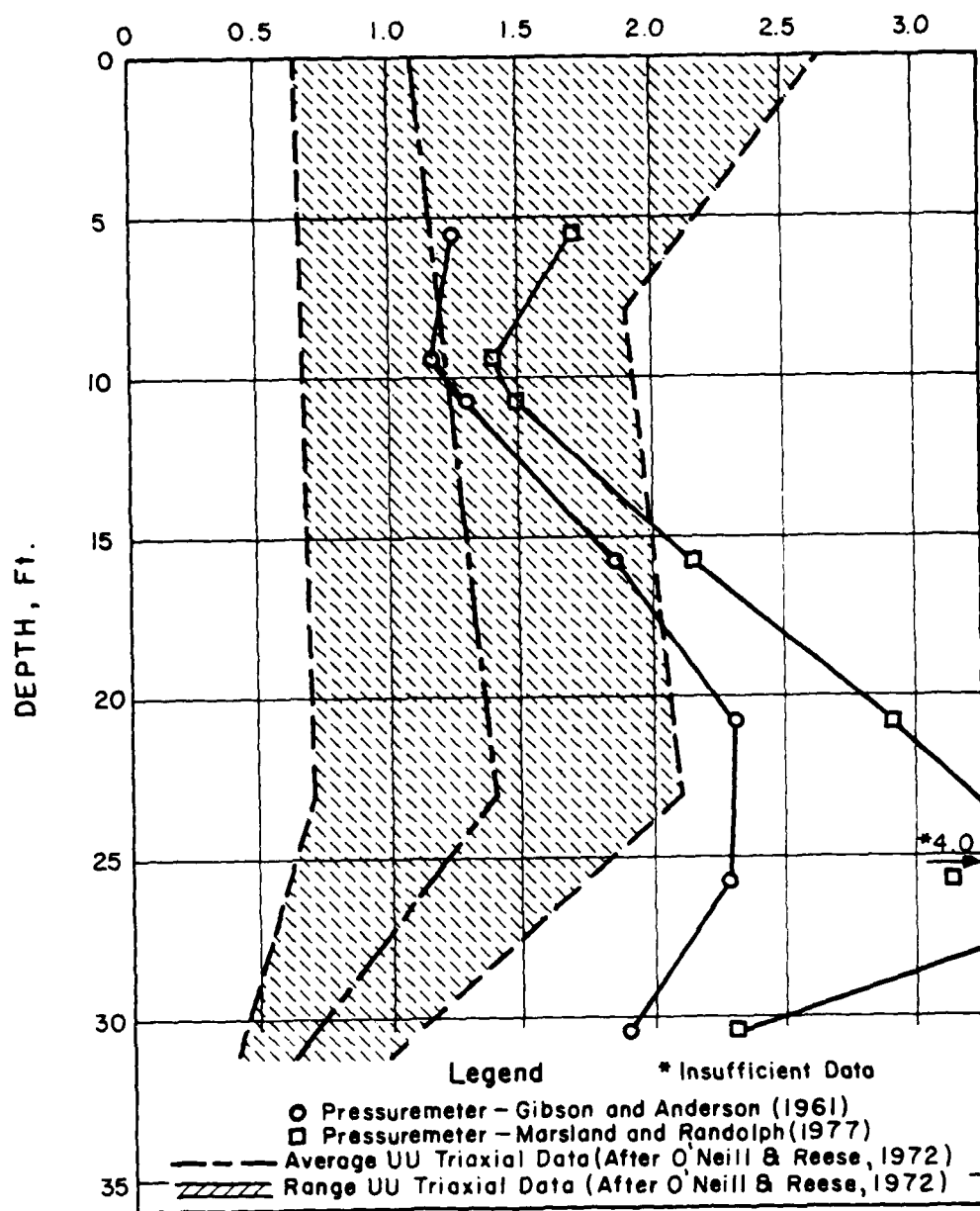


FIGURE 10. UNDRAINED SHEAR STRENGTH

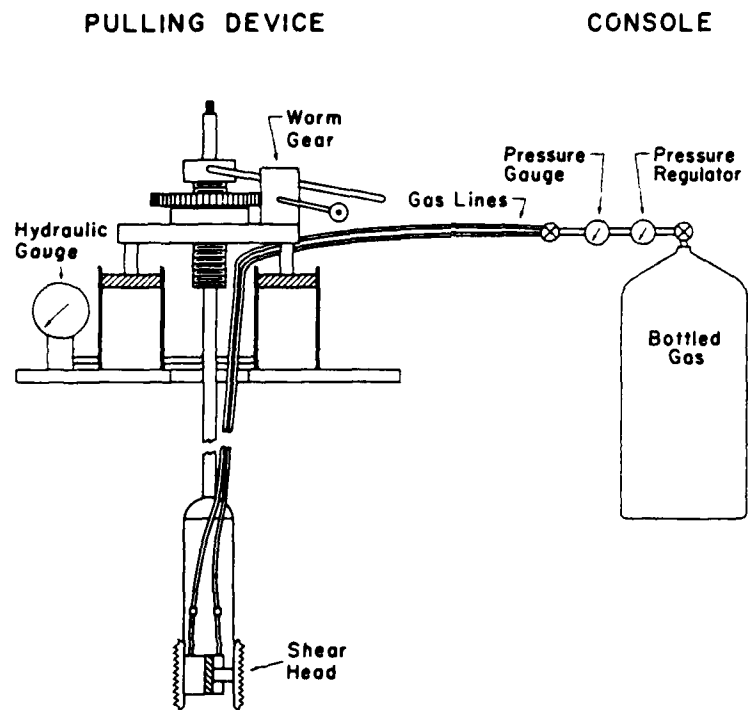


FIGURE 11. THE BOREHOLE SHEAR DEVICE

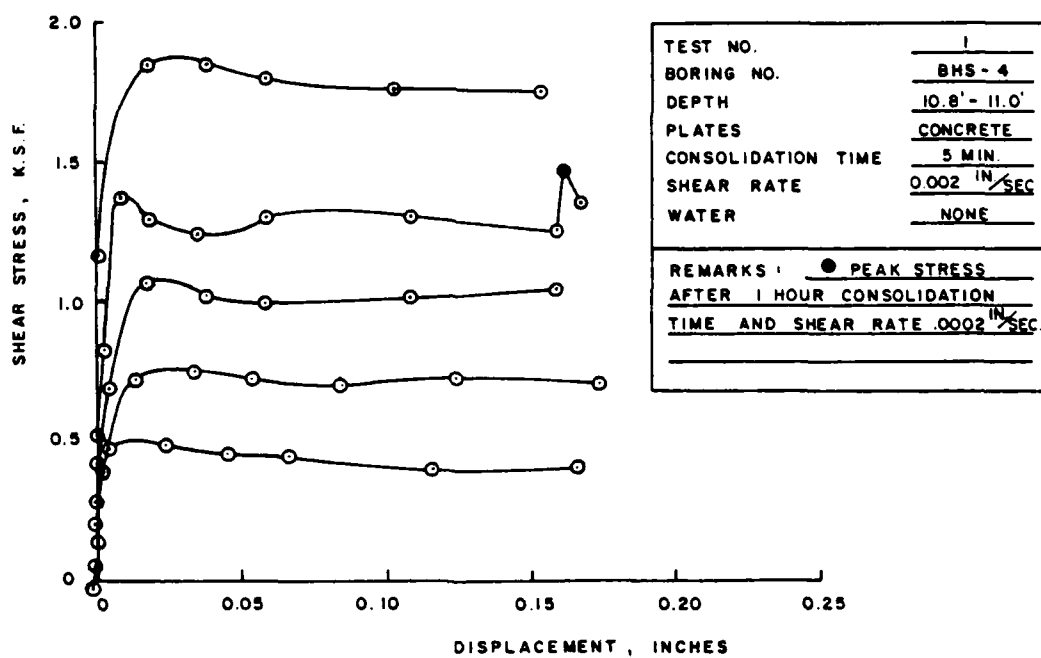
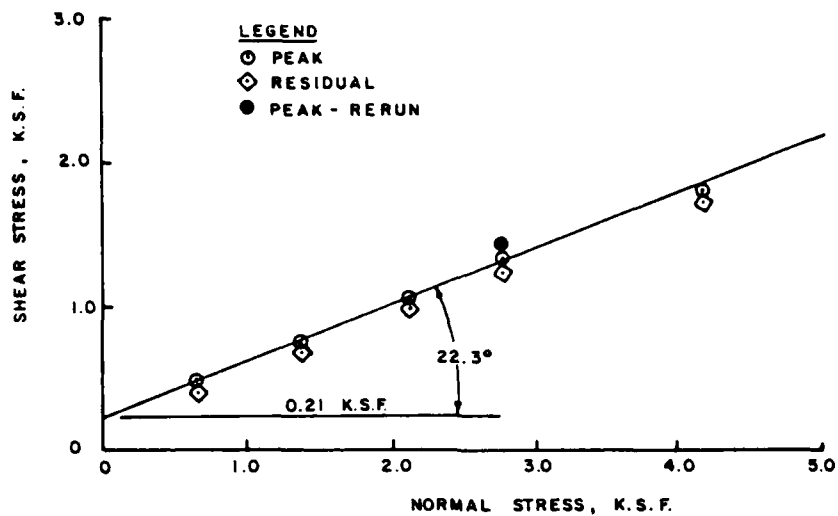


FIGURE 12. BORE HOLE SHEAR TEST RESULTS,  
TEST 1

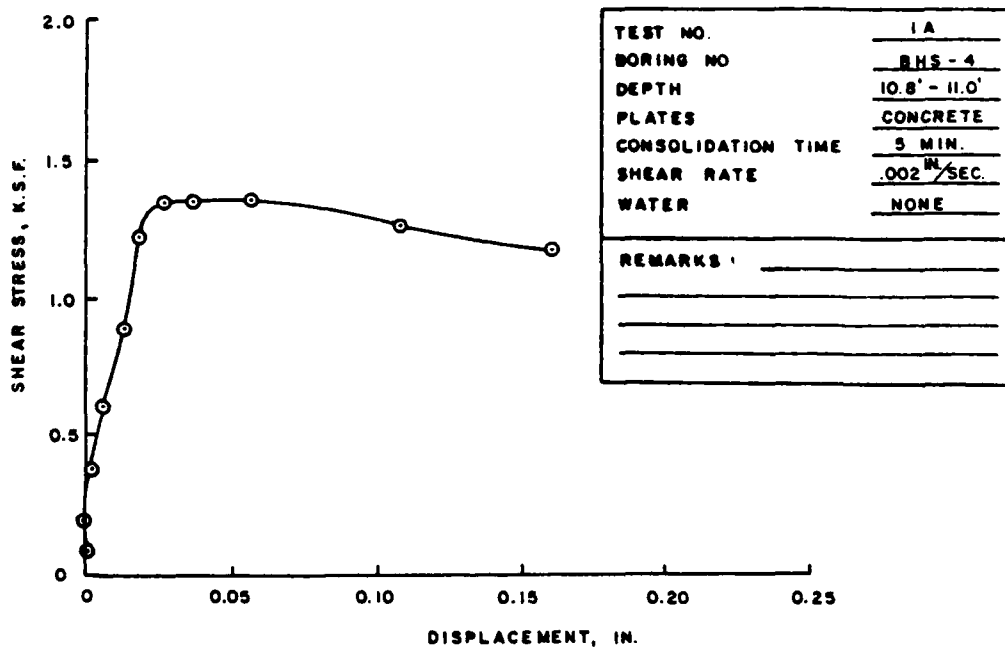
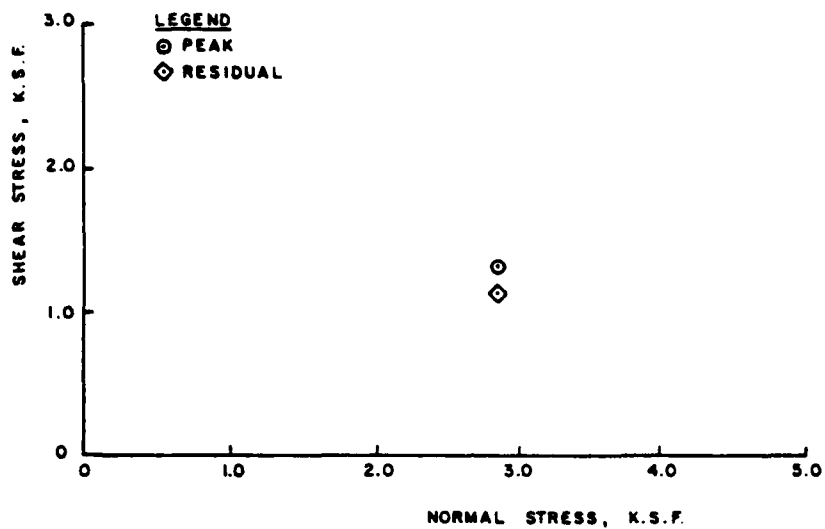


FIGURE 13. BOREHOLE SHEAR TEST RESULTS,  
TEST 1A

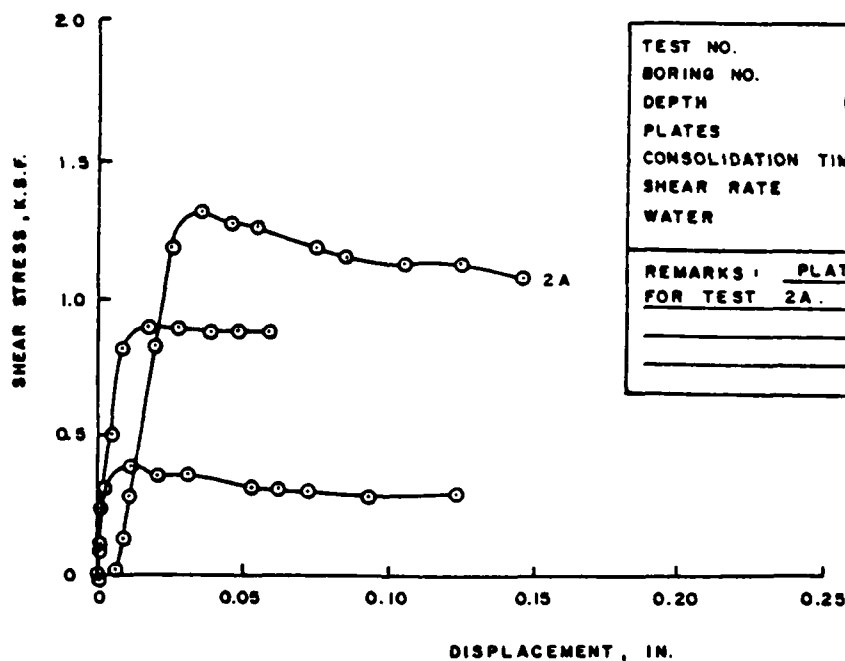
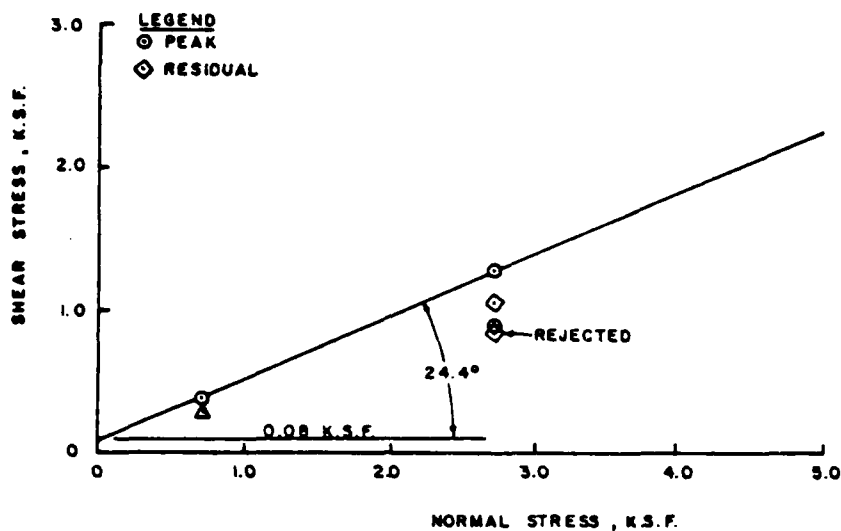


FIGURE 14. BORE HOLE SHEAR TEST RESULTS, TESTS 2 and 2A



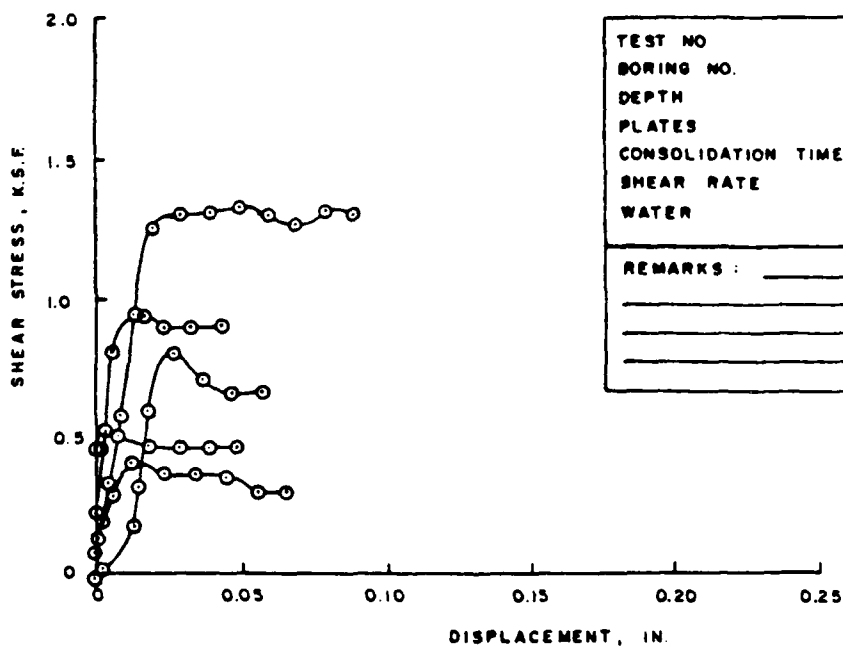
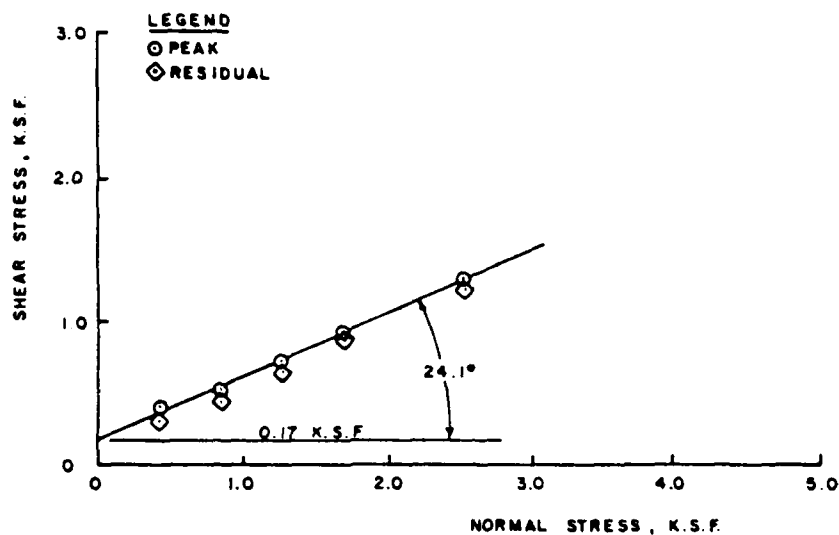


FIGURE 15. BOREHOLE SHEAR TEST RESULTS,  
 TEST 3

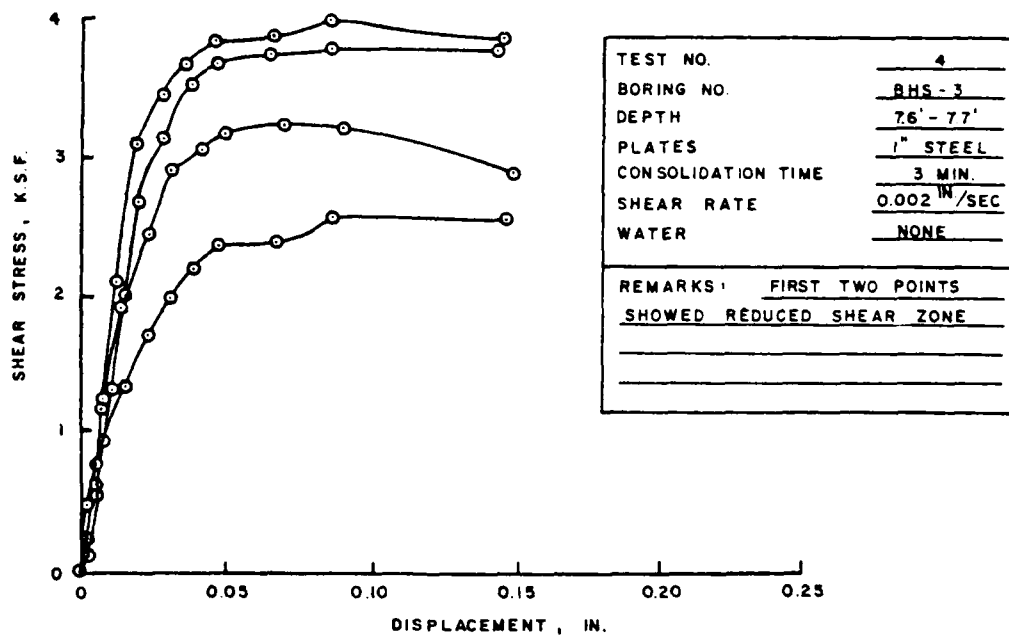
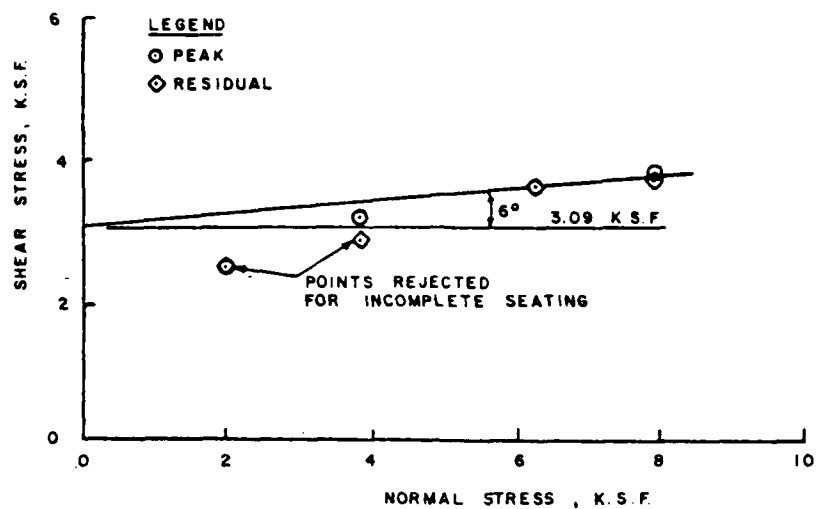
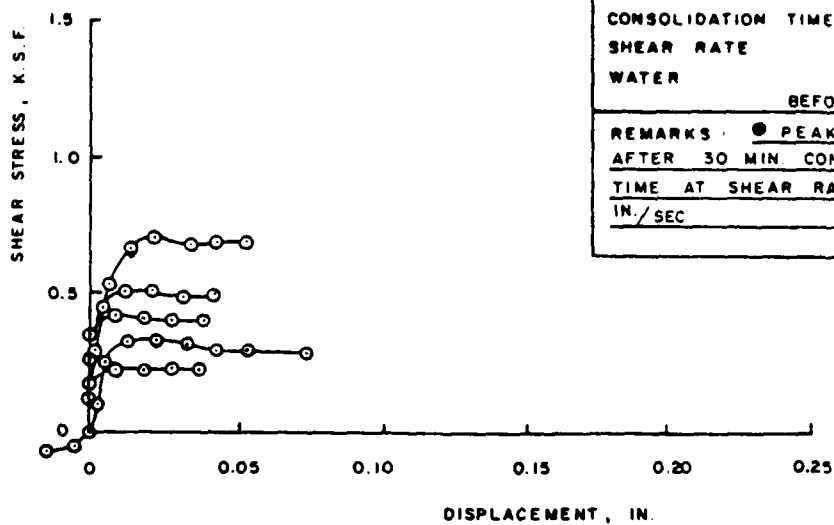
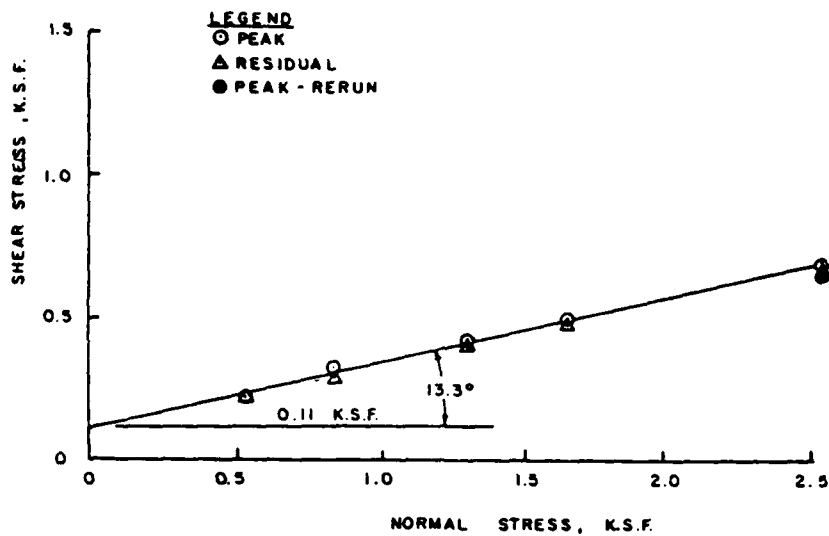


FIGURE 16. BOREHOLE SHEAR TEST RESULTS  
 TEST 4



TEST NO	5
BORING NO.	BHS-3
DEPTH	6.7' - 7.0'
PLATES	CONCRETE
CONSOLIDATION TIME	10 MIN.
SHEAR RATE	.0005 IN./SEC.
WATER	ADDED 1/2 HR
BEFORE TESTING	
REMARKS	● PEAK STRESS
AFTER 30 MIN CONSOLIDATION	
TIME AT SHEAR RATE OF .0001	
IN./SEC	

FIGURE 17. BOREHOLE SHEAR TEST RESULTS,  
TEST 5

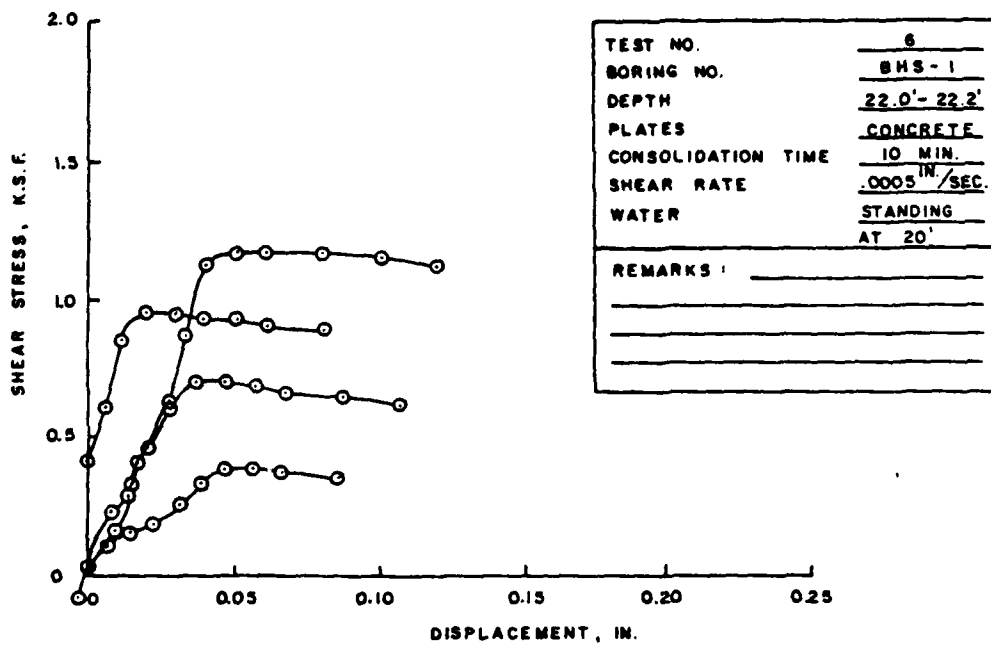
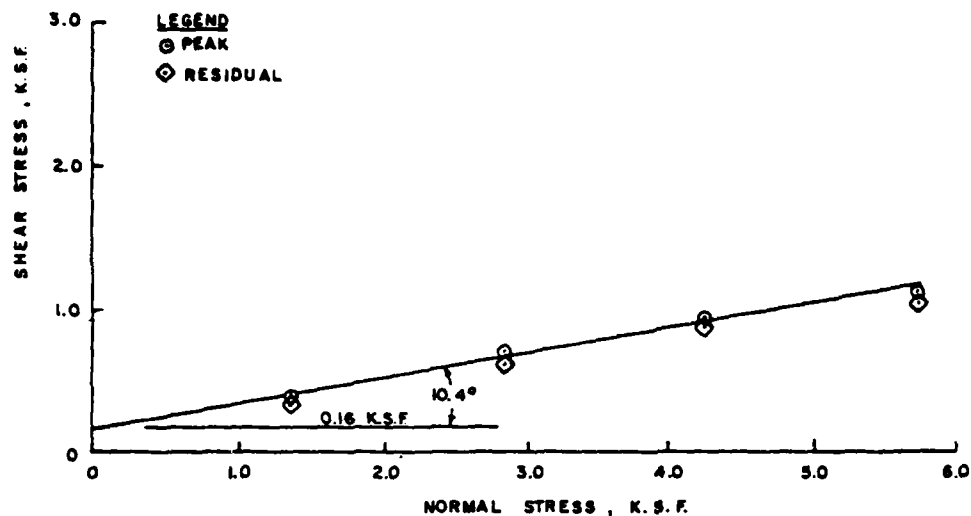
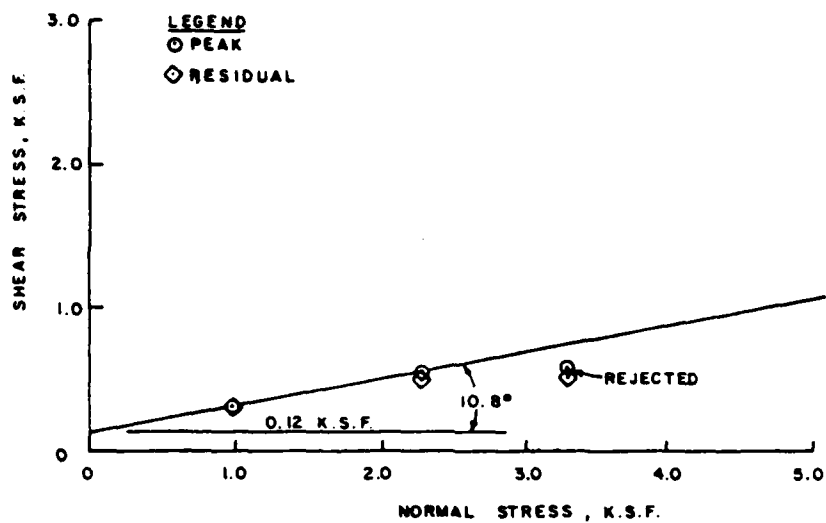


FIGURE 18. BOREHOLE SHEAR TEST RESULTS,  
 TEST 6



TEST NO.	7
BORING NO.	BHS-2
DEPTH	18.8' - 19.0'
PLATES	CONCRETE
CONSOLIDATION TIME	10 MIN.
SHEAR RATE	.0005 IN/SEC
WATER	STANDING
	AT 17'
REMARKS: TEST TERMINATED DUE TO PROBABLE ENLARGEMENT OF HOLE	

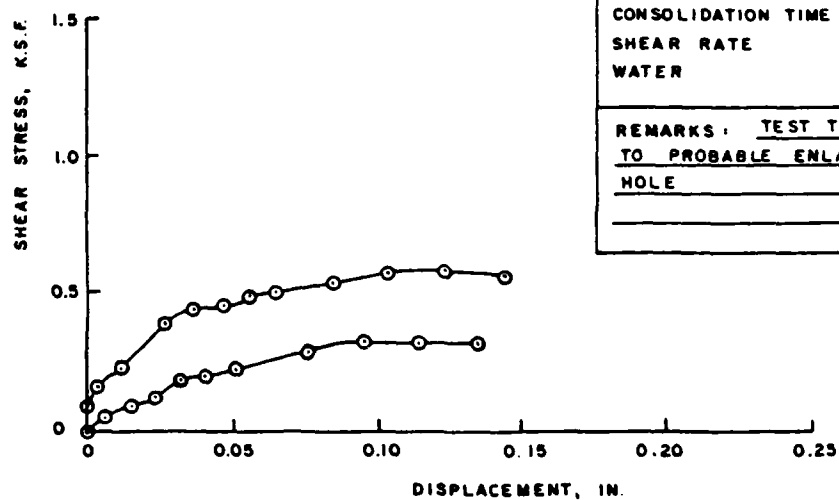
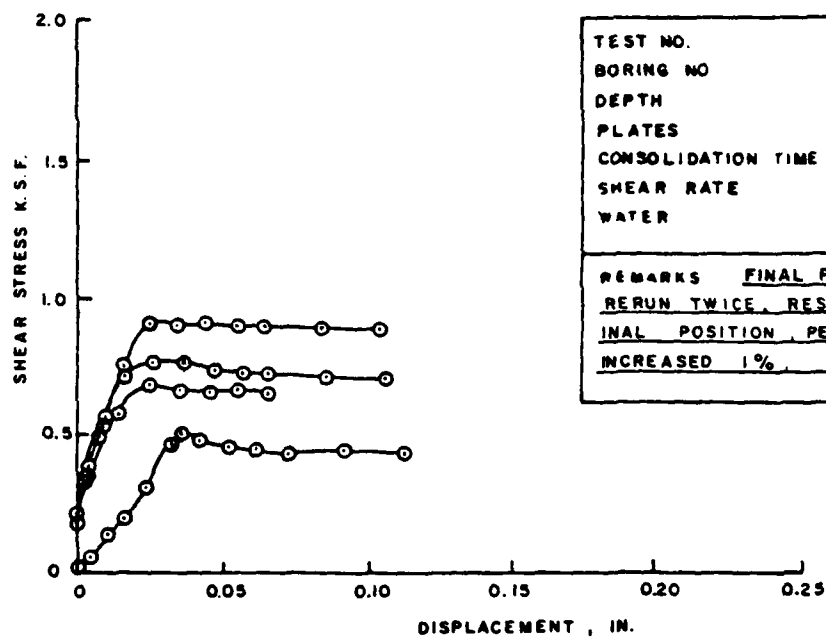
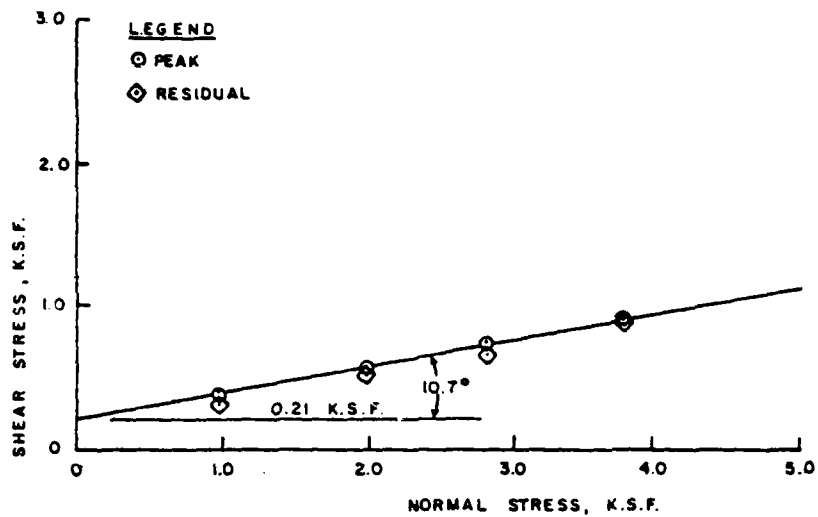


FIGURE 19. BOREHOLE SHEAR TEST RESULTS,  
 TEST 7



TEST NO.	8
BORING NO	BMS-5A
DEPTH	15.2' - 15.4'
PLATES	CONCRETE
CONSOLIDATION TIME	10 MIN.
SHEAR RATE	.0005 IN/SEC.
WATER	TRACE AT 15'
REMARKS	FINAL POINT WAS RERUN TWICE. RESET TO ORIG- INAL POSITION. PEAK STRESS INCREASED 1%.

FIGURE 20. BOREHOLE SHEAR TEST RESULTS,  
 TEST 8

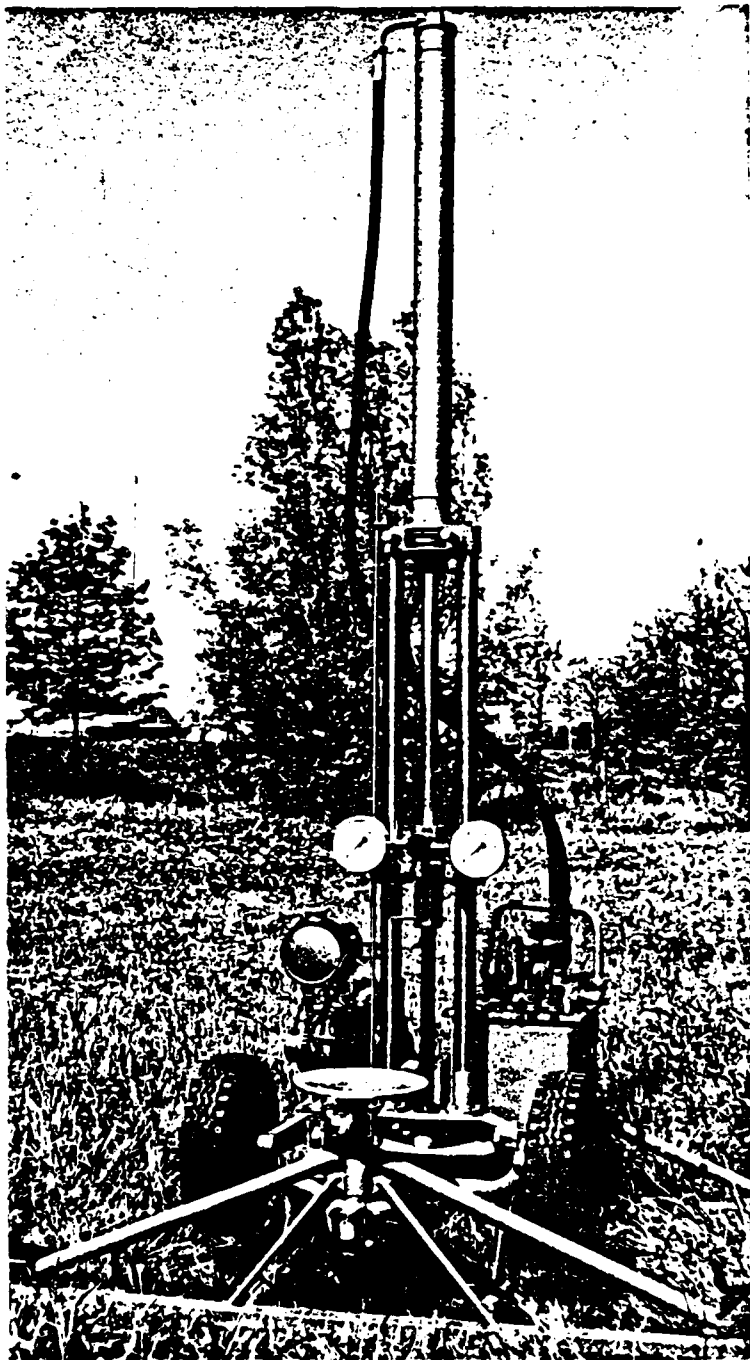


FIGURE 21. THE DUTCH CONE PENETROMETER

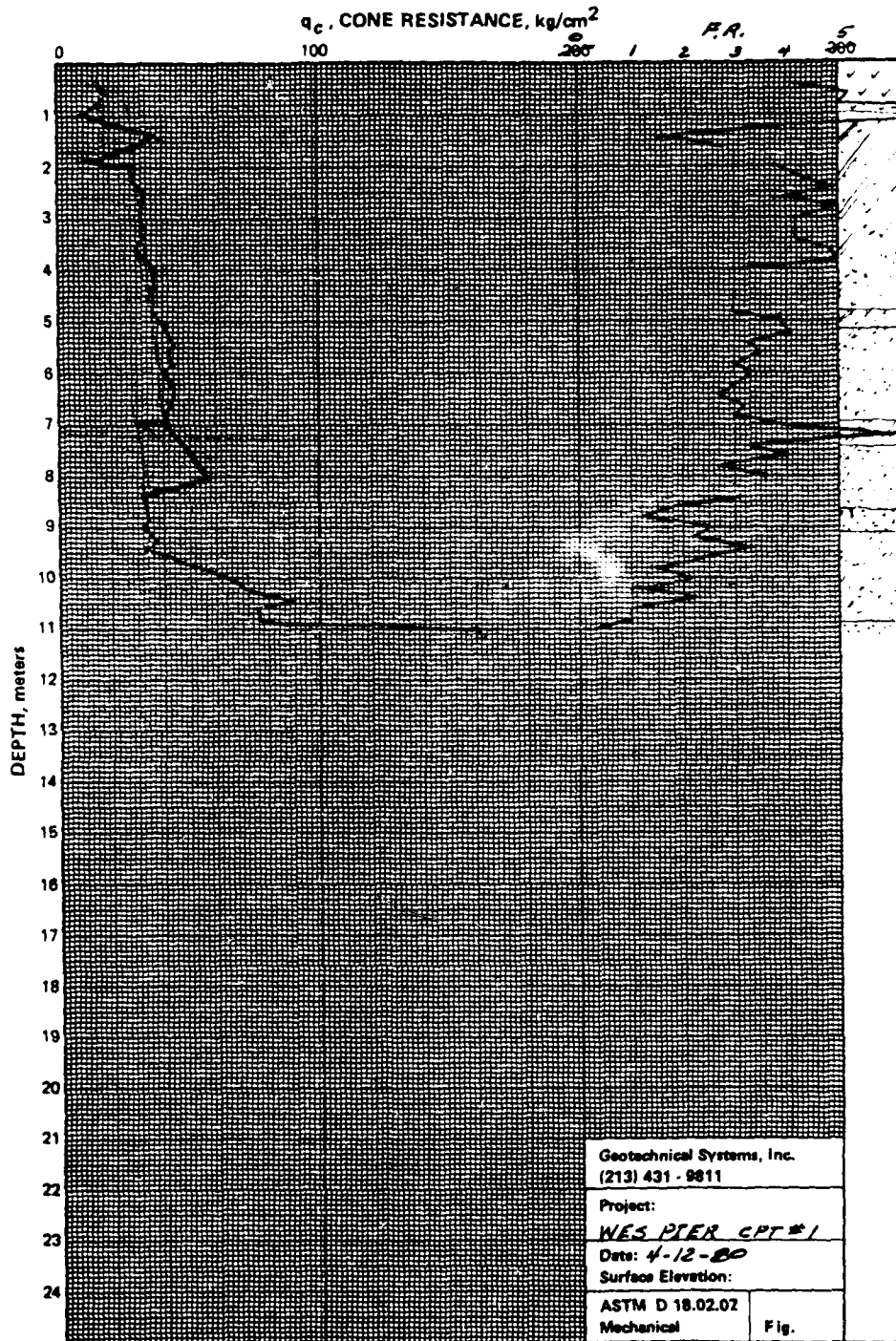


FIGURE 22(a). CONE PENETROMETER TEST DATA (CPT-1)



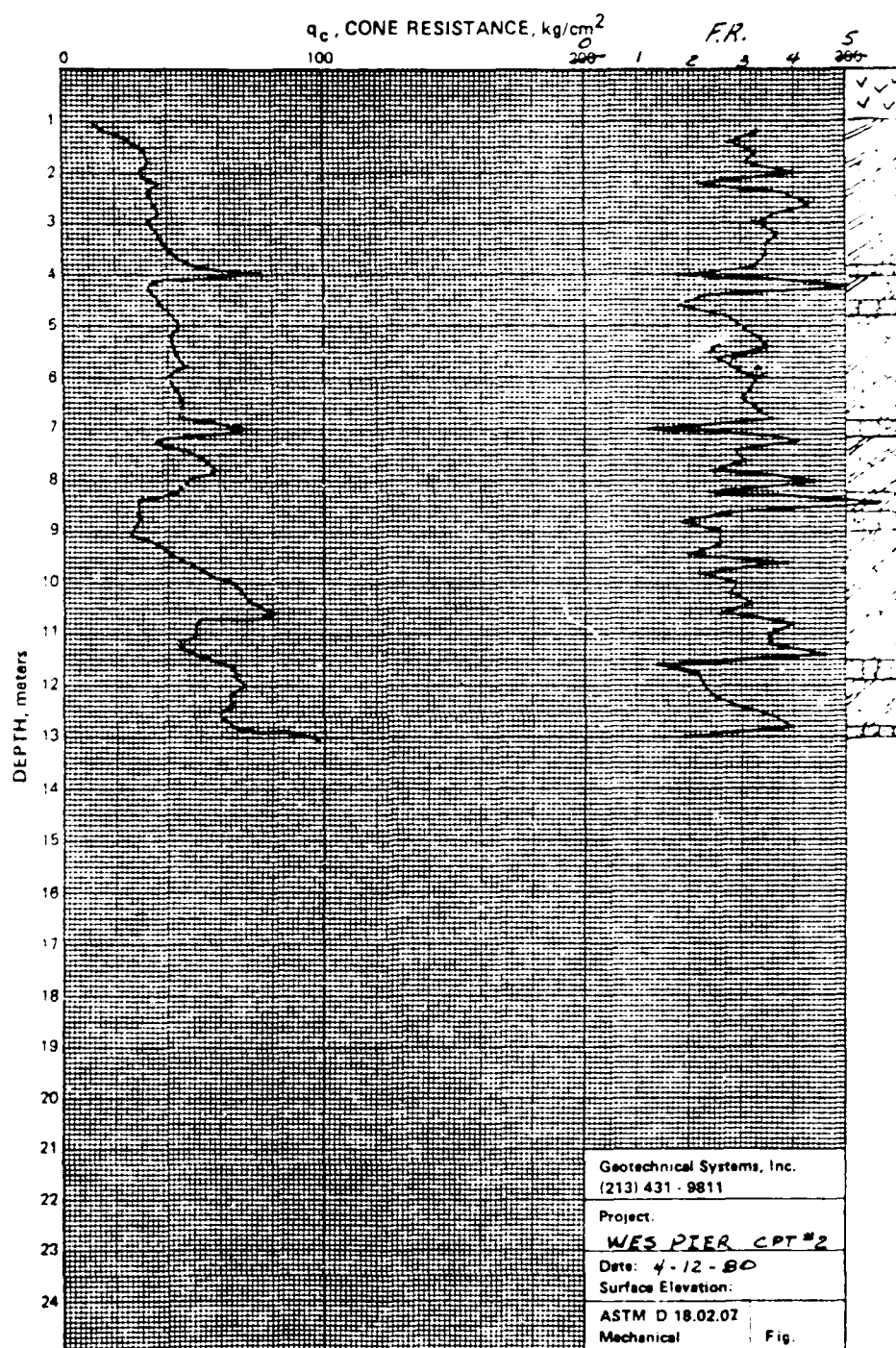


FIGURE 22(b). CONE PENETROMETER TEST DATA (CPT-2)

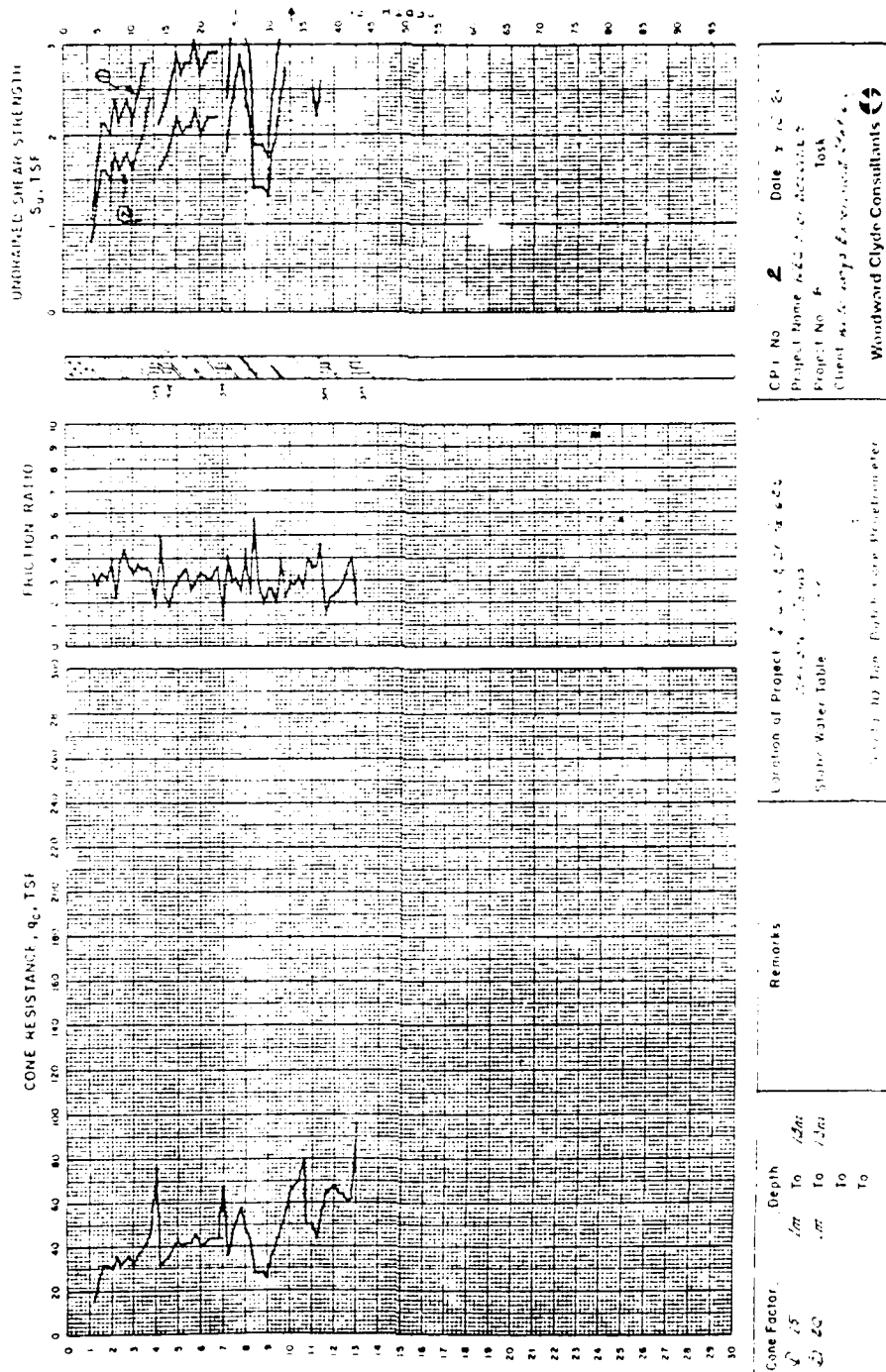


FIGURE 22 (c). TEST DATA AND INTERPRETED SHEAR STRENGTH PROFILE

APPENDIX A  
FIELD LOG OF VERTICAL SOIL BORINGS

# LOG OF BORING

<b>PROJECT:</b> Drilled Shaft Study		<b>BORING NO.:</b> B-1	
<b>CLIENT:</b> U.S. Army Engineer, Waterways Experiment Station		<b>PROJECT NO.:</b> 690112	
<b>LOCATION:</b> 610 East & 225 East, Houston, Texas		<b>DATE:</b> 3-25-80	
<b>BORING TYPE:</b> 4-Inch Diameter Flight Auger (Continuous Shelby Tube Samples)		<b>COMPLETION DEPTH:</b> 34-Ft beneath existing ground level.	
<b>WATER LEVEL:</b>		<b>INITIAL</b>	<b>FINAL</b>
		FT.	FT. MIN.

DEPTH, FEET	SYMBOL	CORES	DESCRIPTION	BLOWS PER FEET	LIQUID LIMIT	PLASTIC INDEX	MOISTURE CONTENT %	UNIT DRY WT. LB/FT <sup>3</sup>	SHEAR STRENGTH, TSF					
									0.5	1.0	1.5	2.0	2.5	
0			Brown and gray clay with calcareous nodules.											
2			Tan and gray clay.											
4			Red and gray mottled clay. Pressure meter test run on this section. (34" push, 24" recovery.)											
7			Gray and brown clay.											
8														
9			Red mottled clay.											
10			Pressure Meter tests run on this section. (34" push and full recovery.)											
12			Red mottled clay.											
14			Light red clay with silt seams and calcareous deposits.											
16														
17														







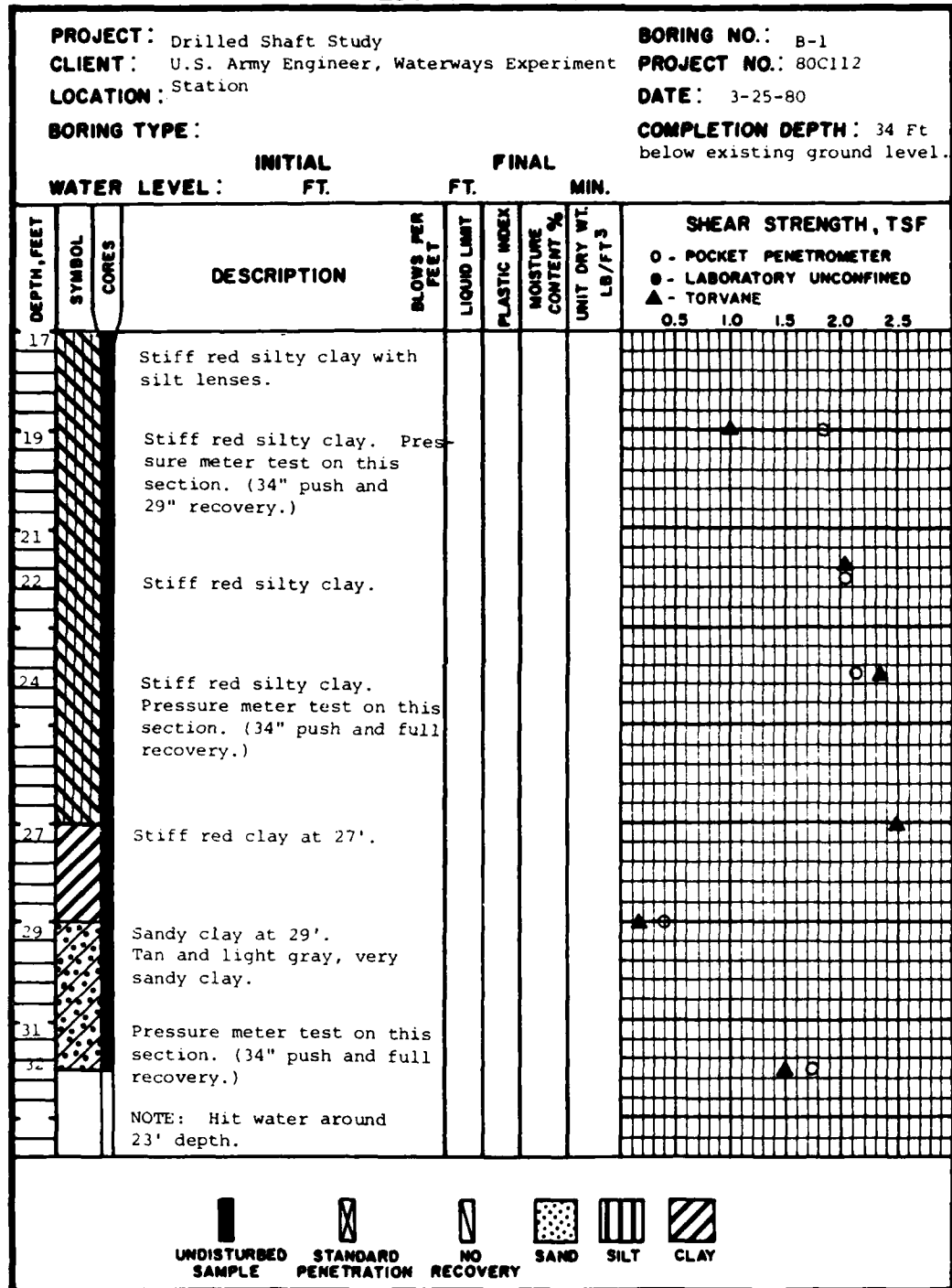
					
UNDISTURBED SAMPLE	STANDARD PENETRATION	NO RECOVERY	SAND	SILT	CLAY

FIGURE A1(a)

WOODWARD-CLYDE CONSULTANTS

# LOG OF BORING



WOODWARD-CLYDE CONSULTANTS

FIGURE A1(b)

# LOG OF BORING


<b>PROJECT:</b> Drilled Shaft Study <b>CLIENT:</b> U.S. Army Engineer, Waterways Experiment Station <b>LOCATION:</b> 610 East and 225 East, Houston, Texas <b>BORING TYPE:</b> 4-inch Diameter Flight Auger				<b>BORING NO.:</b> B-1 <b>PROJECT NO.:</b> 80C112 <b>DATE:</b> 3-25-80 <b>COMPLETION DEPTH:</b>					
<b>WATER LEVEL</b> INITIAL FT.		<b>FINAL</b> FT.		MIN.					
DEPTH, FEET	SYMBOL	CORES	DESCRIPTION	BLOWS PER FEET	LIQUID LIMIT	PLASTIC INDEX	MOISTURE CONTENT %	UNIT DRY WT. LB/FT <sup>3</sup>	SHEAR STRENGTH, TSF
									O - POCKET PENETROMETER ● - LABORATORY UNCONFINED ▲ - TORVANE 0.5   1.0   1.5   2.0   2.5
32			Tan and light gray sandy clay.						
34			TERMINATION DEPTH: 34 Ft.						
<p align="center"><u>DETAILS OF PIEZOMETER INSTALLATION</u></p> <p>1) Piezometer installed at a depth of 26 ft from the top of hole.</p> <div style="display: flex; align-items: center;"> <div style="margin-left: 10px;"> <p>Leads to put into piezometer readout.</p> <p>0</p> <p>-18'</p> <p>-22'</p> <p>-26'</p> <p>-34'</p> <p>Bentonite Pellet Seal 4' thick</p> <p>Pore pressure transducer.</p> <p>Sand.</p> </div> </div>									
<div style="display: flex; justify-content: space-around; align-items: center;"> <div style="text-align: center;"> <p>UNDISTURBED SAMPLE</p> </div> <div style="text-align: center;"> <p>STANDARD PENETRATION RECOVERY</p> </div> <div style="text-align: center;"> <p>NO RECOVERY</p> </div> <div style="text-align: center;"> <p>SAND</p> </div> <div style="text-align: center;"> <p>SILT</p> </div> <div style="text-align: center;"> <p>CLAY</p> </div> </div>									


WOODWARD-CLYDE CONSULTANTS


FIGURE A1(c).


# LOG OF BORING


<b>PROJECT:</b> Drilled Shaft Study					<b>BORING NO.:</b> B-2				
<b>CLIENT:</b> U.S. Army Engineer, Waterways Experiment Station					<b>PROJECT NO.:</b> 80C112				
<b>LOCATION:</b> 610 East and 225 East, Houston, Texas					<b>DATE:</b> 3-14-80				
<b>BORING TYPE:</b> 4-inch Diameter Flight Auger (Continuous Shelby Tube Samples Taken) and then continue in boring B-1A					<b>COMPLETION DEPTH:</b> 14 ft				
<b>WATER LEVEL:</b> <span style="margin-right: 20px;">INITIAL</span> <span style="margin-right: 20px;">FINAL</span> <span style="margin-right: 20px;">MIN.</span>									


DEPTH, FEET	SYMBOL	CORES	DESCRIPTION	BLOWS PER FEET	LIQUID LIMIT	PLASTIC INDEX	MOISTURE CONTENT %	UNIT DRY WT. LB/FT <sup>3</sup>	SHEAR STRENGTH, TSF					
									0.5	1.0	1.5	2.0	2.5	
0			Brown gray clay w/calcareous nodules.											
2			Tan and gray clay.											
4			Red mottled clay slickensided.											
6			Brown and tan clay, slickensided with sand and silt seams and some organic matter.											
8														
10			Red and gray clay with organic matter, slickensided.											
12			Tan and mottled brown silty clay with silt seams.											
14														
16				While sampling from 14 to 16' lost Shelby tube in the boring and moved 6" away from this location and re-sample below 14 ft.										


  
**UNDISTURBED SAMPLE**

  
**STANDARD PENETRATION**

  
**NO RECOVERY**

  
**SAND**

  
**SILT**

  
**CLAY**

WOODWARD-CLYDE CONSULTANTS

FIGURE A2(a)







# LOG OF BORING

<b>PROJECT:</b> Drilled Shaft Study		<b>BORING NO.:</b> B-2A	
<b>CLIENT:</b> U.S. Army Engineer, Waterways Experiment Station		<b>PROJECT NO.:</b> 87C112	
<b>LOCATION:</b> 610 East and 225 East, Houston, Texas		<b>DATE:</b> 3-24-61	
<b>BORING TYPE:</b> 4-in. Diameter Flight Auger (Continuous Shelby Tube Samples Taken)		<b>COMPLETION DEPTH:</b> 34 Ft below existing ground level	
<b>WATER LEVEL:</b>		<b>INITIAL</b>	<b>FINAL</b>
		FT.	FT. MIN.

DEPTH, FEET	SYMBOL	CORES	DESCRIPTION	BLOWS PER FEET	LIQUID LIMIT	PLASTIC INDEX	MOISTURE CONTENT %	UNIT DRY WT. LB/FT <sup>3</sup>	SHEAR STRENGTH, TSF					
									0.5	1.0	1.5	2.0	2.5	
			Augered down to 14 ft and start sampling below 14 ft.											
14			Brown silty clay with silt seams.											
16			Stiff mottled red clay at bottom											
18			Red mottled clay with silt seams, fissured.											
20			Tan and brown silty clay with silt pockets and partings.											
22			Red clay with sand seams and pockets											
24			Red and gray silty clay with sand seams.											
26			Tan and gray clayey sand to sandy clay.											
28														

					
UNDISTURBED SAMPLE	STANDARD PENETRATION	NO RECOVERY	SAND	SILT	CLAY

WOODWARD-CLYDE CONSULTANTS

FIGURE A2(b)



# LOG OF BORING

<b>PROJECT:</b> Drilled Shaft Study <b>CLIENT:</b> U.S. Army Engineer, Waterways Experiment Station <b>LOCATION:</b> 610 East and 225 East, Houston, Texas <b>BORING TYPE:</b>						<b>BORING NO.:</b> B-2A <b>PROJECT NO.:</b> 80C112 <b>DATE:</b> 3-24-80 <b>COMPLETION DEPTH:</b>																	
<b>WATER LEVEL:</b>						<b>INITIAL</b> <b>FT.</b>						<b>FINAL</b> <b>FT.</b>						<b>MIN.</b>					
DEPTH, FEET	SYMBOL	CORES	DESCRIPTION	BLOWS PER FEET	LIQUID LIMIT	PLASTIC INDEX	MOISTURE CONTENT %	UNIT DRY WT. LB/FT <sup>3</sup>	SHEAR STRENGTH, TSF														
									0.5	1.0	1.5	2.0	2.5										
28	[Pattern]		Tan silty clay with sand seams and calcareous nodules																				
30			No recovery. Sandy clay.																				
32			Tan and light gray very sandy clay.																				
34			TERMINATION DEPTH: 34 FT																				
DETAILS OF PIEZOMETER INSTALLATION																							
-21' Bentonite pellets seal 4' thick. -25' -29.5' Pore pressure transducer. -34' Sand.																							
<div style="display: flex; justify-content: space-around; align-items: center;"> <div style="text-align: center;"> <p>UNDISTURBED SAMPLE</p> </div> <div style="text-align: center;"> <p>STANDARD PENETRATION</p> </div> <div style="text-align: center;"> <p>NO RECOVERY</p> </div> <div style="text-align: center;"> <p>SAND</p> </div> <div style="text-align: center;"> <p>SILT</p> </div> <div style="text-align: center;"> <p>CLAY</p> </div> </div>																							

WOODWARD-CLYDE CONSULTANTS

FIGURE A2(c)

## LOG OF BORING

<b>PROJECT:</b> Drilled Shaft Study <b>CLIENT:</b> U.S. Army Engineer, Waterways Experiment Station <b>LOCATION:</b> 610 East and 225 East, Houston, Texas <b>BORING TYPE:</b> 4-in. Diameter Flight Auger & PMT				<b>BORING NO.:</b> B-3 <b>PROJECT NO.:</b> 80C112 <b>DATE:</b> 3-25-80 <b>COMPLETION DEPTH:</b> 12 ft beneath ground level			
<b>WATER LEVEL:</b>		<b>INITIAL</b> FT.	<b>FINAL</b> FT.	<b>MIN.</b>			

DEPTH, FEET	SYMBOL	CORES	DESCRIPTION	BLOWS PER FEET	LIQUID LIMIT	PLASTIC INDEX	MOISTURE CONTENT %	UNIT DRY WT. LB/FT <sup>3</sup>	SHEAR STRENGTH, TSF							
									0.5	1.0	1.5	2.0	2.5			
0			Auger down to 5 ft depth and start logging at 5'.													
2																
4																
5			Stiff red clay.													
6																
7			Stiff red and gray clay.													
8			Slightly silty. Pressuremeter test on this section.													
10																
12			Red mottled clay with organic material at 12'. BORING ABANDONED AT 12' DEPTH													

UNDISTURBED  
SAMPLE

STANDARD  
PENETRATION

NO  
RECOVERY

SAND

SILT

CLAY

WOODWARD-CLYDE CONSULTANTS

FIGURE A3(a)







# LOG OF BORING

<b>PROJECT:</b> Drilled Shaft Study		<b>BORING NO.:</b> 3-A	
<b>CLIENT:</b> U.S. Army Engineer, Waterways Experiment Station		<b>PROJECT NO.:</b> 80C112	
<b>LOCATION:</b> 610 East and 225 East, Houston, Texas		<b>DATE:</b> 4-10-80	
<b>BORING TYPE:</b> 4 in. Diameter Flight Auger (Continuous Shelby Tube Samples)		<b>COMPLETION DEPTH:</b> 34 ft below existing ground level	
<b>WATER LEVEL:</b>		<b>INITIAL</b>	<b>FINAL</b>
		<b>FT.</b>	<b>FT. MIN.</b>

DEPTH, FEET	SYMBOL	CORES	DESCRIPTION	BLOWS PER FEET	LIQUID LIMIT	PLASTIC INDEX	MOISTURE CONTENT %	UNIT DRY WT. LB/FT <sup>3</sup>	SHEAR STRENGTH, TSF					
									O - POCKET PENETROMETER					
									● - LABORATORY UNCONFINED					
									0.5	1.0	1.5	2.0	2.5	
0			Soil disturbed during excavation to locate drilled shaft, 0'-4'											
2														
4			Gray and tan clay with some dark black organic matter											
6			Tan and gray clay with some organic matter											
8			Brown and gray clay, slickensided.											
10			Tan clay at 10'.											
12			Red mottled clay with dark black organic matter at 12'.											
14			Fine light brown sand with light gray and tan clay. Red mottled clay with some tan and gray streaks and scattered dark black organic matter.											
16			Note: Hit water around 13'.											

					
UNDISTURBED SAMPLE	STANDARD PENETRATION	NO RECOVERY	SAND	SILT	CLAY

WOODWARD-CLYDE CONSULTANTS

FIGURE A3(b)

# LOG OF BORING

**PROJECT:** Drilled Shaft Study  
**CLIENT:** U.S. Army Engineer, Waterways Experiment  
**LOCATION:** Station 610 East and 225 East, Houston, Texas  
**BORING TYPE:**

**BORING NO.:** 3-A (cont'd)  
**PROJECT NO.:** 82C112  
**DATE:** 4-10-80  
**COMPLETION DEPTH:**

**WATER LEVEL:** INITIAL FT. FINAL FT. MIN.

DEPTH, FEET	SYMBOL	CORES	DESCRIPTION	BLOWS PER FEET	LIQUID LIMIT	PLASTIC INDEX	MOISTURE CONTENT %	UNIT DRY WT. LB/FT <sup>3</sup>	SHEAR STRENGTH, TSF				
									O - POCKET PENETROMETER ● - LABORATORY UNCONFINED				
									0.5	1.0	1.5	2.0	2.5
16			Mottled red clay with scattered organic matter, slickensided. Recovery only 1 ft.										
18			Red mottled clay.										
20			No recovery. Clay starts softening.										
22			Red and tan mottled clay. Recovery 1 ft.										
24			Red and tan mottled clay.										
26			Red mottled clay at top, light tan clay at bottom. Sandy clay at the very end.										
28			No recovery. Tan sandy clay.										
30			Tan sandy clay with very fine sand seams at top.										
32			Tan clay with very fine sand seams. Slickensided and fissured with dark rust organic matter at bottom.										

 **UNDISTURBED SAMPLE**
 **STANDARD PENETRATION**
 **NO RECOVERY**
 **SAND**
 **SILT**
 **CLAY**

WOODWARD-CLYDE CONSULTANTS

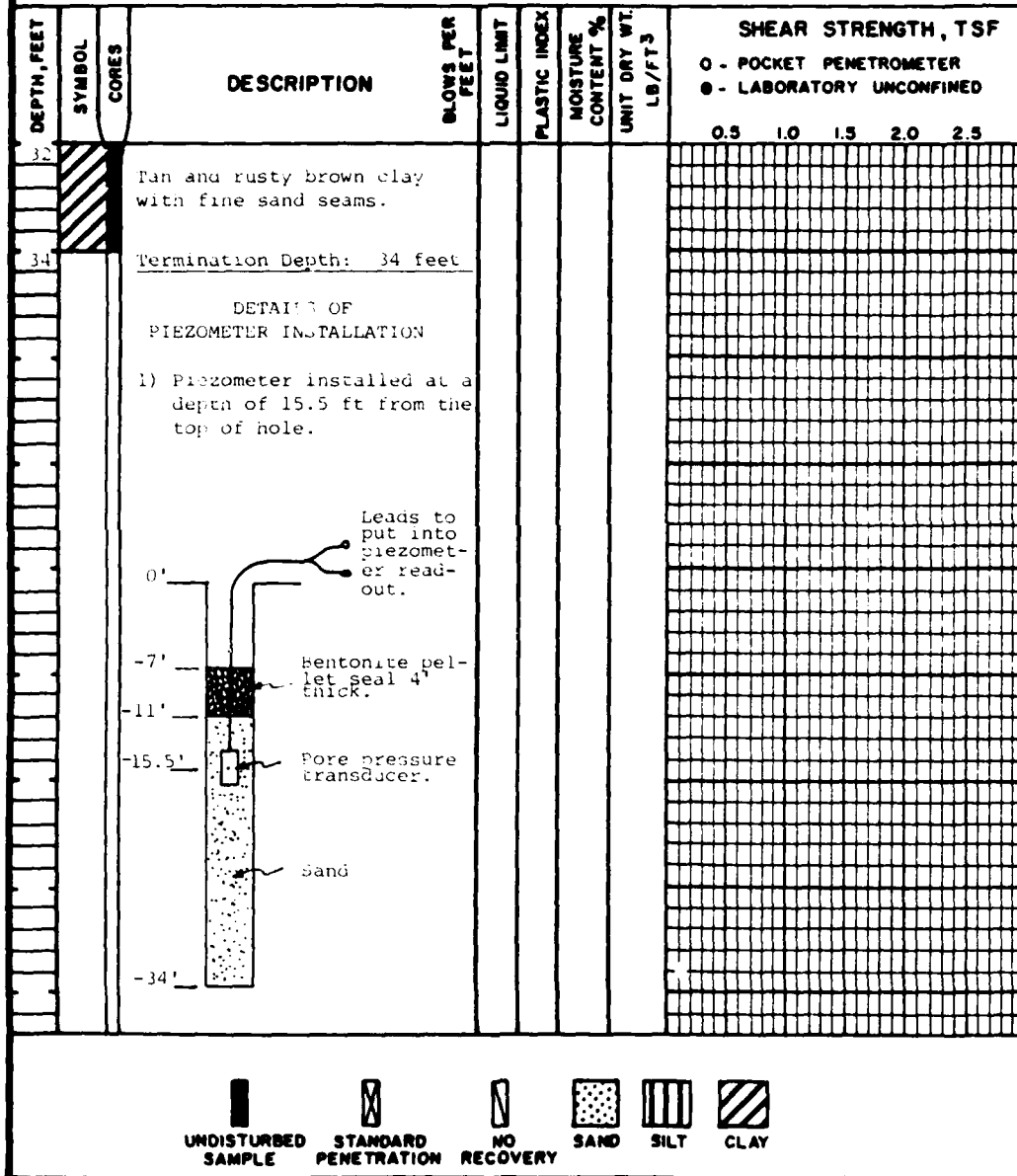
FIGURE A3(c)

# LOG OF BORING

**PROJECT:** Drilled Shaft Study  
**CLIENT:** U.S. Army Engineer, Waterways Experiment Station  
**LOCATION:** 610 East and 225 East, Houston, Texas  
**BORING TYPE:**

**BORING NO.:** 3-A (Cont'd)  
**PROJECT NO.:** 80C112  
**DATE:** 4-10-80  
**COMPLETION DEPTH:**

**WATER LEVEL:** INITIAL FT. FINAL FT. MIN.



WOODWARD-CLYDE CONSULTANTS

FIGURE A3(d)

APPENDIX B

PRESSUREMETER TEST CURVES FOR BORINGS

B-1 AND B-3

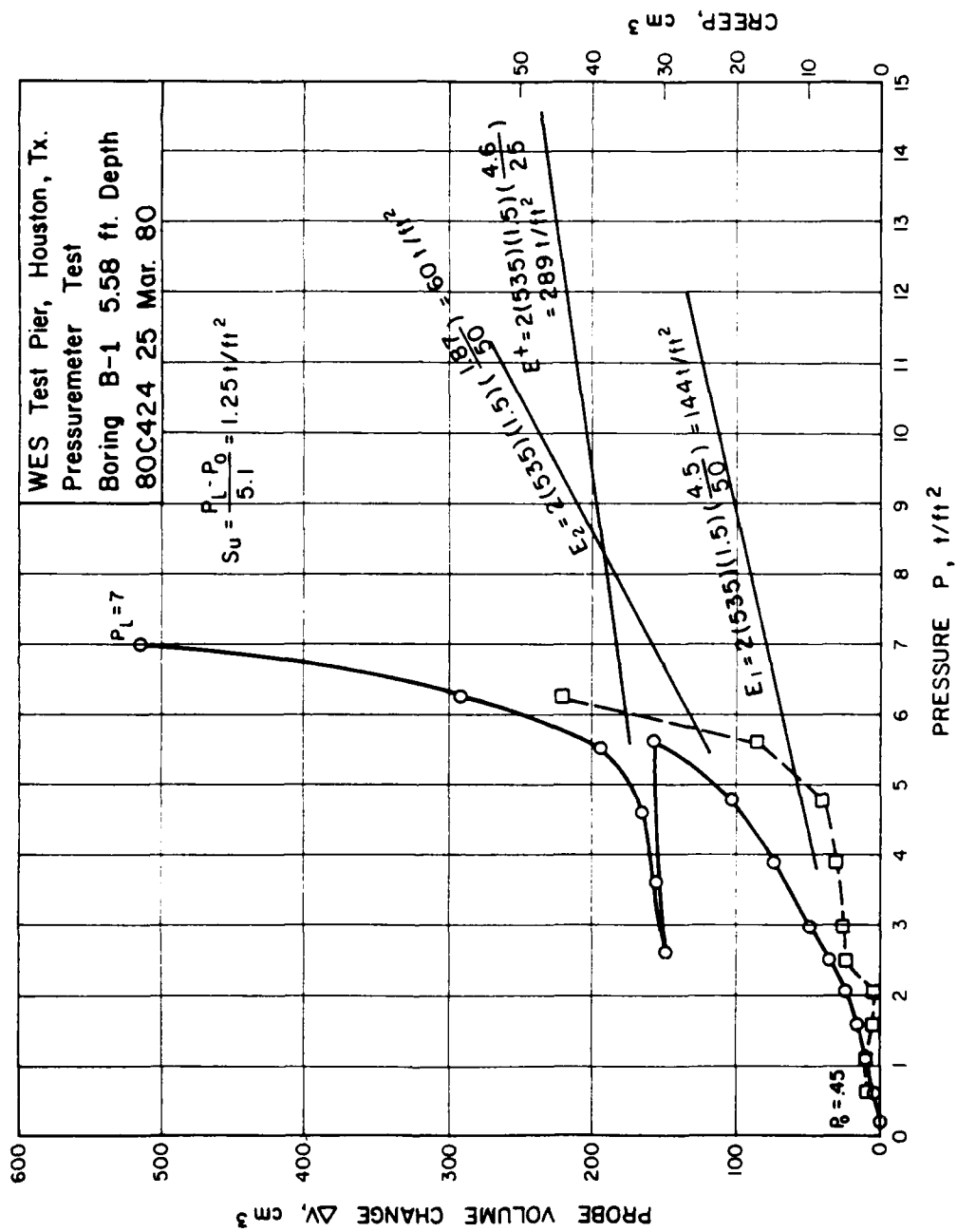


FIGURE B1

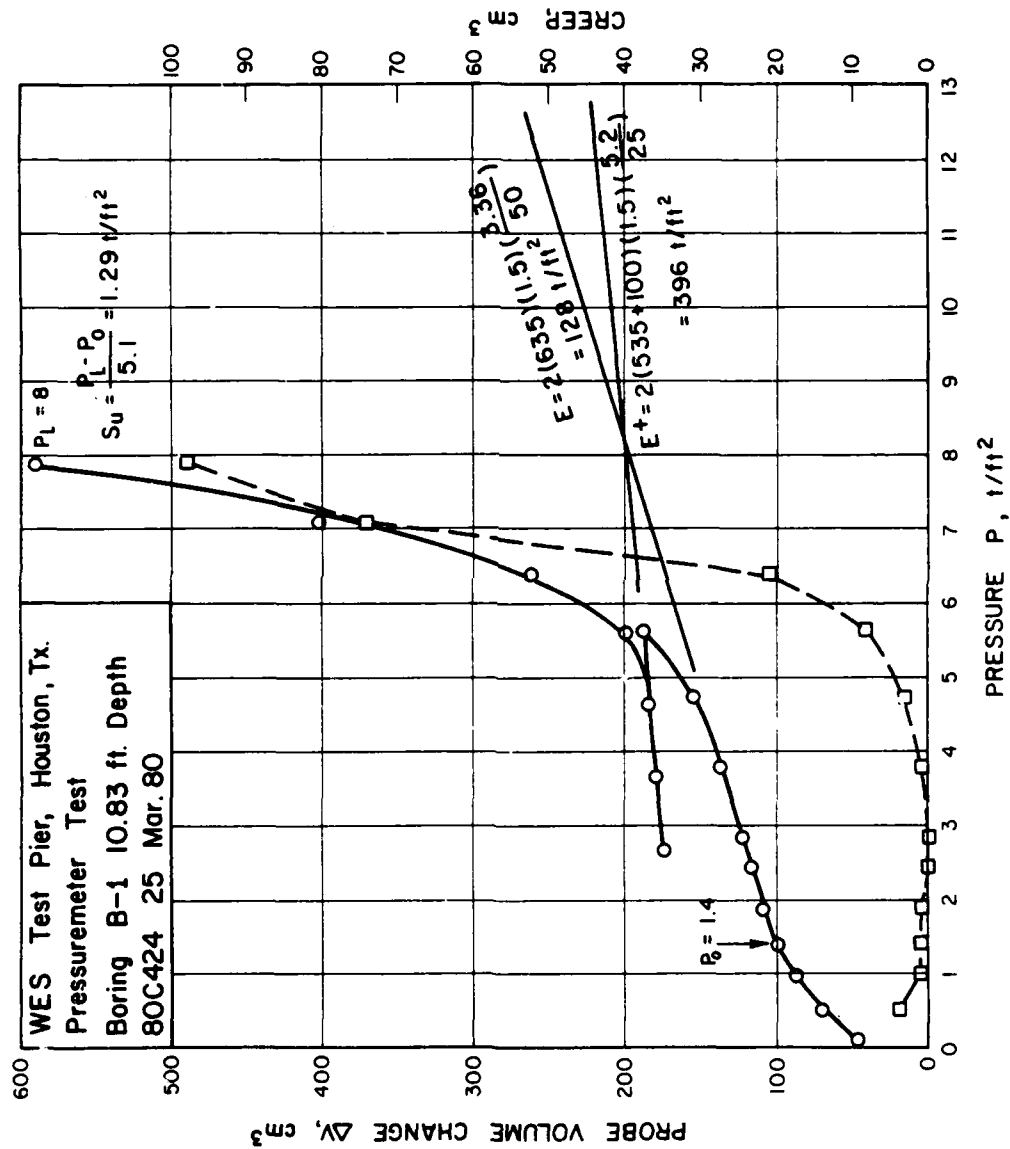


FIGURE B2



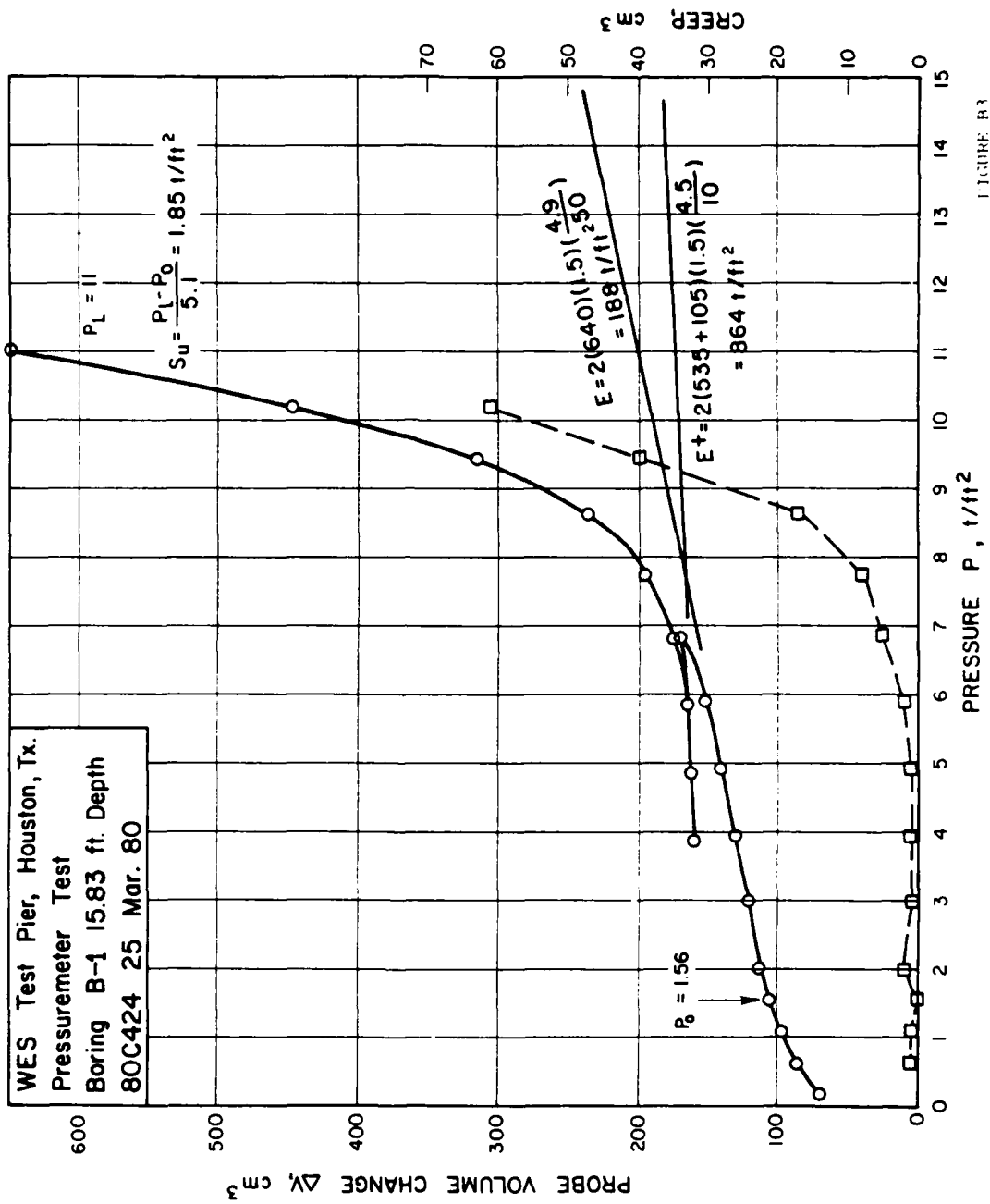
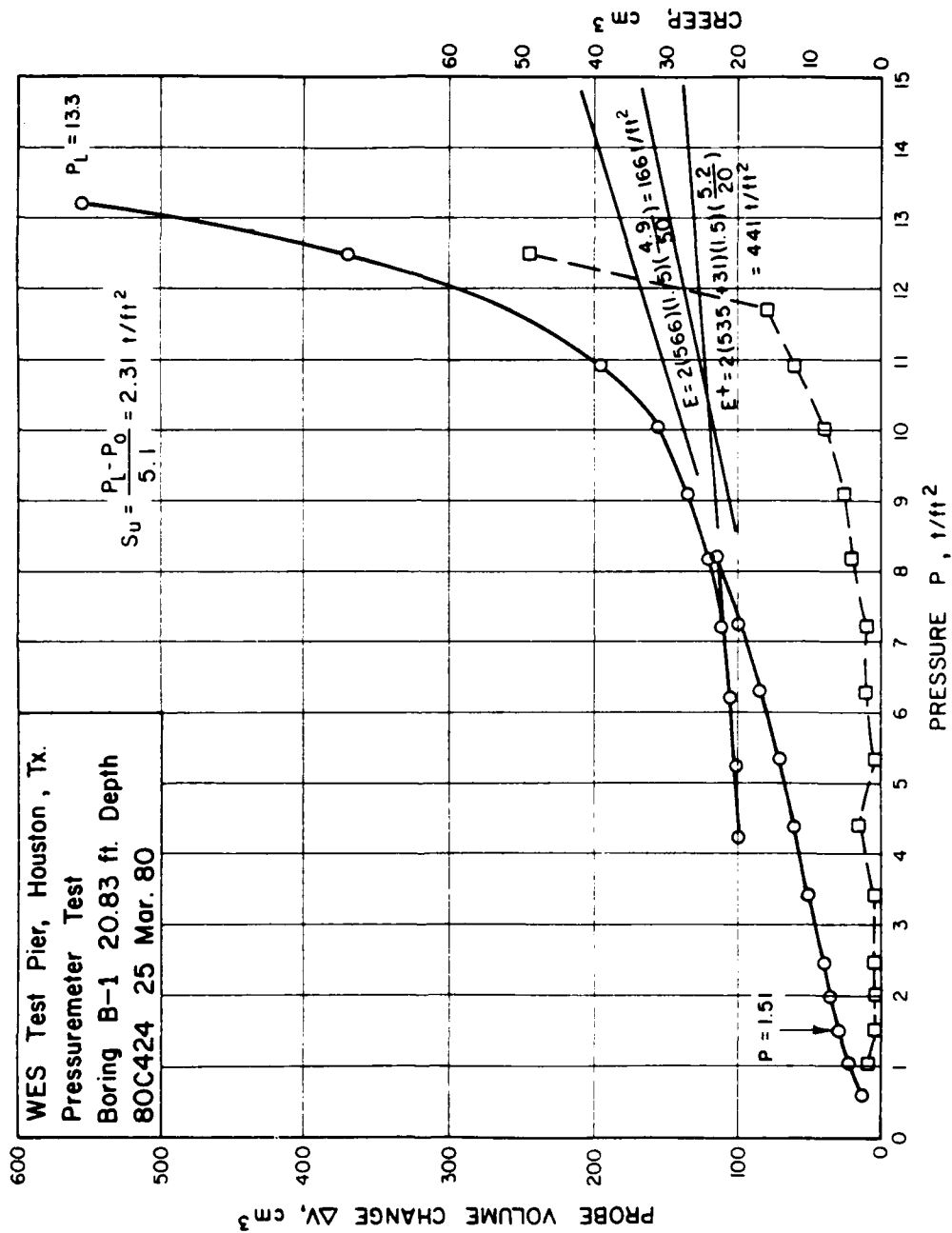


FIGURE B3



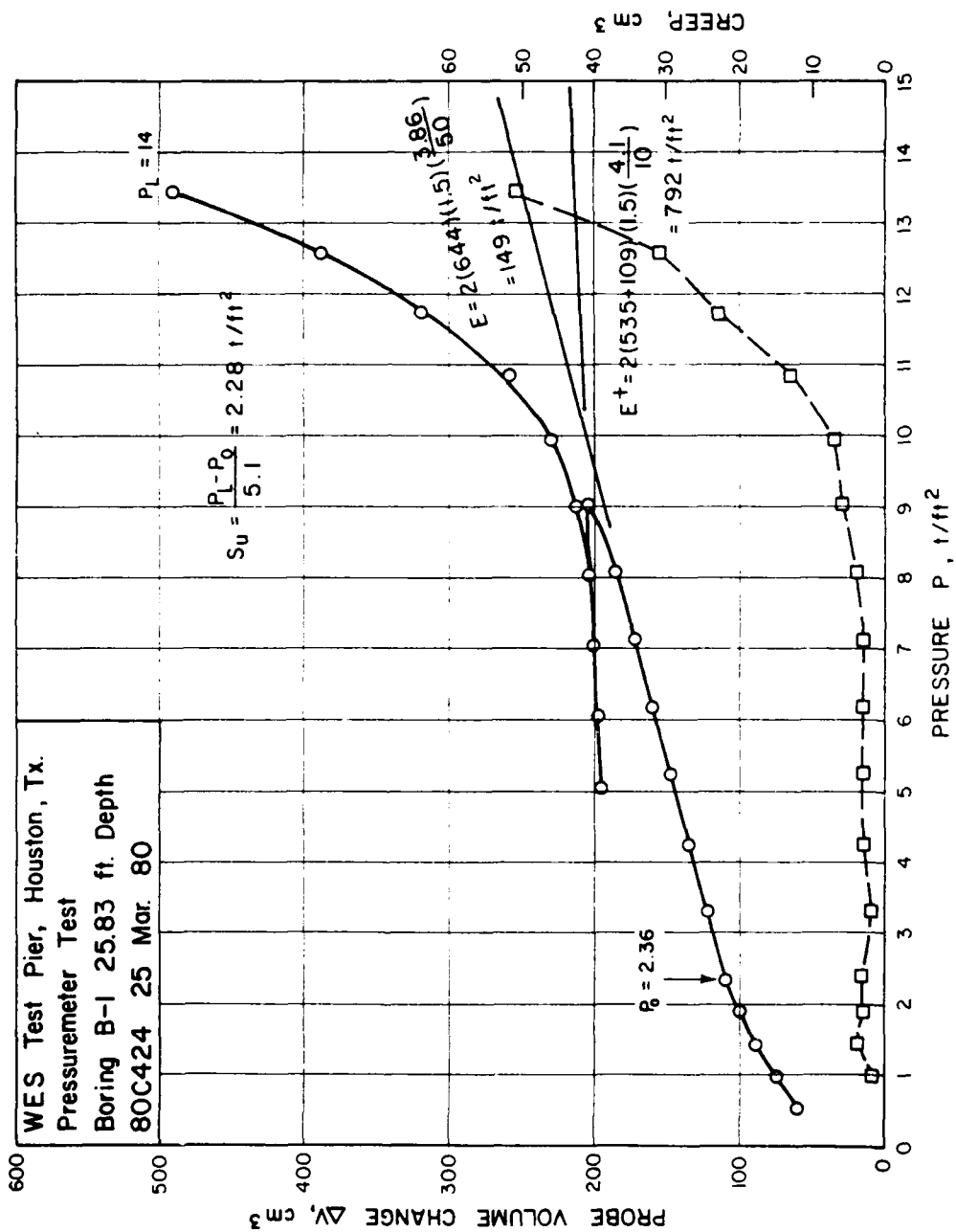


FIGURE 10

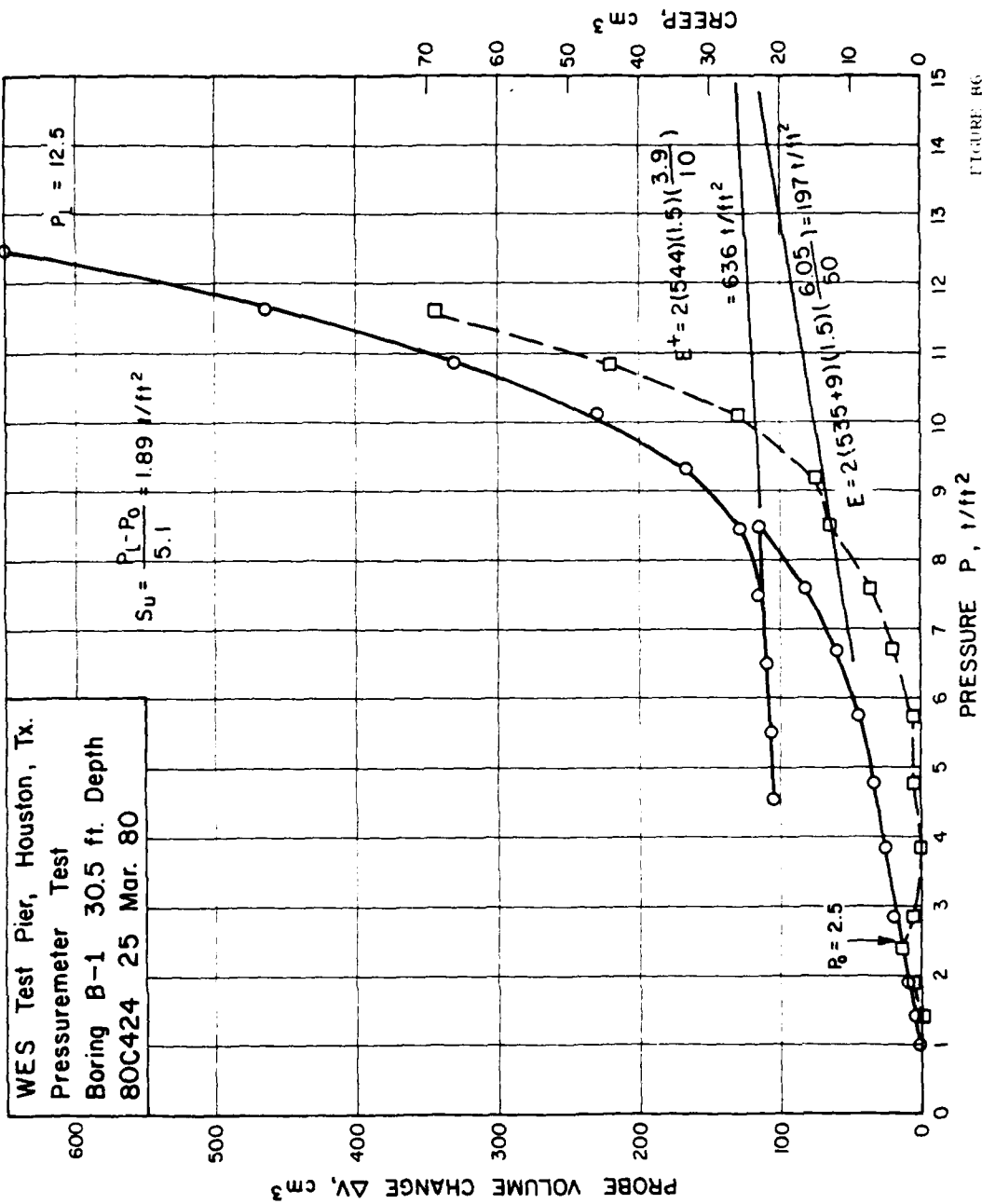


FIGURE 86

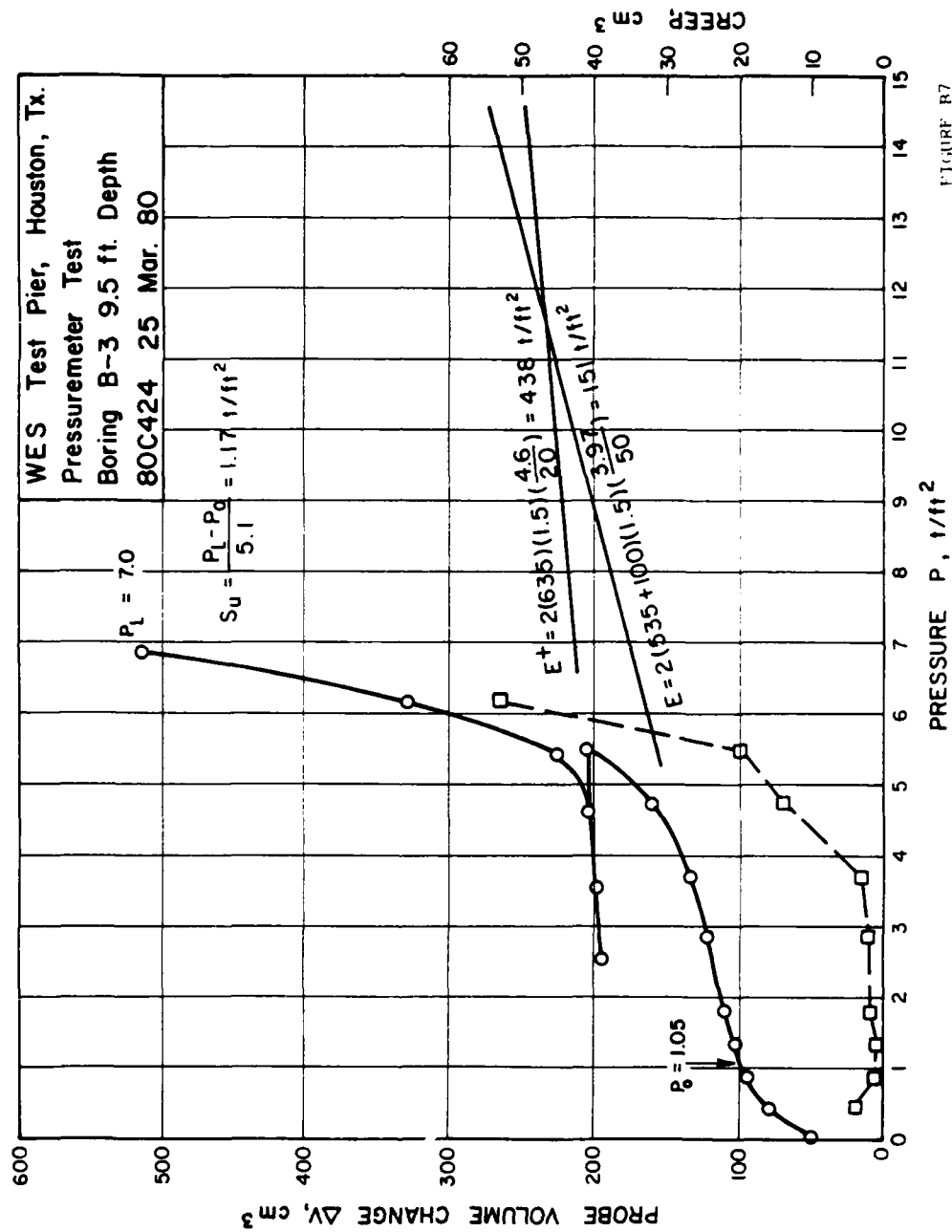
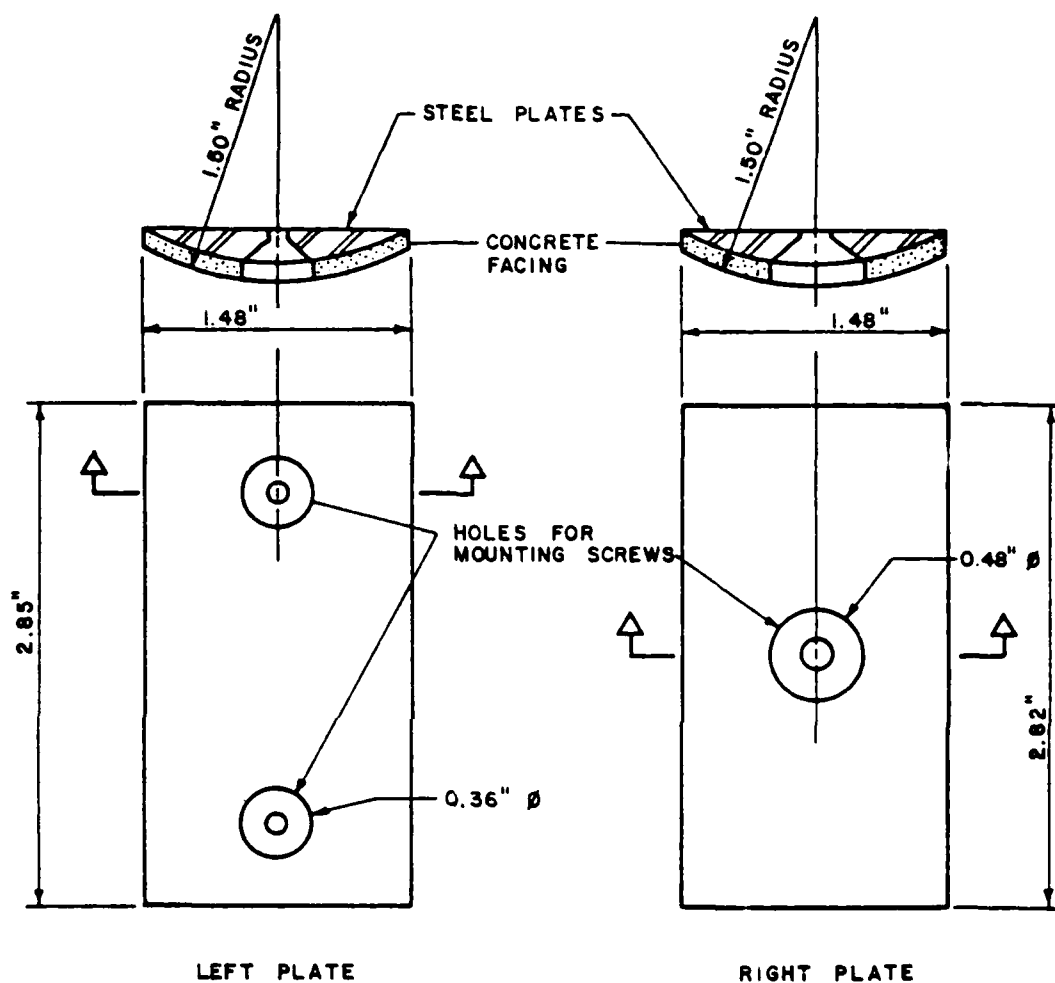


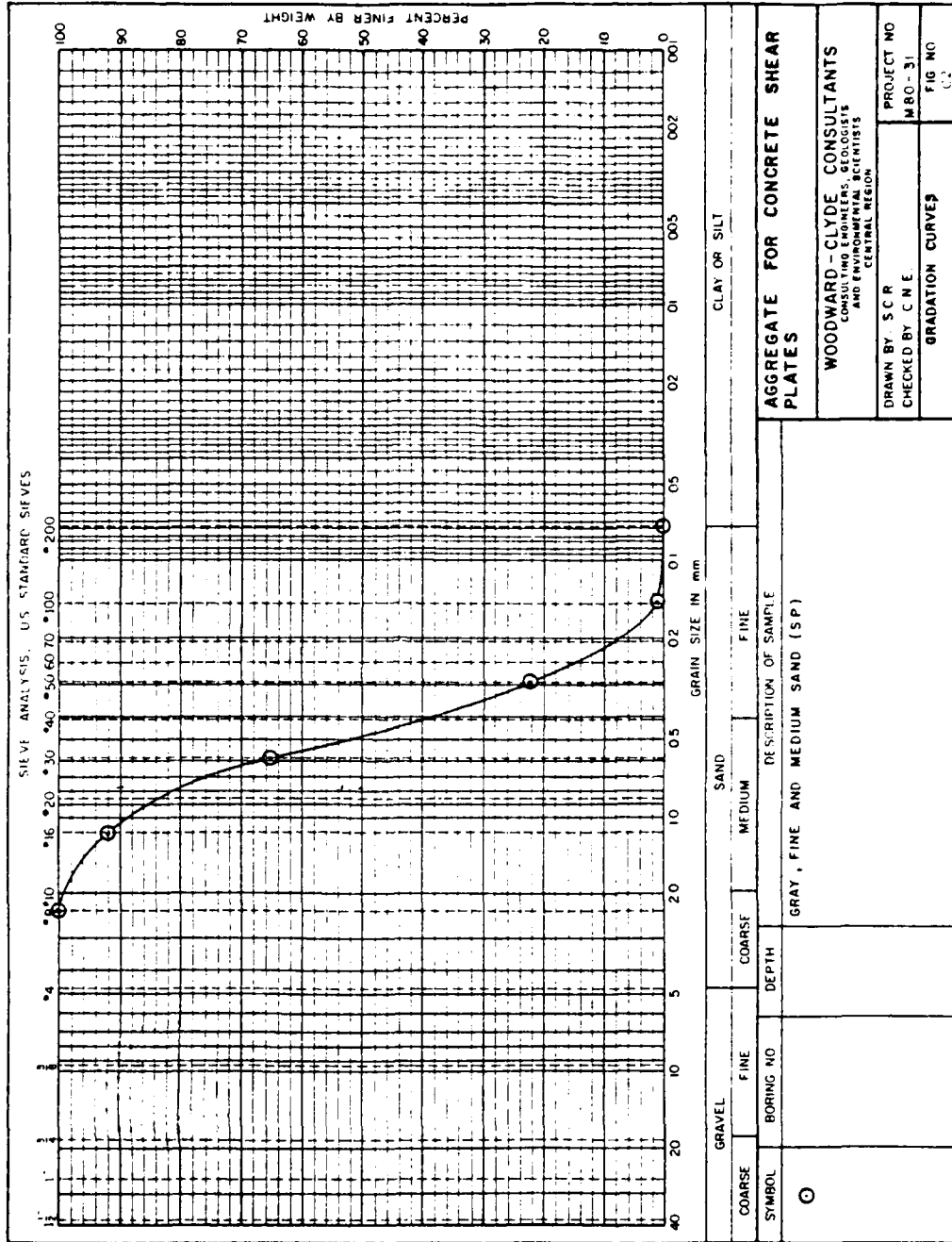
FIGURE R7

APPENDIX C  
CONCRETE-COATED SHEAR PLATE DETAILS  
FOR BOREHOLE SHEAR TESTS



**NOTE:** CONCRETE MIX PROPORTIONS  
 BY WEIGHT: 1 PART TYPE III CEMENT  
 4 PARTS SAND (see Figure C2)  
 0.6 PARTS WATER

FIGURE C1. CONCRETE SHEAR PLATE DETAILS



### AGGREGATE FOR CONCRETE SHEAR PLATES

WOODWARD - CLYDE CONSULTANTS  
CONSULTING ENGINEERS, GEOLOGISTS  
AND ENVIRONMENTAL SCIENTISTS  
CENTRAL REGION

DRAWN BY: S.C.R.  
CHECKED BY: C.N.E.

PROJECT NO.  
MBO - 31

FIG. NO.  
C-2

SYMBOL		BORING NO.	DEPTH	DESCRIPTION OF SAMPLE
O				GRAY, FINE AND MEDIUM SAND (S P)

CLAY OR SILT



APPENDIX D  
CALIBRATION CHARTS,  
BOREHOLE SHEAR TESTS

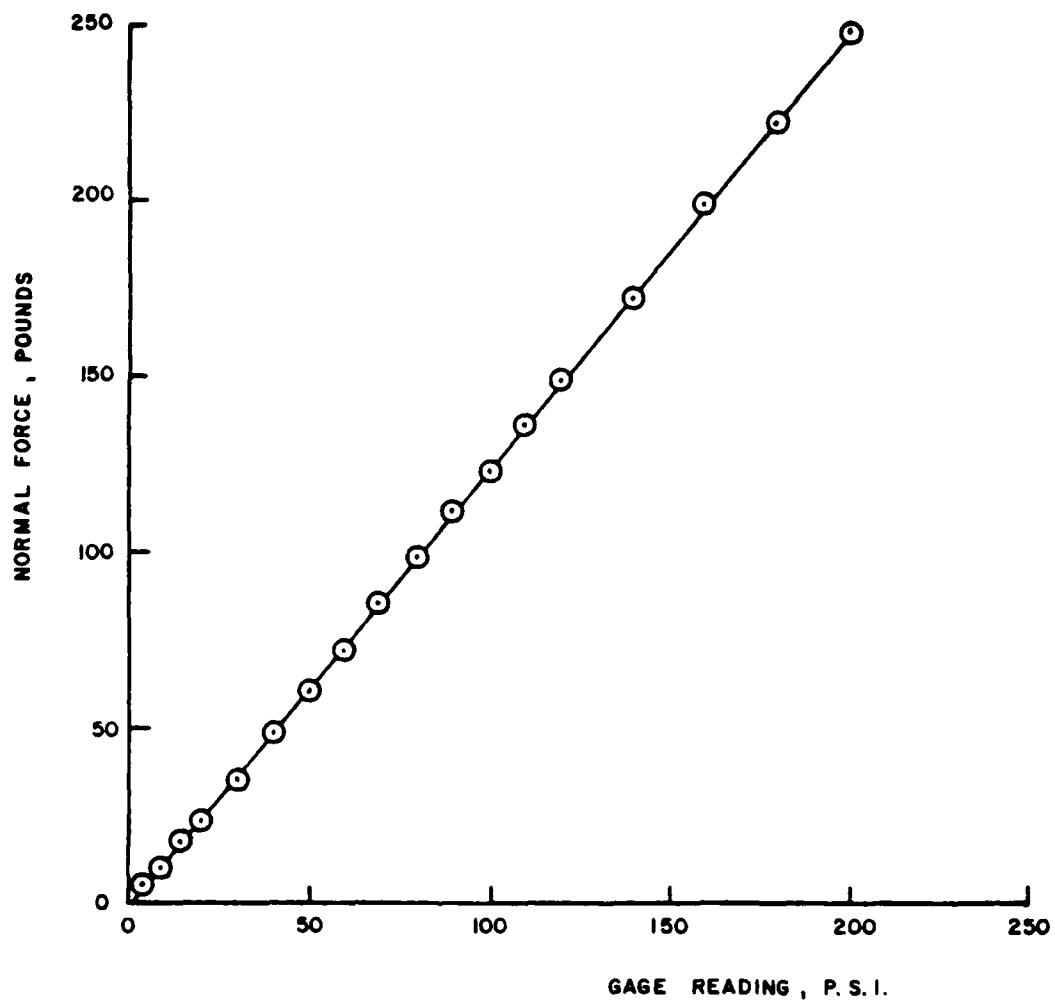


FIGURE D1. BORE - HOLE SHEAR  
NORMAL FORCE  
CALIBRATION CHART  
3-27-80 C.N. EASTON

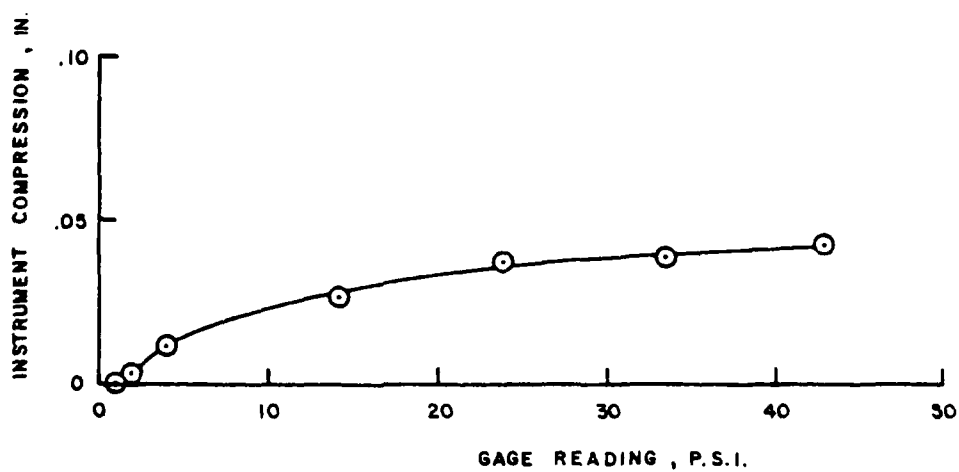
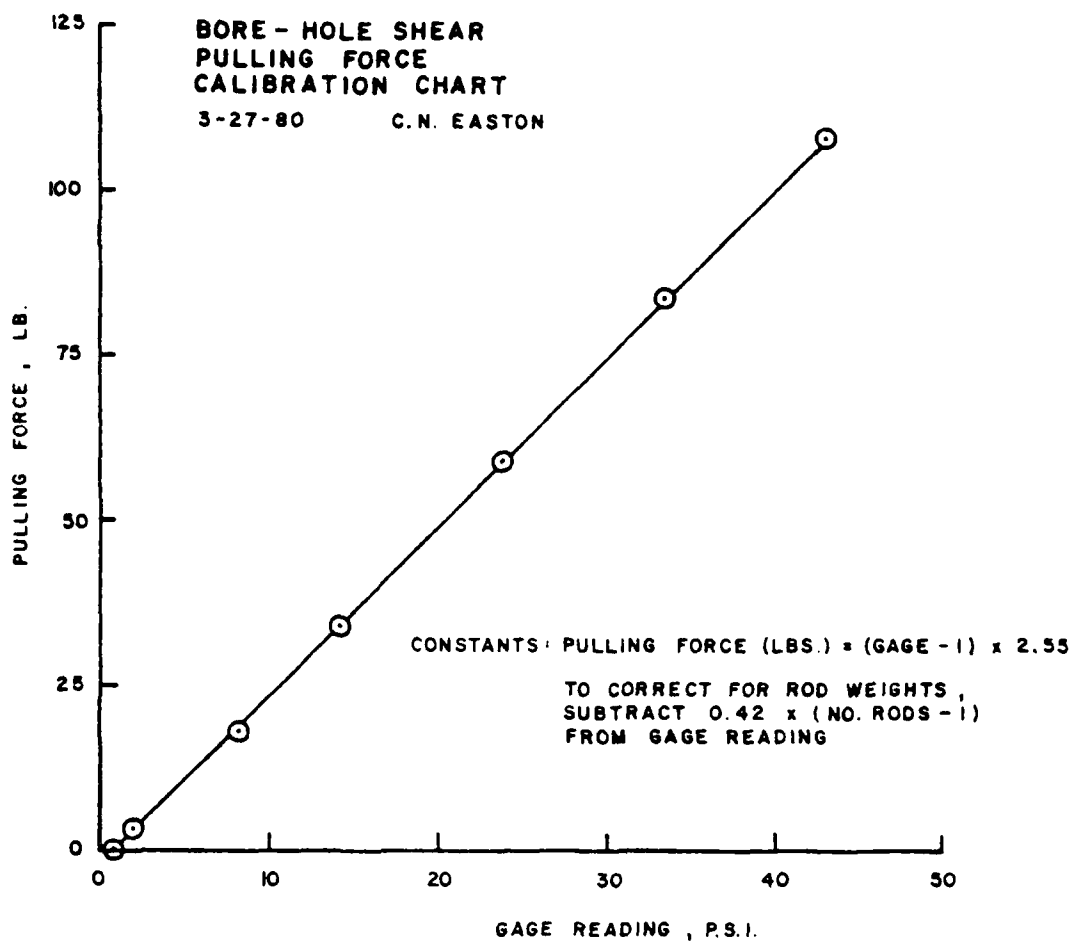


FIGURE D2. **BORE - HOLE SHEAR  
PULLING FORCE  
CALIBRATION CHART**  
3-27-80 C.N. EASTON

APPENDIX E  
PIEZOMETER READINGS

Table E1

Piezometer Readings (P-1)

Piezometer No. P-1  
 Sensor Elevation: E(Ft) -26 Ft

<u>DATE</u>	<u>PIEZOMETER READING, PSI</u>	<u>PRESSURE HEAD P, FT</u>	<u>TOTAL HEAD T, FT</u>
4/3/80	6.4, 6.6 & 6.4 (Ave. 6.47)	14.92	-26 + 14.92 = -11.08
4/7/80	6.4	14.77	-26 + 14.77 = -11.23
4/26/80	6.3	14.54	-26 + 14.54 = -11.46
4/27/80	6.3	14.54	-26 + 14.54 = -11.46
4/28/80	6.3	14.54	-26 + 14.54 = -11.46
4/29/80	6.4	14.77	-26 + 14.77 = -11.23
5/1/80	6.4	14.77	-26 + 14.77 = -11.23
5/3/80	6.4	14.77	-26 + 14.77 = -11.23
5/5/80	6.4	14.77	-26 + 14.77 = -11.23

AD-A114 305

WOODWARD-CLYDE CONSULTANTS HOUSTON TX

F/O 6/13

STUDY TO INVESTIGATE THE EFFECTS OF SKIN FRICTION ON THE PERFOR--ETC(U)

MAR 82 J AUDIBERT, D AGGARWAL, W GARDNER

DACA39-80-C-0001

UNCLASSIFIED

TR-GL-82-1

NL

2 of 4  
AD-A114 305

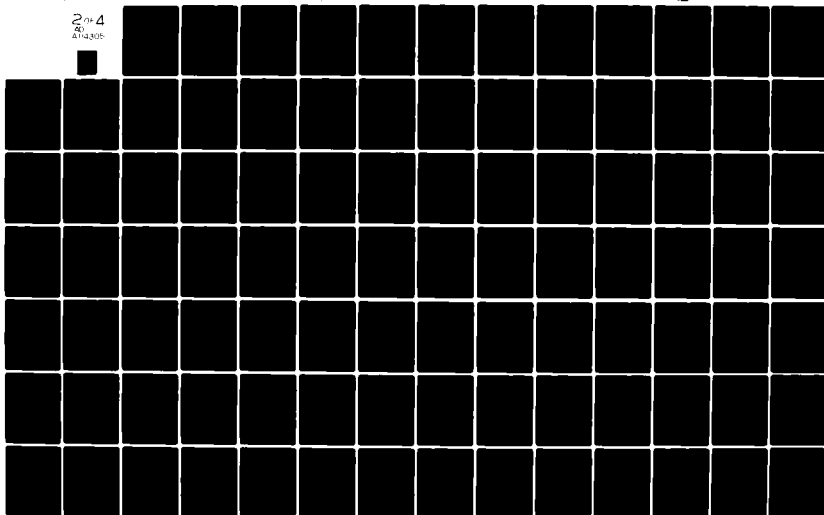


Table E2  
Piezometer Readings (P-2)

Piezometer No. P-2 Sensor Elevation: E(FT) - 29.5 Ft			
<u>DATE</u>	<u>PIEZOMETER READING, PSI</u>	<u>PRESSURE HEAD P, FT</u>	<u>TOTAL HEAD T, FT</u>
4/3/80	8.2	18.92	-29.5 + 18.92 = -10.58
4/7/80	7.8	18.00	-29.5 + 18.00 = -11.50
4/26/80	7.9	18.23	-29.5 + 18.23 = -11.27
4/27/80	7.9	18.25	-29.5 + 18.23 = -11.27
4/28/80	7.9	18.23	-29.5 + 18.23 = -11.27
4/29/80	8.0	18.46	-29.5 + 18.46 = -11.04
5/1/80	8.0	18.46	-29.5 + 18.46 = -11.04
5/3/80	8.0	18.46	-29.5 + 18.46 = -11.04
5/5/80	8.0	18.46	-29.5 + 18.46 = -11.04

Table E3  
Piezometer Readings (P-3)

Piezometer No. P-3 Sensor Elevation: E (FT) -15.5 Ft			
<u>DATE</u>	<u>PIEZOMETER READING, PSI</u>	<u>PRESSURE HEAD P, FT</u>	<u>TOTAL HEAD T, FT</u>
4/26/80	1.9	4.38	-15.5 + 4.38 = -11.12
4/27/80	1.8	4.15	-15.5 + 4.15 = -11.35
4/28/80	1.9	4.38	-15.5 + 4.38 = -11.12
4/29/80	1.9	4.38	-15.5 + 4.38 = -11.12
5/1/80	1.9	4.38	-15.5 + 4.38 = -11.12
5/3/80	1.9	4.38	-15.5 + 4.38 = -11.12
5/5/80	1.9	4.38	-15.5 + 4.38 = -11.12



VOLUME II

LABORATORY TESTING

By  
W. Gardner and R. Singh

## TABLE OF CONTENTS

	Page
PART I: INTRODUCTION .....	3
PART II: LABORATORY TESTING PROGRAM .....	4
PART III: TEST PROCEDURES .....	5
Sample Handling .....	5
Physical and Index Property Tests .....	6
Strength and Compressibility .....	7
Mortar-Soil Interface Tests .....	11
Earth Pressure-At-Rest Tests .....	13
PART IV: LABORATORY TEST RESULTS .....	14
Soil Description and Classification .....	14
Physical Properties .....	15
Soil Shear Strength .....	16
Consolidation Tests .....	18
Coefficient of Earth Pressure-At-Rest ( $K_o$ ) .....	18
Soil-Mortar Interface Shear .....	19
PART V: CHARACTERIZATION OF STRATIGRAPHY .....	20
Physical and Index Property Variation .....	20
Idealized Stratigraphic Section .....	20
PART VI: CHARACTERIZATION OF STRESS STATE .....	21
Effective Overburden Stress .....	21
Maximum Past Pressure .....	21
Effective Horizontal Earth Pressure .....	24
PART VII: DRAINED SHEAR STRENGTH .....	27
$\overline{CIU}$ Test Interpretation .....	27
$K_o$ Test Interpretation .....	28
Characterization of Effective Stress Parameters .....	28
PART VIII: RESIDUAL SHEAR STRENGTH .....	30
Effect of Normal Stress .....	30
Effect of Plasticity .....	31
$\phi'_r$ Characterization .....	31
PART IX: UNDRAINED SHEAR STRENGTH .....	32

Unconfined Compression Tests .....	32
Triaxial Compression Tests .....	32
PART X: DEFORMATION CHARACTERISTICS .....	37
Drained Deformation Parameters .....	37
Undrained Deformation Parameters .....	37
PART XI: INTERFACE SHEAR CHARACTERIZATION .....	39
Natural Water Content Versus Alpha Factor .....	39
Failure Plane Water Content Versus Alpha Factor .....	39
Change in Water Content Versus Alpha Factor .....	40
Interface Shear Characterization .....	41
PART XII: SOIL PROPERTY CHANGES WITH TIME .....	44
Water Content Variation .....	44
Undrained Shear Strength Variation .....	45
PART XIII: LITERATURE CITED .....	47
14 TABLES	
45 FIGURES	
APPENDIX A: LABORATORY TEST RESULTS	

STUDY TO INVESTIGATE THE EFFECTS OF SKIN FRICTION ON THE  
PERFORMANCE OF DRILLED SHAFTS IN COHESIVE SOILS

VOLUME II - LABORATORY TESTING

PART I: INTRODUCTION

Presented herein is the second of a series of three reports prepared by Woodward-Clyde Consultants (WCC) for the U.S. Army Engineer Waterways Experiment Station under contract DACA 39-80-C-0001 entitled, "Study to Investigate the Effects of Skin Friction on Performance of Drilled Shafts in Cohesive Soils." The study has been conducted in three stages, including (1) field investigations, (2) laboratory testing and (3) geotechnical engineering analyses.

As described in the Volume I report entitled "Field Investigation," the area of study is situated on the right-of-way at the intersection of State Highway 225 and Interstate Highway 610 in southeastern Houston, Texas (Fig. 1). Subsurface investigations and in-situ testing were conducted during the period of March through May 1980 in proximity to four drilled shafts constructed and tested in 1969 under the auspices of the Center for Highway Research at the University of Texas at Austin. Geologically, the test site lies within the Beaumont clays, a deposit of Pleistocene age extending over much of south-central Texas.

This report presents a description of the laboratory testing program, the laboratory test results and a characterization of pertinent soil properties and parameters from both the field and laboratory test data.

Descriptions of the scope of the geotechnical laboratory testing and the procedures used during the testing program are presented herein as Parts II and III. Part IV presents the laboratory test results and Parts V through XII describe a characterization of pertinent soil properties and parameters.

## PART II: LABORATORY TESTING PROGRAM

The geotechnical laboratory investigation was performed to provide a characterization of the in-situ soil properties and parameters as well as their state-of-stress. The laboratory testing program consisted of the following:

- a. handling and testing of representative soil samples;
- b. physical and index property tests;
- c. triaxial compression and one-dimensional consolidation tests;
- d. direct shear and residual strength tests;
- e. mortar-soil interface tests; and
- f. earth pressure-at-rest tests.

The laboratory test results were characterized in terms of:

- a. stratigraphy;
- b. stress state;
- c. undrained, drained and residual shear strengths;
- d. deformation characteristics;
- e. interface shear; and
- f. soil property changes with time.

### PART III: TEST PROCEDURES

The handling and testing of representative soil samples recovered as a part of the geotechnical exploration are described below. Where appropriate, reference is made to standard test procedures. Variations from such procedures are also described as are non-standard test methods.

#### Sample Handling

Soil samples used for testing were retrieved by thin-wall tube sampling (ASTM D 1587-74) yielding samples with a nominal 3.0-in. diameter. Denison-barrel samples yielding a nominal sample diameter of 6.0 in. were also retrieved. In addition, horizontally oriented thin-wall tube samples with a nominal 4-1/2 in. diameter were retrieved at different elevations from an access shaft. These samples extended from the access shaft to the face of drilled pier No. S-3. The location of the access shaft with respect to the existing drilled piers is shown on the attached Figure 2.

Undisturbed soil samples were transported from the field site to WCC laboratories in Houston, Texas, and Plymouth Meeting, Pennsylvania, via surface and air transport. The sample containers were packed with vibration energy-absorbing foam rubber and secured during transport. At the laboratories, sample tubes were stored upright in a high humidity room. The cores were removed from storage only as needed for testing.

All undisturbed samples were extruded and prepared for testing under a humidity hood. The samples were extruded from the sample tubes in an upright position with a continuous stroke using a motorized hydraulic piston extruder. Care was taken to minimize moisture loss and sample disturbance at all stages of testing.

Consolidation test specimens were trimmed to a diameter of 2.5 in. (6.35 cm) from their original diameter. Trimming was accomplished as described by Lambe (1951) in accordance with the provisions of ASTM D

2435-70. Triaxial test specimens were trimmed using a soil lathe to 1.4 in. (3.6 cm), 2.0 in. (5.1 cm), or 2.8 in. (7.1 cm) in diameter and cut to a length equal to two times the diameter. The specimen ends were carefully trimmed square. As the Beaumont clay samples often contained slickensided fissures, care was taken to prevent separation of the samples during preparation for testing.

#### Physical And Index Property Tests

Tests to investigate the physical and index properties of representative soil samples were generally conducted according to pertinent ASTM standards. The corresponding standards and test procedure modifications, where used, are described below:

##### Water Content

Samples tested to determine natural water contents were dried in a forced-draft oven in accordance with ASTM D 2216-71 procedures.

##### Liquid Limit

Samples tested to determine the liquid limit were prepared following ASTM D 2217-66, Procedure B, except that samples were not dried but were tested from their natural water content. A standard motorized liquid limit device, operated at a rate of two blows per second, was utilized for all tests.

##### Plastic Limit

Samples tested to determine the plastic limit were prepared as described for the liquid limit test. The test procedure was in accordance with the procedures specified in ASTM D 424-59.

##### Bulk Density

The bulk density was determined from the volume and weight of the test specimens. Volume calculations were made from averages of at least three measurements of sample height and diameter. The samples were carefully trimmed and the ends squared. Moisture contents and unit dry weights were also determined for these specimens.

### Specific Gravity

The procedure used to determine specific gravity essentially followed ASTM D 854. Special care was taken in making and deairing the soil-water mixture. A uniform temperature of the mixture was obtained for each test.

### Sieve And Hydrometer Analysis

The procedures specified by ASTM D 422-63 were used to determine the particle size distribution of representative soil samples.

### Strength And Compressibility

Triaxial compression and one-dimensional consolidation tests were conducted to evaluate the strength and deformation characteristics of the in-situ soils.

Shear strength tests were conducted on both vertically and horizontally oriented undisturbed samples obtained from test borings and an access shaft. The tests on vertically oriented samples were conducted to investigate both the total stress (undrained) and the effective stress (drained) strength parameters of the in-situ clays. Residual strength as well as peak strength parameters were investigated. The tests on horizontally oriented samples focused on pocket penetrometer tests as an index to potential strength changes subsequent to installation of Shaft S-3. The pertinent details of these test procedures are described below.

### Consolidation Tests

All tests were conducted in consolidometers employing highly polished teflon-coated consolidation rings to reduce side friction. The diameter and height of all the specimens tested were 2.5 in. (6.35 cm) and approximately 1.0 in. (2.54 cm), respectively. A load increment ratio\* of 1 was used for all the tests. Loads were applied pneumatically so as to preclude impact loadings. An unload-reload cycle was intro-

---

\* The ratio of the change in load to the previous load applied.



duced after the precompression stress had been exceeded. Reloading was initiated after unloading to approximately the overburden stress or to a minimum of two load decrements, whichever was less.

Time versus deformation records were maintained for each load increment and decrement. Each load was maintained for a duration at least equal to the time required for 90 percent of primary consolidation ( $t_{90}$ ) plus 60 minutes before the next load was imposed. The value of  $t_{90}$  was obtained by the Square Root of Time procedure as defined by Lambe (1951). With this procedure the stress-volumetric strain curves were not significantly influenced by secondary consolidation.

#### Triaxial Compression Tests

Triaxial shear tests were conducted to evaluate both undrained and effective strength parameters. Both consolidated isotropic undrained triaxial compression CIU tests with pore pressure measurements and unconsolidated undrained (UU) tests were conducted. The triaxial tests cells were specially designed to minimize piston friction and end constraint effects, as well as to facilitate consolidation and saturation of the test specimens. Relevant cell features included special bushings, highly polished platens, precision pressure fittings and top and bottom drainage provisions. Pore pressures were measured during all CIU tests using an electronic transducer with a low volume change response.

A minimum back pressure of 60 psi was used to facilitate CIU test specimen saturation. For all tests the pore pressure parameter "B" recorded before shearing was at least 0.95. The rate of undrained loading was approximately three percent per hour to allow pore pressure equalization. The consolidation time of the specimen prior to shearing was controlled to preclude significant secondary consolidation effects on the undrained strength and pore pressure response. Both CIU and UU tests followed the testing procedures outlined by Bishop and Henkel (1962).

At the beginning of the testing program, special shear testing procedures were used to determine if the undrained strength of the subsoils could be normalized as proposed by Ladd and Foott (1974). A

series of CIU tests were consolidated under pressure at least 1.5 times greater than the preconsolidation pressure. Specimens of known overconsolidation ratio were obtained by unloading to predetermined stresses and were sheared after pore pressure stabilization. Several of the test specimens experienced failure along random oriented planes of weakness (fissures) and, therefore, were not well suited to the development of normalized shear strength parameters. Consequently, the special testing program was terminated.

#### Direct Shear Tests

Direct shear tests were conducted with a conventional direct-shear machine with a screw-feed loading system activated by an electric motor capable of running at a constant speed under variable load. Different deformation rates were applied by varying the speed of the motor and were measured by means of a linearly variable differential transducer. Constant vertical load normal to the shear plane was applied by dead loading and the applied horizontal shear force was recorded via a load cell. The loading system was made as rigid as possible and care was taken to align the equipment so that the imposed horizontal load was colinear with the failure plane of the sample.

The tests were conducted on horizontally oriented, "undisturbed" samples. These 4.5-in.-diameter samples were obtained in the access shaft by cross-shaft jacking thin-wall Shelby tubes. Thus, the plane of failure in Direct Shear tests coincided with the plane of slip which would be developed in the soil during the loading of a drilled shaft.

The diameter of the tested soil specimens was 2.5 in. The procedure followed was generally as described in EM 1110-2-1906 of the U. S. Army, Office, Chief of Engineers (1970). To simulate the rate of loading during load tests of drilled shafts, a deformation rate of 0.04 in. (0.10 cm) per minute was selected after O'Neill and Reese (1970). It is likely that this rate approaches that required to approximate undrained conditions. Test samples were consolidated under normal loads equivalent to the estimated overburden pressure ( $\sigma'_{vo}$ ) at the sample depth, the estimated maximum past (consolidation) pressure ( $\sigma'_{vm}$ ) and to a stress midway between  $\sigma'_{vo}$  and  $\sigma'_{vm}$ .

### Residual Strength Tests

Special direct shear tests were run to assess the residual strength of the soil. For these tests, a shear failure plane was performed to coincide with the induced failure plane (which is perpendicular to the axis of the horizontal undisturbed sample) by cutting a plane surface through an intact specimen with a fine wire. The precut shear plane was used to preclude failure plane irregularities which could prevent measurement of the true residual shear strength. A deformation rate of  $4 \times 10^{-3}$  in. per minute was used to minimize development of significant pore pressure during shear. Otherwise the details of the residual strength test were the same as those discussed for intact soil specimens.

An investigation into the effects of repeated load reversals on shear strength was also conducted using loading rates ranging from 0.01 to 0.04 in. per minute. Although some researchers have reported that a strength degradation occurs which is independent of the rate of cyclic loading, no significant change in strength was noted under as many as 12 load reversals. It was judged that strength degradations under cyclic loading sufficient to define residual strength would occur only with shear strain rates which approach drained rather than undrained shear conditions. Consequently, the "rapid" reversed loading tests were terminated.

The residual friction angle ( $\phi'_r$ ) of the soil was also measured by performing a shear plane in a triaxial compression test specimen at an angle  $(45 + \phi'_r/2)$  to the horizontal. As demonstrated by Chandler (1966), the measured values of  $\phi'_r$  are not much influenced by small inaccuracies in the choice of the angle of shear plane. The specimen was cut at an angle of 55 degrees to the horizontal (assuming  $\phi'_r = 20$  deg) using a specially constructed form. The displacement at the peak deviator stress was small; therefore, no special platen was utilized in the tests. The data obtained was corrected for changes in the cross-sectional area and the influence of the rubber membrane. These corrections are described in detail by Chandler (1966).

Since quite small strains were required to mobilize the maximum strength for the precut specimens, a multi-stage loading test technique was used to define the failure envelope in terms of residual strength. The rate of deformation used was 0.0025 in. per minute. This slow rate of deformation was chosen to insure that shear occurred under drained conditions and the strength measured was truly residual.

#### Mortar-Soil Interface Tests

Special shear tests were conducted to study the effect of wet concrete placement in drilled shafts on the shear strength of the exposed soil. It has been hypothesized by O'Neill and Reese (1970) that water not required for hydration of cement tends to migrate into and soften the sidewalls of shafts drilled into cohesive soils. This softening is thought to cause a reduction in the undrained strength. There is also some evidence that when drilled shafts are loaded to failure, the failure plane may not coincide with the soil-concrete interface, but will occur within the soil immediately adjacent to the shaft. To investigate this strength reduction hypothesis, a number of special direct shear tests were conducted on soil-mortar specimens together with a special triaxial shear test.

#### Direct Shear Tests

The procedure followed for mortar-soil shear tests was essentially the same as described by O'Neill and Reese (1970). Specimens were trimmed to 2.5 in. in diameter and placed in the bottom half of the direct shear box with 0.375 in. (0.95 cm) of soil protruding above the shear plane. Then the shear box was assembled and cement mortar was cast on the top of the soil. The mortar contained Type I cement. The water-cement ratio was 0.6 and the sand-cement ratio was 3.0. A normal pressure of 2 psi, sufficient only to assure tight contact between the

mortar and the soil\*, was then applied to the assembly and the specimen was allowed to cure in a high humidity room for one week. Soil-mortar specimens were kept moist during this period by wrapping with moist cloth.

After the curing period, the soil-mortar specimen assembly was installed in the direct shear machine and the specimen was sheared using a 0.04-in.-per-minute deformation rate. Before shear, a normal stress was imposed which was maintained throughout the test. This stress was varied to define the failure envelope as described for the conventional direct shear tests. After the specimen was sheared, moisture content at various distances from the interface was obtained.

#### Triaxial Test

One mortar-soil interface test was conducted in a triaxial cell. The bottom half of the specimen was obtained by precutting a soil sample at 55 degrees as for the residual strength test. This sample was put at the bottom of a form and the top half of the form was filled with cement mortar. The mix of the mortar was the same as that described in the section entitled "Direct Shear Tests" in Part III. The assembly was allowed to cure in the high humidity room and moist cloth was used to prevent drying.

After a seven-day curing period, the specimen was installed in the triaxial cell. The rate of deformation applied was 0.0025 in. (0.0064 cm) per minute. The specimen did not fail along the pre-cut failure plane. Upon disassembly, failure was observed to have occurred along slickensided planes present in the test specimen. This was similar to the failure mode in many of the unconsolidated-undrained triaxial tests. Consequently, further testing of this type was not conducted.

---

(\*) Although it has been postulated that the consolidation pressure ( $\sigma_c$ ) applied to mortar-soil specimens during curing is one of the variables influencing moisture migration (O'Neill and Reese, 1970), a review of available information suggests that  $\sigma_c$  has only a secondary effect. Consequently, a variation of  $\sigma_c$  during curing was not incorporated in the testing program.

### Earth Pressure-At-Rest Tests

Triaxial compression tests were conducted to evaluate the coefficient of earth pressure-at-rest ( $K_0$ ), defined as the ratio of the in-situ effective horizontal to the effective vertical pressure. In setting up the test, special care was taken to prevent entrapment of air between the sample and the membrane. This was facilitated by provisions for double drainage in the triaxial test cells. After the assembly of the triaxial cell, a backpressure of 60 psi was applied to saturate the specimen. A pore water pressure response of at least 0.95 of the cell pressure was obtained prior to shear for each specimen. To insure complete saturation, these specimens were backpressured for at least three days before being tested.

As the volumetric changes and the axial deformations were expected to be small, sensitive burettes with a 0.010-cc accuracy were used to measure the volume change within the sample. The volume of water flowing both out of and into the triaxial cell was monitored. The premise of the  $K_0$  test procedure was that for a no lateral strain condition, the measured volume change of the saturated sample must be equal to the axial compression of the sample multiplied by the initial cross-section area of the sample, i.e., volumetric strain equals axial strain. Correspondingly, axial load was controlled in accordance with the burette readings using a precalculated no lateral strain relationship between these two parameters. Other details of the test were the same as described by Bishop and Henkel (1962).

#### PART IV: LABORATORY TEST RESULTS

The results of the various laboratory tests conducted as part of this study are summarized herein.

##### Soil Description And Classification

The predominantly cohesive soils encountered at the site are associated with the Pleistocene, Beaumont clay formation. These soils are reported to have been deposited during the later stages of the Wisconsin glaciation and were deposited in deltas and in shallow waters. The formation, in general, is somewhat heterogeneous consistent with its alluvial deposition origin.

##### Mineralogy And Structure

The soils encountered by site explorations were usually classified as stiff to hard, mottled red or tan and gray silty clay. Based on available data (Al-Layla, 1970) the mineralogical composition includes montmorillonite (23-47 percent), illite (28-55 percent), kaolinite (7-18 percent) and quartz (15-18 percent). The silty clays also contain occasional calcareous nodules and traces of organic material as well as silty and sandy seams. The silty clay samples usually revealed randomly oriented fissures and occasional relict joint features. Most of the fissures were observed to be small and discontinuous and were often characterized by slickensided surfaces. The fissures are postulated to be a product of cyclic wetting and drying and the associated swelling and shrinking activity. It is likely that this desiccation also acted to preconsolidate the subsoils, particularly in the upper part of the deposit.

##### Liquid And Plastic Limits

Liquid and plastic limits were determined to provide data for soil classification and property correlation. These test results are presented in Appendix A (Tables A1 through A4). A summary of these data is shown in Figure 3 in terms of the liquid limit versus the plasticity

index, i.e., the Casagrande A-line chart. As indicated, samples obtained from the upper 0 to 17 feet were usually classified in accordance with the Unified Classification System as a clay of medium to high plasticity (CH) as were those samples taken from 20 to 26.5 ft. With the exception of a CL-ML interval from 29 to 31 ft, the remaining samples to a depth of 32 ft were classified as silty clays (CL). Data from a total of 30 tests are shown on the plasticity chart.

#### Physical Properties

The results of tests to investigate the water content, unit weight, specific gravity and grain-size distribution from representative soil samples are included in Appendix A. This presentation provides a tabulation of test results in Tables A1 through A4 and curves of grain-size distribution determined from representative samples. A summary of the maximum, minimum and statistical mean physical property test results for each of the generalized strata encountered by the exploration is given in Table 1. It is noted that discrimination of the strata is made on the basis of property variations, together with classification data and is somewhat arbitrary.

The variation with depth of the natural water content and liquid and plastic limit data is shown in Figure 4. These data incorporate tests conducted only on vertically oriented soil samples. (The results of water content tests conducted only on horizontally oriented soil samples are shown in Figures 36 through 39. In these figures, the test results are plotted as a function of the distance from the face of Shaft S-3.) Figure 5 depicts the soil composition of representative samples in terms of the differentiation according to percentage of sand, silt and clay sizes from borings 2/2A and 3A.



## Soil Shear Strength

### Unconfined Compression (UC) Tests

The results of UC tests on samples obtained from Borings B-2 and B-3A have been plotted as a function of depth in Figure 6. Observations made during the conduct of these 22 tests indicated that the failure surface was often controlled by planes of weakness coincident with the orientation of fissures. Those samples which appeared to be unaffected by fissuring usually yielded significantly higher UC strengths (Table 2a).

### Unconsolidated-Undrained (UU) Triaxial Tests

The undrained shear strength variation with depth was investigated by UU tests conducted on representative samples obtained from the test borings. A summary of these data is presented in Table 2(b) and in Figure 7 as a plot of the undrained shear strength versus depth. As indicated in this figure, the scatter in data (primarily attributed to the clay fissures) is similar to that obtained from the UC tests. Again, only the test results near the upper bound of the measurement appear not to be significantly influenced by the effect of fissures.

To further investigate the hypothesis that comparatively low strength UC and UU tests results represent failure modes controlled by fissures, additional UU tests were conducted on Denison soil samples. Two sets of tests were made on each of three samples secured from the same sampling tube. As it is known that the size of sample will influence the probability of the test being influenced by fissures, sample diameters of 1.4, 2.0 and 2.8 in. were used in these tests. The test results are shown on Figures 8 and 9. The test series on samples taken from a depth of 18.5 to 19.5 ft did not exhibit readily apparent failure modes controlled by fissures. However, a trend towards increasing strength with smaller sample size can be detected. The second test series graphically demonstrates the influence of a fissure-controlled failure. Note that the fissure-controlled failure occurred in the smallest sample, contrary to expectations.

#### Consolidated-Undrained ( $\overline{CIU}$ ) Triaxial Tests

The  $\overline{CIU}$  test results are summarized in Table 2(c) and the undrained shear strength is plotted in Figure 10 as a function of the total normal stress  $(\sigma_1 + \sigma_3)/2$  using all the test data.

The slope of a regression line through the data can be interpreted in terms of the apparent friction angle of the clay. Note that the undrained strength as given by the  $\overline{CIU}$  tests may also be influenced by the effects of fissuring. The upper bound line of the failure envelope likely represents the consolidated undrained shear strength of samples whose failure mode is not significantly influenced by fissures. Some differences may also be attributed to the differences in plasticity index as shown for the effective stress parameter interpretations presented in Part VII.

#### Direct Shear Tests

A summary of the direct shear test results is presented in Table 3 and Figure 11, which shows the peak undrained shear strength versus the effective normal stress prior to shearing.

There is some uncertainty relative to the drainage conditions during direct shear as well as to the degree of saturation of the test samples. It is likely that the results represent a near undrained case considering the relatively rapid shearing rate. When comparing the results of direct shear tests to those of triaxial tests, consideration must be given to rotation of the principal stress direction imposed by the direct shear test and the difference in the sampling orientation. These effects would be expected to produce somewhat lower undrained shear strengths in direct shear.

#### Residual Strength Tests

As described in Part III, residual strength determinations were made by both direct and triaxial shear tests on representative test specimens with precut failure planes. A summary of these test data is presented in Table 4.

### Consolidation Tests

Table 5(a) summarizes the physical and index properties of the consolidation test samples and presents stress state and compressibility parameters interpreted from the test data. The results of the consolidation test curves are contained in Appendix A.

The maximum past consolidation stress ( $\sigma'_{vm}$ ) has been interpreted by three techniques. The coefficients of compressibility in virgin compression ( $C'_c$ ) and in recompression ( $C'_r$ ) represent the slopes of the log stress versus volumetric strain curves in the range of virgin compression and recompression, respectively. It is noted that the stress state and compressibility parameters are sensitive to sample disturbance and that the general effect of disturbance is to decrease  $\sigma'_{vm}$  and decrease  $C'_c$ .

### Coefficient of Earth Pressure-At-Rest ( $K_o$ )

The results of these tests are shown on Table 5(b). The effective vertical consolidation pressure ( $\sigma'_1$ ) versus  $K_o$  values are summarized in Figure 12.

Where  $K_o$  becomes constant, the test specimen has reached a state of normal consolidation ( $OCR = 1$ ). The estimated in-situ  $K_o$  values are derived from the test results by entering Figure 12 with a  $\sigma'_1$  equivalent to the  $\sigma'_{vo}$  of each sample. It is noted that such  $K_o$  tests are extremely sensitive to sample disturbance as well as to the effects of stress relief upon sampling. Consequently, conventional laboratory  $K_o$  tests underpredict the in-situ  $K_o$  value. Where samples are not highly structured, much more representative measurements can be made using SHANSEP testing procedures (Ladd and Foott, 1974).

### Soil-Mortar Interface Shear

The results of the interface shear tests are presented in Table 6. The water content of the test specimens at and in proximity to the failure plane of the test specimens is also documented. Figure 13 shows the peak shear strength from the soil-mortar interface shear tests versus the effective normal stress prior to shearing.

For most tests, the difference between the soil strength of companion samples tested in direct shear and the interface shear resistance is very small. The comparison is undoubtedly affected by the natural variation in specimen properties even though the companion samples were carefully selected. If the interface shear tests are interpreted as a single data base, the apparent friction angle between the mortar and soil is essentially identical to the apparent friction angle as determined by the direct shear tests on the companion soil specimens. This is demonstrated by comparison of the direct shear test results shown in Figures 11 and 13. Further consideration of this observation is made in Part XI.

## PART V: CHARACTERIZATION OF STRATIGRAPHY

For the purpose of engineering analysis, an idealization of the stratigraphy at the test site has been developed from the subsurface exploration data and the laboratory test data contained in Part IV in the section entitled "Soil Description and Classification," and in Appendix A. This interpretation includes characterization of the variation of the plasticity index, liquid limit, natural water content, specific gravity and unit dry weight of the subsoils.

### Physical And Index Property Variation

To assist in evaluation of a general stratigraphy representative of the test site, a careful examination of the variation in liquid limit, plasticity index and water content was conducted as shown by Figures 4 and 14. Based upon this evaluation, generalized strata were identified and the variation of plasticity, unit dry weight and natural water content were assessed within each of the generalized strata. This evaluation has been summarized in Table 1.

As indicated by the standard deviation of the data, there is a substantial scatter of some of the physical and index properties. This is consistent with the depositional history and structure of the Beaumont clay and provides some insight to the natural variation of the engineering soil parameters to be characterized in this study. This profile variation is also vividly demonstrated by the static cone penetrometer logs reproduced as Figures 29 and 30.

### Idealized Stratigraphic Section

Based on the boring records and the foregoing analyses, an idealized stratigraphic section has been prepared for the purposes of subsequent analyses. This section is shown as Figure 15 and is presented together with a summary characterization of the pertinent physical and index properties for each generalized stratum.

## PART VI: CHARACTERIZATION OF STRESS STATE

The in-situ stress state parameters of interest are the effective overburden pressure ( $\sigma'_{vo}$ ), the maximum past consolidation pressure ( $\sigma'_{vm}$ ) and the ambient effective horizontal stress ( $\sigma'_{ho}$ ) existing within the soil deposits. The characterization of each of these parameters is described in the following subsections.

### Effective Overburden Stress

The  $\sigma'_{vo}$  within the subsoils is directly related to the unit weight of the subsoils and to the depth of groundwater below the surface. As  $\sigma'_{vo}$  changes with seasonal variations of groundwater level, the current (1980)  $\sigma'_{vo}$  would be expected to be different from the condition prevailing at the time of the pier load tests (1969). Based on the reported groundwater level during the pier load test (O'Neill and Reese, 1970), the variation of  $\sigma'_{vo}$  with depth is shown in Figure 16 for both periods of time. The measured unit dry weights ( $\gamma_d$ ) presented in Figure 15 have been used in the  $\sigma'_{vo}$  analysis. Total unit weights ( $\gamma_t$ ) below groundwater level were calculated assuming a 100 percent saturation condition. Above water level ( $\gamma_t$ ) was calculated as  $(1 + w_n) \cdot \gamma_d$  where  $w_n$  is the appropriate mean natural water content.

### Maximum Past Pressure

Estimates of the maximum past pressure ( $\sigma'_{vm}$ ) have been primarily derived from the results of consolidation tests described in Part IV in the section entitled "Consolidation Tests." The  $\sigma'_{vm}$  has been interpreted following the procedures of Burmister (1951), Casagrande (1936) and Rutledge (1944). In addition, interpretations have been made from the results of pressuremeter tests (PMT), as presented in Volume I, and from the results of the UU tests described in Part IV under "Unconsolidated-Undrained Triaxial Tests."

### Consolidation Test Evaluation

The  $\sigma'_{vm}$  interpretation by the Burmister technique and by the combined Casagrande and Rutledge techniques\* are shown on Figure 17. It is noted that the effect of sample disturbance is to reduce the predicted  $\sigma'_{vm}$  values and that the least disturbed test specimens would be expected to be those trimmed from the large diameter Denison samples. It is noted that the Burmister interpretation produces the upper bound  $\sigma'_{vm}$  prediction and has the least data scatter. There are usually only minor differences in the  $\sigma'_{vm}$  interpretations made by the Casagrande and Rutledge procedures. Figure 18 presents the data contained in Figure 17 in terms of overconsolidation ratio, i.e.,  $\sigma'_{vm}/\sigma'_{vo}$ .

### Pressuremeter Test Evaluation

The  $\sigma'_{vm}$  predictions from the pressuremeter test (PMT) are also shown in Figure 17. Direct comparison of these test results with other techniques entails some difficulties. First, the PMT measurement is in a horizontal rather than vertical direction and, therefore, is related to the maximum past horizontal stress ( $\sigma'_{hm}$ ) not  $\sigma'_{vm}$ . Secondly, the interpretation technique assumes that porewater pressures induced by the probe expansion have dissipated during the typical one-minute incremental loading period.

The relationship of  $\sigma'_{vm}$  to  $\sigma'_{hm}$  would be differently interpreted depending upon the cause of the overconsolidation of a soil deposit. If the cause were a geologic erosion, then equating  $\sigma'_{vm}$  to  $\sigma'_{hm}$  would be entirely erroneous. In this circumstance, the relationship between  $\sigma'_{hm}$  and  $\sigma'_{vm}$  would be derived for an initial state of normal consolidation, i.e.,  $\sigma'_{vm}$  would be about twice  $\sigma'_{hm}$ . Should, on the other hand, the overconsolidation of the deposit be primarily due to desiccation, then equating  $\sigma'_{hm}$  to  $\sigma'_{vm}$  may not be significantly in error.

The assumption that no significant porewater pressure remains at the time of the PMT measurement would tend to overpredict  $\sigma'_{hm}$  and,

---

\* Only the largest  $\sigma'_{vm}$  interpretations of the two techniques are shown on Fig. 17.

therefore,  $\sigma'_{vm}$ . There is some reason to believe that in the heavily overconsolidated Beaumont clays, dissipation of pore pressures would proceed relatively rapidly and may not be too significant after the one-minute time period that the load increment is maintained. In summary, considering all aspects, predictions of  $\sigma'_{vm}$  by the PMT should be utilized with extreme caution. In the future, the use of self-boring pressuremeters with the capability to measure pore water pressures during probe expansion should resolve some of the uncertainties connected with the test.

#### Prediction from $S_u$ and OCR

The results of the triaxial compression tests can also be used to provide an approximate evaluation of OCR provided the test samples are not unduly disturbed or the strength significantly affected by the presence of fissures. This interpretation is made using the concept of normalized undrained strength parameters (Ladd and Foott, 1974) in accordance with Equation 1:

$$S_u / \sigma'_{vo} = K(OCR)^n \quad (1)$$

In Equation 1, K represents the normalized shear strength of the soil in a normally consolidated state and the exponent, n, is primarily a function of the type of shear test used. For triaxial tests on soils with a plasticity index over 30 percent, K is approximately 0.35. The parameter n for triaxial tests is typically about two-thirds and would generally be in the range of 0.60 to 0.75 (Gardner, 1977).

To provide estimates of OCR, the upper bound strength envelope for UU tests (Fig. 28) was chosen for analysis. The results of this interpretation are shown in Table 7 for n parameters of 0.67 to 0.75. The n = 0.75 prediction shows a reasonable conformance with the upper bound consolidation test results but significantly higher OCR's are predicted for the n = 0.67 solution.



### OCR Characterization

Based on the foregoing analyses it is concluded that the upper limit of the  $\sigma'_{vm}$  consolidation test predictions is a conservative characterization of the past stress history of the Beaumont clay within the depth of exploration. These bounds are expressed in terms of OCR in Figure 19 for the assumed OCR existing at the time of load testing (1969). Note that this characterization is given for a groundwater level of 15 ft as reported by O'Neill & Reese (1970).

### Effective Horizontal Earth Pressure

As the effective ambient horizontal earth pressure ( $\sigma'_{ho}$ ) is usually expressed in terms of the Coefficient of Earth Pressure-At-Rest ( $K_o$ )\*, the  $K_o$  parameter is usually of specific interest. In the characterization of  $K_o$ , consideration has been given to both the  $K_o$  triaxial tests and PMT measurements conducted as part of this study. Indirect methods of  $K_o$  prediction from basic soil properties have also been incorporated in the characterization process.

### $K_o$ Triaxial Compression

As indicated by Figure 12,  $K_o$  measurements from "no lateral strain" triaxial compression tests range from 0.78 to 0.84. The test results also indicate that  $K_o$  for the normally consolidated state ranges from 0.66 to 0.54. Consistent with the recognition that  $K_o$  laboratory measurements are highly sensitive to sample disturbance as well as to the test procedures, the test results are judged to be lower than exist in-situ. This judgement is confirmed by the subsequent evaluations.

### Estimates From Soil Properties

Equation 2 expresses the ratio of the overconsolidated  $K_o$  to normally consolidated ( $K_{nc}$ ) values as a function of the OCR of the deposit (Gardner, 1977):

---

\* 
$$\sigma'_{ho} = K_o \cdot \sigma'_{vo}$$

$$\frac{K_o}{K_{nc}} = OCR^m \quad (2)$$

As  $K_{nc}$  is closely approximated by  $(1 - \sin \phi')$  and  $m$  can be estimated from the plasticity index, an estimate of  $K_o$  for the Beaumont clay can be made by Equation 3:

$$K_o = (1 - \sin \phi') (OCR)^m \quad (3)$$

assuming the effective friction angle ( $\phi'$ ) and OCR vary with depth as shown by Figures 25 and 18. These calculations are summarized in Table 8 for comparison with the  $K_o$  tests. Note that the exponent  $m$  is predicted as a function of plasticity index\* based on the work of Brooker and Ireland (1965).

Figure 20 presents the  $K_o$  measurements together with the predicted variation of  $K_o$  with depth based on the foregoing procedure. It is noted that the parameters used in these calculations incorporate the upper bound consolidation test values of OCR as interpreted from both  $\sigma'_{vm}$  (Fig. 17) and  $S_u$  (Fig. 28) for UU tests.

#### Pressuremeter Tests

Interpretations of  $K_o$  from the pressuremeter tests are summarized in Table 9 and are plotted on Figure 20. The  $K_o$  derivation is based on the effective in-situ horizontal stress ( $\sigma'_{ho}$ ) interpretation made from the configuration of the PMT curve. This interpretation is quite sensitive to the probe hole preparation, as well as the assumption that significant pore water pressure is not induced at strains induced by the probe sufficient to define  $\sigma'_{ho}$ . The effects of disturbance and/or excess pore pressure would be to increase the  $\sigma'_{ho}$  prediction.

PMT predictions of  $K_o$  using the Ménard type of pressuremeter may be somewhat greater than the true  $K_o$  value. The degree of potential overprediction is, of course, a function of the care taken during the

---

\*  $m = 0.58/I_p^{-0.12}$

probe hole preparation. In this regard, extreme care was taken during the pressuremeter testing at the site as described in Volume I, "Field Investigation."

#### Summary

It is concluded that  $K_o$  predictions from the upper bound consolidation test interpretation OCR and the  $\phi'$  profiles presented in Figures 18 and 25 represent a reasonable degree of conservatism and are appropriate for engineering analysis. This conservatism is particularly appropriate considering the little known effect of the fissured clay structure on predictions of  $K_o$  from either laboratory or field data. It is likely that the most reliable techniques will eventually be developed from in-situ testing incorporating a self-boring pressuremeter having the capability to measure excess pore water pressures during probe expansion. The Ménard PMT and upper limit UU test interpretations presented in Figure 20 are probably closer to the in-situ state but incorporate a fair degree of uncertainty.

## PART VII: DRAINED SHEAR STRENGTH

The effective stress parameters required to characterize the drained shear strength of the subsoils are the effective friction angle ( $\phi'$ ), the effective cohesion ( $c'$ ), and the excess pore water parameter at failure ( $A_f$ ). The  $\phi'$  parameter has been primarily developed from the results of the  $\overline{CIU}$  tests and secondarily from the  $K_o$  triaxial tests; whereas  $c'$  and  $A_f$  have been interpreted from the  $\overline{CIU}$  tests. A correlation between  $\phi'$  and plasticity index has also been developed to facilitate engineering analyses. The various drained shear strength characterizations are summarized as follows.

### CIU Test Interpretation

Figures 21 through 23 demonstrate the interpretation of  $\phi'$  from the stress path plots of the  $\overline{CIU}$  test data. Note that the test data are grouped in accordance with the plasticity index of the test specimens. In each of the figures, the failure envelope is represented by a line tangent to the stress path peaks. The slope of this line represents  $\sin \phi'$ ; whereas the deviator stress intercept represents  $c'/\cos \phi'$  (Lambe and Whitman, 1969). Table 10 summarizes the results of the  $\overline{CIU}$  test interpretations.

It is likely that the wide variation in  $c'$  is the effect of fissures within the test samples and/or sample disturbance. Disturbance effects may be significant as the largest  $c'$  was obtained on test specimens trimmed from the large diameter Denison samples. Figure 24 presents the pore water parameter ( $A_f$ ) versus the OCR of the test specimens. The OCR's were estimated from the upper bound of the consolidation tests shown in Figure 18. Note that  $A_f$  is given for the maximum deviator stress failure criteria. Also shown for comparative purposes is the same relationship derived for London clay (Bishop and Henkel, 1962) which is a stiff fissured clay similar to that of the Beaumont formation.

### K<sub>o</sub> Test Interpretation

The effective friction angle can be interpreted from the K<sub>o</sub> tests described in Part IV in the section entitled "Coefficient of Earth Pressure-at-Rest" by equating the K<sub>o</sub> values derived from the normally consolidated range of the test to the quantity (1 - sin  $\phi'$ ). The results of this assessment are tabulated in Table 8. Note that the  $\phi'$  interpreted from two of the three K<sub>o</sub> tests appear to be in substantial agreement with the derivations from CIU tests when consideration is given to the plasticity index of the test specimens as demonstrated by Figure 25.

### Characterization Of Effective Stress Parameters

The effective stress parameters  $\phi'$ ,  $c'$  and  $A_f$  have been characterized from the preceding interpretations with due consideration of the special mineralogical and structural features of Beaumont clay.

#### Effective Friction Angle

The relationships between  $\phi'$  and plasticity index shown in Figure 25 are concluded to be a reasonable characterization which is not greatly sensitive to the effects of fissures on the test results. Comparison of the derived relationship with published data, however, indicates the effective friction angle of the Beaumont clay is generally lower than the median  $\phi'$  which would be predicted from the plasticity indices of the deposit. It is likely that this condition can be attributed to the dominant montmorillonite clay mineral of the Beaumont clay.

#### Effective Cohesion

Unlike  $\phi'$ , it is probable that  $c'$ , as derived from the laboratory tests, is significantly affected by the presence of fissures within the test samples and/or sample disturbance. There is also some limited evidence that as the plasticity index decreases,  $c'$  similarly decreases. The relatively high  $c'$  interpreted in Figure 23(a) is believed to

more closely represent in-situ behavior. Note that the test samples used in this analysis were trimmed from the large diameter Denison samples obtained from the location of the test shaft. It is judged that  $c'$  can be conservatively approximated as 0.4 tsf for plasticity indices less than 20 percent. Between these limits a linear interpretation appears reasonable.

The  $A_f$  factors measured during the  $\overline{CIU}$  tests are probably most representative of the in-situ behavior of the clay in the higher OCR range. The excess pore water pressure at failure would undoubtedly be influenced by the effects of sample fissuring, as well as disturbance. In summary, it is concluded that Figure 25 can be used to provide a suitable estimate of  $\phi'$  as a function of plasticity, and that  $A_f$  can be conservatively predicted from the upper bound curve through the data shown on Figure 24.

## PART VIII: RESIDUAL SHEAR STRENGTH

The residual shear strength of clay represents the minimum shearing resistance developed upon significant movement along a failure plane. The appreciable reduction in peak shear strength required to reach residual strength is explained by the preferred orientation of the clay fabric induced along the failure plane by the sliding soil mass. As described in Parts III and IV in the sections entitled "Residual Strength Tests," residual shear tests were conducted using both triaxial and direct shear methods. The results of these tests are interpreted in terms of the residual friction angle ( $\phi'_r$ ) as follows.

### Effect Of Normal Stress

If the triaxial and direct residual shear tests are interpreted separately,  $\phi'_r$  values of 9.0 degrees and 10.2 degrees, respectively, are obtained without consideration of the effects of stress dependency. However, when these data are combined, as shown on Figure 26, a good agreement between the results of the two different types of tests is evident and  $\phi'_r$  for the combined data is 9.0 degrees. Based on the work of Bishop et al. (1971) it has been recognized that the residual friction angles of many clays are stress dependent, i.e., are related to the effective stress ( $\sigma'_n$ ) imposed normal to the plane of shear during testing. In this regard,  $\phi'_r$  has been shown to decrease with increasing  $\sigma'_n$  up to stresses at least on the order of 40 to 50 psi. This behavior is particularly evidenced by the data points representing  $\sigma'_n$  values less than about 1.5 tsf. For example, in the  $\sigma'_n$  range between about 0.5 and 1.5 tsf,  $\phi'_r$  is more correctly characterized as 15 degrees; whereas  $\phi'_r$  for  $\sigma'_n$  greater than about 3.0 tsf is 9 degrees.

### Effect Of Plasticity

It was first recognized by Skempton (1957) that the residual friction angle is a function of the clay mineralogy as measured either by the activity number or the plasticity index. A compilation of data presented in the literature has been published by Kanji and Wolle (1977) and is presented as Figure 27(a). Shown in Figure 27(b) is the interpreted  $\phi'_r$  for stress levels above about 3.0 tsf. Note that there is a reasonably good agreement of this data with the published  $\phi'_r$  versus plasticity index relationship.

### $\phi'_r$ Characterization

The expression derived for the locus of the published data shown on Figure 27(a) can be used to extrapolate the test results as a function of plasticity and effective normal stress. The proposed relationship is given as Equation 4:

$$\phi'_r = \beta 46.6 PI^{-0.446} \quad (4)$$

The normal stress influence parameter  $\beta$  is a function of  $\sigma'_n$  and can be conservatively represented by Figure 27(b). Note that derivation of  $\beta$  from the residual shear strength test data is somewhat subjective but is quite typical of the  $\phi'_r$  versus  $\sigma'_n$  trends shown by Bishop and subsequent investigators.



## PART IX: UNDRAINED SHEAR STRENGTH

The undrained shear strengths of the subsoils at the test site have been investigated by unconfined compression, unconsolidated undrained and consolidated undrained triaxial tests, the latter employing pore-water pressure measurements. In addition, shear strength interpretations have been made from the results of field Torvane, Static Cone Penetration and Pressuremeter tests. A characterization of  $S_u$  from the results of the various tests is described as follows.

### Unconfined Compression Tests

The unconfined shear strength, interpreted as one-half of the unconfined compression strength, has been shown as a function of depth in Figure 6. The upper bound of the data envelope represents tests believed to be largely unaffected by fissures. This line is also similar to the mean unconfined shear strength profile presented by O'Neill and Reese (1970). Conversely, the low bound line of the data envelope is believed to represent compressive strengths that are controlled by the presence of fissures within the sample. It has also long been recognized that the shear strength from UC tests is usually significantly lower than that produced by UU tests.

### Triaxial Compression Tests

Unconsolidated undrained and  $\overline{CIU}$  tests were conducted on both 2.8-in.-O.D. thin-wall tube samples obtained from conventional borings and on 5-1/2-in.-O.D. Denison barrel samples. Tests conducted on specimens trimmed from the large diameter samples are identified on the subsequent graphic interpretations.

### UU Tests

The undrained shear strength ( $S_u$ ), representing one-half the maximum deviator stress, has been shown for the UU tests in Figure 7 as a

function of depth. Similar to the unconfined compression tests, the upper bound interpretation of  $S_u$  from the UU tests is believed to represent tests which have not been materially affected by the presence of fissures within the test specimens. The upper bound of the  $S_u$  envelope in the top 22 ft of the profile is in substantial agreement with the "mean strength" line interpreted by O'Neill and Reese (1970). However, below this depth the upper bound  $S_u$  interpretation is significantly greater than the O'Neill and Reese interpretation. Because of the limited data base derived from this study, however, comparisons with the extensive O'Neill and Reese  $S_u$  data should be made with caution.

#### CIU Tests

The CIU tests have been interpreted in terms of total stress as shown in Figure 10. As indicated, two failure envelopes are apparent. The upper bound interpretation probably represents sample failure modes not appreciably influenced by fissures. Note that both the apparent friction ( $\phi_u$ ) of 17 degrees and cohesion ( $c_u$ ) of 0.5 tsf are significantly reduced by fissure-controlled failures.

As there are water content changes during consolidation, strengths interpreted from Figure 10 would usually be higher than exist in-situ. Consequently, CIU test results interpreted in terms of total stress are not recommended for assessment of the undrained shear strength of soil deposits.

#### Pressuremeter And Torvane Tests

As described in the preceding Volume I report,  $S_u$  has been interpreted from pressuremeter tests after Gibson and Anderson (1961) and Marsland and Randolph (1977). The results of this interpretation are summarized in Table 11. It is noted that  $S_u$  (1) after Gibson and Anderson (1961) is reported to represent a post peak shear strength; whereas  $S_u$  (2) after Marsland and Randolph (1977) represents the peak undrained shear strength.

Torvane tests were also run in the field on Shelby tube samples immediately after recovery. The results of these tests as conducted on samples from Boring B-1 are included in Figure 28 along with

the  $S_u$  range interpreted from the UU, PMT and CPT results. Note the lower bound PMT and the Torvane results are remarkably similar. Both also follow the trend of the upper bound UU test data. The greater  $S_u$  measured by the PMT and Torvane is consistent with failure modes which are essentially independent of the effects of sample fabric discontinuities such as fissures.

#### Cone Penetrometer Tests

Indirect assessment of  $S_u$  can be obtained from results of the quasi-static cone penetrometer tests (CPT) as described in the Volume I report. The cone resistance ( $q_c$ ) assessment is related to the ultimate bearing capacity of the clay in accordance with Equation 5,

$$q_c = N_c S_u + \sigma_{vo} \quad (5)$$

where  $N_c$  and  $\sigma_{vo}$  are the cone (bearing capacity) factor and the total overburden pressure, respectively.  $N_c$  may be calculated if correlative  $S_u$  measurements are available or may be assumed. Correlation of  $N_c$  with the upper bound  $S_u$  measurements from the UU tests yield  $N_c$  values well above those reported in the literature. This may be the result of reduced  $S_u$  measurements due to the fissured structure of the clay.

It is of interest to evaluate, solely from soil properties, an undrained shear strength which is essentially unaffected by the fissured structure. Consequently, the CPT records included as Figures 29 and 30, were analyzed to characterize the average slope of those parts of the records where  $q_c$  increases approximately linearly with depth. In this analysis, the undrained shear strength, normalized with respect to the effective overburden pressure ( $S_u/\sigma'_{vo}$ ), can be expressed as a function of the measured  $q_c/\sigma'_{vo}$  in accordance with Equation 6:

$$\frac{S_u}{\sigma'_{vo}} = \frac{1}{N_c} \frac{(q_c - \sigma_{vo})}{\sigma'_{vo}} \quad (6)$$

As  $S_u/\sigma'_{vo}$  has also been shown to be uniquely expressed as  $K(OCR)^n$ , it follows that the  $n$  and  $K$  parameters can be readily determined from Equation 6 if  $N_c$  is assumed. Equation 7 has been derived from  $N_c = 20$ , which represents a typical upper bound value for non-structured clays:

$$S_u/\sigma'_{vo} = 0.43 (OCR)^{0.85} \quad (7)$$

The specific solutions were  $K = 0.44$  and  $0.43$  and  $n = 0.83$  and  $0.87$  for CPT locations No. 1 and No. 2, respectively.

Figure 28 represents the variation of  $S_u$  with depth for  $N_c = 20$  in accordance with Equation 5. Also shown on this figure are the upper limits of  $S_u$  as determined by the UU, torvane, and pressuremeter tests.

#### Summary

Application of the  $S_u$  data presented in Figure 28 to drilled shaft capacity analysis must consider that shaft-soil interface failure will not be substantially controlled by the random orientation of the fissured structure of the Beaumont clay. However, some degradation of the  $S_u$ , as represented by the homogeneous elements of the soil mass should be anticipated. Such tests as the PMT and Torvane would be expected to yield the highest "baseline" strength profiles; whereas "upper bound" UU strength would represent a more conservative and more conventional reference "baseline" (Fig. 31).

From an applied practice view, the undrained shear strength characterization for application to shaft design must consider:

- a. Only a limited number of routine shear tests are typically provided.
- b.  $S_u$  measurements should be made by only one type of shear test to preclude differences due to different failure modes.
- c. Laboratory shear tests of fissured clays should be conducted on 1.4-in.-diameter specimens so as to minimize the effects of fissures.
- d. Tests should be conducted in such a manner so as to prevent changes in water content prior to and during shear.

Based on these considerations, it is concluded that the unconsolidated undrained triaxial test represents the most practical and conservative representation of  $S_u$  for highly structured soils such as the fissured Beaumont clays. It is also concluded that the best UU strength reference is that which is least affected by fissuring.

A sufficient number of samples should be run so as to define an upper bound of the variation of  $S_u$  with depth. For design purposes, the upper bound  $S_u$  "baseline" may be reduced so as to empirically simulate any degree of strength degradation desired. CPT data calibrated to the upper bound UU strength clearly provides a superior method for  $S_u$  profile characterization.

## PART X: DEFORMATION CHARACTERISTICS

Both the drained and undrained characteristics of the Beaumont clays encountered at the site have been characterized from laboratory tests on representative samples. Drained deformation behavior has been investigated by consolidation tests; whereas the undrained deformation has been investigated by both UU and CIU tests as described below.

### Drained Deformation Parameters

One-dimensional virgin compression ( $C'_c$ ) and recompression ( $C'_r$ ) indices have been derived from the consolidation tests in terms of axial strain. The variation of  $C'_c$  with liquid limit is shown by Figure 32. These data can also be used to estimate the drained deformation moduli ( $E_d$ ) as a function of the change in vertical stress ( $\Delta\sigma_v$ ) and the effective overburden pressure ( $\sigma'_{vo}$ ) in accordance with Equation 8:

$$E_d = \frac{\sigma'_{ave}}{0.435C} \frac{(1 + \nu)(1 - 2\nu)}{(1 - \nu)} \quad (8)$$

Where  $\sigma'_{ave}$  \* is less than the maximum past pressure ( $\sigma'_{vm}$ ), then  $C = C'_r$ ; otherwise  $C = C'_c$ . Poisson's Ratio ( $\nu$ ) for the stiff overconsolidated clay is estimated to be on the order of  $0.25 \pm 0.05$ .

### Undrained Deformation Parameters

The undrained modulus ( $E_u$ ) and the axial strain of UU test specimens have been calculated for a stress level corresponding to one-half of the maximum deviator stress. Figure 33(a) presents  $E_{50}$  as a function of consolidation pressure ( $\sigma'_c$ ). The strain ( $\epsilon$ ) corresponding to 50 percent of the maximum deviator stress ( $\epsilon_{50}$ ) is also shown as a function of OCR in Figure 33(b). The data points corresponding to the upper

---

\*  $\sigma'_{ave} = \sigma'_{vo} + \Delta\sigma_v/2$

bound  $S_u$  test data which are least affected by fissures within the test specimens are identified on these figures.

An alternative interpretation relating  $E_{50}/S_u$  to OCR indicates that Beaumont clay does not behave similarly to typical overconsolidated clays in that  $E_{50}/S_u$  increases rather than decreases with OCR. This is undoubtedly the result of the fissured structure of the clay. This observation is also consistent with the  $E_u$  interpretations made from the pressuremeter tests and presented in Table 11. It is noted that moduli interpreted from the PMT and UU tests are within a similar range, the upper bound from the UU tests being somewhat greater.

## PART XI: INTERFACE SHEAR CHARACTERIZATION

The subsequent interpretations of the soil-mortar interface tests follow the interface shear and moisture migration study procedures used by Chuang and Reese (1969) and O'Neill and Reese (1970). The objective of these interpretations is to relate the ultimate resistance in direct shear of the soil-mortar to the undrained strength of the soil in direct shear as a simulation of drilled shaft friction behavior. The postulated mechanism is that the soil in contact with the drilled shaft (mortar) takes on water from the fresh concrete (mortar) and loses strength so that the ratio of shaft friction to the undrained shear strength of the soil becomes less than unity. This ratio is generally termed the Cohesion or Alpha Factor in design applications. A summary of the Alpha Factors calculated for each test set is given in Table 12.

### Natural Water Content Versus Alpha Factor

The Alpha Factor versus the natural water content of the interface shear test specimens is plotted on Figure 34. Also superimposed on this figure is a regression line representing the test results of moisture migration studies made by Chuang and Reese (1969) on a variety of undisturbed samples. Note that this line falls below all but one point derived from this study. It is also evident that the scatter of the test data is fairly large.

### Failure Plane Water Content Versus Alpha Factor

The largest water content measured from a series of test on samples taken at and in near proximity to the failure plane of the test specimen have been related to the Alpha Factor as shown on Figure 35. Also indicated on this figure is a similar relationship developed by O'Neill and Reese (1970) using the average of all their test data. The data from this study seem to fall just below the O'Neill and Reese line and to have a very similar trend.



As would be expected, the scatter of the data seems to be somewhat less than that shown for the natural water content versus Alpha Factor plot. However, Figure 35 is sensitive to the choice of the failure plane location during the testing. As described in Part III, the failure plane for the testing was set at  $3/8$  in. from the mortar-soil interface, consistent with the findings of O'Neill and Reese that maximum water content after moisture migration usually occurs at a  $3/8$ -in. offset from the mortar-soil interface. This offset then represents the location of the lowest shearing resistance.

The test results are also sensitive to the variation of natural water content which occurs over very small distances within the samples as demonstrated by Figures 36 through 39. This is further demonstrated by the irregularity of the measured change in water content of the clay from the natural to after-test state. For example, of the eleven test samples described in Table 6, five indicated a positive moisture content change and six indicated a negative moisture content change (Table 12). Thus, the reliability of Alpha prediction from moisture migration data is of a low order when applied to a complex structured clay such as the Beaumont formation.

#### Change In Water Content Versus Alpha Factor

The moisture content change versus Alpha Factor obtained from the mortar-soil interface tests conducted as part of this study are summarized in Figure 40. Also indicated in this figure are similar data points derived from the published O'Neill and Reese (1970) data. It is evident that the latter data base is essentially random and that any derived relationship would have an extremely low correlation coefficient. From the limited data obtained from this study, there does appear to be some trend of decreasing Alpha Factor with a reduction in moisture content change expressed algebraically. However, the consolidated data scatter reinforces the perceived insensibility of the moisture migration technique to highly structured or otherwise micro-heterogeneous soils.

### Interface Shear Characterization

In addition to investigation of the mortar-soil interface shearing resistance ( $\tau_f$ ) by laboratory tests, a similar study has been conducted in-situ by borehole shear tests. The characterization of  $\tau_f$  by both of these methods is described as follows.

#### Laboratory Tests

It is concluded that prediction of the Alpha Factor from moisture migration tests has a relatively low reliability in soils such as the Beaumont clays. The use of the interface shear results to characterize the shaft friction represents an alternate approach which deserves some study. In this regard, the interface shear strength has been shown as a function of the effective normal stress on the plane of shear ( $\sigma'_n$ ) as in Figure 13. The regression line through the data expresses the peak interface shear in terms of  $\sigma'_n$ , the interface cohesion ( $c_i$ ) and the interface friction angle ( $\delta$ ) in accordance with Equation 9:

$$\tau_f = 0.30 + \sigma'_n \tan 18.2 \quad (9)$$

Note that  $c_i = 0.30$  tsf and  $\delta = 18.2$  degrees suggests a partially undrained shear behavior.

A comparison of the foregoing data with the results of direct shear tests given in Figure 11 shows the direct shear and the interface shear expressions to be identical. The conclusion can only be that there is no significant difference between the mortar-soil and soil-soil failure in direct shear from a composite data standpoint. However, there is a significant difference between the interface shear and the undrained shear strength as predicted from UU tests and other tests with differing failure modes than direct shear. As an example, Alpha Factors have been calculated from interface shear tests using the upper bound shear strength line of the UU tests as shown by Figure 28. The results of these calculations are shown in Table 13.

As indicated, the average Alpha Factor predicted from the interface shear and UU tests is approximately 0.48 for the CH soils. This corresponds to load test interpretations conducted in London clays by Skempton (1959), and Whitaker and Cooke (1966). For comparison, the average Alpha Factors reported by O'Neill and Reese were 0.40 to 0.44 (Shaft 1), 0.35 to 0.52 (Shaft 2) and 0.54 (Shaft 3), where these factors represent the peak and the ultimate shearing resistance.

#### In-Situ Borehole Shear Tests

A series of eight in-situ borehole shear tests was conducted as described in Volume I. The tests of interest to this characterization incorporated mortar shear plates to engage the sidewall of the borehole. The mortar plates were judged to yield a more realistic mortar-soil interface failure; whereas the conventional grooved steel plate appears to yield a failure plane in the soil.

Borehole shear test results were presented in Volume I. The interpretation of these tests results above the groundwater level and of three tests conducted below the water level are summarized in Table 14.

From Table 14, it is evident that the above groundwater tests yield essentially drained test results when compared to Figure 25. Further, the interface friction angle ( $\delta$ ) appears to correspond to the effective friction angle of the soil; e.g., there is no reduction in  $\phi'$ . There is, however, some indication that interface cohesion ( $c_i$ ) may be less than  $c'$  from CIU tests not significantly influenced by the fissured structure of the clay. The  $c_i$  parameter also appears to be sensitive to the time of consolidation (see Tests 1A and 2A).

The tests below groundwater level resemble consolidated undrained tests in that  $\delta$  is reduced by at least one-half. This effect can also be seen to some degree from the results of Test No. 3 where water was added to the borehole.

In summary, it is likely that the boundary effects of the small size of the mortar shear plates (1.5 x 2.8 in.) prevented the development of representative interface shear behavior. It can be concluded,

however, that the borehole shear test shows promise as an in-situ test to investigate the shear strength properties of subsoils which are not unduly disturbed by preparation of the access hole.

## PART XII: SOIL PROPERTY CHANGES WITH TIME

During the field investigations at the test site, horizontal samples were obtained from an access shaft. The samples were jacked at various levels below the surface approximately 4.3 ft to the concrete face of Shaft S-3. The 4-1/2 inch O.D. thin-wall tube samples were subsequently tested to determine the variation in water content and undrained shear strength with horizontal distance from the shaft. The results of these tests are summarized herein and are compared to similar original test data presented by O'Neill and Reese (1970).

### Water Content Variation

The water content was determined at 1-in. horizontal intervals on horizontal samples taken at depths below the ground surface of 7, 11, 15 and 19 ft. The results of these tests are shown in Figures 36 through 39. For comparison, the O'Neill and Reese data are shown in each figure for the closest comparative elevation. Note that the original tests extended 2-1/2 in. from the shaft face; whereas the current data extend at least 23 in. With one exception, the sampling depths of the two studies have a 1-ft difference in elevation.

### Natural Variation

From review of Figures 36 through 39, it is evident that there is as much as four percentage points difference in water content over distances of as little as 2 in. This variation can also be observed on a macro-scale as evidenced by Figure 4 and by the standard deviations of water content within each generalized stratum (Table 1). A well-defined trend in the water content distribution away from the shaft face is not evident except at the 19-ft depth. However, like the 19-ft record, there is a suggestion of a decrease in water content with distance from the shaft within an interval of about 7 to 15 in.

### Data Comparison

In comparing the initial and current water content data distribution, it is evident that only gross trends are meaningful considering the extreme natural water content variation in the Beaumont clay. Further, an exact match in sampling depths for the two data bases is obtained only at the 15-ft sampling depth. Any conclusions from comparison of the two data bases would, therefore, tend to be highly subjective.

In all cases, the O'Neill and Reese data show water content maximums within 1/8 in. of the face of the concrete shaft for the 2-1/2-in. interval tested. Note that with the natural variation, a higher water content would be likely at greater distance from the shaft. Comparison of the two data sets indicate a gross difference only at the 15-ft test level. As indicated by Figure 38, the current water content measurement is about 4.5 percentage points above the original data within the interval of comparison. This appears to be consistent with the rise in the original groundwater level (15 ft) to the current level (11 ft from the surface). It is also pertinent to note that at this level the depth of the data bases coincide. Other changes in water content since the time the original data were obtained are not evident and the differences between the data are well within the range of natural variation.

### Undrained Shear Strength Variation

The variation in undrained shear strength with horizontal distance from the shaft face was investigated as a potential indicator of the change in soil properties with time since construction of the test shaft. Consequently, pocket penetrometer tests on the horizontal samples were conducted as an index to the undrained shear strength. Four penetrometer tests were conducted for each inch of the sample length. The variation of the average penetrometer measurement and with variation of one standard deviation from the mean are shown in Figures 41 through 44 as a function of distance from the shaft face.

#### Natural Variation

Similar to the water content data, it is evident from Figures 41 through 44 that there is a significant variation in shear strength over very small distances within the deposit. Undoubtedly, the variation indicated is accentuated by variations inherent in the pocket penetrometer test and in the complex fissured structure of the clay.

Data trends are evident only at the 11-ft test depth (Fig. 42). Here there is a well-defined increase in strength at increasing distances from the shaft face. However, this trend is not clearly evident at any of the other test levels. Conversely, a reverse trend (although not as well defined) is shown at the 7-ft test level.

#### Data Comparison

In the absence of initial and current data which can be directly compared, a comparison of the pocket penetrometer data made closest to the shaft with similar data made from the test borings has been made. This comparison is shown on Figure 45 which incorporates data from both the original and current test borings. As indicated, the near shaft data are less than the mean of the O'Neill and Reese data at two levels, approximately equal to and significantly greater than the mean strength at the remaining two test depths. Consequently, no apparent correlation is evident concerning the relationship between the near shaft and free field shear strength of the subsoils.

PART XIII: LITERATURE CITED

Al-Layla, M.T.H. 1970. Study of certain geotechnical properties of Beaumont clay, Ph.D. Thesis, Texas A&M University at College Station.

American Society for Testing and Materials. 1980 annual book of ASTM standards, Part 19, soil and rock; building stones.

Bishop, A.W. and Henkel, D.J. 1962. The measurement of soil properties in the triaxial test, 2nd Ed. Edward Arnold, Ltd., London.

Bishop, A.W., et. al. 1971. A new ring shear apparatus and its application to the measurement of residual strength. Geotechnique. Vol 21, (4):273-328.

Brooker, E.W. and Ireland, H.R. 1965. Earth pressure-at-rest related to stress history. Canadian Geotechnical Journal. Vol II (1).

Bureau of Yards and Docks. 1971. Soil mechanics, foundations and earth structures, Department of the Navy, Design Manual, NAVDOCKS DM-7, Washington, D.C.

Burmister, D.M. 1951. The application of controlled test methods in consolidation testing, ASTM Special Technical Publication No. 126, pp. 83, ASTM, Philadelphia, PA.

Casagrande, A. 1936. "The Determination of the Preconsolidation Load and its Practical Significance", Proceedings 1st International Conference on Soil Mechanics & Foundation Engineering, Cambridge, MA, pp. 60.

Chandler, R.J. 1966. The measurement of residual strength in triaxial compression. Geotechnique. Vol 16, (3): 181-186.

Chuang, J. W., and Reese, L. C. 1969. Studies of shearing resistance between cement mortar and soil, Research Report 89-3, Center for Highway Research, University of Texas at Austin, Austin, Texas.

Gardner, W.S. 1977. Soil property characterization in geotechnical engineering practice. Geotechnical/Environmental Bulletin, Vol X, (2), Woodward-Clyde Consultants, San Francisco.

Gibson, R.E. and Anderson, W.F. 1961. In situ measurement of soil properties with the pressuremeter. Civil Engineering. Vol 56: 615-620.

Kanji, M.A. and Wolle, C.M. 1977. "Residual Strength - New Testing and Microstructure," Proceedings of the 9th International Conference on Soil Mechanics and Foundation Engineering, Tokyo, Japan, Vol I: 153-154.



- Ladd, C.C. and Foott, R. 1974. New design procedure for stability of soft clays. *Journal of the Geotechnical Engineering Division, ASCE*. Proc. Paper 10664. Vol 100 (GT7):763-786.
- Lambe, T.W. 1951. *Soil testing for engineers*. John Wiley and Sons, Inc., New York.
- Lambe, T.W. and Whitman, R.V. 1969. *Soil mechanics*. John Wiley and Sons, Inc., New York.
- Marsland, A. and Randolph, M.F. 1977. Comparisons of the results from pressuremeter tests and large in situ plate tests in London clays. *Geotechnique*. Vol 27, (2):217-243.
- O'Neill, M.W. and Reese, L.C. 1970. Behavior of axially loaded drilled shafts in Beaumont clay, Research Report No. 89-8, Center for Highway Research, The University of Texas at Austin, Dec., 1970, 569 pp.
- Rutledge, P. 1944. Relation of undisturbed sampling to laboratory testing, Transactions ASCE. Vol 109, Paper No. 2229, pp. 1155-1216.
- Skempton, A.W. 1957. Discussion on "Planning and design of the New Hong Kong Airport," Proceedings of the Institute of Civil Engineers. Vol VII.
- U. S. Army, Office, Chief of Engineers. 1970. Laboratory soils testing, Engineer Manual EM 1110-2-1906.
- Whitaker, T. and Cooke, R.W. 1966. An investigation of the shaft and base resistances of large bored piles in London clay, Proceedings of Symposium on Large Bored Piles, London.

Table 1  
Summary of Physical Properties for Each Stratum

Stratum	Water Content (%)			Liquid Limit (%)			Plastic Limit (%)			Dry Unit Weight (pcf)			Specific Gravity		
	Max	Min	$\bar{x}$	Max	Min	$\bar{x}$	Max	Min	$\bar{x}$	Max	Min	$\bar{x}$	Max	Min	$\bar{x}$
① (CH) 0-17	30.2	22.3	25.4	70	51	60	26	18	22	108.7	92.3	99.9	2.68	2.60	2.63
② (CL) 17-20	26.1	20.1	23.5	55	41	47	27	18	21	105.6	99.7	102.9	2.62	2.62	2.62
③ (CH) 20-26.5	31.4	17.3	23.7	61	46	58	25	19	23	108.7	91.6	101.0	2.65	2.60	2.63
④ (CL) 26.5-29	26.3	20.1	23.2	25	25	25	15	12	13.5	104.6	92.2	99.9	--	--	2.60*
⑤ (CL-ML) 29-31	23.7	16.5	19.5	--	--	21*	--	--	16*	110.3	97.2	102.1	--	--	--
⑥ (CL) 31-34	--	--	15.2*	--	--	33*	--	--	13*	--	--	108.1*	--	--	--

\*Less than three data points.

Table 2(a)  
Summary of Unconfined Compression Test Data

Boring No.	Depth (ft)	w <sub>n</sub> (%)	γ <sub>d</sub> (pcf)	S <sub>u</sub> (tsf)	Remarks
B-2	0-2	24.6	103.2	0.27	
B-2	2-4	23.4	100.1	0.73	
B-2	4-6	23.7	96.4	0.30	Slickensided Failure
B-2	6-8	30.7	92.0	0.45	
B-2	10-12	32.7	94.2	0.34	Slickensided Failure
B-2	12-14	22.8	106.0	0.43	
B-2	14-15	23.4	105.9	0.62	Slickensided Failure
B-2	15-16	22.3	107.0	0.51	Slickensided Failure
B-2	18-20	24.5	104.3	1.01	
B-2	20-22	26.3	101.8	0.67	Slickensided Failure
B-2	22-23	31.4	94.7	0.57	Slickensided Failure
B-2	23-24	25.2	104.4	0.46	Slickensided Failure
B-2A	24-26	26.4	100.0	0.96	
B-2A	26-28	17.7	112.1	0.27	
B-2A	28-30	18.2	113.4	0.36	
B-2A	32-34	16.5	121.7	1.26	
B-3A	4-6	28.9	101.3	0.84	Slightly Slickensided Failure
B-3A	8-10	29.5	96.8	0.56	Slickensided Failure
B-3A	12-14	20.5	106.4	0.52	
B-3A	16-18	23.2	104.2	0.13	(Sample disturbed)
B-3A	24-26	27.4	98.1	0.51	
B-3A	30-32	16.2	120.0	1.29	

Note: The sample size is about 2.80 in. in diameter.

Table 2(b)  
Summary of Unconsolidated Undrained Triaxial Test Data

Boring No.	Depth (ft)	w <sub>n</sub> %	γ <sub>d</sub> pcf	σ <sub>c</sub> tsf	(σ <sub>1</sub> -σ <sub>3</sub> ) <sub>max</sub> tsf	1/2(σ <sub>1</sub> +σ <sub>3</sub> ) tsf	Diam (in.)	Remarks
B-1	3.0	23.9	100.2	0.22	0.96	0.480	2.87	
	10.4	11.8	106.7	0.67	0.86	0.430	2.36	
	20.0	24.0	102.6	1.50	3.20	1.600	2.00	
	25.4	22.7	104.6	2.0	3.63	1.815	2.00	
	30.4	16.5	114.4	2.6	2.90	1.450	2.36	
V-1	4.5	21.6	103.7	0.31	2.05	1.025	2.80	
	5.0	24.0	102.5	0.31	2.14	1.070	2.00	
	5.5	23.6	100.8	0.31	1.30	0.650	1.44	Slickensided Fissure Failure
V-5	18.5	25.7	99.7	1.08	2.20	1.100	2.80	
	19.0	25.1	101.7	1.08	2.35	1.175	2.00	
	19.5	24.1	105.3	1.08	2.90	1.450	1.44	

(continued)

Table 2(b) (Concluded)  
Summary of Unconsolidated Undrained Triaxial Test Data

Boring No.	Depth (ft)	w <sub>n</sub> %	γ <sub>d</sub> pcf	σ <sub>c</sub> tsf	(σ <sub>1</sub> -σ <sub>3</sub> ) <sub>max</sub> tsf	½(σ <sub>1</sub> -σ <sub>3</sub> ) tsf	Diam (in.)	Remarks
B-2A	14-16	25.1	99.8	0.79	0.29	0.145	2.80	Slickensided Failure
B-2A	18-20	27.8	101.2	0.94	1.76	0.880	2.80	
B-2A	22-24	25.8	101.2	1.08	1.22	0.610	2.80	
B-2A	26-28	30.4	100.6	1.23	0.68	0.340	2.80	
B-2A	32-34	22.9	95.0	1.51	0.37	0.185	2.80	
B-3A	4-6	26.0	98.4	0.36	0.97	0.485	2.80	
B-3A	8-10	30.3	94.8	0.65	0.64	0.320	2.80	
B-3A	12-14	26.0	99.1	0.79	0.92	0.460	2.80	
B-3A	16-18	26.9	101.5	0.94	0.73	0.365	2.80	
B-3A	24-26	27.2	101.6	1.22	0.64	0.320	2.80	

Table 2(c)  
Summary of Data from Consolidated Undrained (CIU) Triaxial Compression Tests

Boring and Sample Number	Sample Depth (ft)	Test No.	W <sub>o</sub> (%)	W <sub>f</sub> (%)	Y <sub>d</sub> (pcf)	LL (%)	PL (%)	σ <sub>c</sub> max (tsf)	σ <sub>c</sub> (tsf)	σ <sub>c</sub> max / σ <sub>c</sub>	At (σ <sub>1</sub> -σ <sub>3</sub> ) max.				A at (σ <sub>1</sub> /σ <sub>3</sub> ) max.	E <sub>50</sub> (tsf)	E <sub>50</sub> /s <sub>u</sub>	Strain Rate (1/hr)	H/D Ratio	Remarks	
											σ <sub>1</sub> -σ <sub>3</sub> (tsf)	ε (%)	A <sub>f</sub>	σ <sub>1</sub> /σ <sub>3</sub>							
B-1	8.0	1	27.5	29.9	94.5	57	33	5.10	0.54	9.4	0.304	10.02	- .503	1.714	.555	170	559	3-inch Samples	STRAIN RATE FOR ALL TESTS = 2.54/hr	HEIGHT/DIAMETER RATIO FOR ALL TESTS = 2.0	
	13.5	2	24.1	26.3	100.8	51	31	5.55	0.70	7.9	0.448	15.38	- .133	2.094	.210	219	489				
	24.7	3	23.6	24.8	102.8	46	27	6.45	2.00	3.2	0.828	3.11	.322	2.128	.339	733	440				
	14.7	4	25.8	25.0	99.2	51	31	5.60	5.40	1.0	2.018	4.11	.541	2.254	.546	551	273				
	19.7	5	22.8	23.8	104.3	41	22	6.1	1.60	3.8	1.354	2.22	.213	3.644	.243	261	193				
	13.0	6	21.1	22.4	105.2	35	15	5.5	1.40	3.9	1.230	4.70	.082	3.053	.179	372	302				
	12.5	7	19.4	19.7	108.3	35	15	5.5	2.70	2.0	2.123	6.84	.120	2.940	.243	400	148				
V-6	22.7	8	18.6	21.3	105.9	58	35	6.3	2.00	3.2	1.500	12.00	.033	2.578	.292	343	69	6-inch diameter Samples			
	23.3	9	17.3	19.0	108.7	58	35	6.3	4.00	1.6	2.280	5.50	.281	2.678	.374	588	258				
B-1	8.5	10	25.1	24.5	98.2	57	24	5.2	12.00	1.0	3.168	4.41	.681	1.823	.680	1012	84	3-inch Samples			
	3.0	11	27.2	28.6	96.2	57	18	6.7	0.22	30.5	0.264	0.804	.143	4.651	.170	297	1125				

Table 3  
Beaumont Clay Direct Shear Tests: Peak Strength

Test No.	Tube No. Depth (ft)	$w_n$ (%)	$\sigma_n$ (tsf)	Final Water Content			Peak Strength $\tau_f$ (tsf)	$\tau_f/\sigma_n$
				Top 0-1/8	Middle 1/8-1/4	Bottom 1/4-3/4		
1	H-2 11.0	24.8	6.0	--	--	--	2.375	0.396
2	H-2 11.0	25.8	6.0	26.5	--	27.5	2.527	0.421
3	H-2 11.0	23.8	6.0	16.8	--	20.4	2.090	0.348
4	H-1 7.0	25.3	6.0	26.2	25.2	25.9	2.096	0.349
5	H-1 7.0	26.8	0.5	29.9	27.5	27.7	0.350	0.700
6	H-3 15.0	26.6	0.9	27.2	25.8	27.0	0.685	0.760
7	H-3 15.0	30.2	3.0	27.0	24.7	25.1	1.240	0.413
8	H-4 19.0	25.1	4.6	23.1	20.3	22.3	1.677	0.365
9	H-4 19.0	33.2	4.6	22.0	14.6	22.6	2.000	0.435
10	H-4 19.0	32.8	0.6 1.2 2.9	-- -- --	-- -- --	-- -- --	0.455 0.704 1.379	0.758 0.587 0.476

Table 4

Residual Shear Strength Summary

Sample No.	$W_n$ (%)	$I_p$ (%)	$\tau_f$ (tsf)	$\sigma'_n$ (tsf)	$(\sigma_1 - \sigma_3)_f$ (tsf)	$\sigma_{3c}$ (tsf)	$\sigma_n^*$ (tsf)
DS-1	30.2	38	0.205	0.90			
DS-2	24.1		0.264	1.80			
DS-3	25.7		0.484	2.70			
TX-1 (a)	29.9	36			0.45	0.50	0.56
TX-1 (b)					1.05	3.27	3.62
TX-1 (c)					1.95	6.00	6.64
TX-2 (a)	24.0	38			0.65	0.90	1.11
TX-2 (b)					0.70	1.80	2.03
TX-2 (c)					0.79	2.70	2.96
TX-2 (d)					1.49	4.00	4.49

$$* \sigma_n = \frac{\sigma_1 + \sigma_3}{2} + \frac{\sigma_1 - \sigma_3}{2} \cos 2\theta$$

$\theta$  = angle of the failure plane from horizontal

(Note that the two triaxial compression tests utilized staged testing techniques to facilitate the testing and assure sample uniformity.)



Table 5(a)  
Summary of Consolidation Test Results

BORING NUMBER	SAMPLE NUMBER	DEPTH (ft)	w <sub>n</sub> (%)	Y <sub>d</sub> (pcf)	LL (%)	PL (%)	e <sub>o</sub>	e <sub>f</sub>	C <sub>c</sub> <sup>(4)</sup> LAB	C <sub>f</sub> <sup>(4)</sup>	$\bar{\sigma}_{vo}$ (tsf)	PRECONSOLIDATION PRESSURE		
												(1)	(2)	(3)
B-1		7.67	24.9	95.0	57	24	0.748	0.730	0.119	0.025	0.469	5.9	6.8	12.0
B-1		12.3	24.2	102.9	50	20	0.601	0.636	0.080	0.027	0.753	2.6	2.4	5.1
B-1		19.3	22.7	101.7	41	19	0.609	0.593	0.090	0.017	1.047	3.9	2.8	6.0
B-1		24.3	23.7	92.2	46	19	0.723	0.754	0.096	0.029	1.197	3.5	3.2	6.4
(Dentison boring)	V-1	4.2	24.1	101.6	52	18	0.621	0.614	0.106	0.019	0.257	4.3	5.0	5.6
	V-2	6.7	28.0	92.3	58	22	0.766	0.728	0.109	0.024	0.410	3.0	3.1	5.1
	V-3	10.8	28.6	94.5	62	22	0.728	0.711	0.113	0.023	0.661	3.0	3.2	5.4
	V-6	22.6	31.4	91.6	58	23	0.797	0.781	0.115	0.030	1.146	3.6	3.2	6.3
B-2		7.0	27.7	-	57	24	0.729	0.577	0.139	0.040	0.428	5.4	8.0	8.0
B-2		15.8	22.1	-	62	24	0.665	0.486	0.150	0.030	0.942	6.0	6.0	6.0
B-2		23.0	23.1	-	53	23	0.586	0.479	0.126	0.044	1.158	5.0	-	5.0

- (1) Based on Casagrande method  
(2) Based on Rutledge method  
(3) Based on Burmister method  
(4) Unit Strain Basis

Table 5(b)  
Summary of  $K_o$ -Consolidation Test Data

Boring and Sample No.	Depth (ft)	$W_n$ (%)	LL	PL	$\sigma_c$ (tsf)	$\sigma_l$ (tsf)	$K_o$
V-6	22.3	27.9	66	23	0.36	0.39	0.92
					1.08	1.52	0.71
					1.44	2.15	0.67
					1.80	2.81	0.64
					2.16	3.38	0.64
					2.88	4.50	0.64
V-3	11.0	28.6	70	22	0.72	0.86	0.84
					1.08	1.46	0.74
					1.44	1.97	0.73
V-1	4.3	20.0	52	18	0.36	0.50	0.72
					0.72	1.06	0.68
					1.08	2.00	0.54
					1.44	2.67	0.54
					2.16	4.00	0.54
					2.88	5.33	0.55

NOTE: All samples trimmed from 6-in.-diameter samples (Denison boring).

Table 6  
Summary of Direct Shear Interface Property Test Data

Test No.	Boring	Depth (ft)	$w_n$ (%)	$\bar{\sigma}_n$ (tsf)	$w_f$ (%)			$\tau_I$ (tsf)	$\tau_I/\bar{\sigma}_n$
					Top 0-1/8"	Middle 1/8"-1/4"	Bottom 1/4"-3/8"		
1	H-2	11.0	24.2	3.30	24.2	24.6	24.0	1.537	0.466
2	H-2	11.0	25.3	0.54	25.0	28.2	31.1	0.467	0.865
3	H-2	11.0	24.5	6.0	26.0	20.7	25.0	2.456	0.409
4	H-1	7.0	26.0	0.54	27.3	27.1	27.1	0.769	1.424
5	H-4	19.0	34.0	1.50	25.1	25.4	25.6	0.829	0.553
6	H-4	19.0	19.1	4.60	24.2	23.3	23.6	1.477	0.321
7	H-1	7.0	27.9	6.0	23.3	20.5	24.3	2.230	0.372
8	H-1	7.0	27.7	6.0	25.6	--	27.0	3.130	0.522
9	H-3	15.0	25.3	0.87	24.4	23.7	22.8	0.616	0.708
10	H-3	15.0	24.6	1.80	22.5	21.8	23.6	1.056	0.587
11	H-3	15.0	26.8	2.70	22.7	19.8	25.8	1.085	0.402

Table 7  
OCR Interpretation from Soil Properties

Depth (ft)	$S_u^*$ (tsf)	$\frac{S_u}{\sigma'_{vc}}$	OCR**	
			n = 2/3	n = 3/4
4.75	1.07	3.60	33.0	22.4
7.5	1.15	2.45	18.6	13.4
10.0	1.20	1.92	12.8	9.7
15.0	1.42	1.75	11.2	8.5
20.0	1.60	1.65	10.2	7.9
25.0	1.82	1.62	9.9	7.7

\* From UU tests; upperbound  $S_u$  profile (Fig. 28)

\*\* For  $K = 0.35$

Table 8  
 $K_o$  Interpretation from Soil Properties

Depth (ft)	$I_p$ (%)	$\phi'$ (deg)	OCR*	OCR**		$K_o^*$	$K_o^{**}$	
				n=3/4	n=2/3		n=2/3	n=3/4
5.0	37	21.8	18.0	21.4	32.0	1.88	2.32	1.99
7.5	37	21.8	11.9	13.4	18.6	1.54	1.89	1.67
10.0	37	21.8	8.2	9.7	12.8	1.39	1.63	1.48
15.0	35	22.5	7.0	8.6	11.2	1.30	1.54	1.40
20.0	27	24.25	6.4	7.9	10.2	1.25	1.46	1.32
25.0	31	23.2	5.9	7.7	9.9	1.20	1.46	1.33

\* OCR from upperbound  $\sigma'_{vm}$  interpretation

\*\* OCR from upperbound  $S_u$  interpretation from UU tests

Table 9  
Interpretation of Stress State from Pressuremeter Tests

Depth (ft)	$\sigma'_{ho}$ (tsf)	$K_o$	$\sigma'_{hm}$ (tsf)	OCR <sup>*</sup>
5.58	0.45	1.22	2.1	6.0
9.50	1.05	1.78	3.7	6.2
10.83	1.40	2.06	4.0	5.9
15.83	1.53	1.39	5.9	7.0
20.83	1.33	1.19	5.2	5.2
25.83	2.02	1.58	7.8	6.8
30.50	2.02	1.42	4.5	3.5

\* Assumes  $\sigma'_{hm} = \sigma'_{vm}$

Table 10  
Summary of CIU Test Data Interpretations

Boring No.	Sample Depth	w <sub>n</sub> (%)	LL (%)	PI (%)	γ <sub>d</sub> (pcf)	$\bar{\sigma}_c$ (tsf)	Effective Strength Parameters	
							c' (tsf)	φ' (deg)
B-1	19.7	22.8	41	22	104.3	1.6	0.18	28.5
	13.0	21.1	35	15	105.2	1.4		
	12.5	19.4	35	15	108.3	2.7		
B-1	8.0	27.5	57	33	94.5	0.54	0.0	23.1
	13.5	24.1	51	31	100.8	0.70		
	24.7	23.6	46	27	102.8	2.00		
	14.5	25.8	51	31	99.2	5.40		
V-6	22.7	18.6	58	35	105.9	2.00	0.42	22.6
	23.3	17.3	58	35	108.7	4.00		

Table 11  
S<sub>u</sub> from Pressuremeter Tests

Depth (ft)	Soil Classification	Est. I <sub>p</sub> (%)	S <sub>u</sub> (tsf)		E+ <sup>*</sup> (tsf)	E/S <sub>u</sub>	
			**	†		**	†
5.53	CH	37	1.25	1.70	289	170	231
10.83	CH	38	1.29	1.48	396	268	307
15.83	CH	35	1.85	2.15	864	402	467
20.83	CL	35	2.31	2.90	441	152	191
25.83	CH	31	2.28	4.00	792	198	347
30.50	CL-ML	5	1.89	2.30	636	277	337

\* Represents the reloading cycle of the PMT.

\*\* Interpretation after Gibson and Anderson (1961).

† Interpretation after Marsland and Randolph (1977).

Table 12  
Summary of Calculations for Factor Alpha ( $\alpha$ )

Test No.	Boring	Depth (ft)	$w_n$ (%)	$w_f$ (%)	$\Delta w_n$ (%)	$\bar{\sigma}_n$ (tsf)	$T_I$ (tsf)	$T_S$ (tsf)	$\alpha = T_I/T_S$
1*	H-2	11.0	24.2	24.0	-0.2	3.3	1.537	1.384 1.552	1.111 0.990
2*	H-2	11.0	26.3	31.1	+4.8	0.54	0.467	0.477 0.547	0.979 0.854
3	H-2	11.0	24.5	25.0	+0.5	6.0	2.456	2.090 2.375 2.527	1.175 1.034 0.972
4	H-1	7.0	26.0	27.1	+1.1	0.54	0.769	0.350	2.197
5*	H-4	19.0	34.0	25.6	-8.4	1.50	0.829	0.793 0.896	1.045 0.925
6	H-4	19.0	19.1	23.6	+4.5	4.6	1.477	1.677 2.000	0.881 0.739
7*	H-1	7.0	27.9	24.3	-3.6	6.0	2.230	2.271 2.560	0.982 0.871
8	H-1	7.0	27.7	27.0	-0.7	6.0	3.130	2.096	1.493
9	H-3	15.0	25.3	22.8	-2.5	0.87	0.616	0.685	0.899
10*	H-3	15.0	24.6	23.6	-1.0	1.8	1.056	0.891 1.006	1.185 1.050
11*	H-3	15.0	26.8	25.8	+1.0	2.7	1.085	1.187 1.334	0.914 0.813

\*Values of  $T_S$  for these tests estimated from test data in Fig. 11.



Table 13  
Alpha Factor from Interface Shear Upper Bound UU Strength Reference

Depth (ft)	$K_o^*$	$S_u$ (tsf)	$\sigma'_n$ (tsf)	$\tau_f^\dagger$ (tsf)	$\tau_f/S_u$ ( $\alpha$ )
5.75	1.75	1.07	0.63	0.51	0.48
10.0	1.38	1.25 **	0.86	0.58	0.47
15.0	1.31	1.42 **	1.06	0.65	0.46
19.0	1.24	1.45	1.16	0.68	0.47
20.0	1.24	1.62	1.20	0.70	0.43
25.5	1.21	1.83	1.38	0.75	0.41

\* Estimated from Fig. 20.

\*\* Estimated from Fig. 7.

†  $\tau_f = 0.3 + \sigma'_n \tan 18.2^\circ$ ;  $\sigma'_n = K_o \sigma'_{vo}$

Table 14  
Summary of Borehole Shear Test Results

Test No.	Boring No.	Depth (ft)	Cohesion (tsf)	Friction Angle (Deg)	Remarks
1 & 1A	BHS-4	10.8-11.0	0.105	22.3	5 Minutes Consolidation
2 & 2A	BHS-4	11.3-11.7	0.040	24.4	30 Minutes Consolidation
3	BHS-3	7.2-7.5	0.085	24.1	
4	BHS-3	6.7-7.0	0.055	13.3	Water Added to Hole
5	BHS-1	22.0-22.2	0.080	10.4	Below Ground-water Level
6	BHS-2	18.8-19.0	0.060	10.8	Below Ground-water Level
7	BHS-5A	15.2-15.4	0.105	10.7	Below Ground-water Level

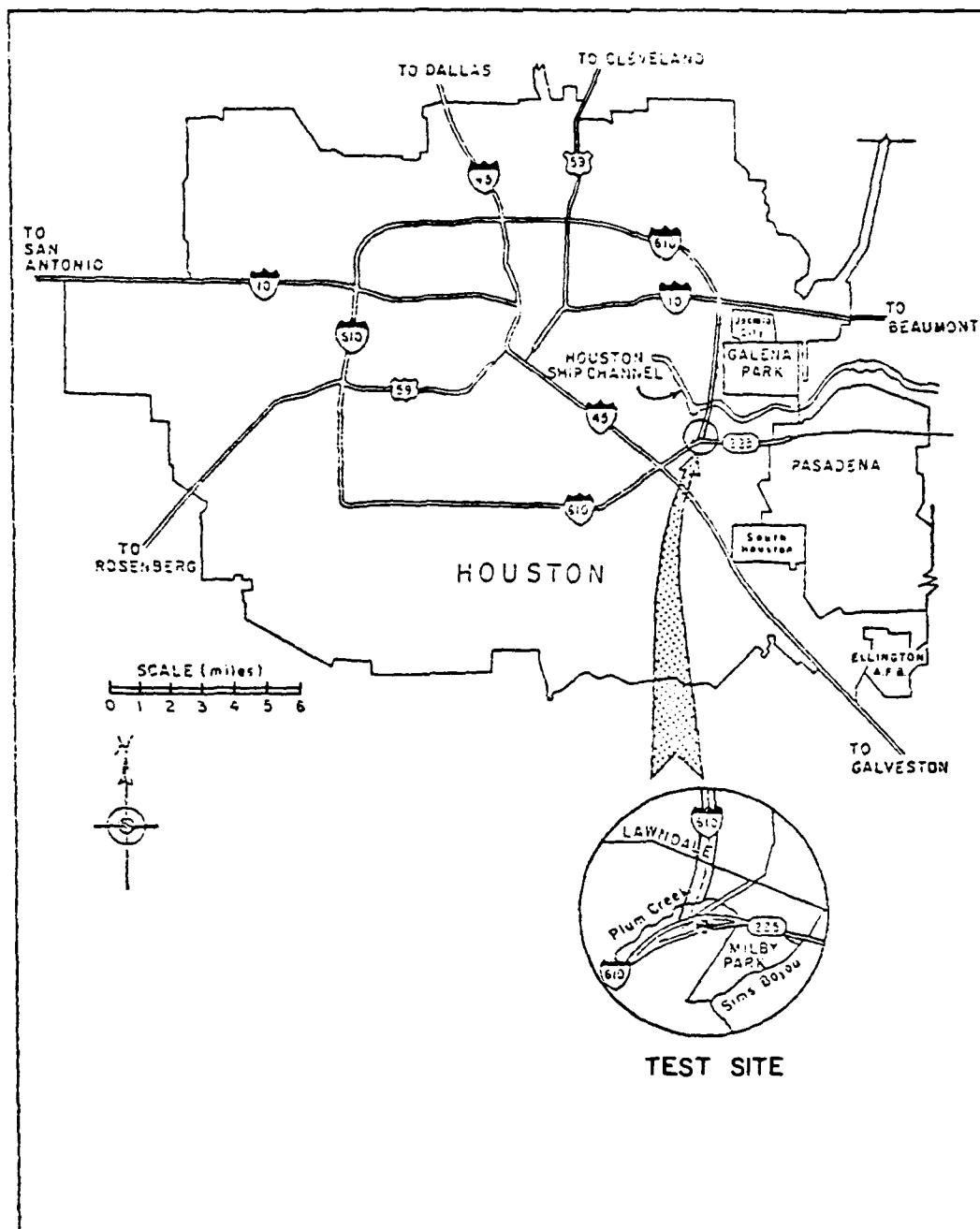
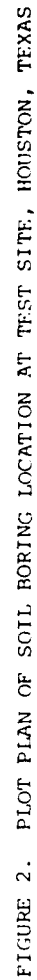


FIGURE 1. LOCATION MAP FOR THE SELECTED TEST SITE



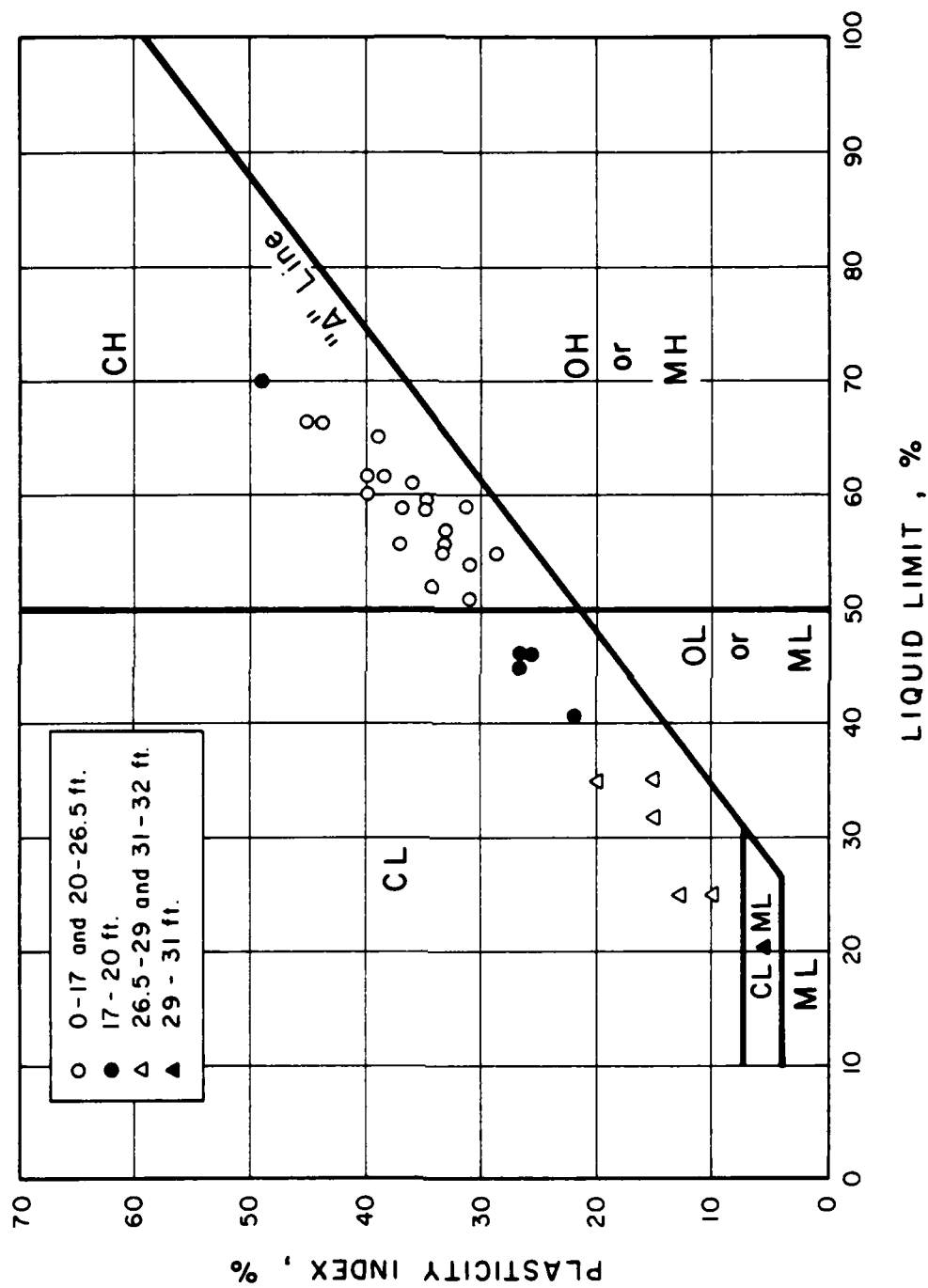


FIGURE 3. PLASTICITY CHART

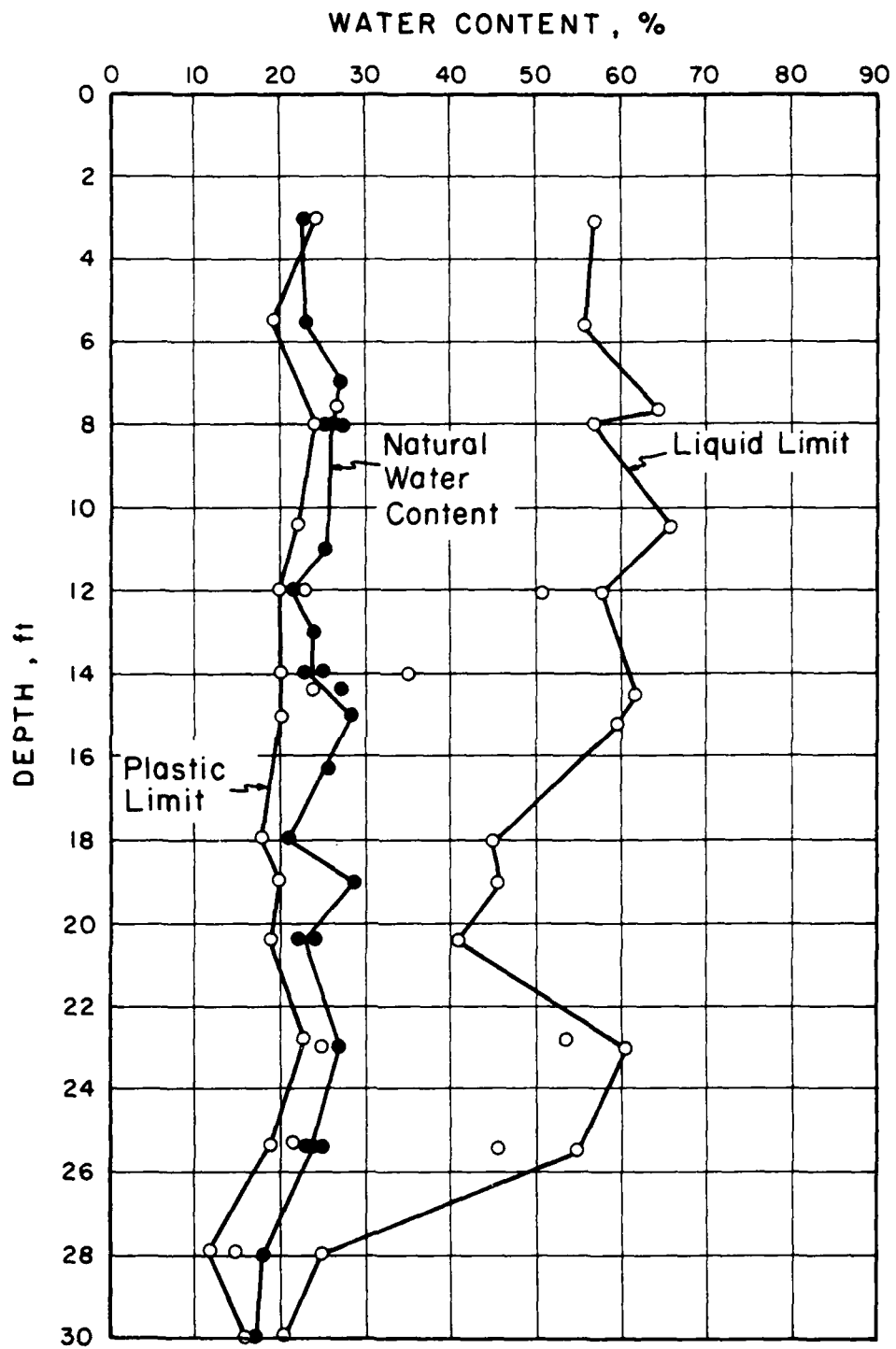


FIGURE 4. LIQUID AND PLASTIC LIMITS DATA

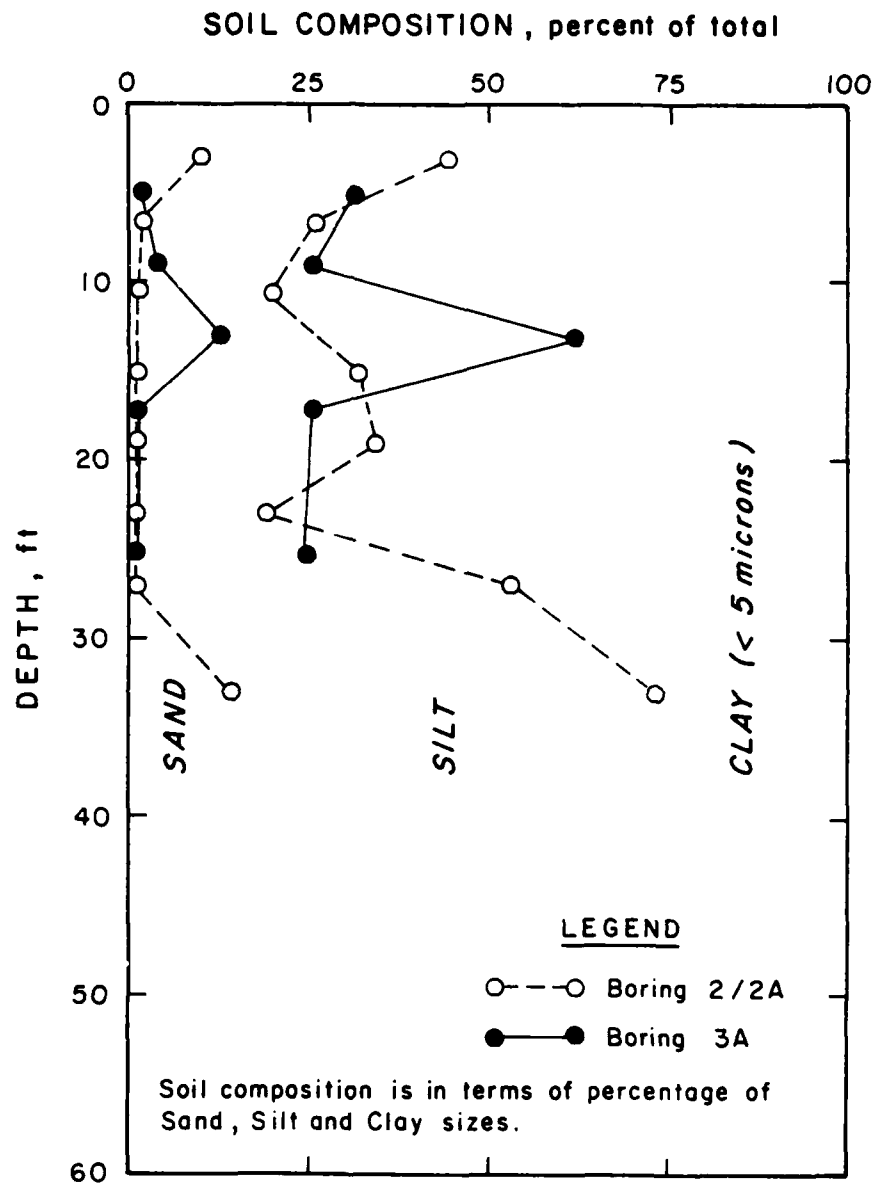


FIGURE 5. COMPOSITION OF BEAUMONT CLAY VS. DEPTH BELOW GROUND SURFACE

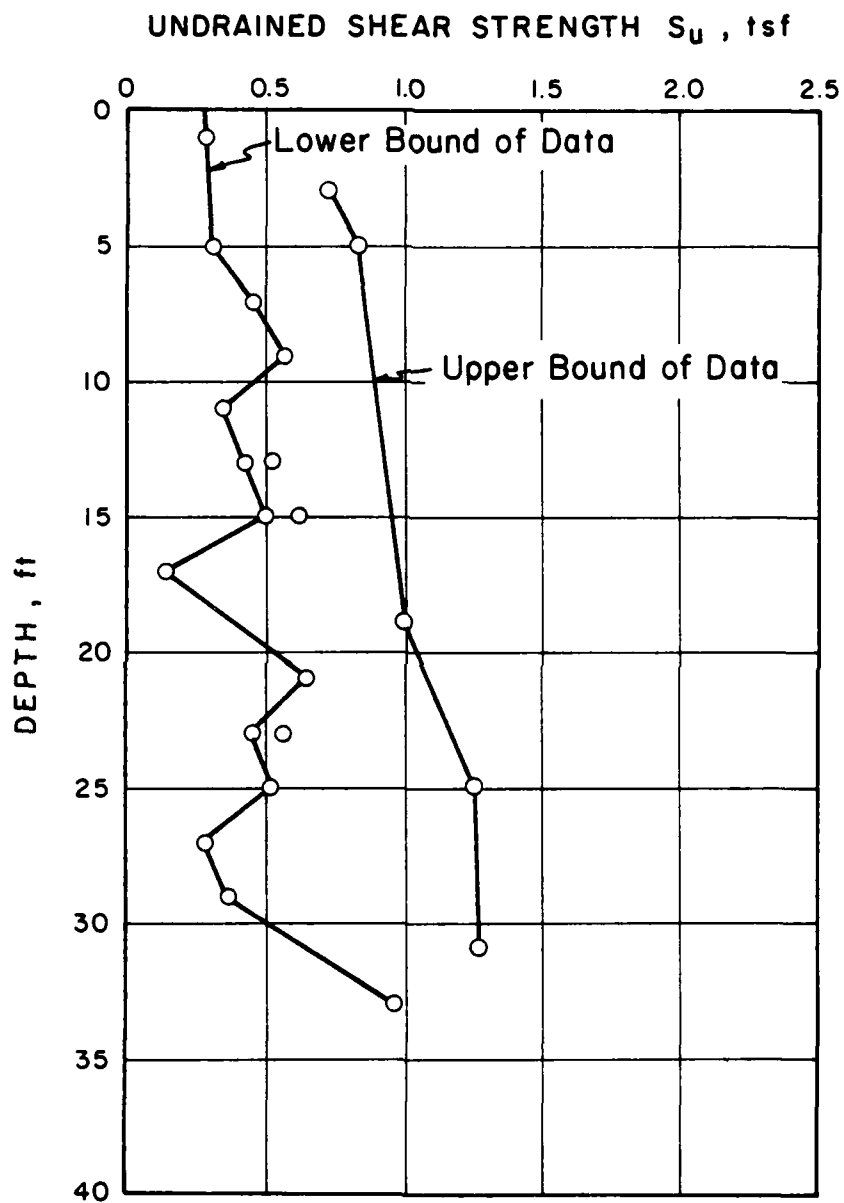


FIGURE 6. UNCONFINED COMPRESSION STRENGTH TEST RESULTS

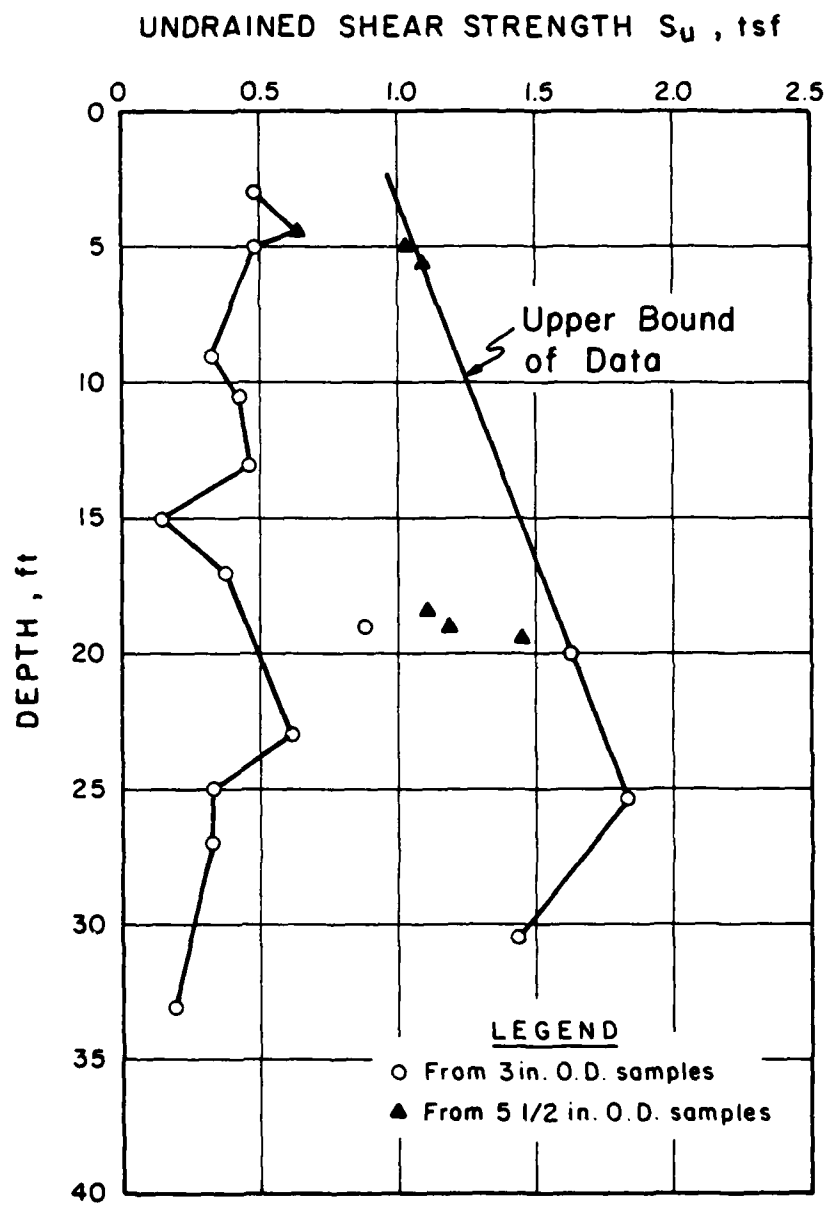


FIGURE 7. UNCONSOLIDATED UNDRAINED TRIAXIAL STRENGTH TEST RESULTS



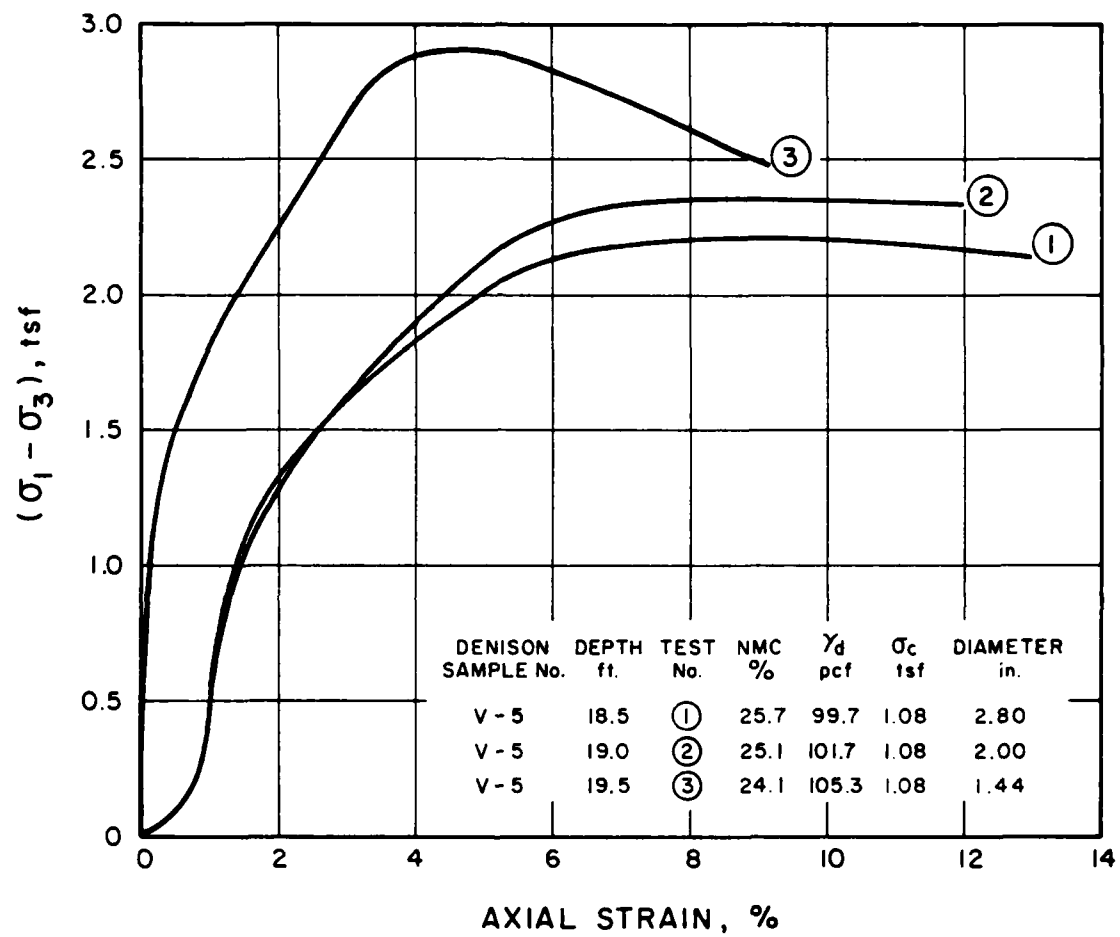


FIGURE 8. EFFECT OF SAMPLE SIZE  
AND FISSURE-CONTROLLED FAILURE  
ON UU STRENGTH (V-5)

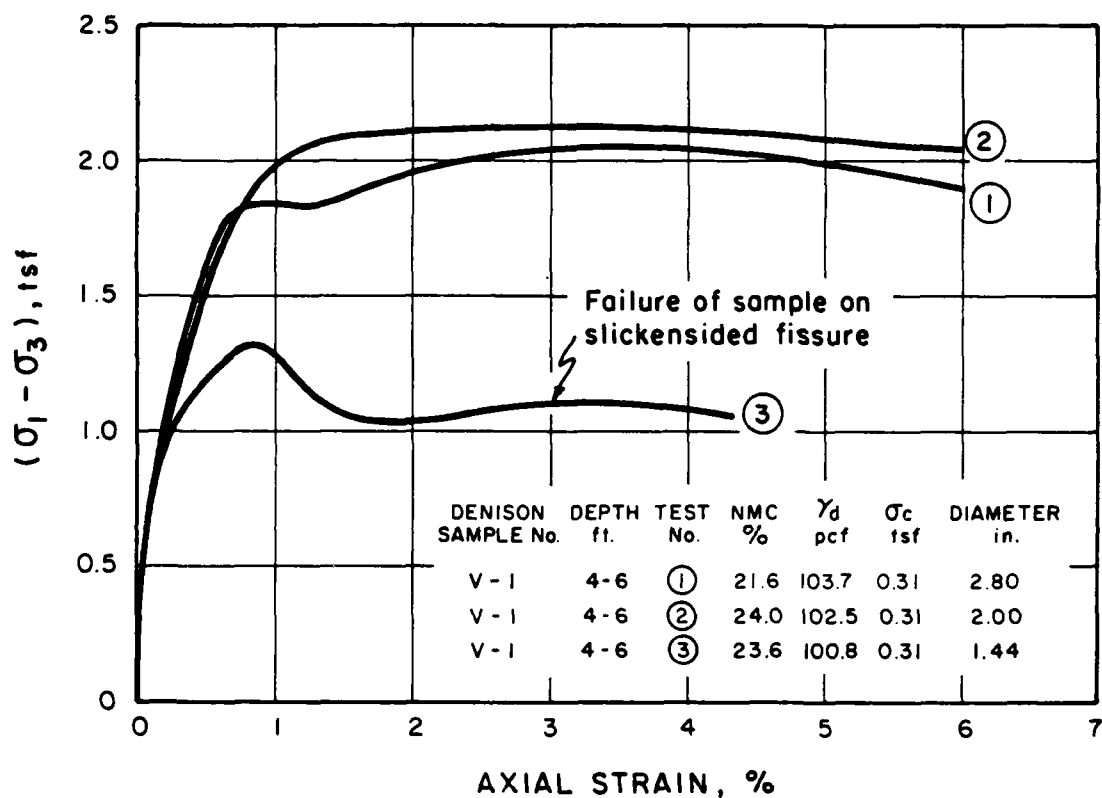


FIGURE 9. EFFECT OF SAMPLE SIZE  
AND FISSURE-CONTROLLED FAILURE  
ON UU STRENGTH (V-1)

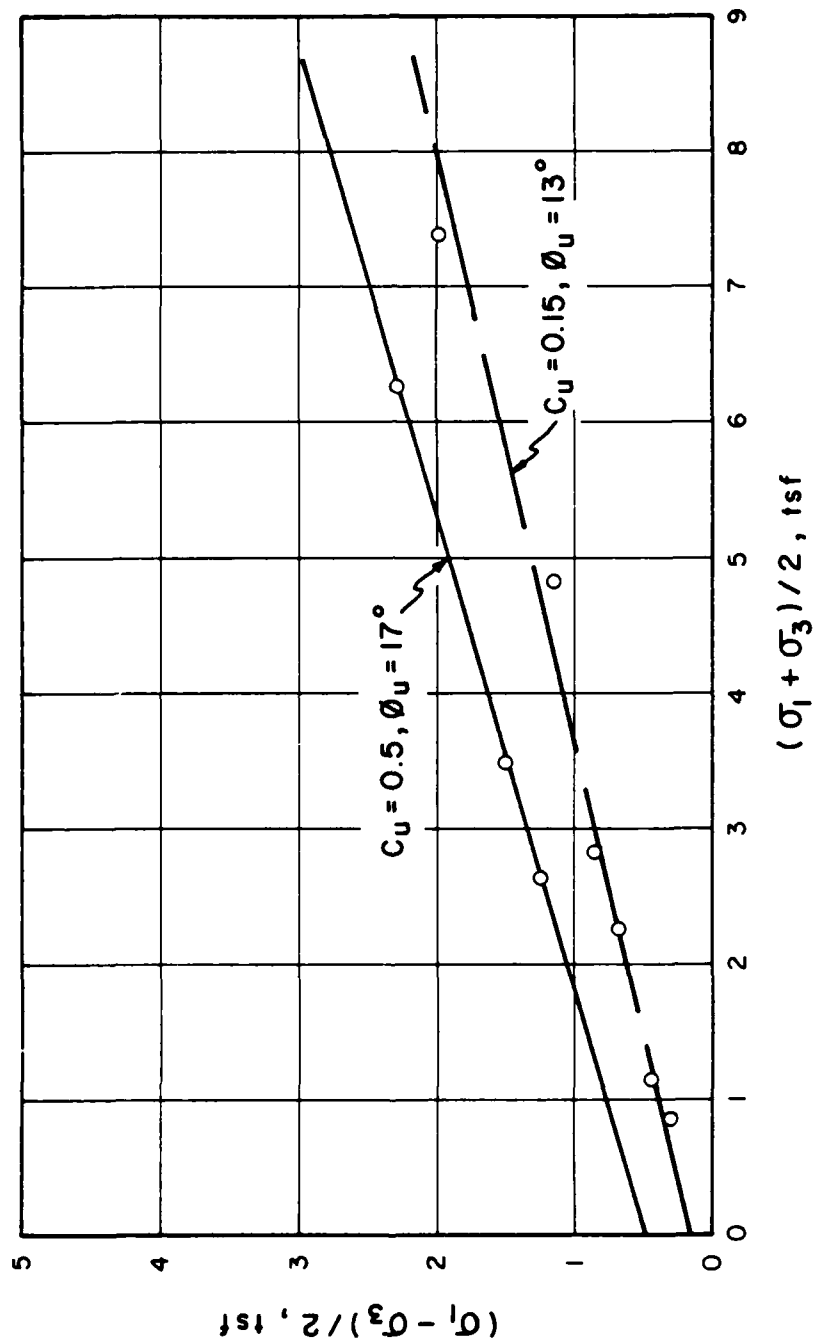


FIGURE 10. TOTAL STRESS INTERPRETATION OF CIU TESTS

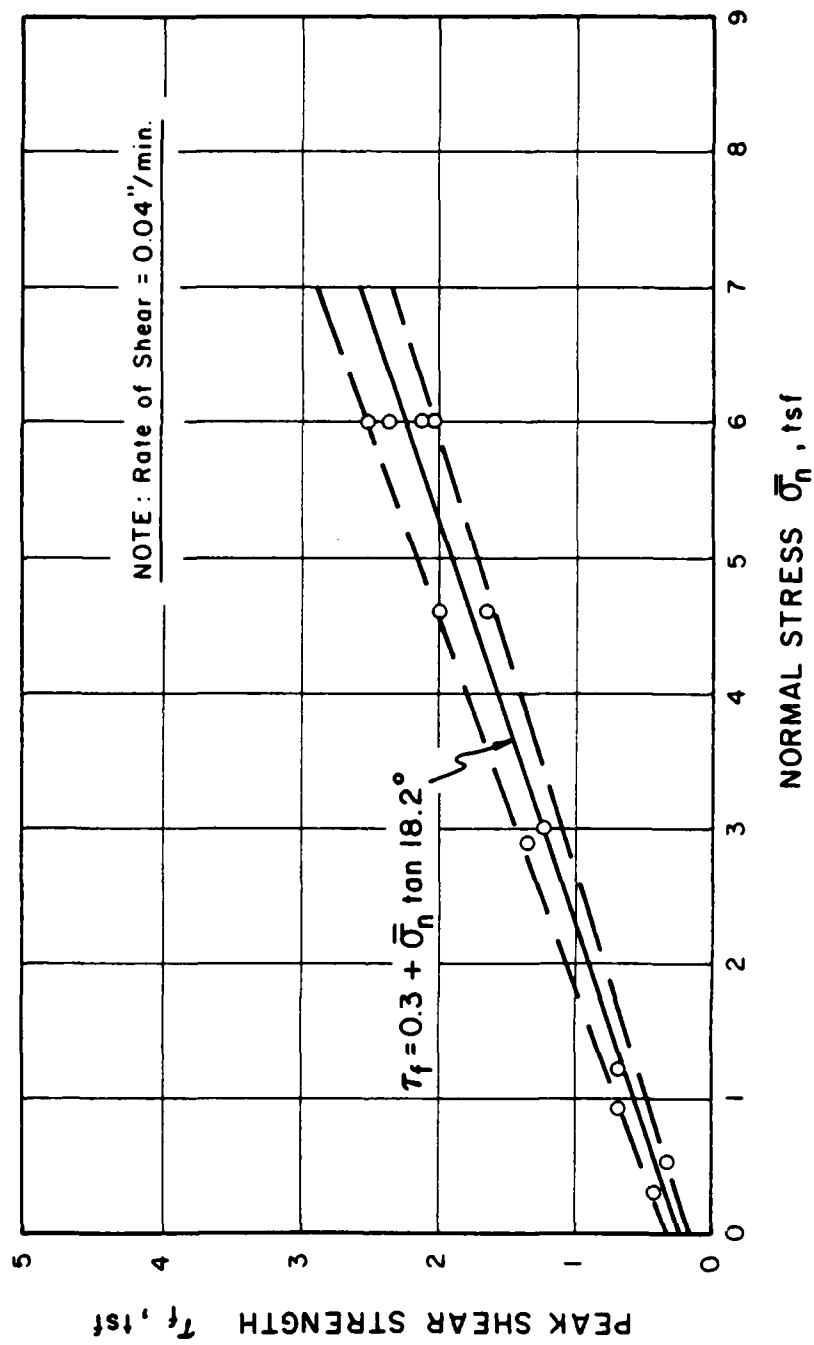


FIGURE 11. PEAK SHEAR STRENGTH FROM DIRECT SHEAR TESTS  
VS. EFFECTIVE NORMAL STRESS

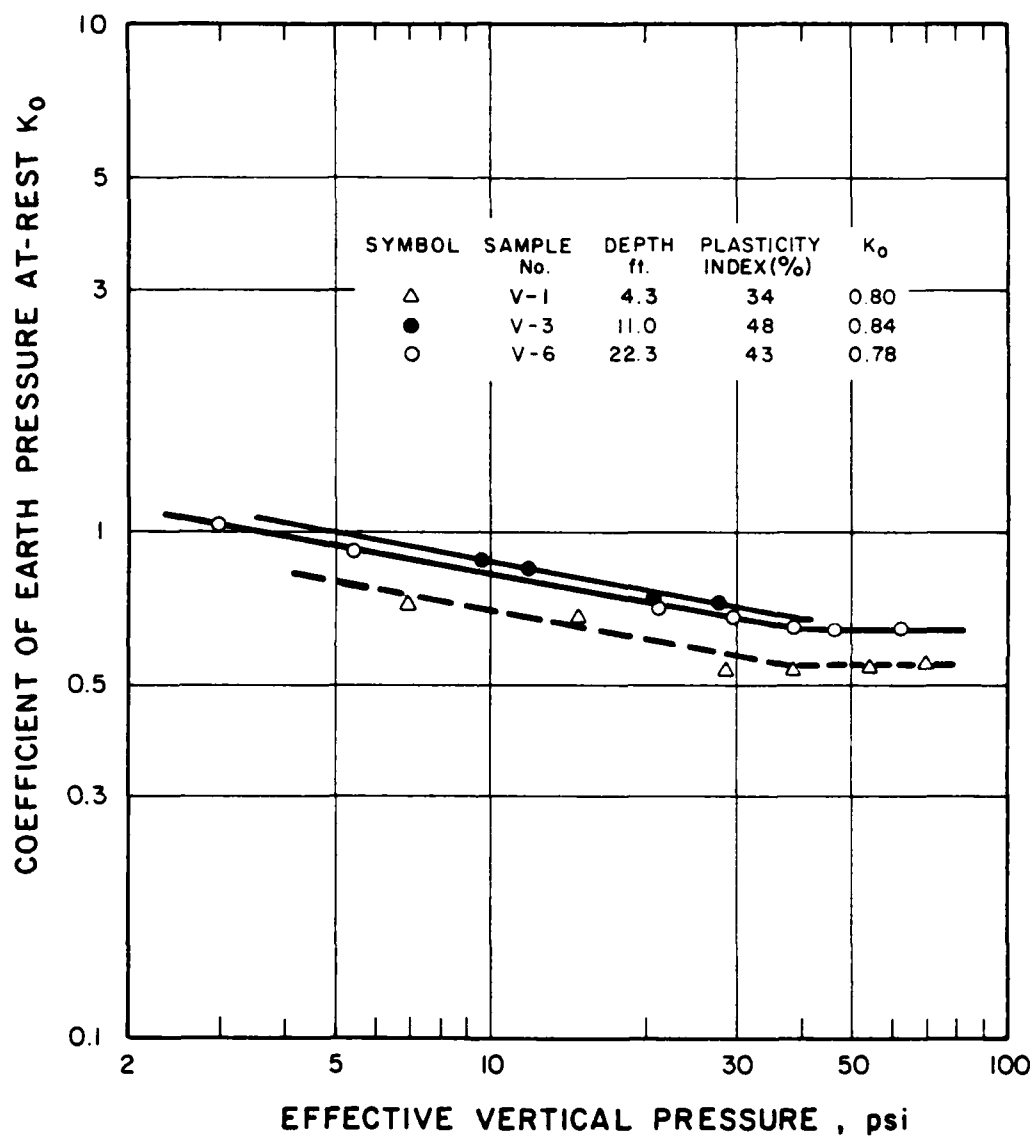


FIGURE 12. VERTICAL CONSOLIDATION PRESSURE VS.  
COEFFICIENT OF EARTH PRESSURE-AT-REST

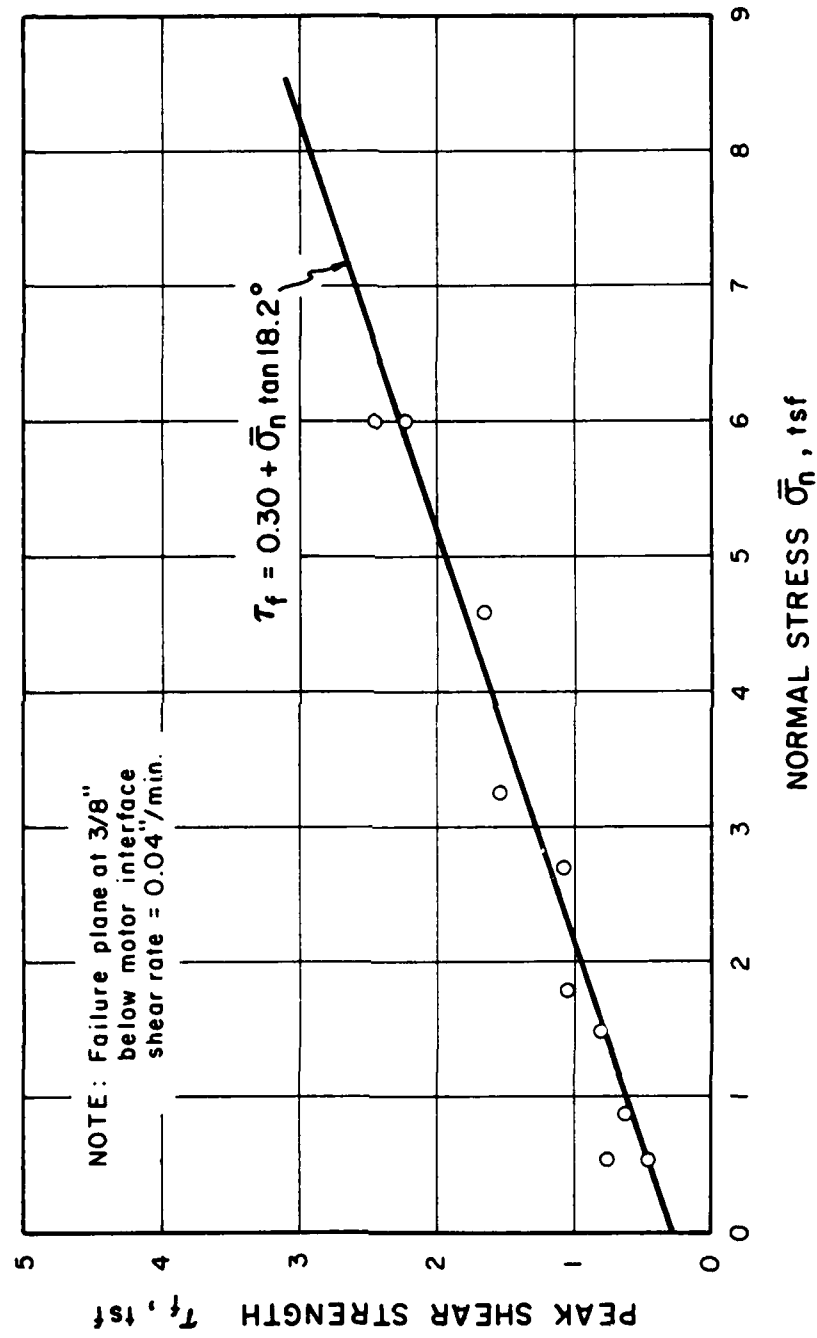


FIGURE 13. PEAK SHEAR STRENGTH FROM INTERFACE SHEAR TESTS  
VS. EFFECTIVE NORMAL STRESS

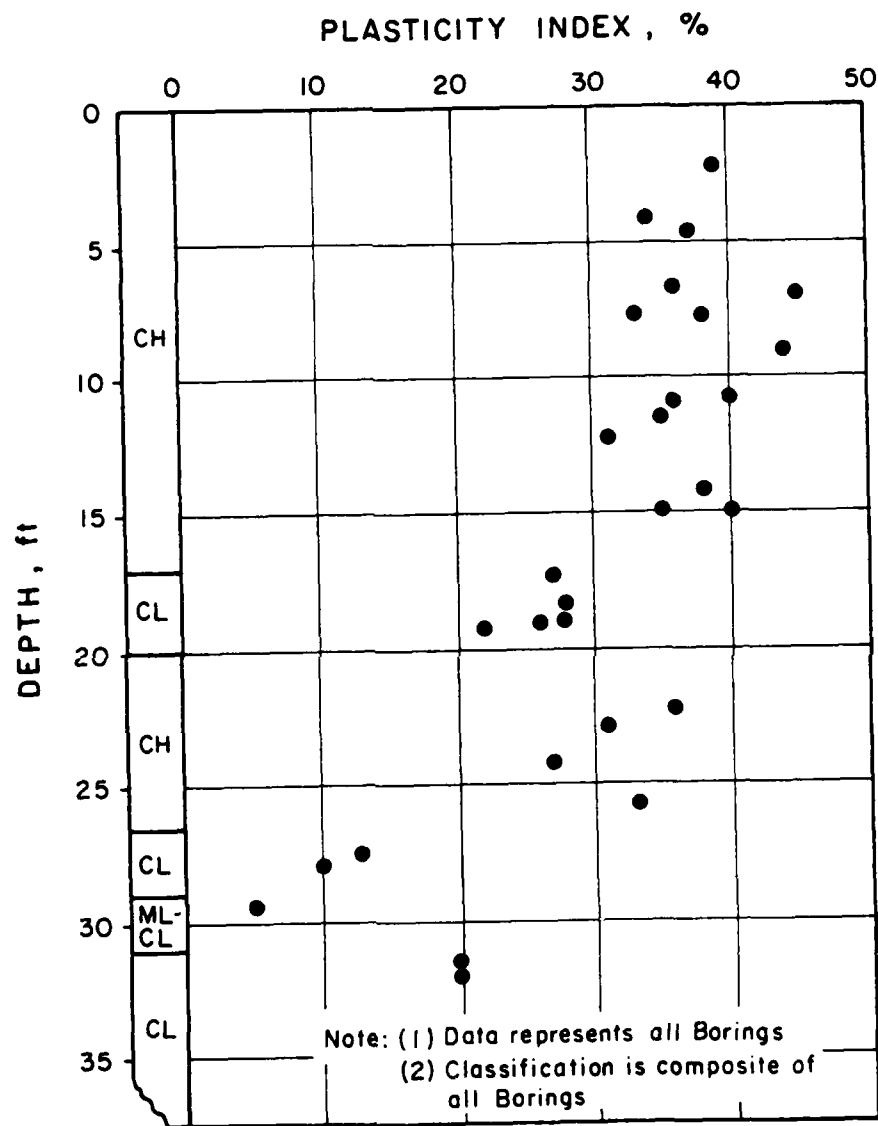


FIGURE 14. PLASTICITY INDEX AND CLASSIFICATION  
VS. DEPTH BELOW GROUND SURFACE

DEPTH, FT	STRATUM NO. & SOIL CLASSIFI.	W % n		PI %		LL %		$\gamma_d$ pcf	
		$\bar{x}$	s	$\bar{x}$	s	$\bar{x}$	s	$\bar{x}$	s
5									
10	① CH	25.4	2.3	37	4	60	5	111.7 (125)	4.1
(1980)									
15									
(1969)									
20	② CL	23.5	1.3	26	3	47	6	102.9* (127)	2.2
25	③ CH	23.7	4.9	32	4	58	6	101.0 (125)	7.3
30	④ CL	23.2	2.6	12*	-	25*	-	99.9 (123)	6.7
	⑤ CL-ML	19.5	2.6	5*	-	21*	-	102.1* (122)	4.5
35	⑥ CL	15.2*	-	20*	-	33*	-	108.1* (125)	-

\* REPRESENTS ONLY TWO TESTS  
 ( ) REPRESENTS ASSUMED AVERAGE TOTAL UNIT WEIGHT OF SOIL

FIGURE 15. IDEALIZED STRATIGRAPHY AND  
 SELECTED SOIL PROPERTIES



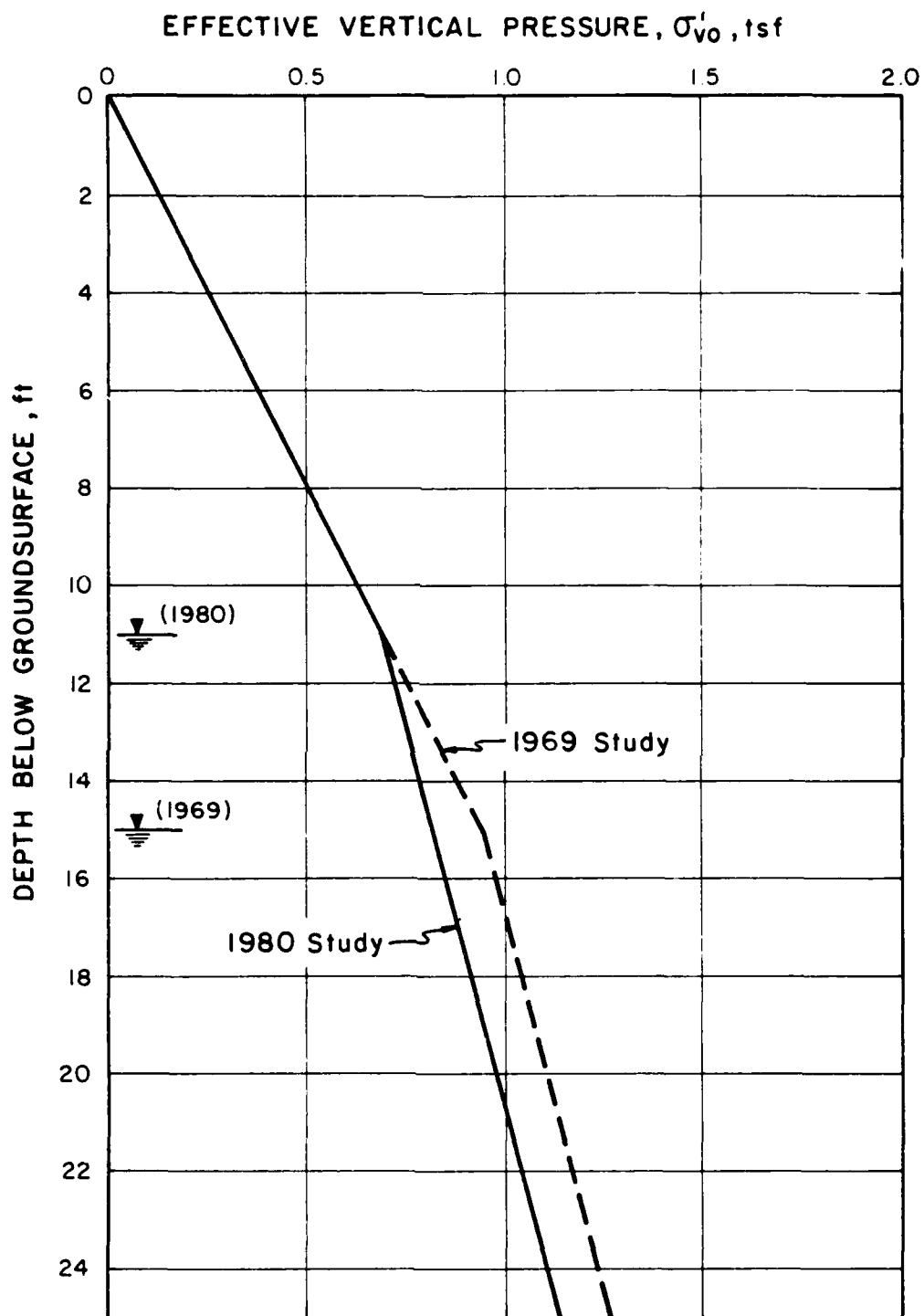


FIGURE 16. EFFECTIVE VERTICAL PRESSURE FOR  
GROUNDWATER LEVELS  
DURING 1969 AND 1980 STUDIES

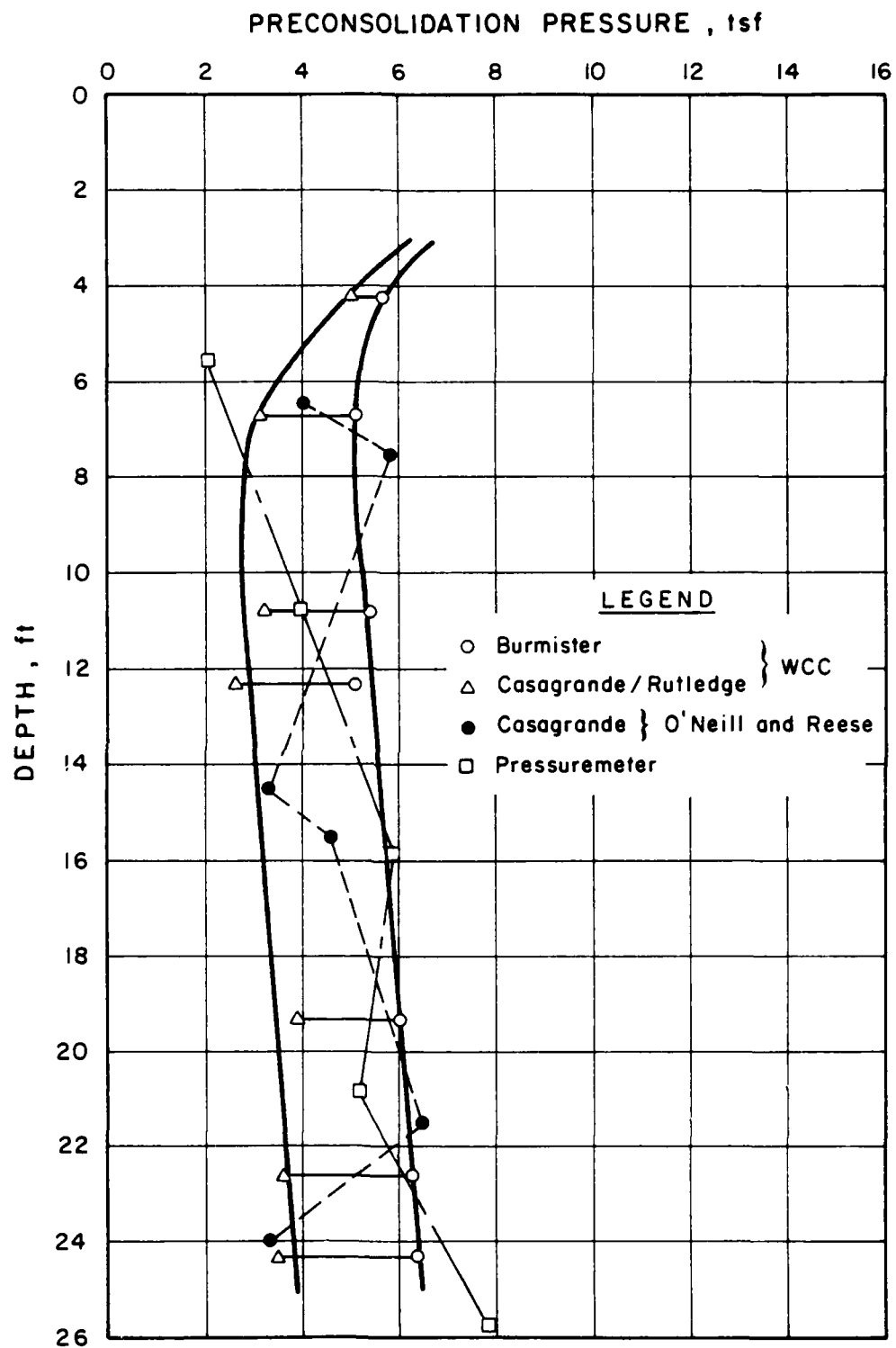


FIGURE 17. PRECONSOLIDATION PRESSURE INTERPRETATION FROM CONSOLIDATION AND PRESSUREMETER TESTS

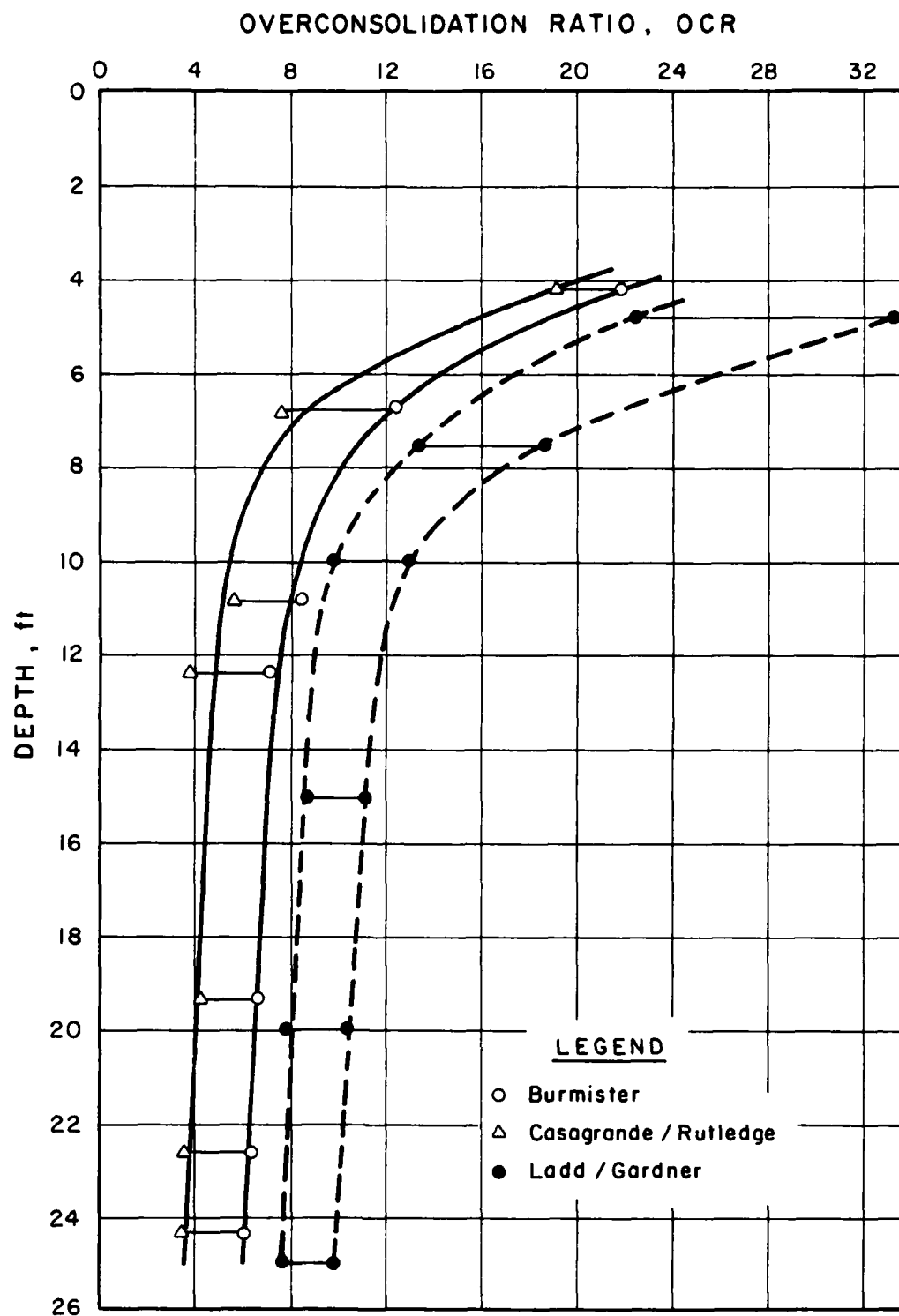


FIGURE 18. OVERCONSOLIDATION RATIO INTERPRETATION FROM CONSOLIDATION AND UU TESTS

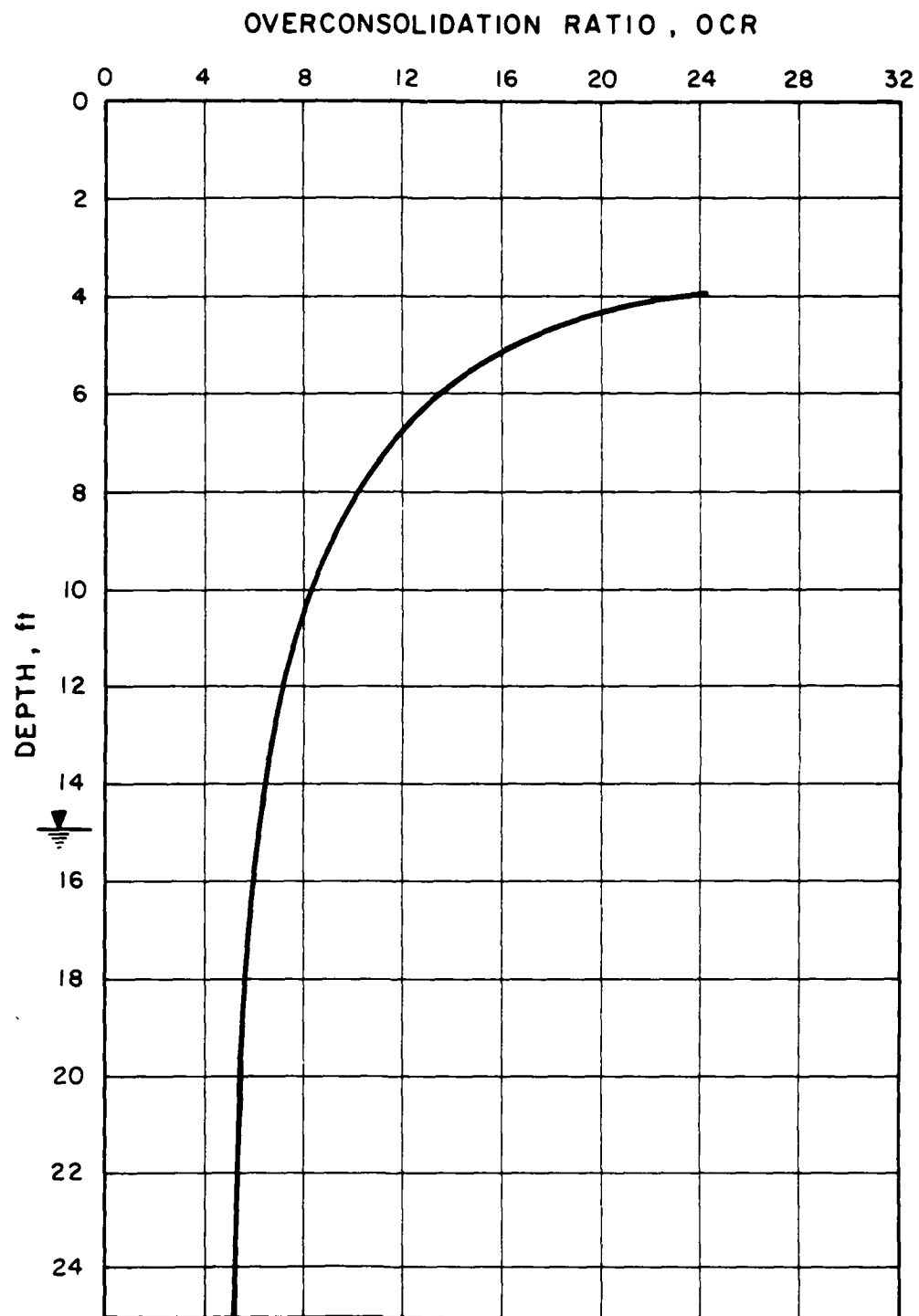


FIGURE 19. PREDICTED OVERCONSOLIDATION PROFILE  
FOR 15-FT GROUNDWATER LEVEL

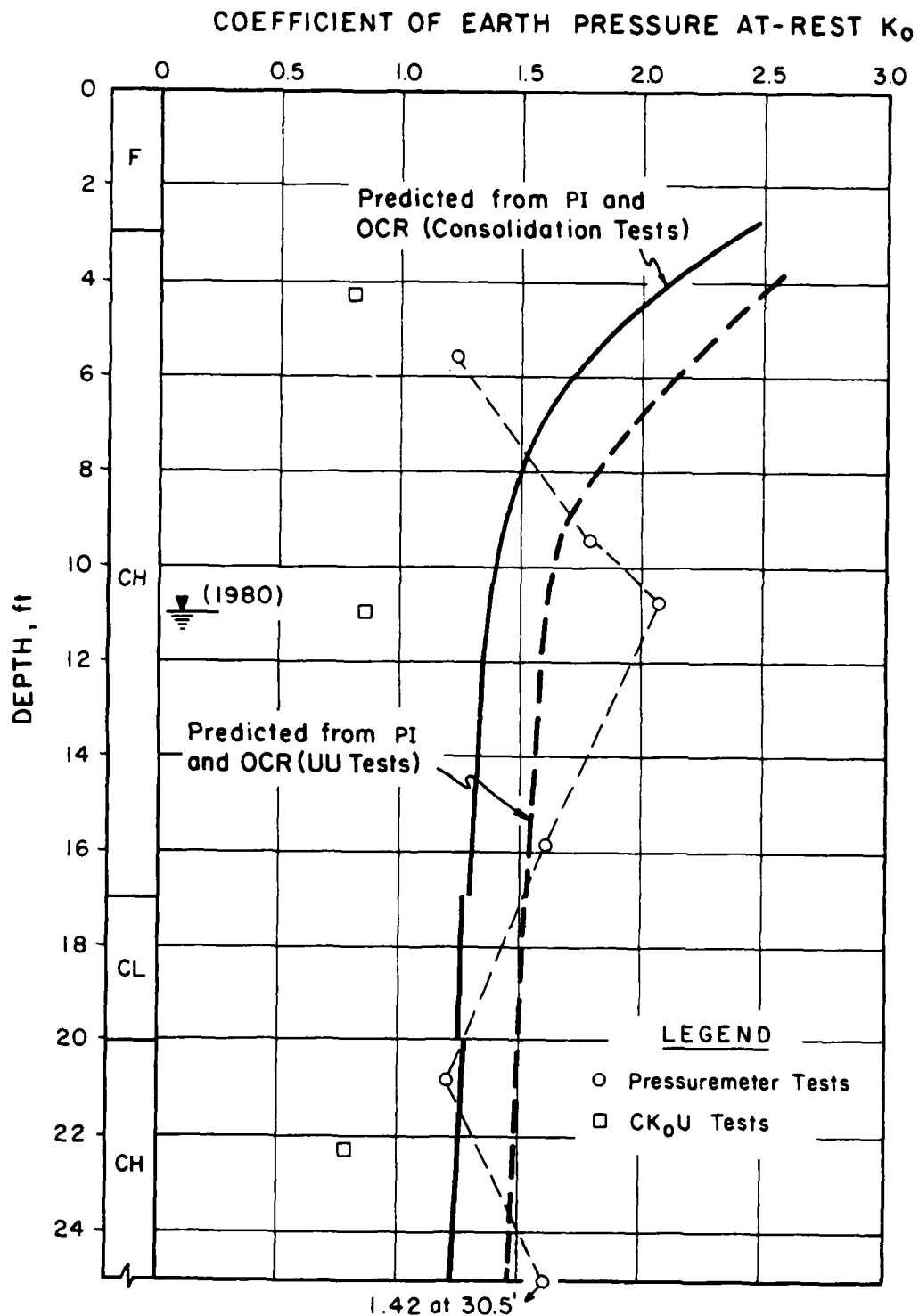


FIGURE 20. COEFFICIENT OF EARTH PRESSURE-AT-REST  
INTERPRETATION FROM  
LABORATORY AND PRESSUREMETER TESTS

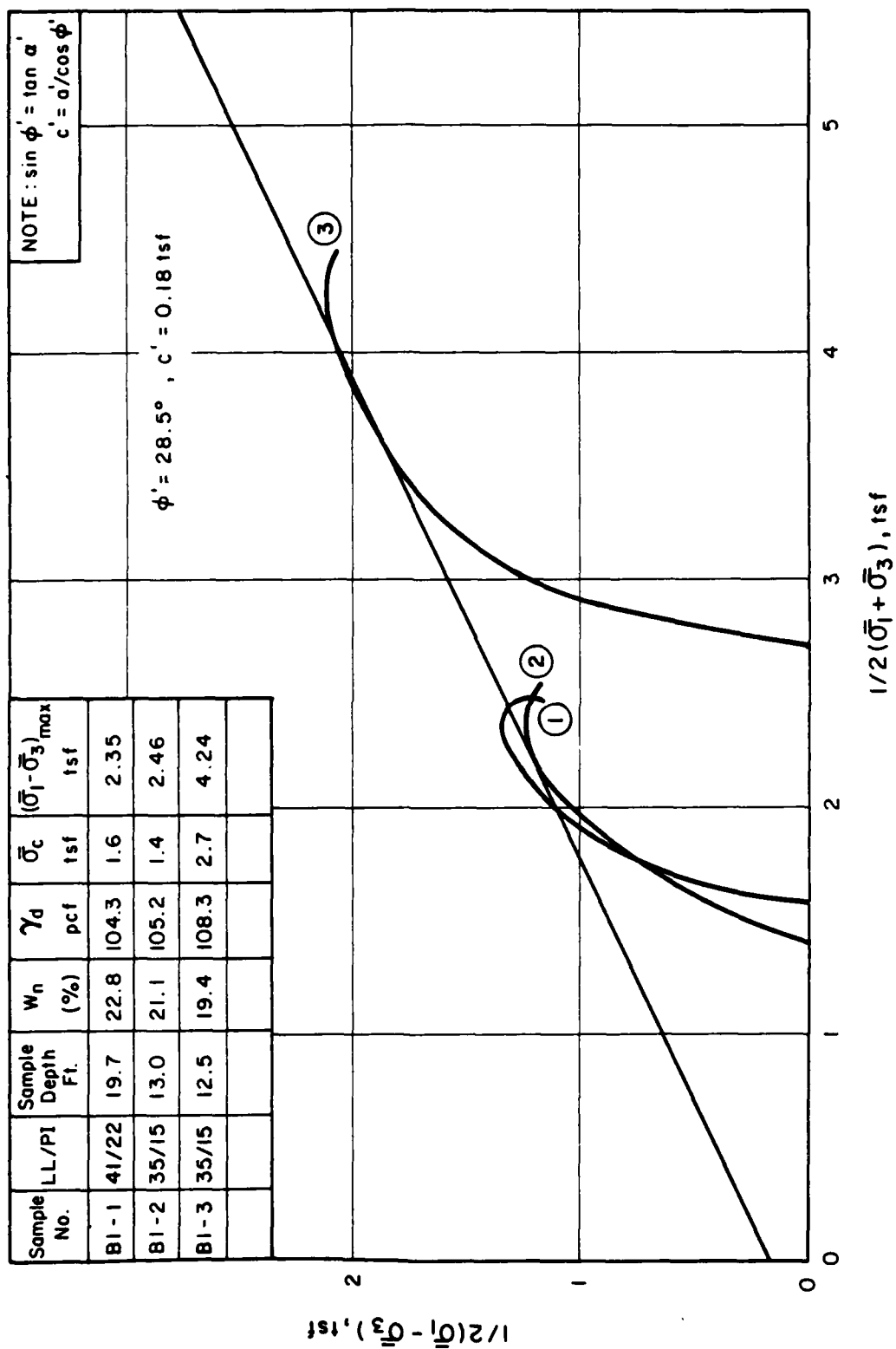


FIGURE 21(a). STRESS PATHS FOR CIU TESTS, BORING NO. B-1

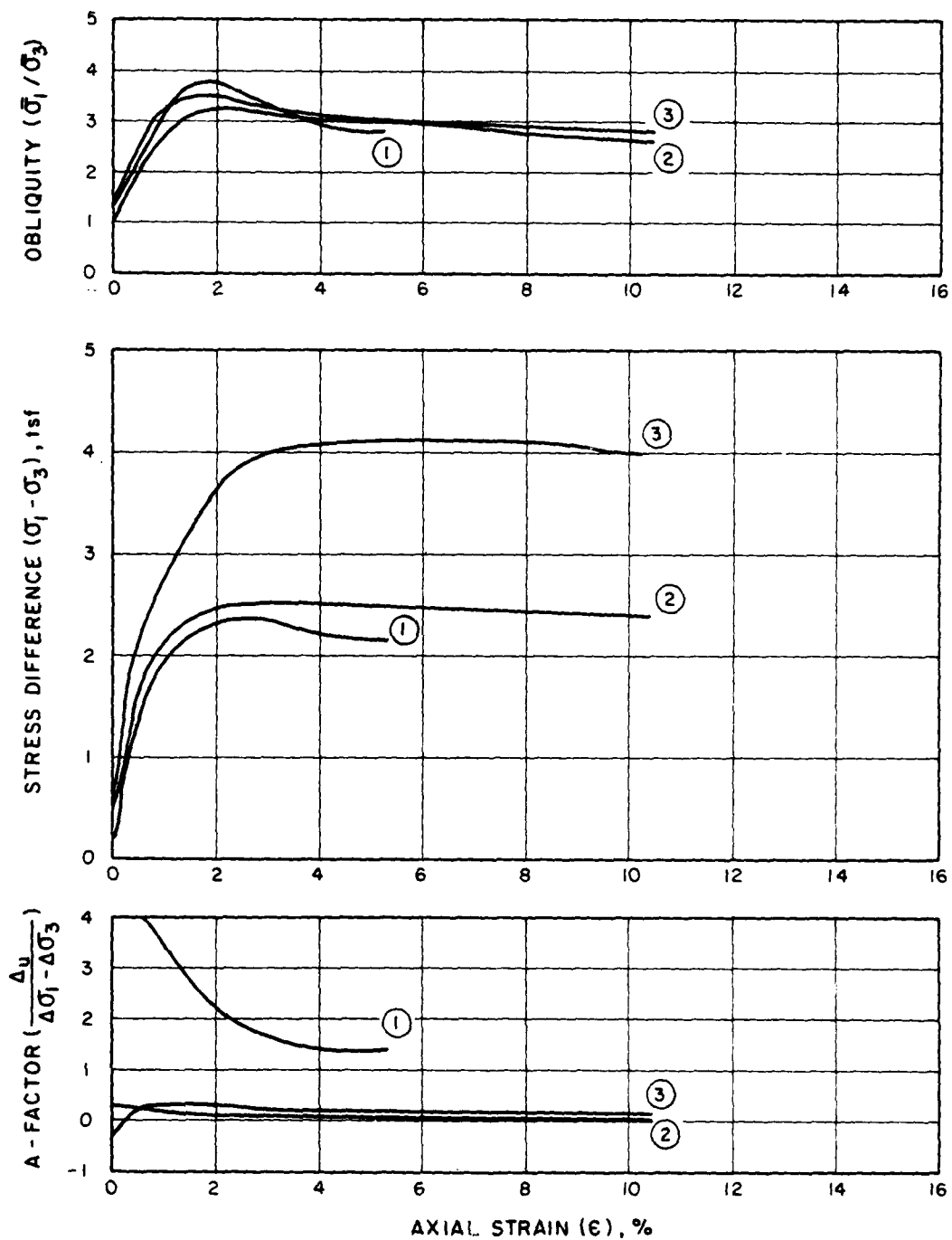


FIGURE 21(b). STRAINS FOR CIU TESTS, BORING NO. B-1

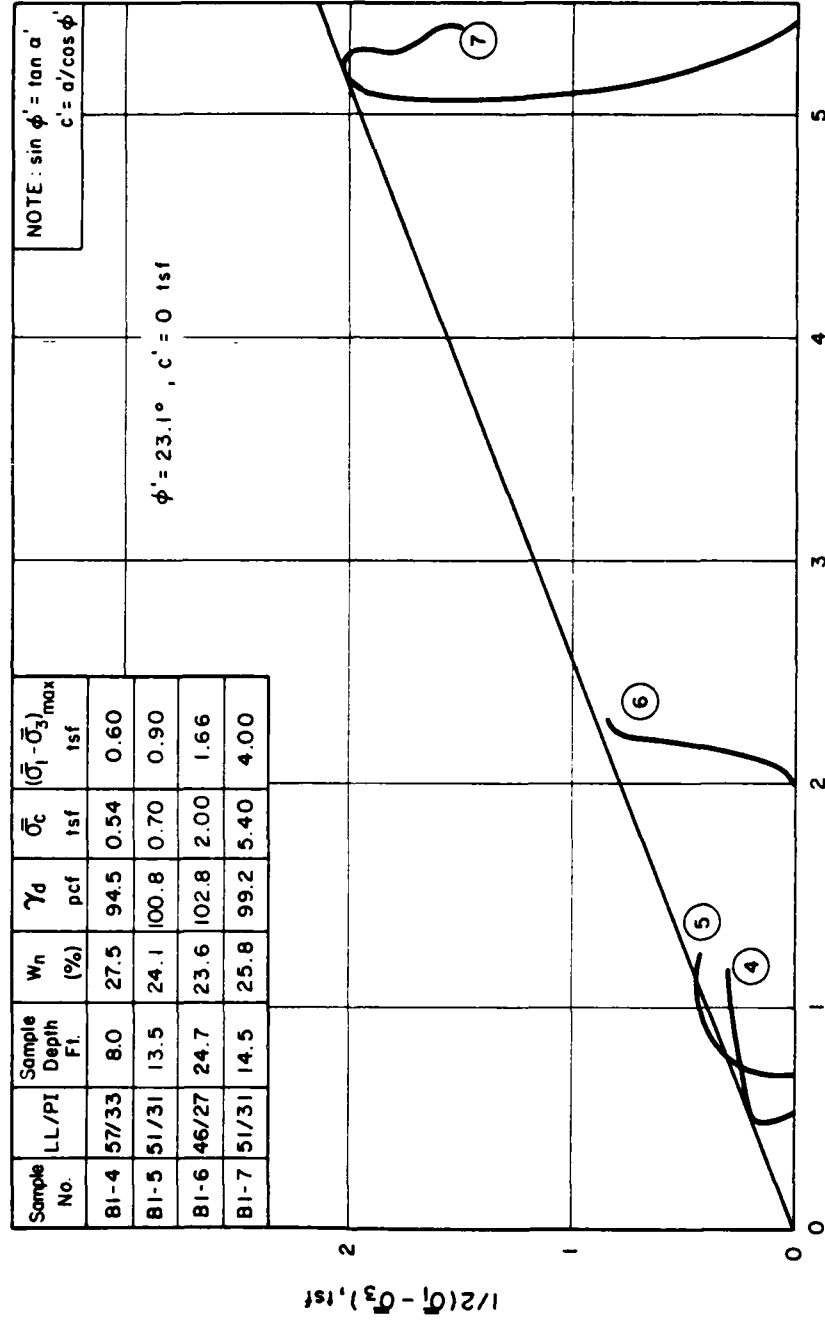


FIGURE 22(a). STRESS PATHS FOR CIU TESTS, BORING NO. B-1



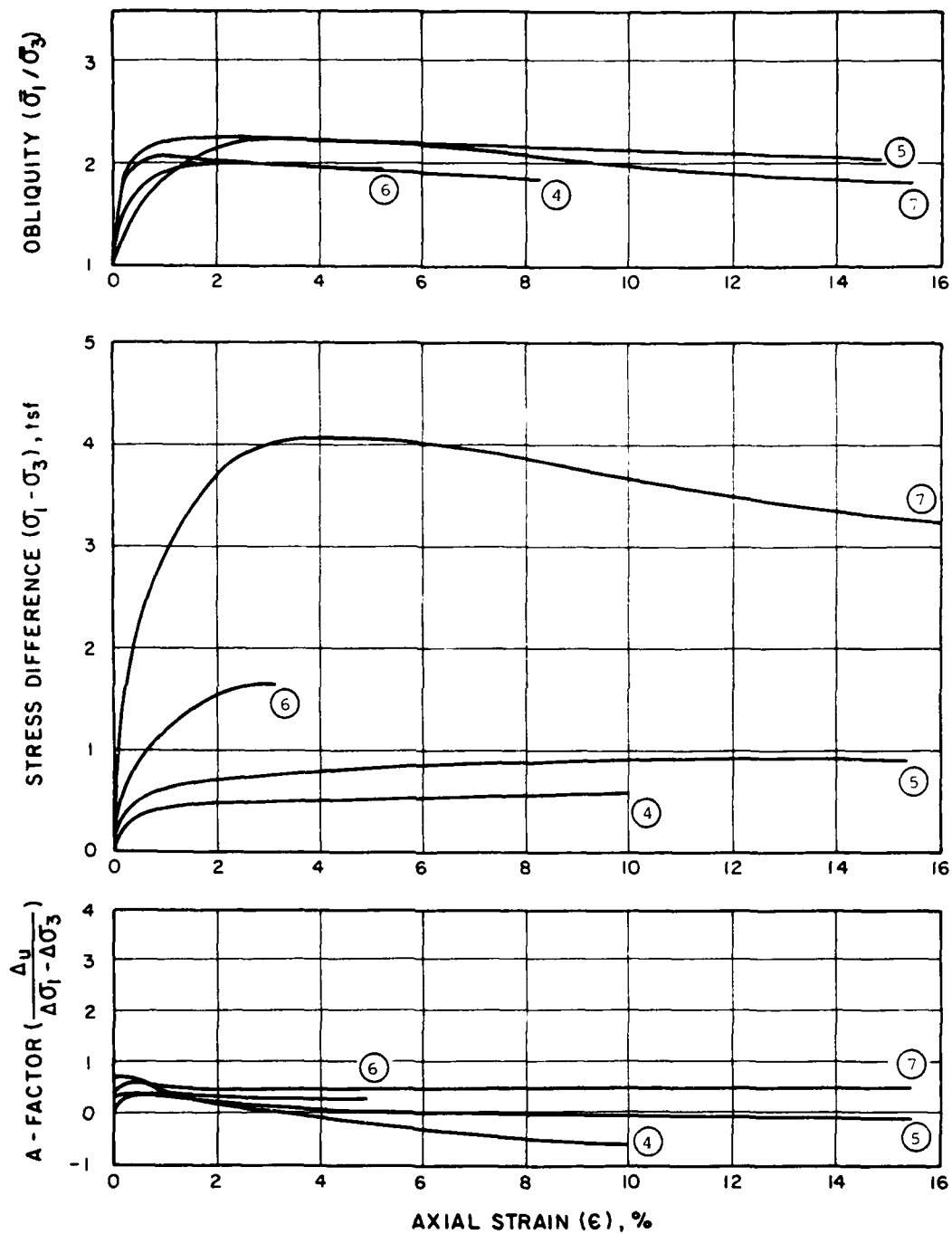


FIGURE 22(b). STRAINS FOR CIU TESTS, BORING NO. B-1

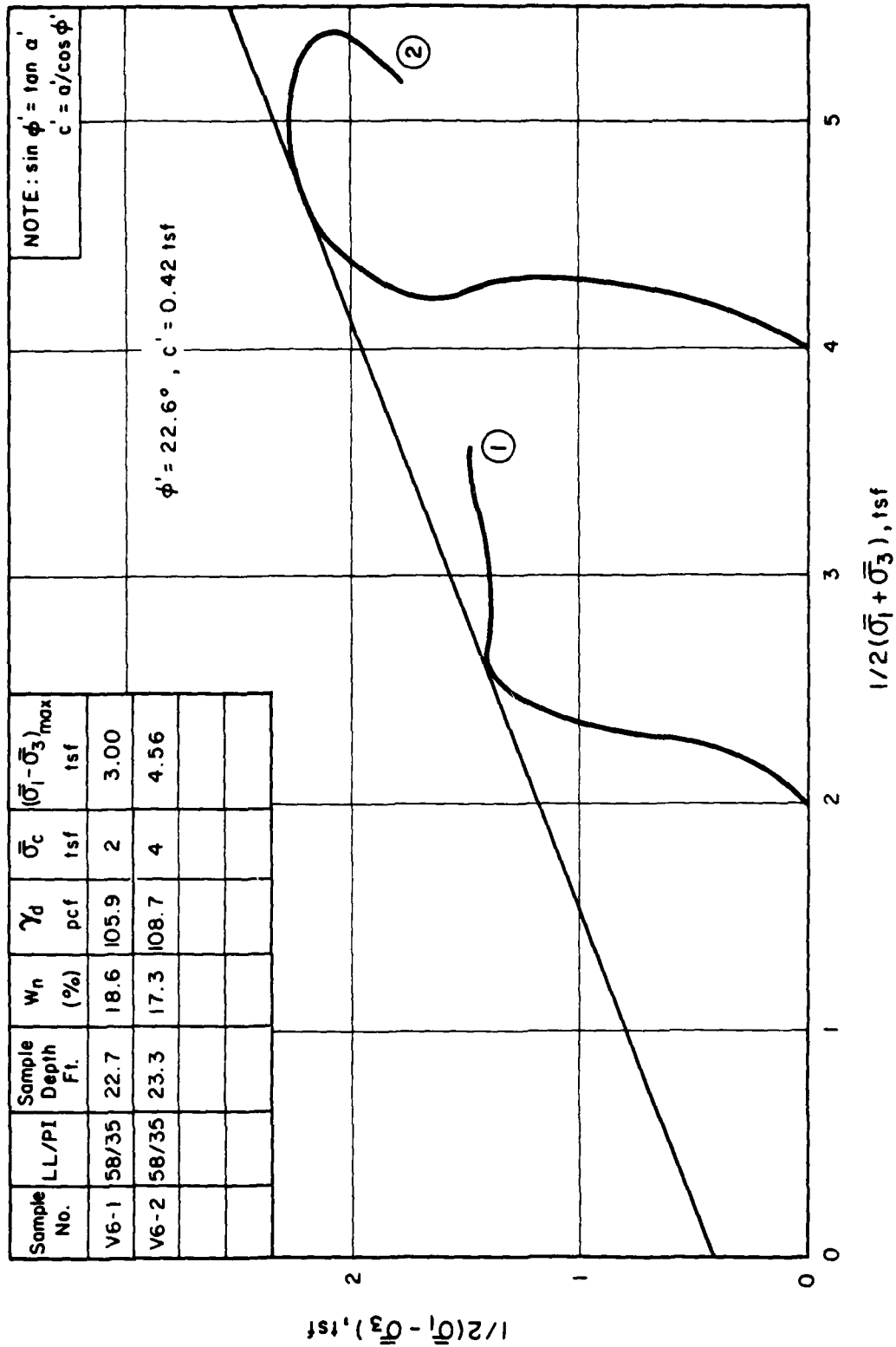


FIGURE 23(a). STRESS PATHS FOR CIU TESTS, BORING NO. V-6

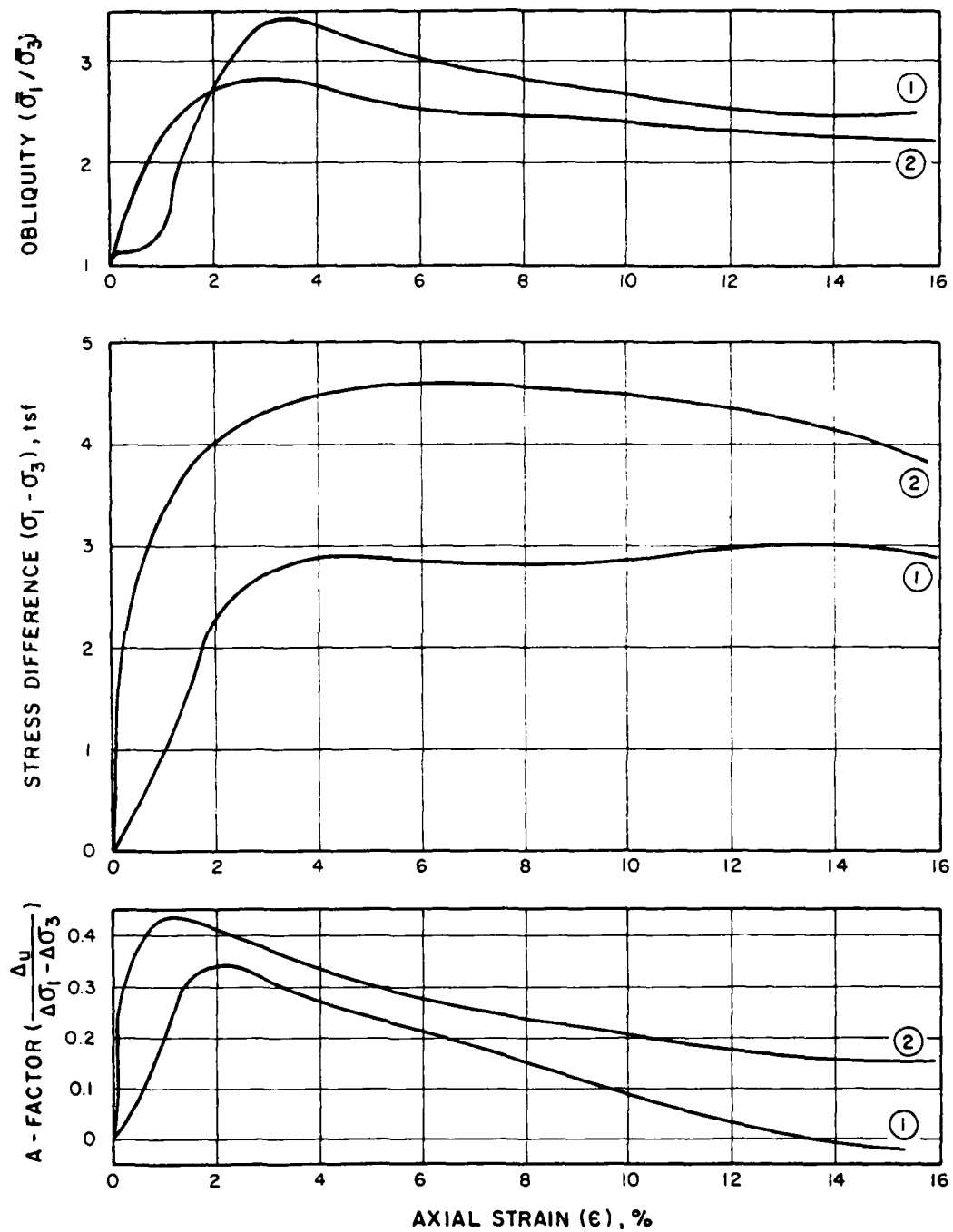


Figure 23(b). Strains for CIU tests, Boring No. V-6

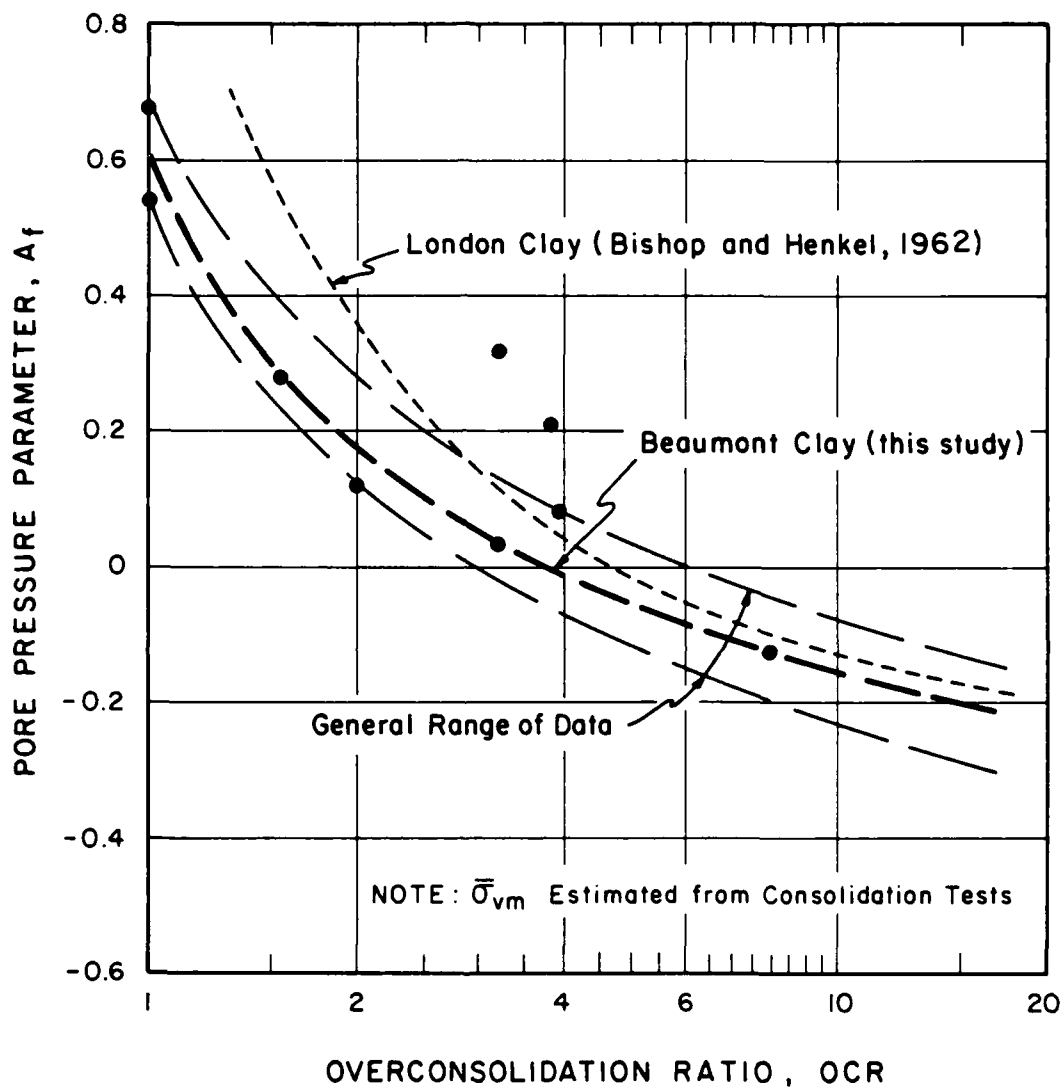


FIGURE 24.  $A_f$  FACTOR VS. OCR  
FROM CIU TESTS

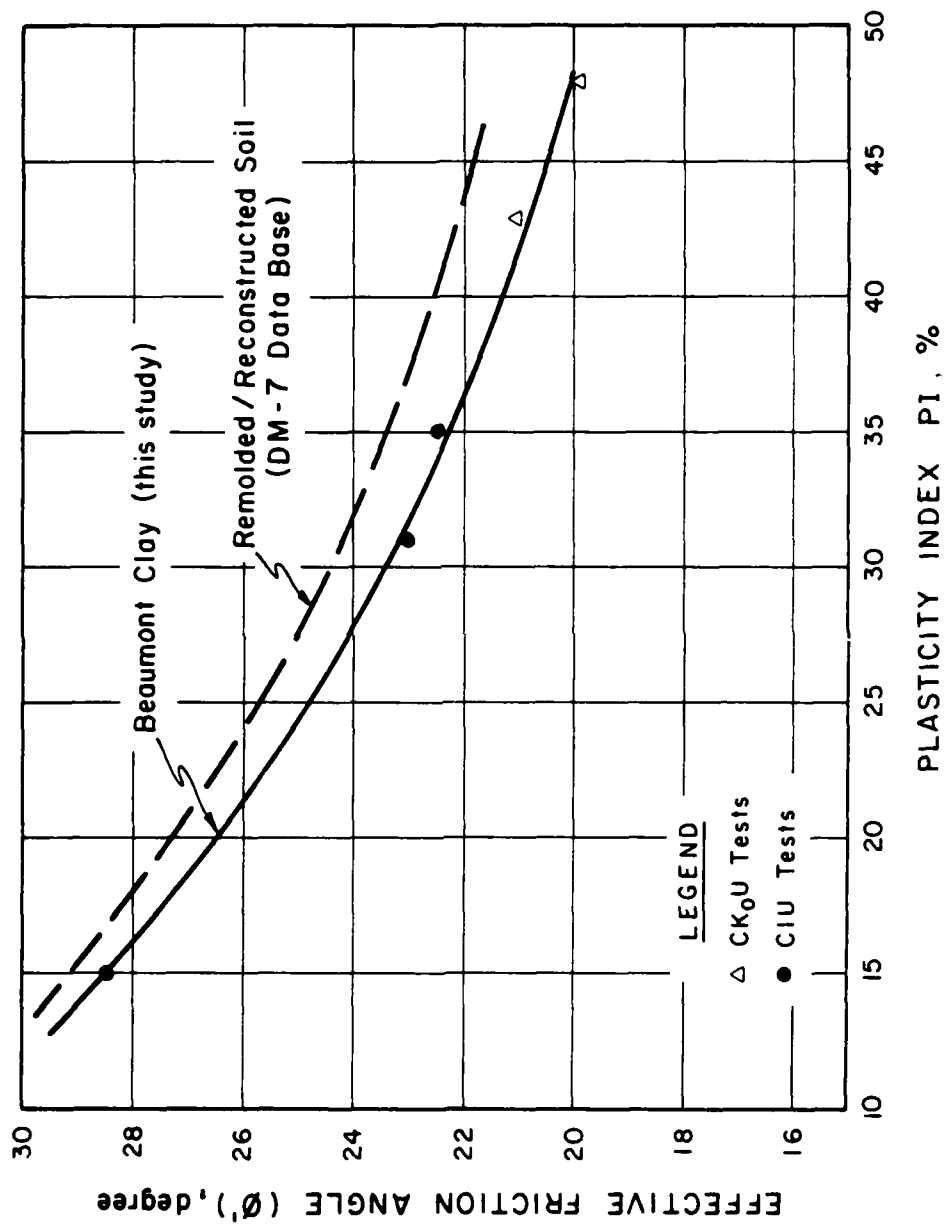


FIGURE 25. EFFECTIVE FRICTION ANGLE VS. PLASTICITY INDEX

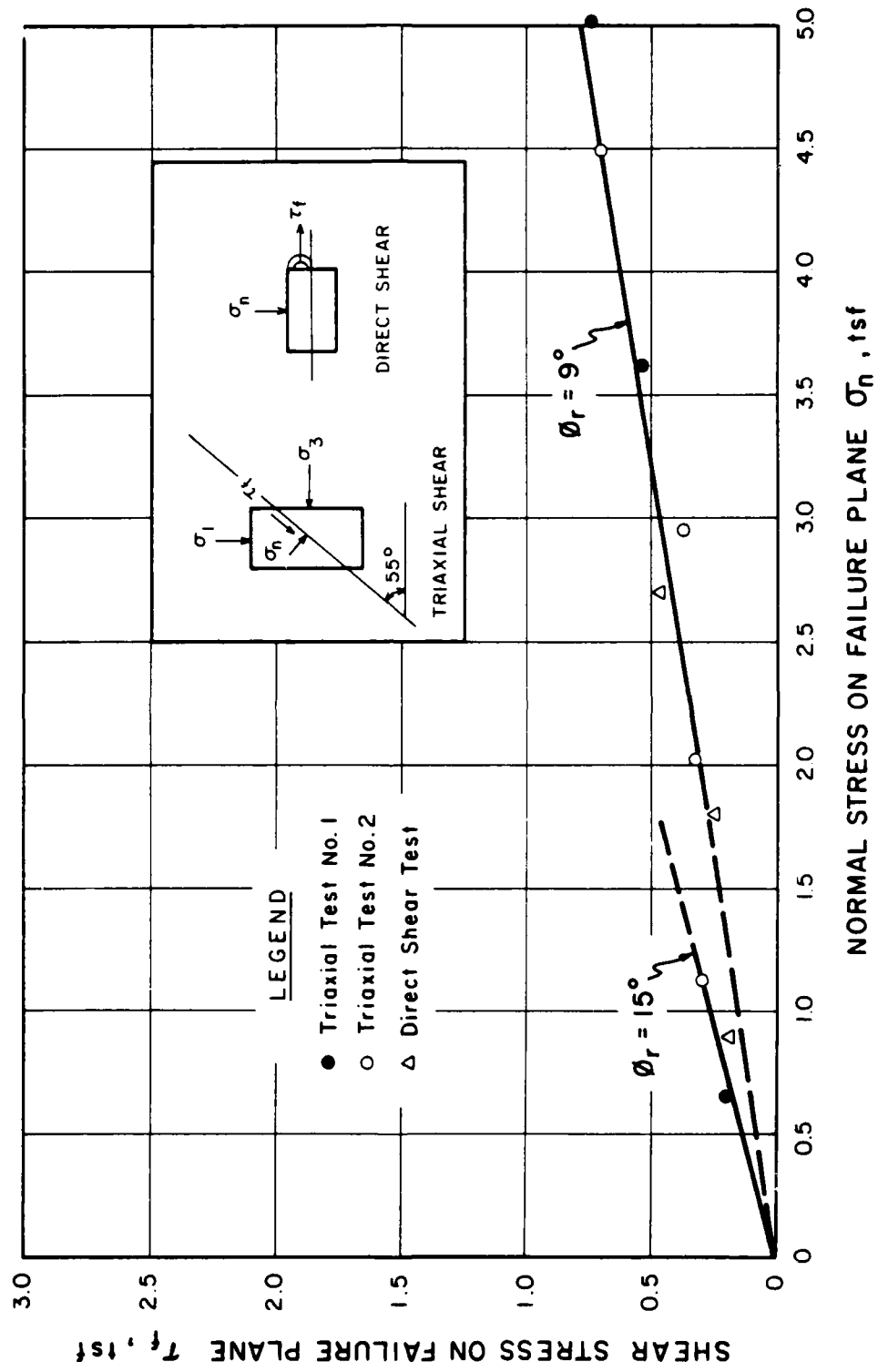


FIGURE 26. NORMAL STRESS VS. SHEAR STRESS FROM RESIDUAL STRENGTH TESTS

AD-A114 305

WOODWARD-CLYDE CONSULTANTS HOUSTON TX

F/S 8/13

STUDY TO INVESTIGATE THE EFFECTS OF SKIN FRICTION ON THE PERFOR--ETC(U)

MAR 82 J AUDIBERT, D AGGARWAL, W GARDNER

DACA39-80-C-0001

UNCLASSIFIED

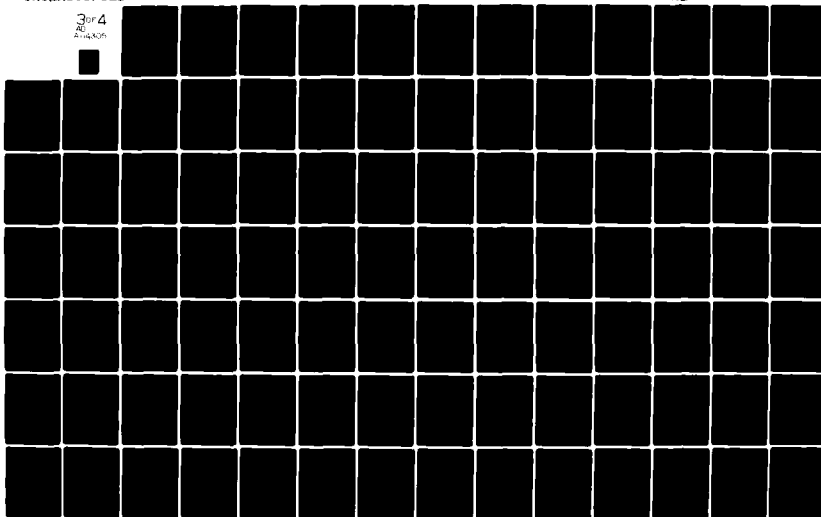
TR-8L-82-1

NL

3 of 4

26

24-44000



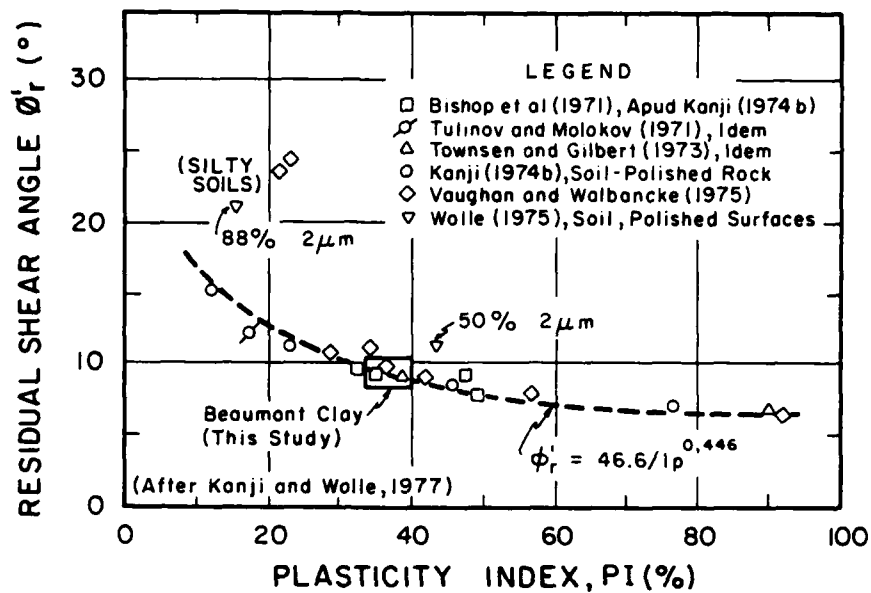


FIGURE 27(a). DRAINED RESIDUAL SHEAR ANGLE VS. PLASTICITY INDEX

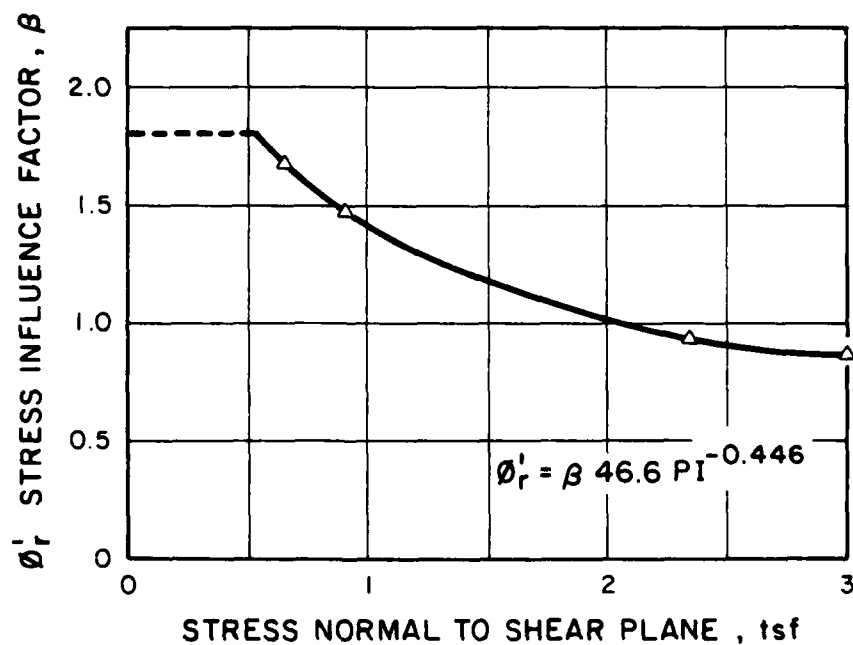


FIGURE 27(b). INFLUENCE OF NORMAL STRESS ON RESIDUAL STRENGTH



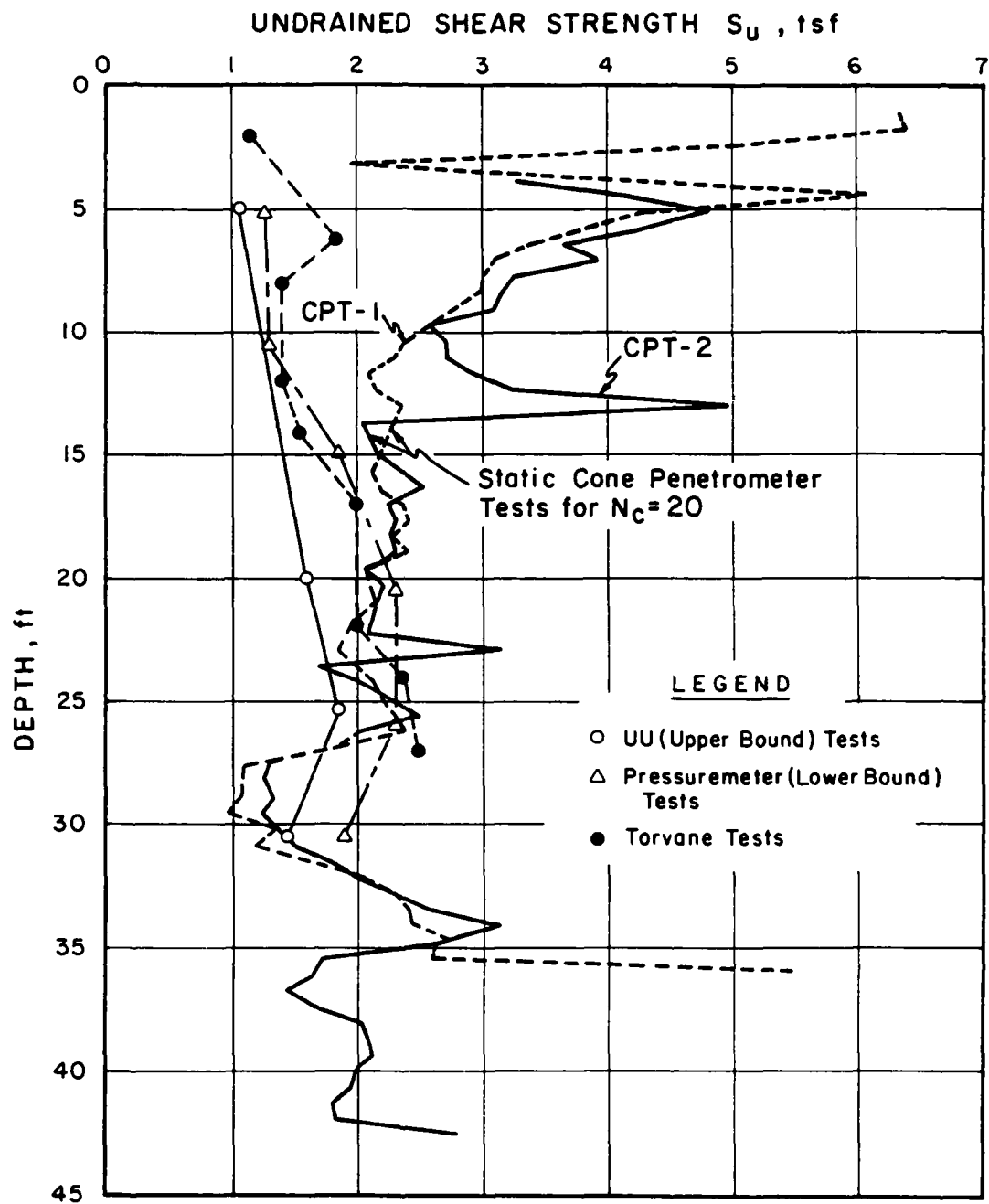


FIGURE 28. INTERPRETATION OF UNDRAINED SHEAR STRENGTH MINIMALLY AFFECTED BY FISSURES

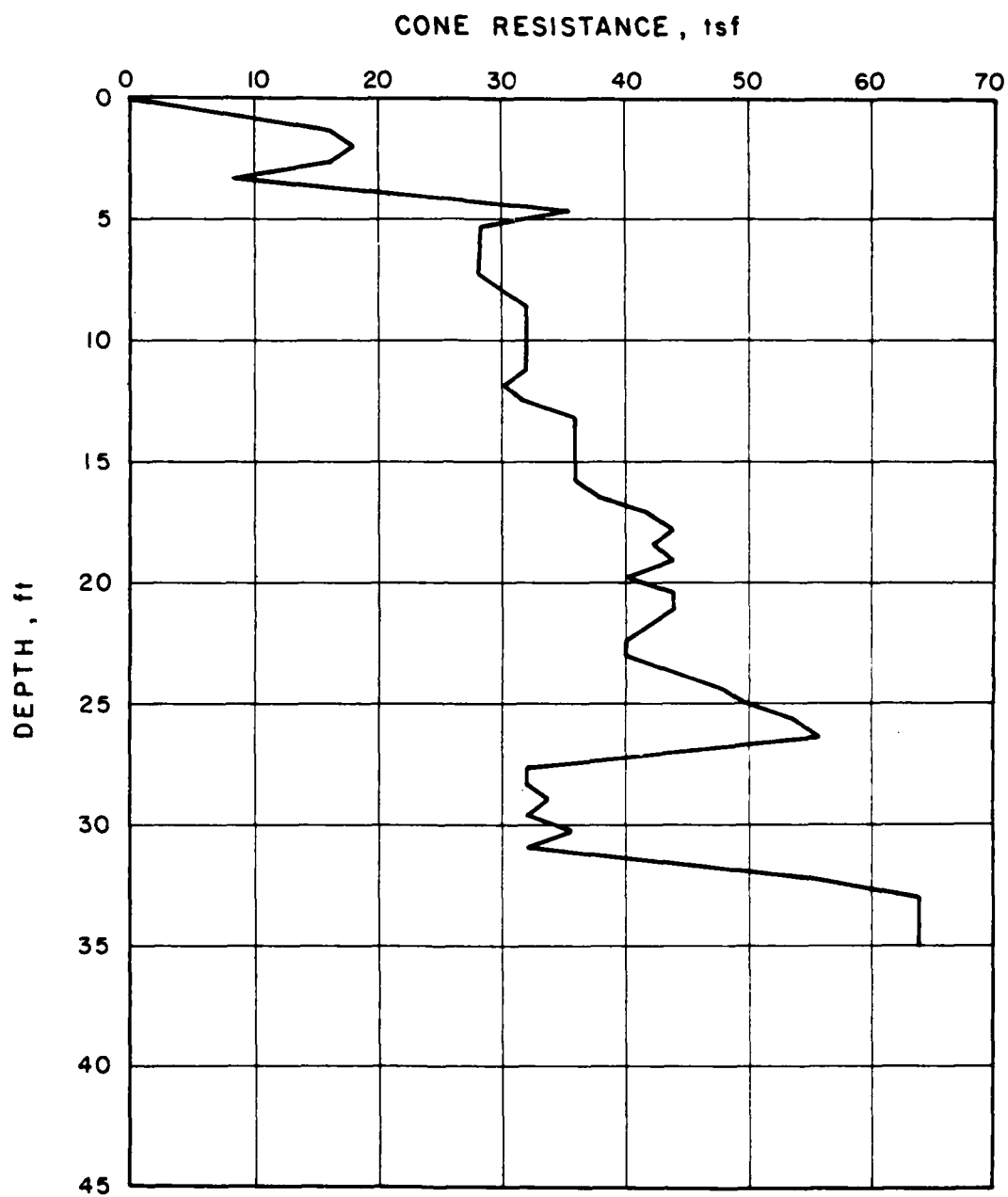


FIGURE 29. STATIC CONE RESISTANCE VS. DEPTH  
BELOW GROUND SURFACE (TEST NO. CPT-1)

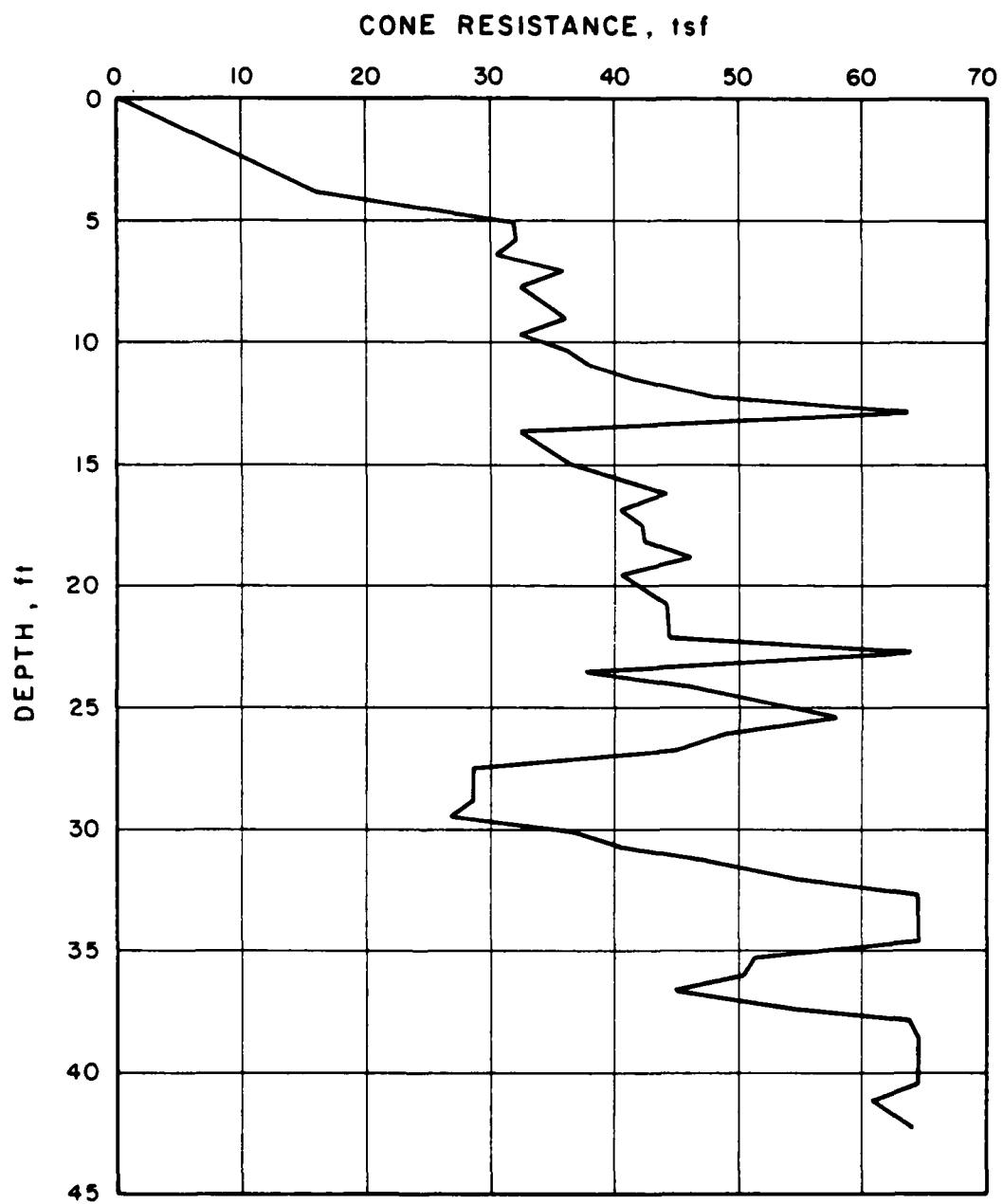


FIGURE 30. STATIC CONE RESISTANCE VS. DEPTH  
BELOW GROUND SURFACE (TEST NO. CPT-2)

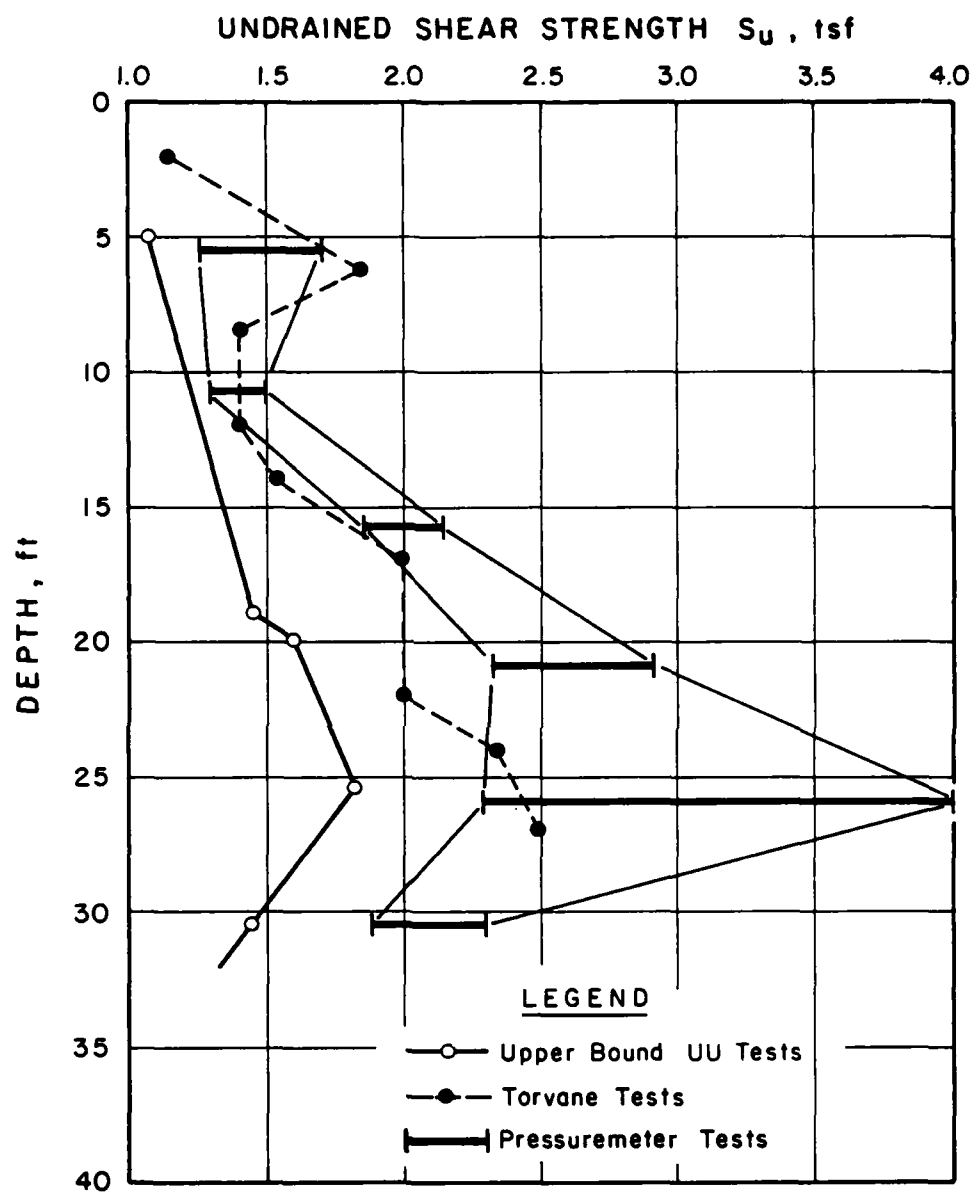


FIGURE 31. UNDRAINED SHEAR STRENGTH FROM  
VARIOUS TYPES OF TESTS

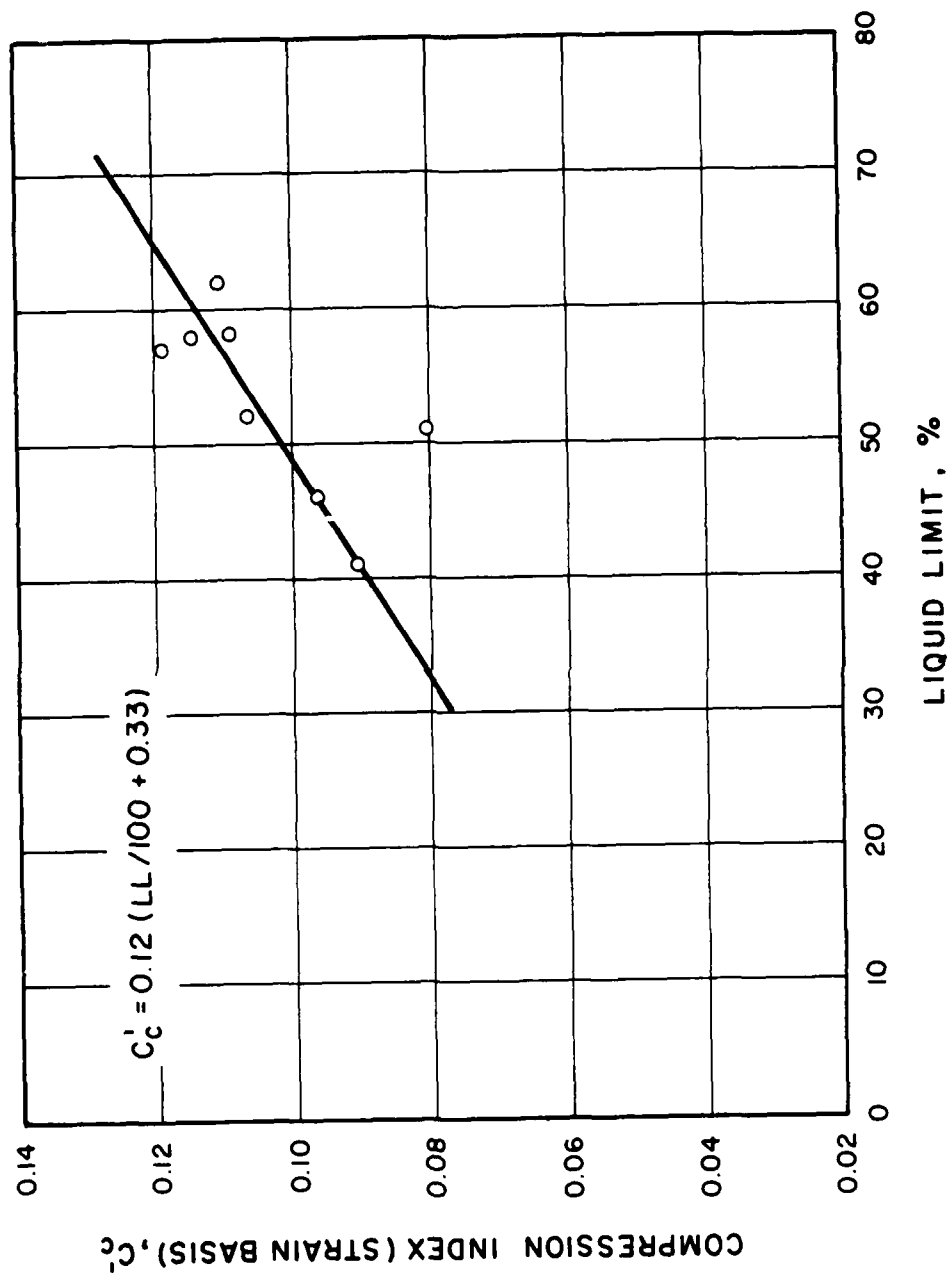


FIGURE 32. ONE-DIMENSIONAL COMPRESSION INDEX VS. LIQUID LIMIT

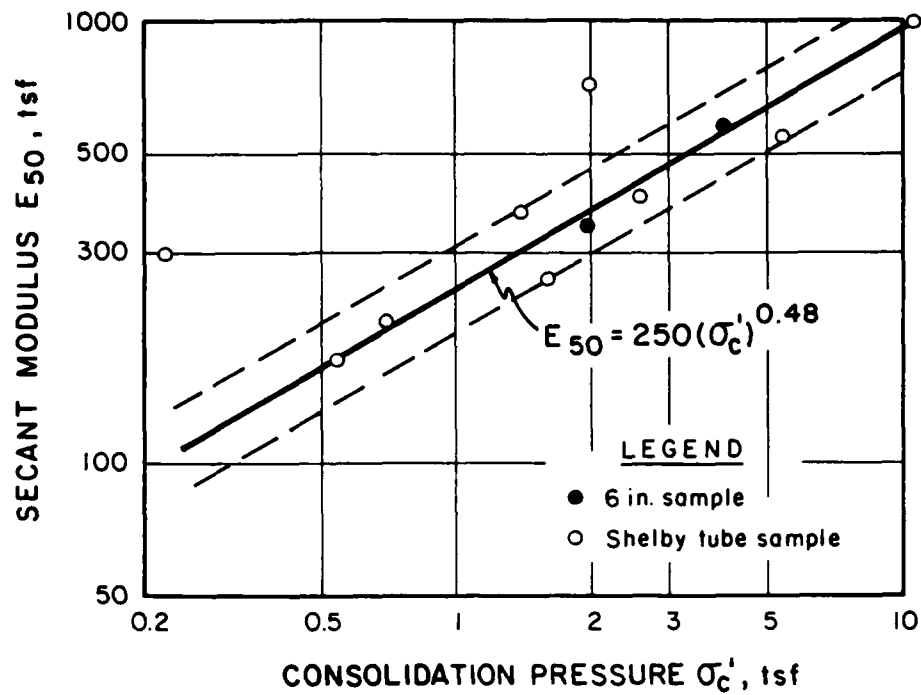


FIGURE 33(a). UNDRAINED SECANT MODULUS AT 50% OF PEAK STRENGTH FROM UU SHEAR TESTS

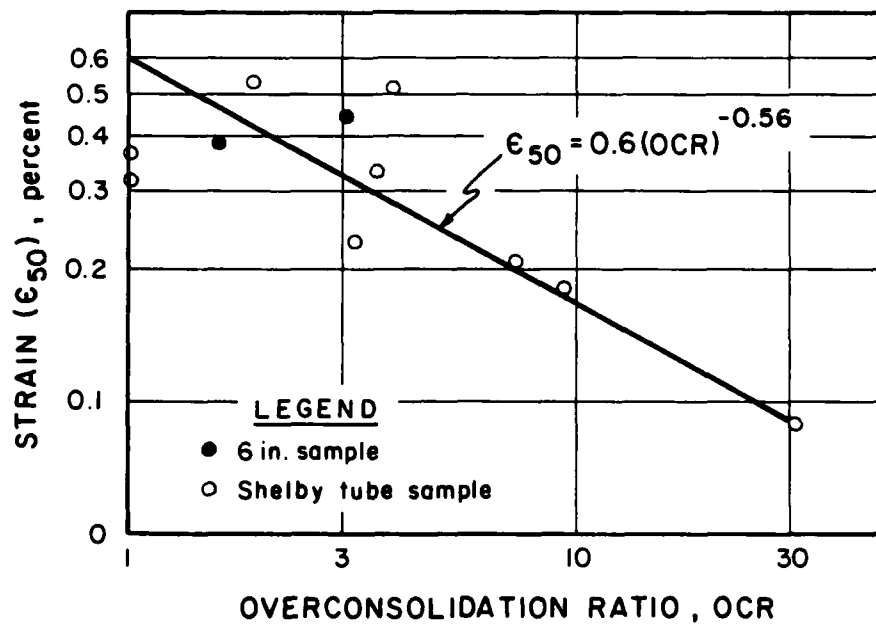


FIGURE 33(b). STRAIN 50% OF PEAK STRENGTH FROM CONSOLIDATED UNDRAINED TRIAXIAL SHEAR TEST

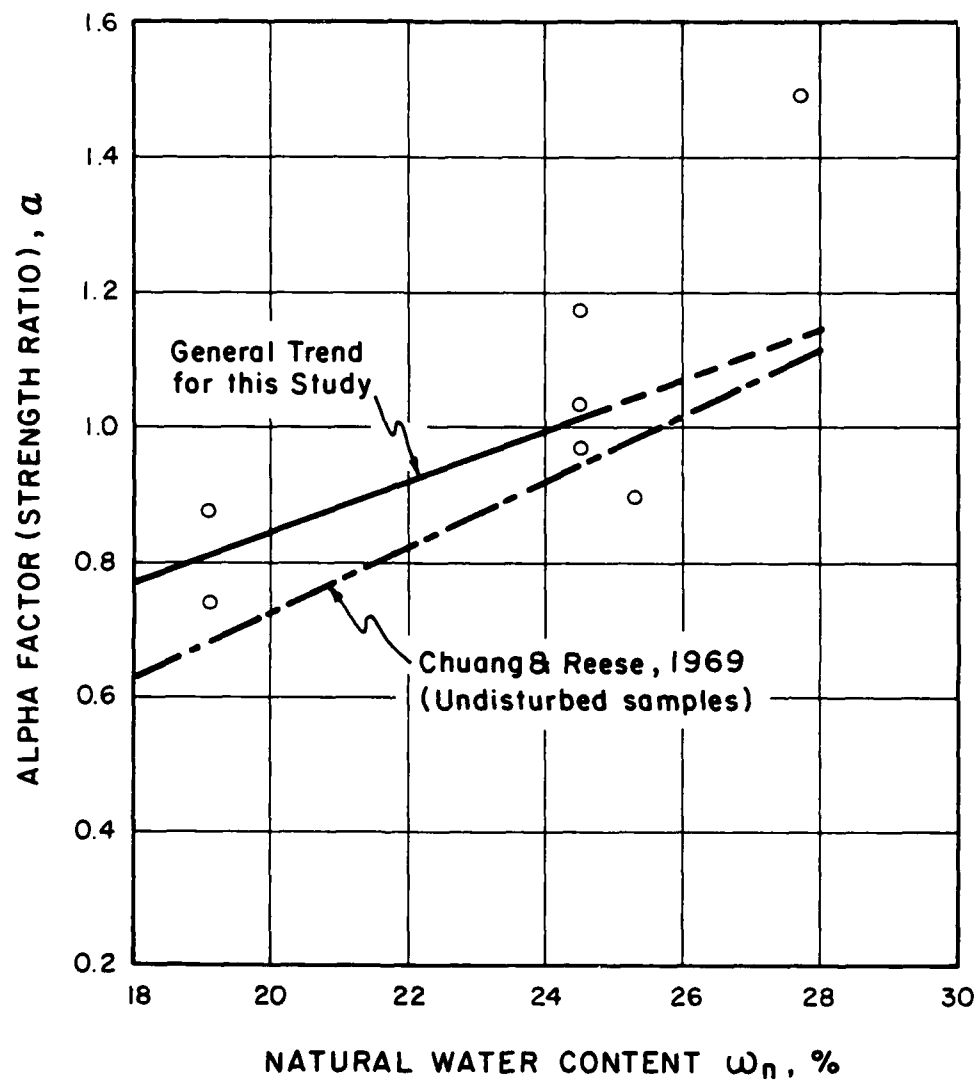


FIGURE 34. NATURAL WATER CONTENT FROM INTERFACE  
SHEAR TESTS VS. STRENGTH RATIO  
(ALPHA FACTOR)

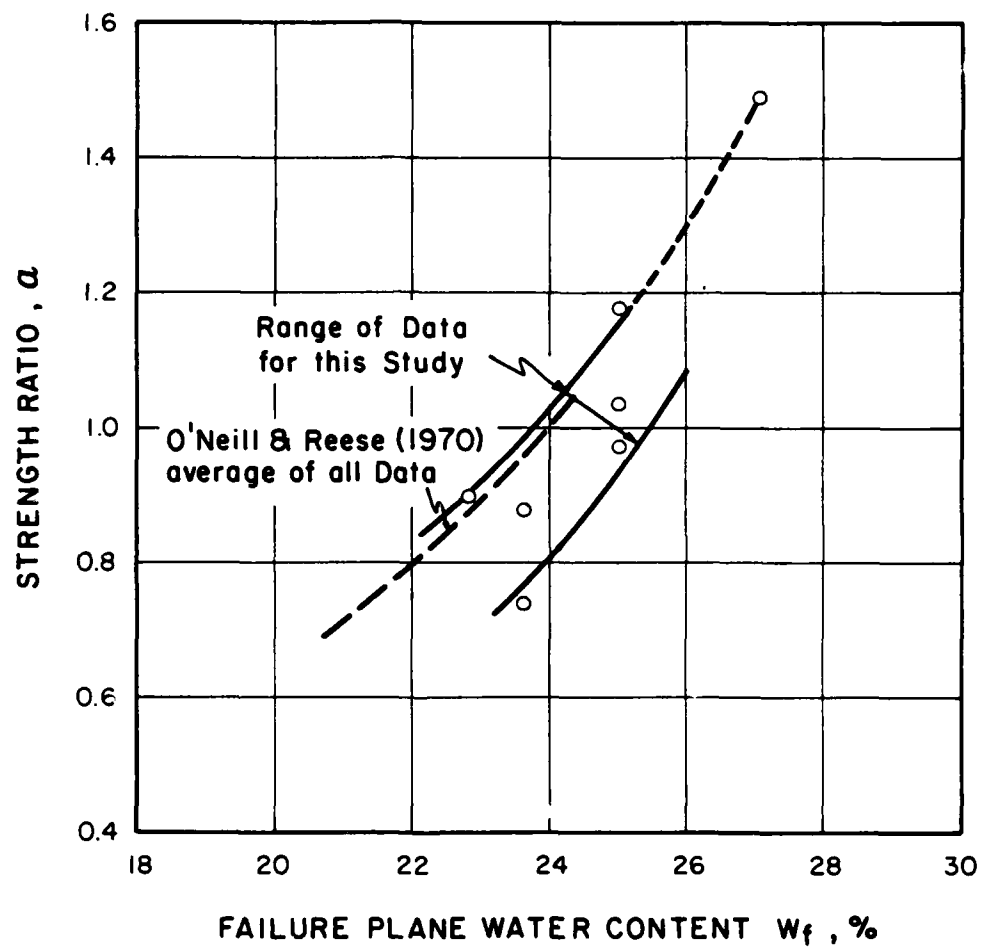


FIGURE 35. FAILURE PLANE WATER CONTENT INTERFACE  
SHEAR TEST VS. STRENGTH RATIO  
(ALPHA FACTOR)



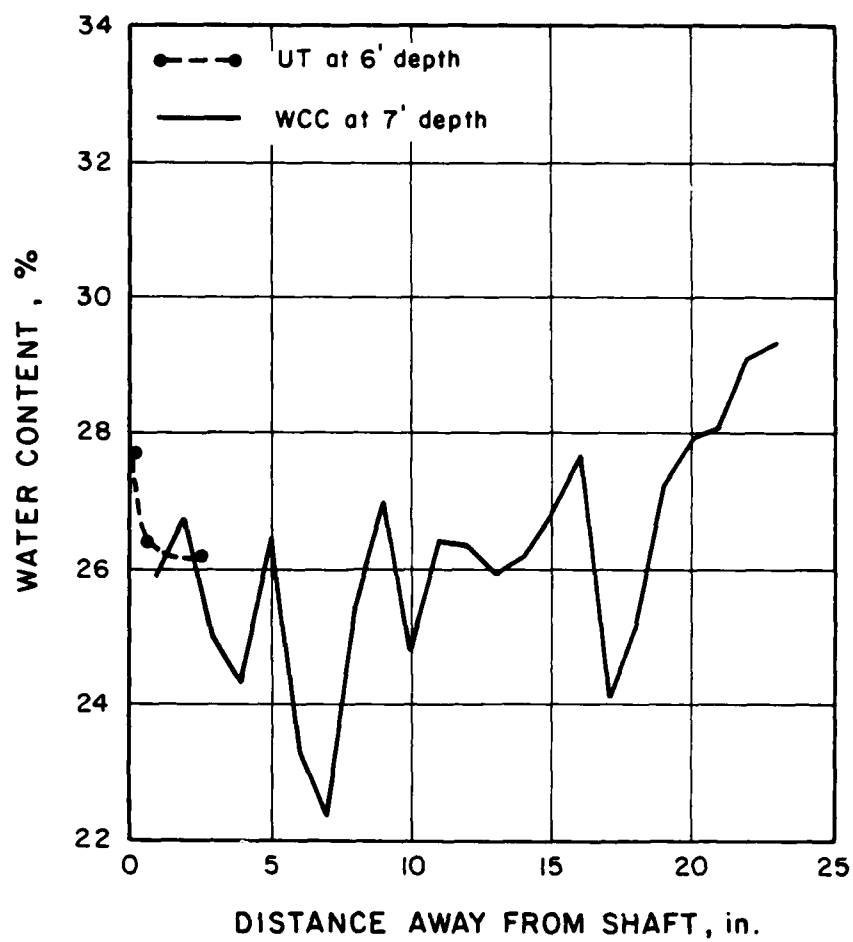


FIGURE 36. VARIATION OF NATURAL WATER CONTENT (TEST DEPTH 7 FT)

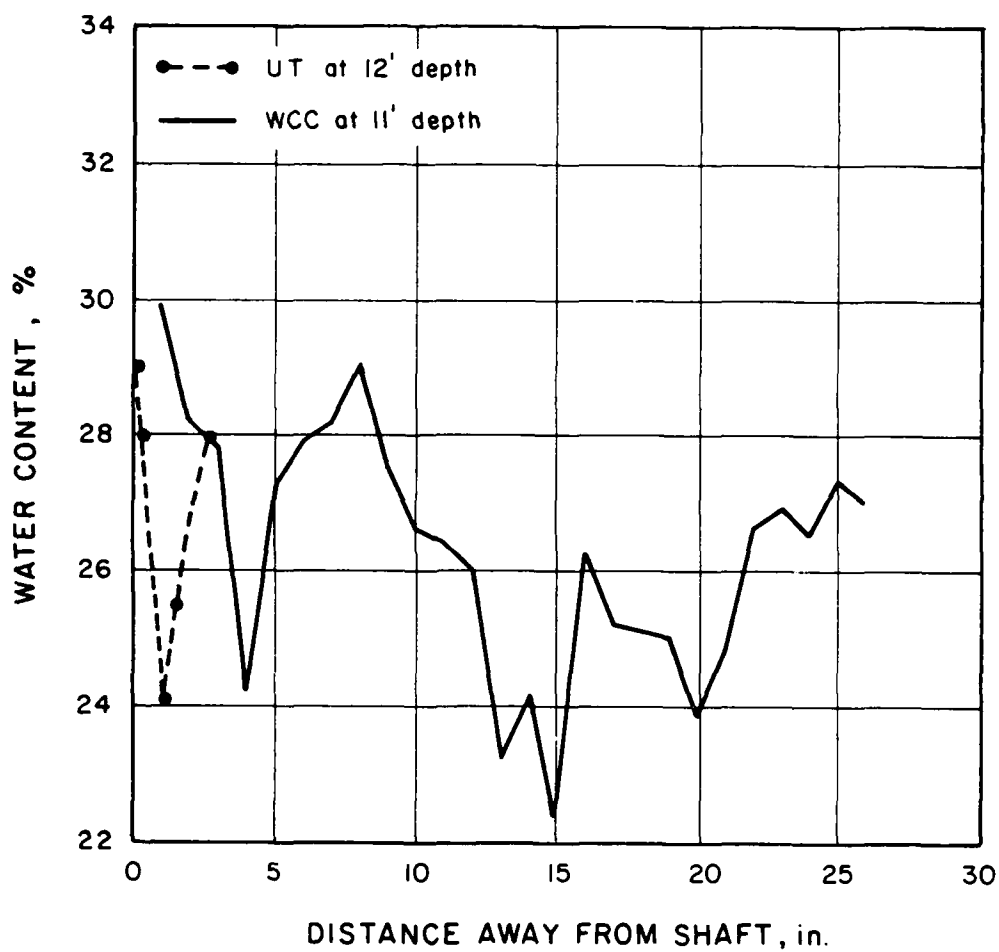


FIGURE 37. VARIATION OF NATURAL WATER CONTENT  
(TEST DEPTH 11 FT)

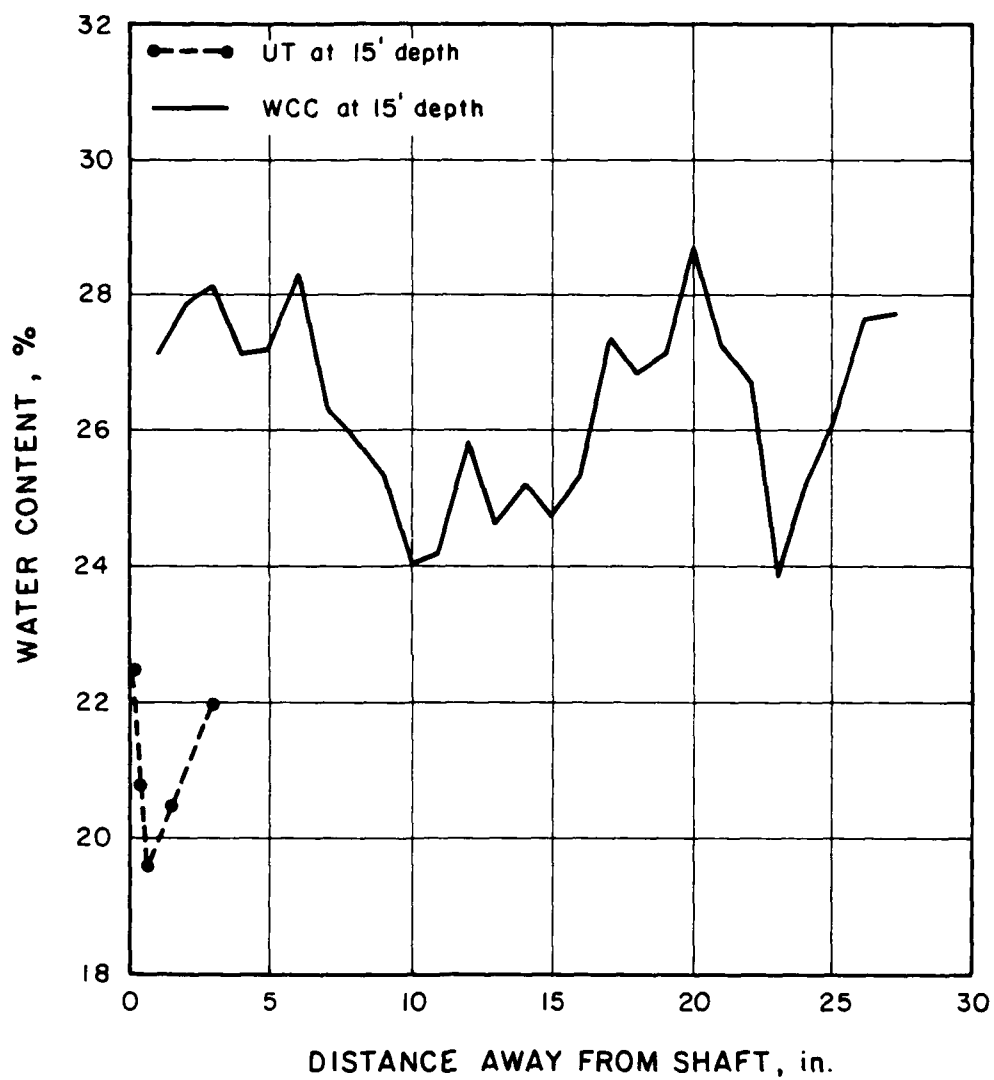


FIGURE 38. VARIATION OF NATURAL WATER CONTENT  
(TEST DEPTH 15 FT)

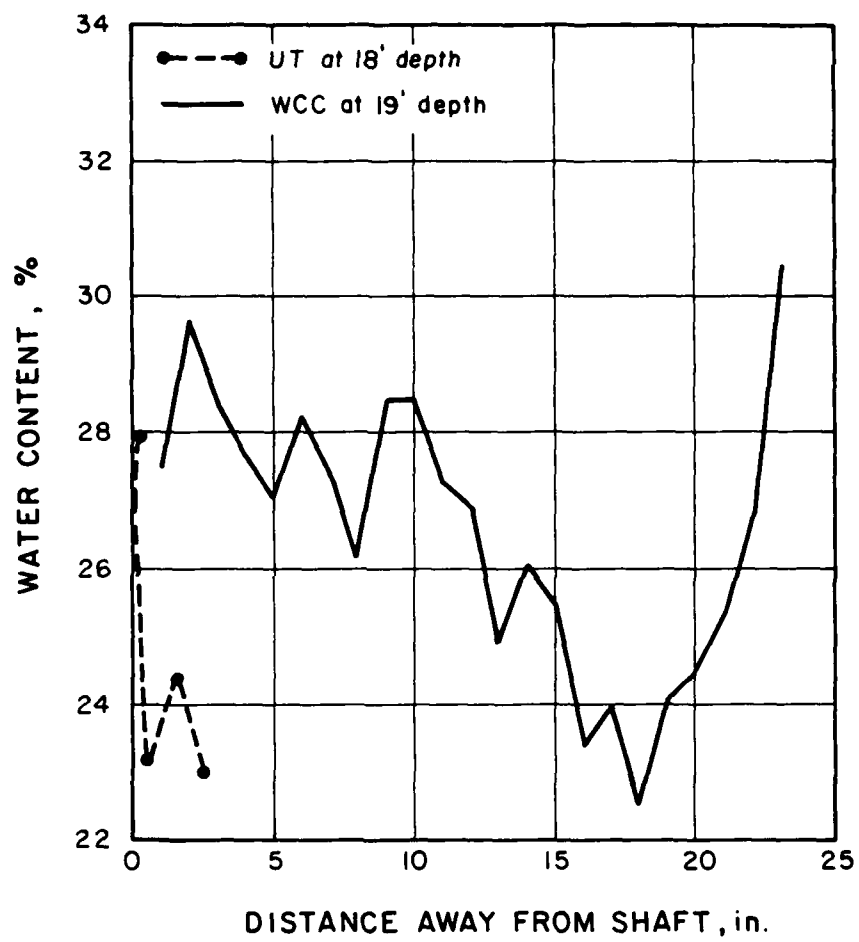


FIGURE 39. VARIATION OF NATURAL WATER CONTENT  
(TEST DEPTH 19 FT)

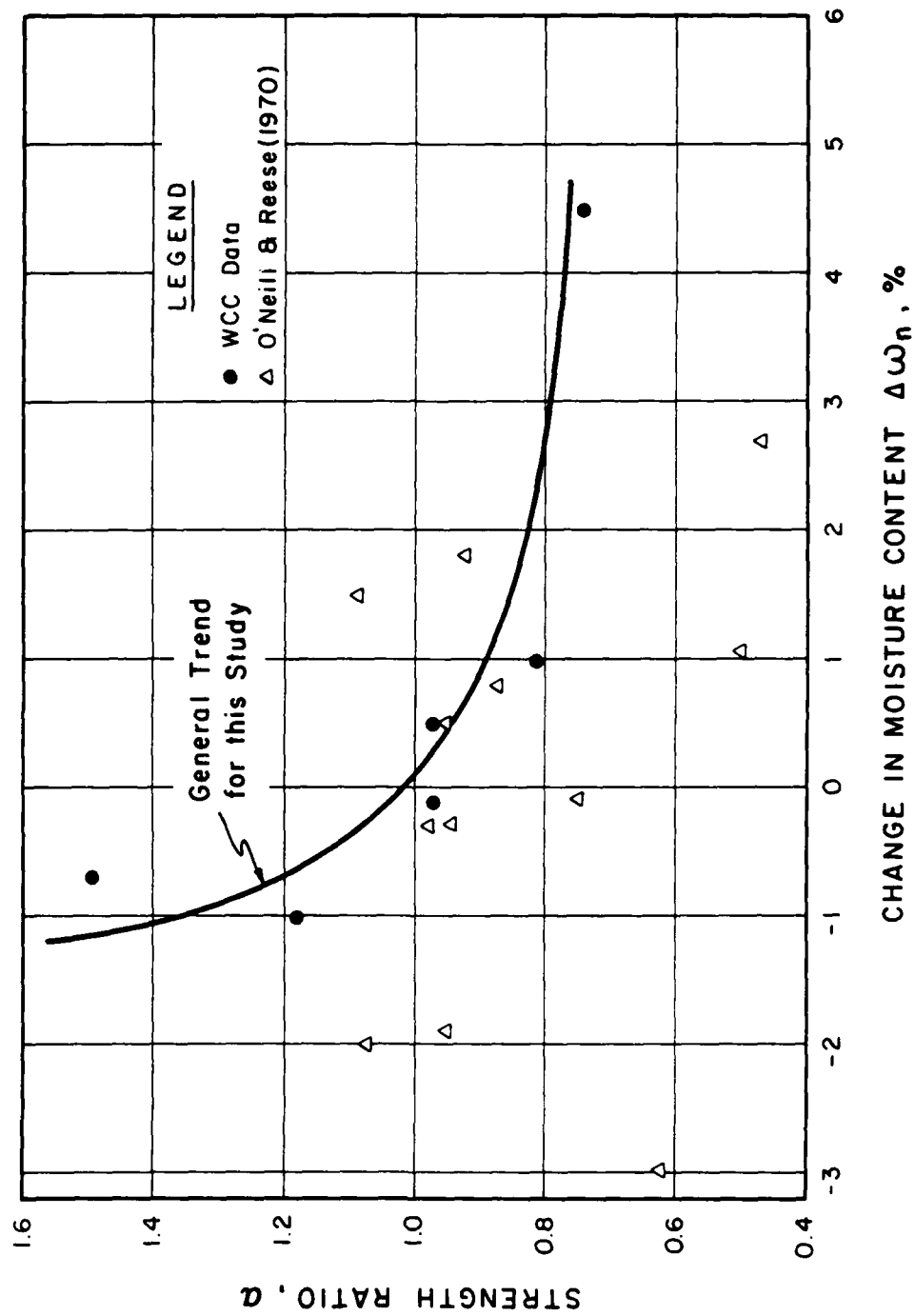


FIGURE 40. WATER CONTENT CHANGE IN INTERFACE SHEAR TESTS VS. STRENGTH RATIO (ALPHA FACTOR)

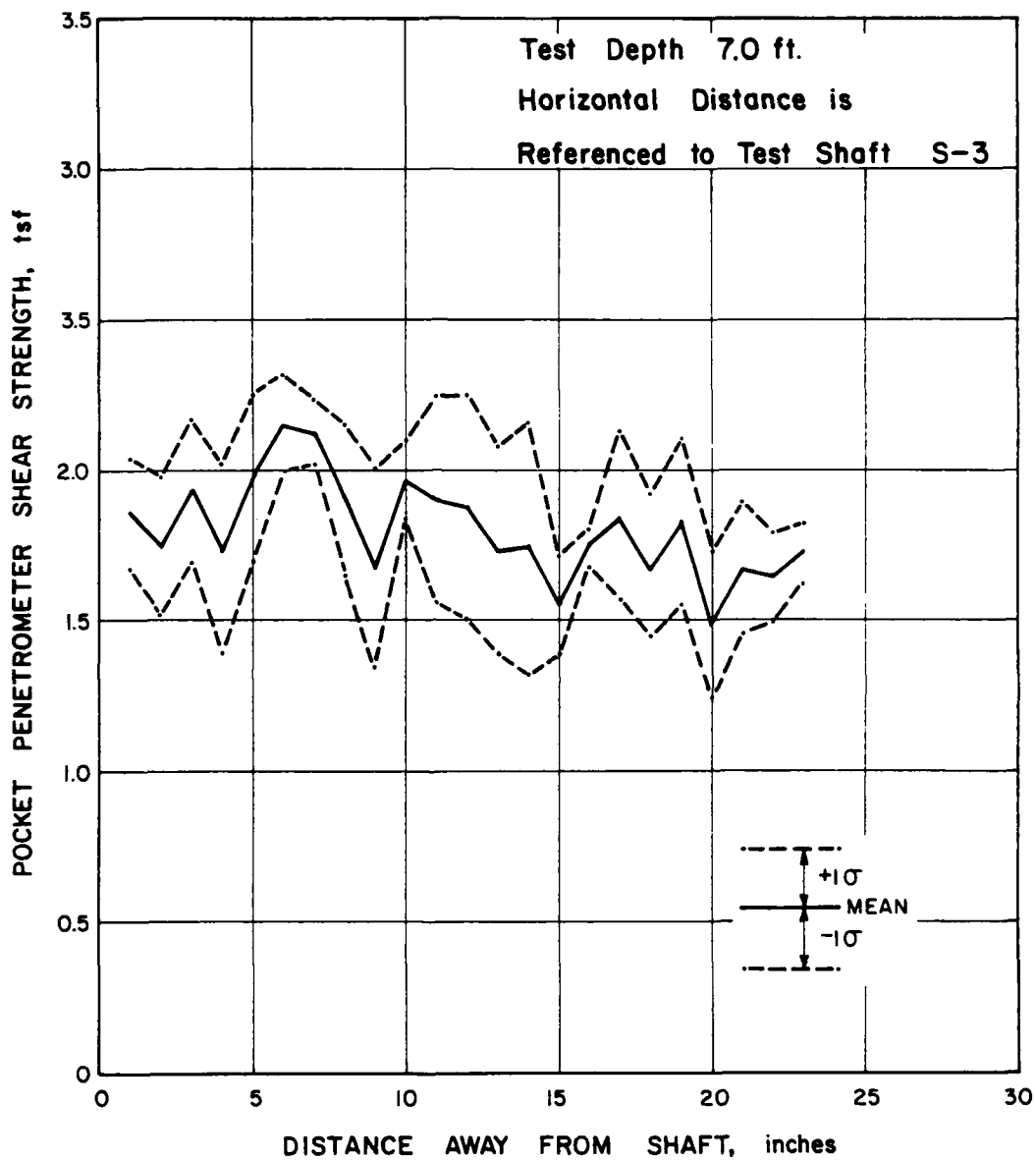


FIGURE 41. VARIATION IN UNDRAINED SHEAR STRENGTH WITH  
HORIZONTAL DISTANCE FROM THE SHAFT FACE  
(TEST DEPTH 7 FT)

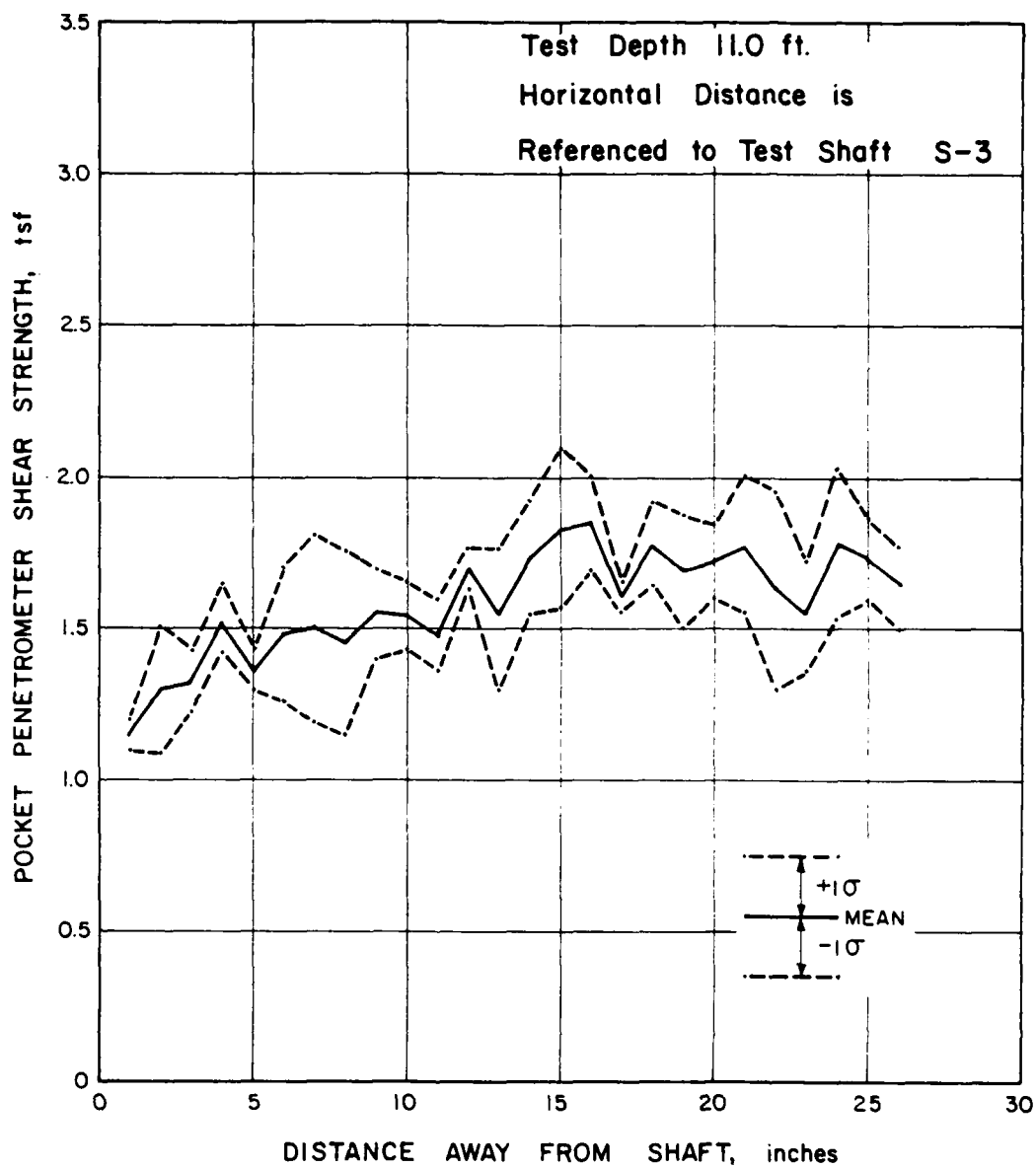


FIGURE 42. VARIATION IN UNDRAINED SHEAR STRENGTH WITH  
HORIZONTAL DISTANCE FROM THE SHAFT FACE  
(TEST DEPTH 11 FT)

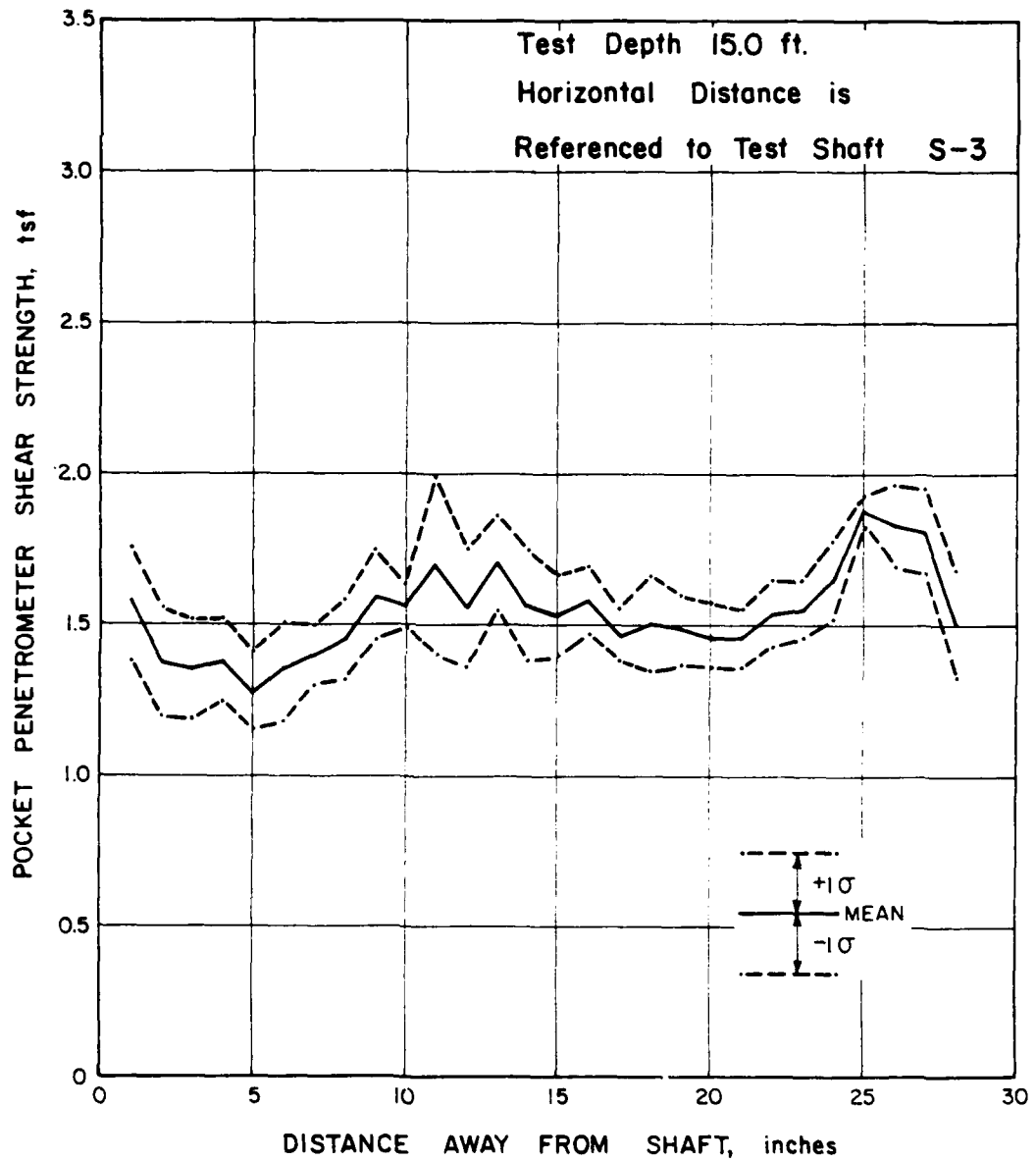


FIGURE 43. VARIATION IN UNDRAINED SHEAR STRENGTH WITH  
HORIZONTAL DISTANCE FROM THE SHAFT FACE  
(TEST DEPTH 15 FT)



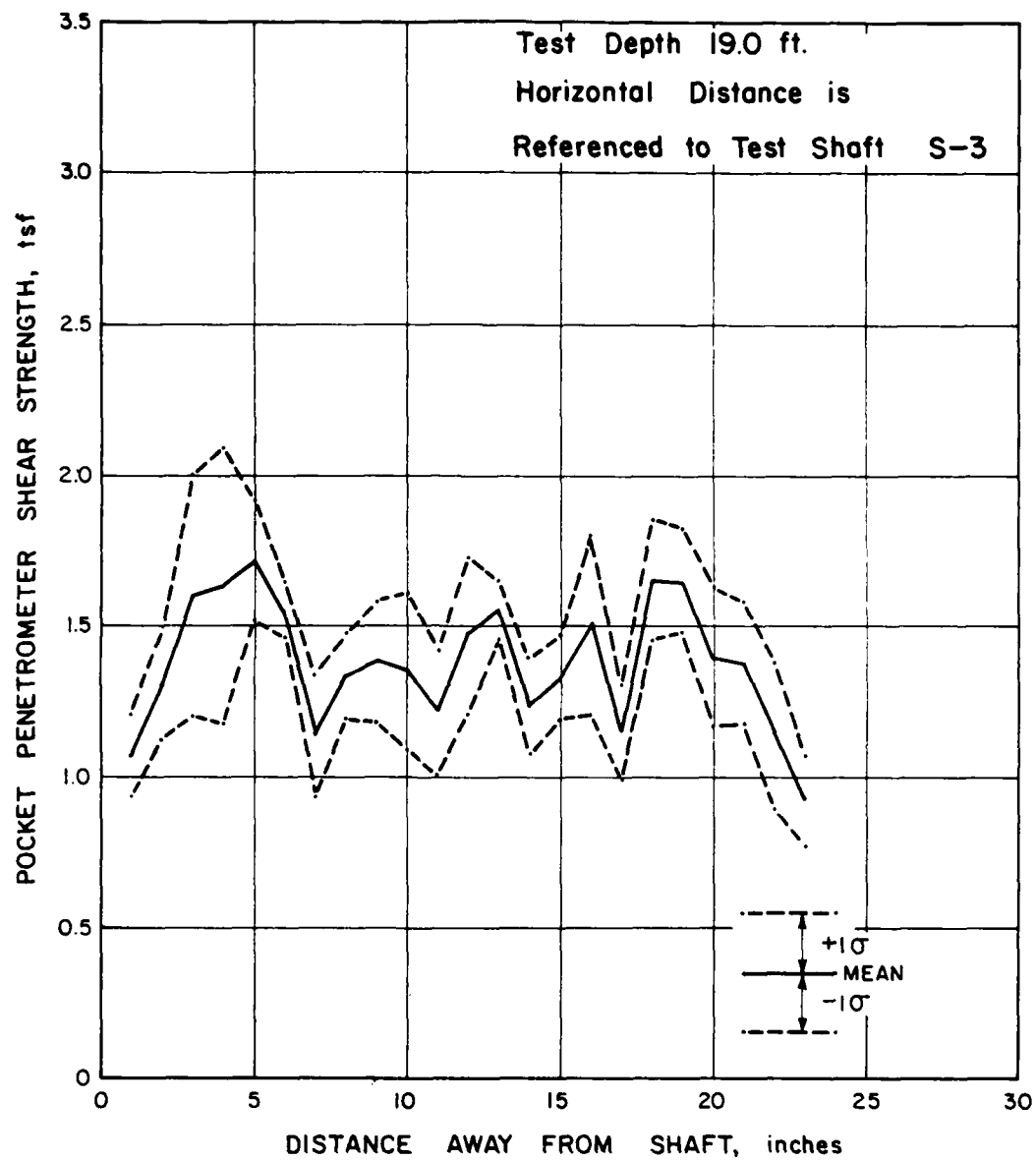


FIGURE 44. VARIATION IN UNDRAINED SHEAR STRENGTH WITH  
HORIZONTAL DISTANCE FROM THE SHAFT FACE  
(TEST DEPTH 19 FT)

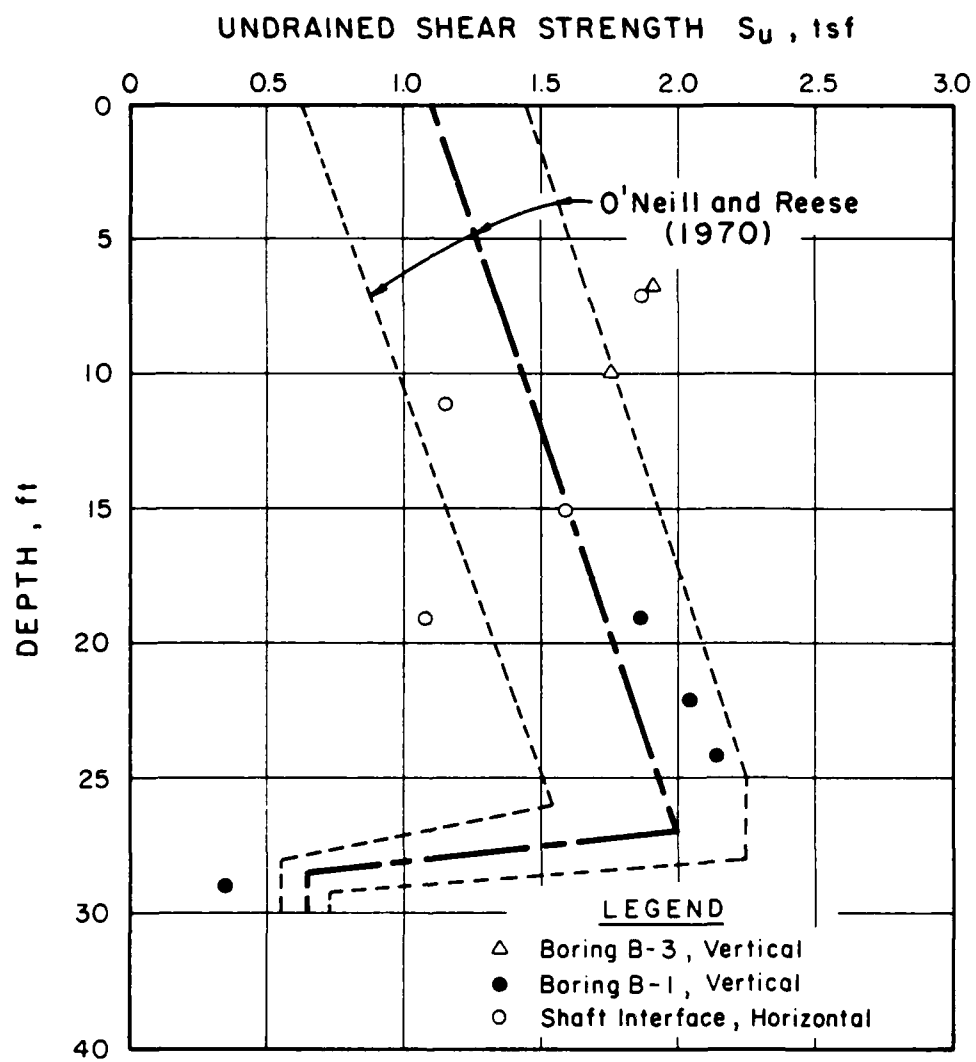


FIGURE 45. COMPARISON OF ORIGINAL AND CURRENT MEASUREMENT FROM POCKET PENETROMETER TESTS

APPENDIX A  
LABORATORY TEST RESULTS

JOE NO.: 80C112 DATE: \_\_\_\_\_

• SEE ATTACHED CURVES

Table A2: RESULTS OF LABORATORY TESTS

PROJECT: WES Drilled Shaft Study

JOB NO.: 80C112 DATE: \_\_\_\_\_

HOLE NO.	DEPTH BELOW GROUND	% MOIST	DRY DENSITY PCT	ATTERBERG LIMITS			COMPRESSION TEST				REL. DENSITY BLOWS/FT	SIEVE ANALYSIS	Specific Gravity	CONSOLIDATION	TYPE OF MATERIAL
				LL	PL	PI	COMPRESSION TEST	% STRAIN	LATERAL PRESSURE PSI	TYPE FAILURE					
	17-19	21.0	105.6	45	18										
	19-21.8	24.0	102.6												
		22.7	101.7	41	19								2.62		
		22.8	104.3												
	22-24	26.8		61	25										
	24-26.8	22.7	104.6												
		24.3	92.2	46	19								2.60		
		23.6	102.8												
	27-29	18.0	111.7	25	12										
		20.1													
	29-31.8	16.5	114.4	21	16										
		23.7													
		20.8													
		18.9													
		17.9													
	32-34	15.2	118.1	33	13										

\* SEE ATTACHED CURVES

**Table A3: RESULTS OF LABORATORY TESTS - Denison Samples**

PROJECT: WES Drilled Shafts

[illegible][illegible]

**• SEE ATTACHED CURVES**

## RESULTS OF LABORATORY TESTS

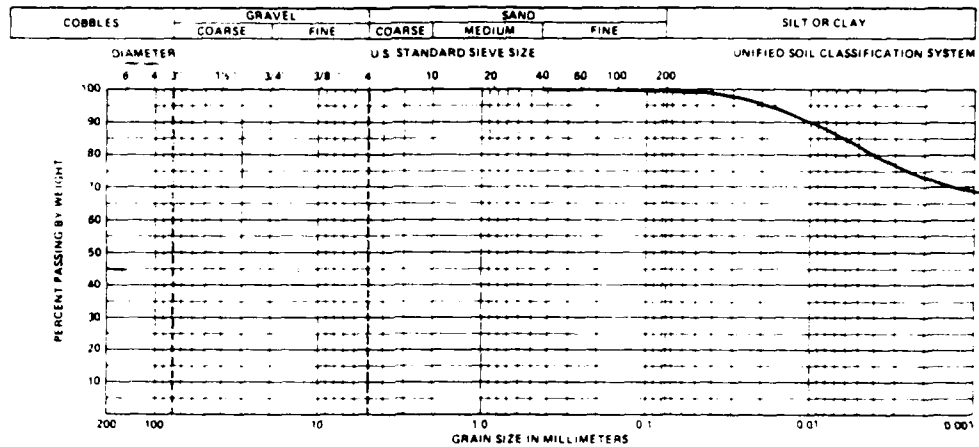
WFS Drilled Shaft Study

DATE 11-11-54

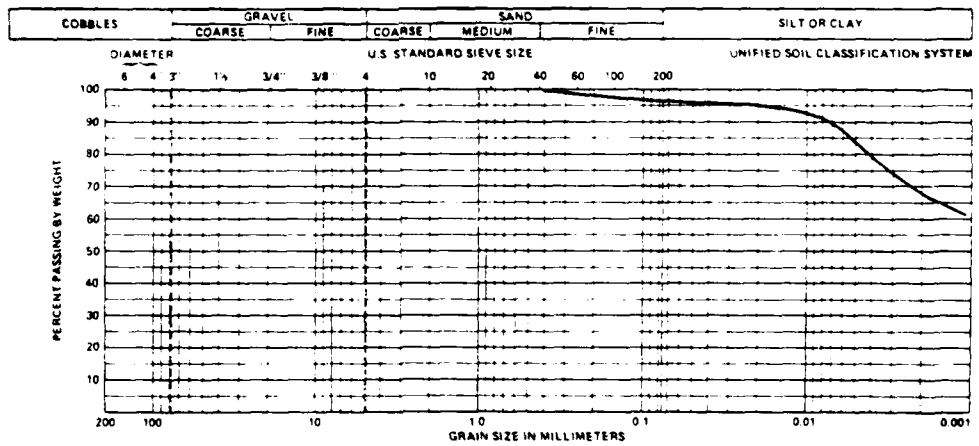
[illegible]

**• SEE ATTACHED CURVES**

# GRAIN-SIZE DISTRIBUTION



BORING	SAMPLE	DEPTH (ft)	SYMBOL	CLASSIFICATION	w (%)	w <sub>L</sub> (%)	w <sub>p</sub> (%)
-	H-1	7'		Brown and gray silty CLAY			

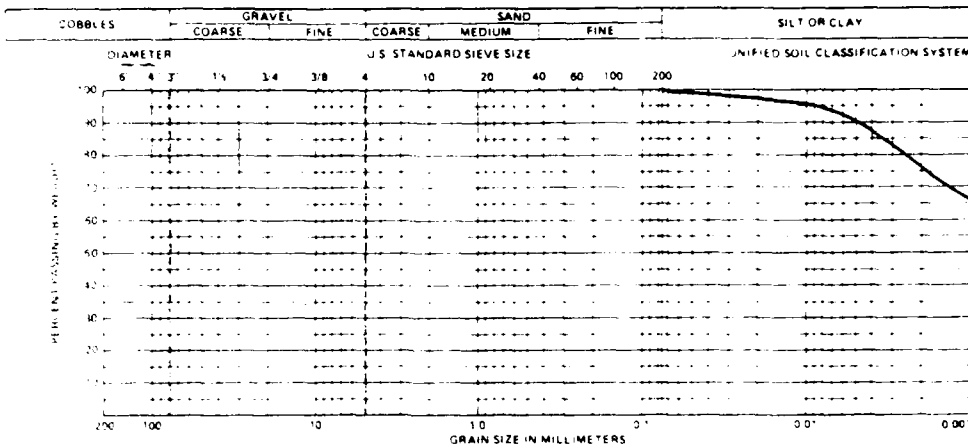


BORING	SAMPLE	DEPTH (ft)	SYMBOL	CLASSIFICATION	w (%)	w <sub>L</sub> (%)	w <sub>p</sub> (%)
-	H-2	11'		Brown and gray silty CLAY			

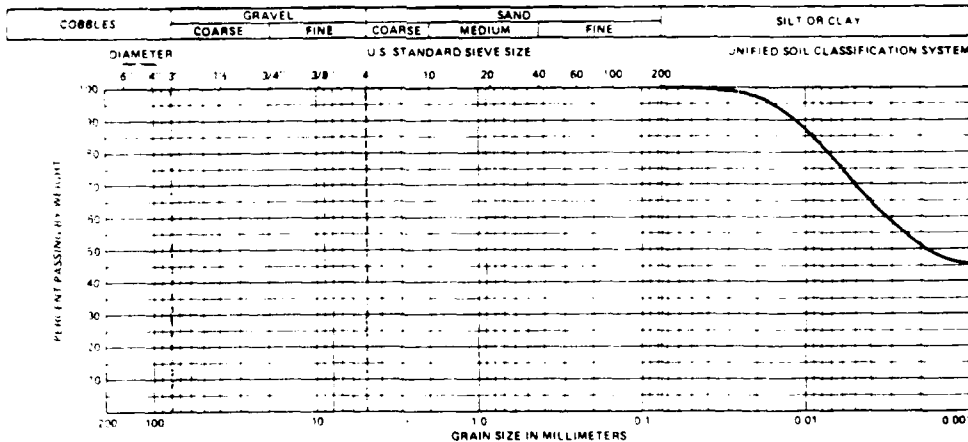
FIGURE A1



## GRAIN-SIZE DISTRIBUTION



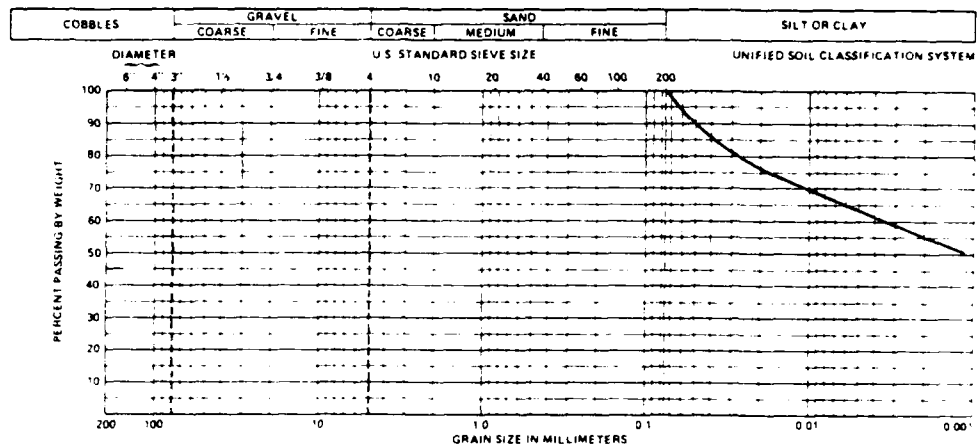
NO.	SAMPLE	DEPTH IN	SYMBOL	CLASSIFICATION	...	...	...	...
-	H-3	15'		Brown and gray silty CLAY				



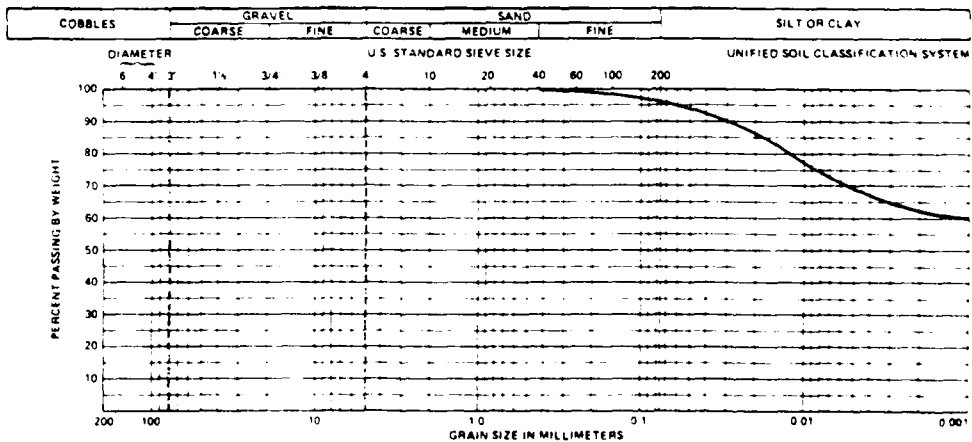
BORING	SAMPLE	DEPTH (ft)	SYMBOL	CLASSIFICATION	w (%)	w <sub>L</sub> (%)	w <sub>p</sub> (%)
-	H-4	19'		Brown and gray silty CLAY			

REF A2

1



BORING	SAMPLE	DEPTH	SYMBOL	CLASSIFICATION
W-1	-	4'-6'		red brown and brown gray mottled clay CLAY



BORING	SAMPLE	DEPTH (')	SYMBOL	CLASSIFICATION	w, %	w <sub>L</sub> , %	w <sub>p</sub> , %
2-1	-	11.40'		Red brown and brown gray mottled clay			
				CLAY			

• 1 • 121 A3

# GRAIN-SIZE DISTRIBUTION

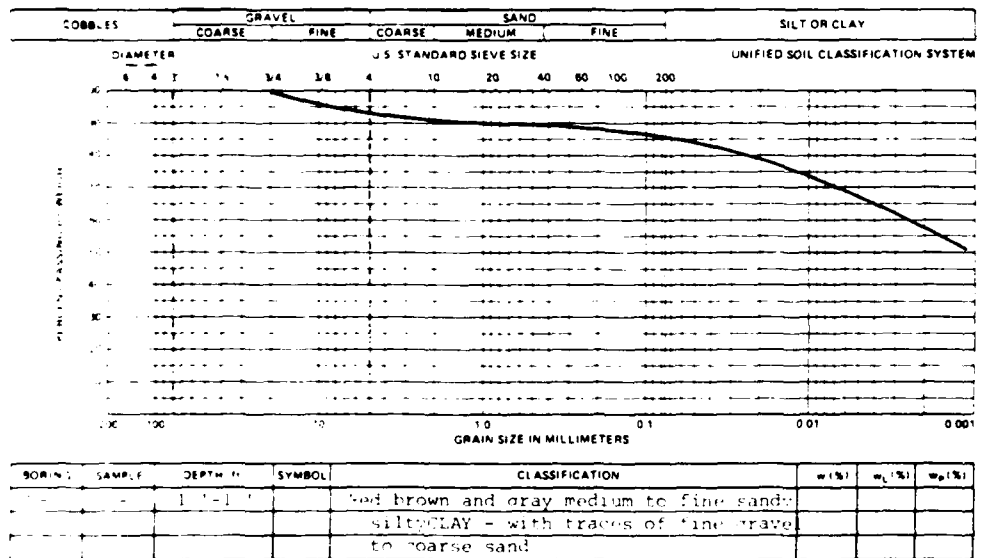
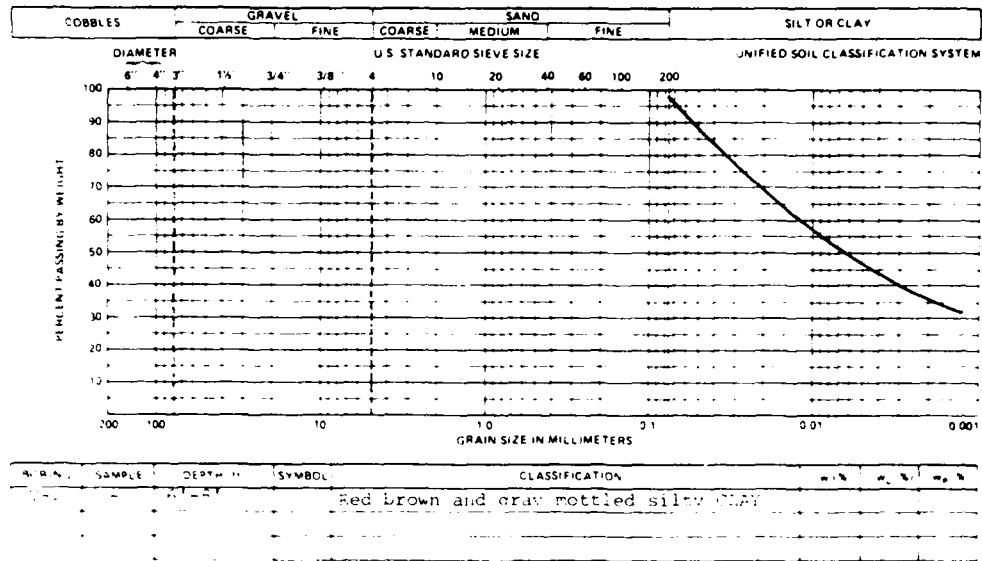
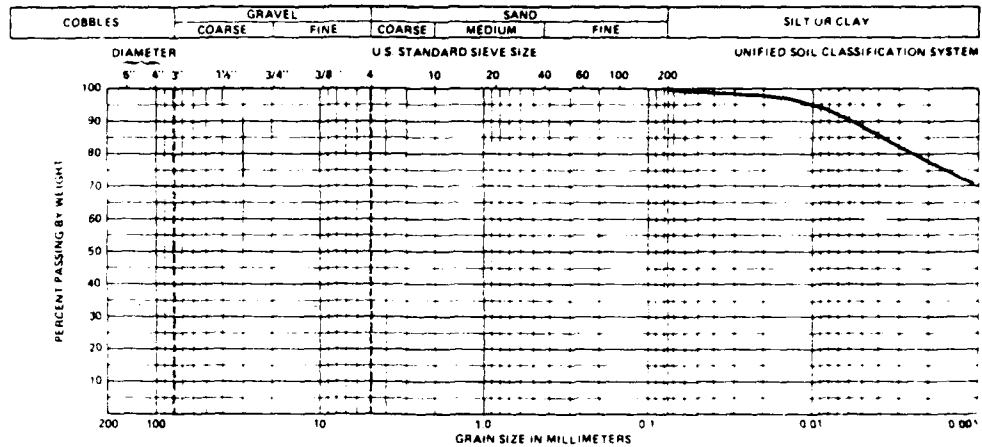
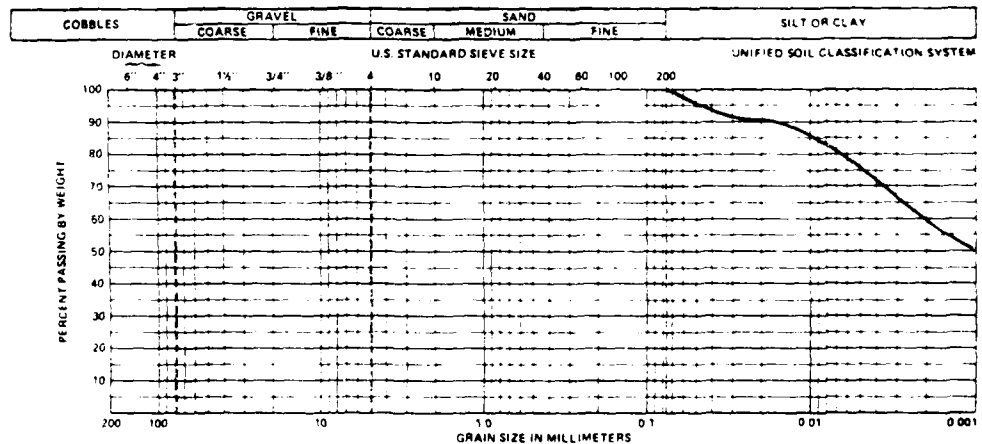


FIGURE A4

# GRAIN-SIZE DISTRIBUTION



BORING	SAMPLE	DEPTH (ft)	SYMBOL	CLASSIFICATION
W-4	-	14'-16'		Brown and Gray Silty CLAY



BORING	SAMPLE	DEPTH (ft)	SYMBOL	CLASSIFICATION	w (%)	w <sub>L</sub> (%)	w <sub>p</sub> (%)
W-5	-	18'-20'		Red brown silty CLAY			

UNITED A5

# GRAIN-SIZE DISTRIBUTION

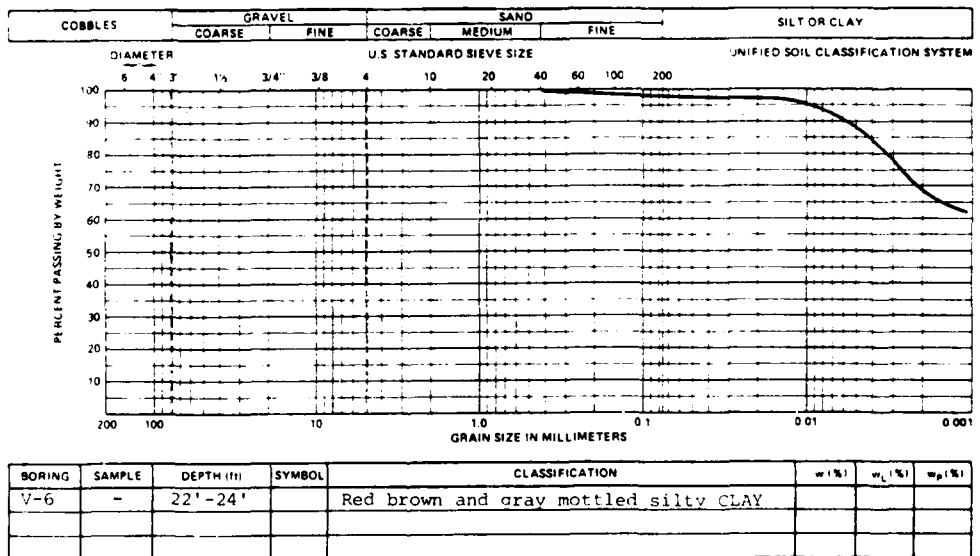
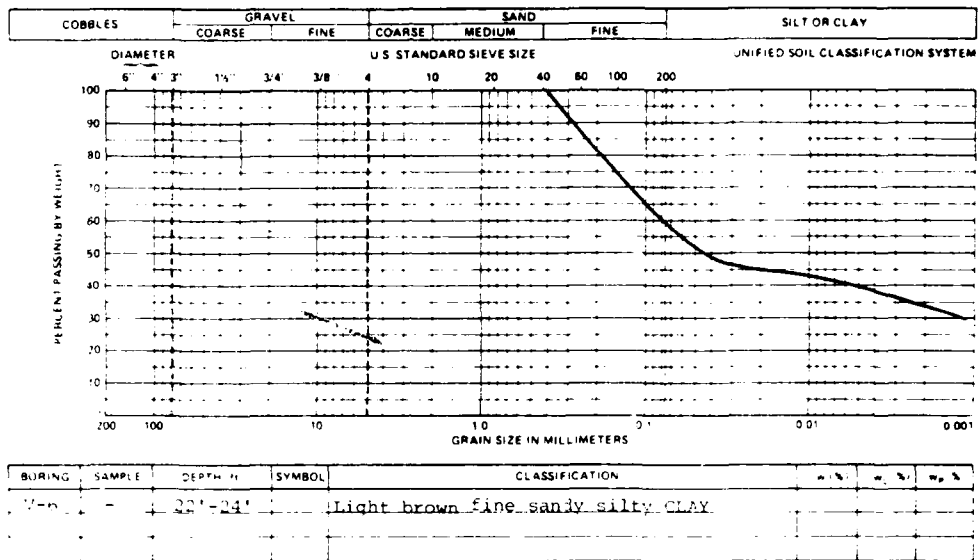
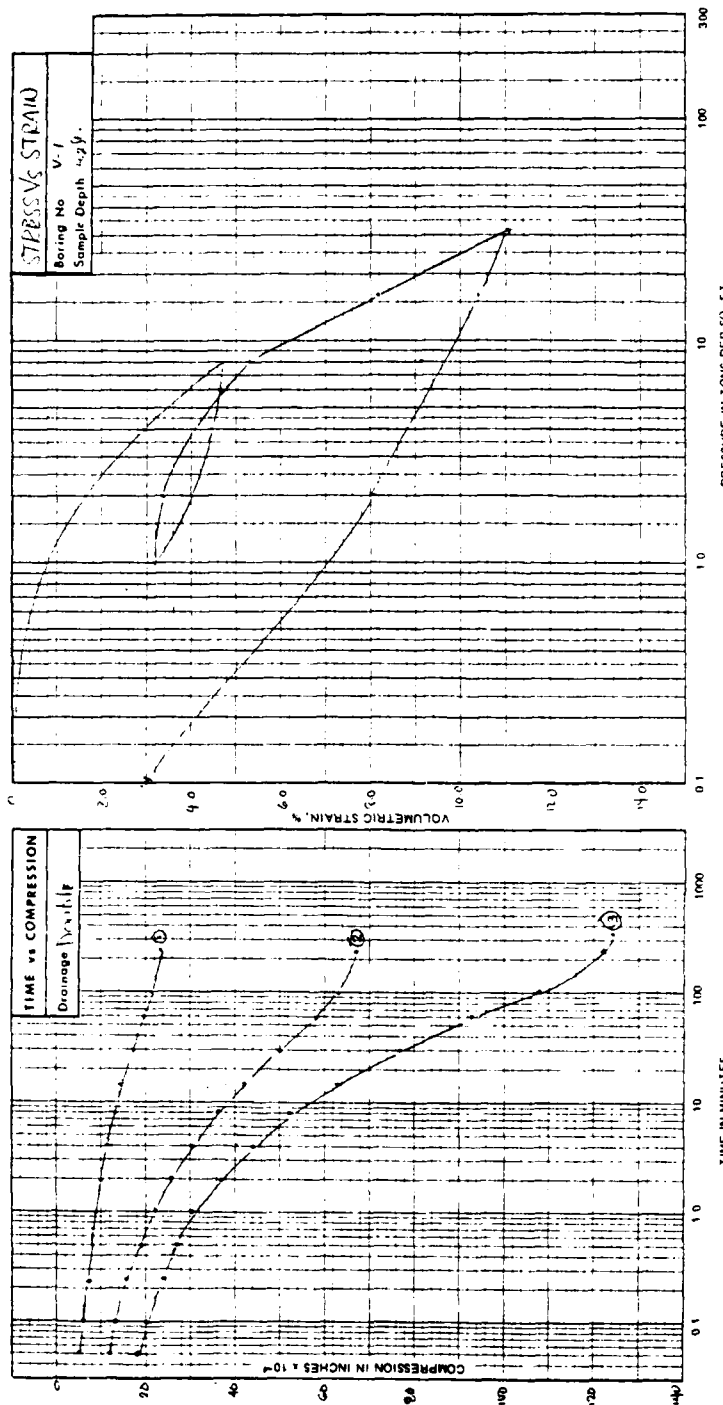


FIGURE A6



PRESSURE INCREMENTS ON CURVE			TIME IN MINUTES	COEFFICIENT OF CONS (1/1000)	DESCRIPTION OF SPECIMEN	CONSOLIDATION PROPERTIES	TEST SPECIMEN PROPERTIES								CONSOLIDATION TEST							
FROM (psi)	TO (psi)	TIME (min)					COMPRESSION INDEX	RECOMPRESSION INDEX	SWELLING INDEX	PRECONSOLIDATION STRESS, psi	EXISTING OVERBURDEN STRESS, psi	WATER CONTENT, %	VOID RATIO	SATURATION, %	SAMPLE HEIGHT, in	SAMPLE DIAMETER, in	UNIT DRY WEIGHT, pcf	LIQUID LIMIT, %	PLASTIC LIMIT, %	SPECIFIC GRAVITY	TESTED BY	DATE
1	11.5	24.8	2.48						0.164						24.1	1.41						
2	24.8	44.8	4.48						0.070						2.21	0.74						
3	44.8	84.8	8.48						5.560						100	1.00						
4	84.8	124.8	12.48						0.257						372	0.73						
5	124.8	164.8	16.48												2.410							
6	164.8	204.8	20.48												121	52						
7	204.8	244.8	24.48																			
8	244.8	284.8	28.48																			
9	284.8	324.8	32.48																			
10	324.8	364.8	36.48																			
11	364.8	404.8	40.48																			
12	404.8	444.8	44.48																			
13	444.8	484.8	48.48																			
14	484.8	524.8	52.48																			
15	524.8	564.8	56.48																			
16	564.8	604.8	60.48																			
17	604.8	644.8	64.48																			
18	644.8	684.8	68.48																			
19	684.8	724.8	72.48																			
20	724.8	764.8	76.48																			
21	764.8	804.8	80.48																			
22	804.8	844.8	84.48																			
23	844.8	884.8	88.48																			
24	884.8	924.8	92.48																			
25	924.8	964.8	96.48																			
26	964.8	1004.8	100.48																			
27	1004.8	1044.8	104.48																			
28	1044.8	1084.8	108.48																			
29	1084.8	1124.8	112.48																			
30	1124.8	1164.8	116.48																			
31	1164.8	1204.8	120.48																			
32	1204.8	1244.8	124.48																			
33	1244.8	1284.8	128.48																			
34	1284.8	1324.8	132.48																			
35	1324.8	1364.8	136.48																			
36	1364.8	1404.8	140.48																			
37	1404.8	1444.8	144.48																			
38	1444.8	1484.8	148.48																			
39	1484.8	1524.8	152.48																			
40	1524.8	1564.8	156.48																			
41	1564.8	1604.8	160.48																			
42	1604.8	1644.8	164.48																			
43	1644.8	1684.8	168.48																			
44	1684.8	1724.8	172.48																			
45	1724.8	1764.8	176.48																			
46	1764.8	1804.8	180.48																			
47	1804.8	1844.8	184.48																			
48	1844.8	1884.8	188.48																			
49	1884.8	1924.8	192.48																			
50	1924.8	1964.8	196.48																			
51	1964.8	2004.8	200.48																			
52	2004.8	2044.8	204.48																			
53	2044.8	2084.8	208.48																			
54	2084.8	2124.8	212.48																			
55	2124.8	2164.8	216.48																			
56	2164.8	2204.8	220.48																			
57	2204.8	2244.8	224.48																			
58	2244.8	2284.8	228.48																			
59	2284.8	2324.8	232.48																			
60	2324.8	2364.8	236.48																			
61	2364.8	2404.8	240.48																			
62	2404.8	2444.8	244.48																			
63	2444.8	2484.8	248.48																			
64	2484.8	2524.8	252.48																			
65	2524.8	2564.8	256.48																			
66	2564.8	2604.8	260.48																			
67	2604.8	2644.8	264.48																			
68	2644.8	2684.8	268.48																			
69	2684.8	2724.8	272.48																			
70	2724.8	2764.8	276.48																			
71	2764.8	2804.8	280.48																			
72	2804.8	2844.8	284.48																			
73	2844.8	2884.8	288.48																			
74	2884.8	2924.8	292.48																			
75	2924.8	2964.8	296.48																			
76	2964.8	3004.8	300.48																			
77	3004.8	3044.8	304.48																			
78	3044.8	3084.8	308.48																			
79	3084.8	3124.8	312.48																			
80	3124.8	3164.8	316.48																			
81	3164.8	3204.8	320.48																			
82	3204.8	3244.8	324.48																			
83	3244.8	3284.8	328.48																			
84	3284.8	3324.8	332.48																			
85	3324.8	3364.8	336.48																			
86	3364.8	3404.8	340.48																			
87	3404.8	3444.8	344.48																			
88	3444.8	3484.8	348.48																			
89	3484.8	3524.8	352.48																			
90	3524.8	3564.8	356.48																			
91	3564.8	3604.8	360.48																			
92	3604.8	3644.8	364.48																			
93	3644.8	3684.8	368.48																			
94	3684.8	3724.8	372.48																			
95	3724.8	3764.8	376.48																			
96	3764.8	3804.8	380.48																			
97	3804.8	3844.8	384.48																			
98	3844.8	3884.8	388.48																			
99	3884.8	3924.8	392.48																			
100	3924.8	3964.8	396.48																			
101	3964.8	4004.8	400.48														</					

FIGURE A-7

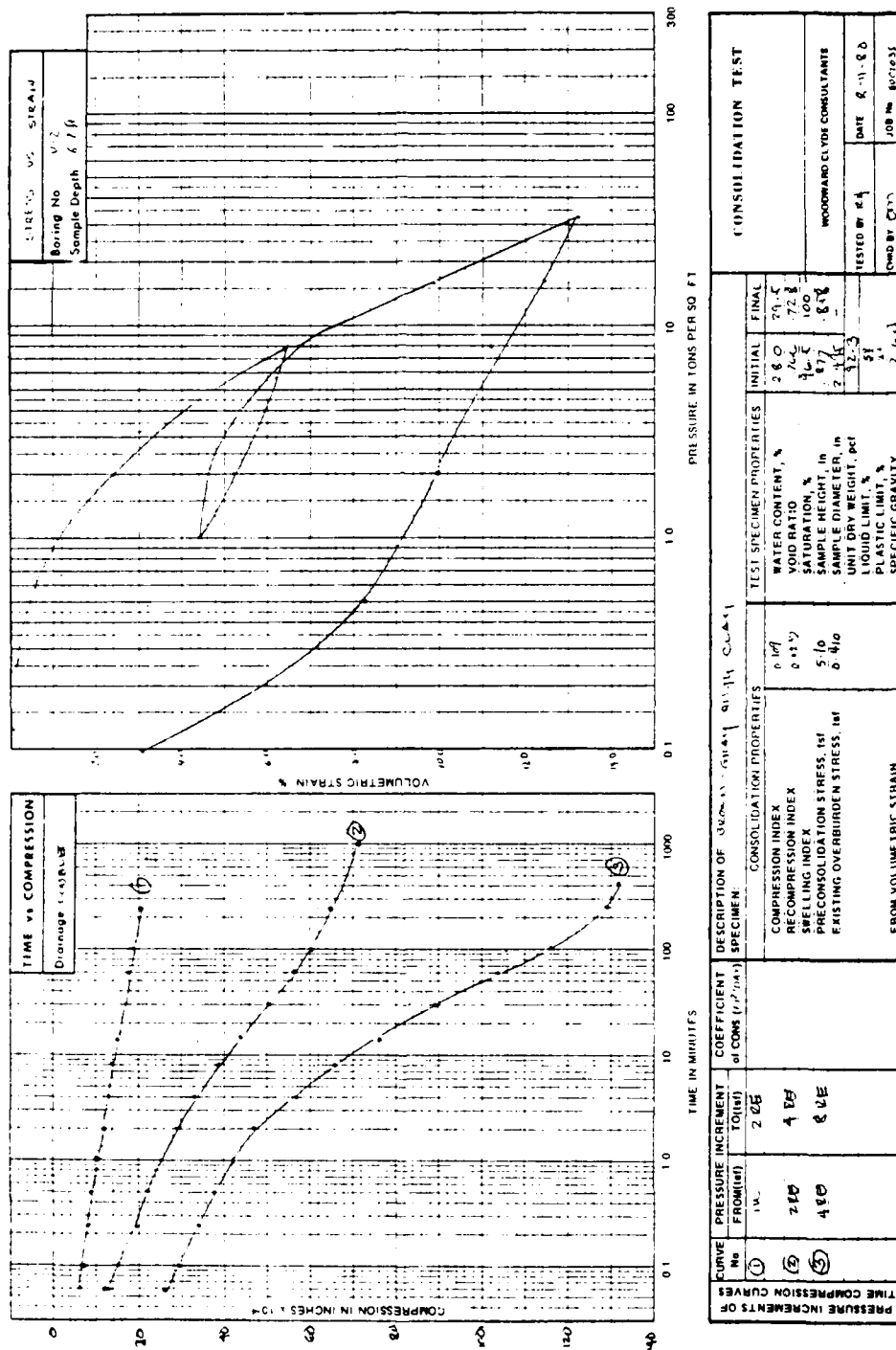


FIGURE AB

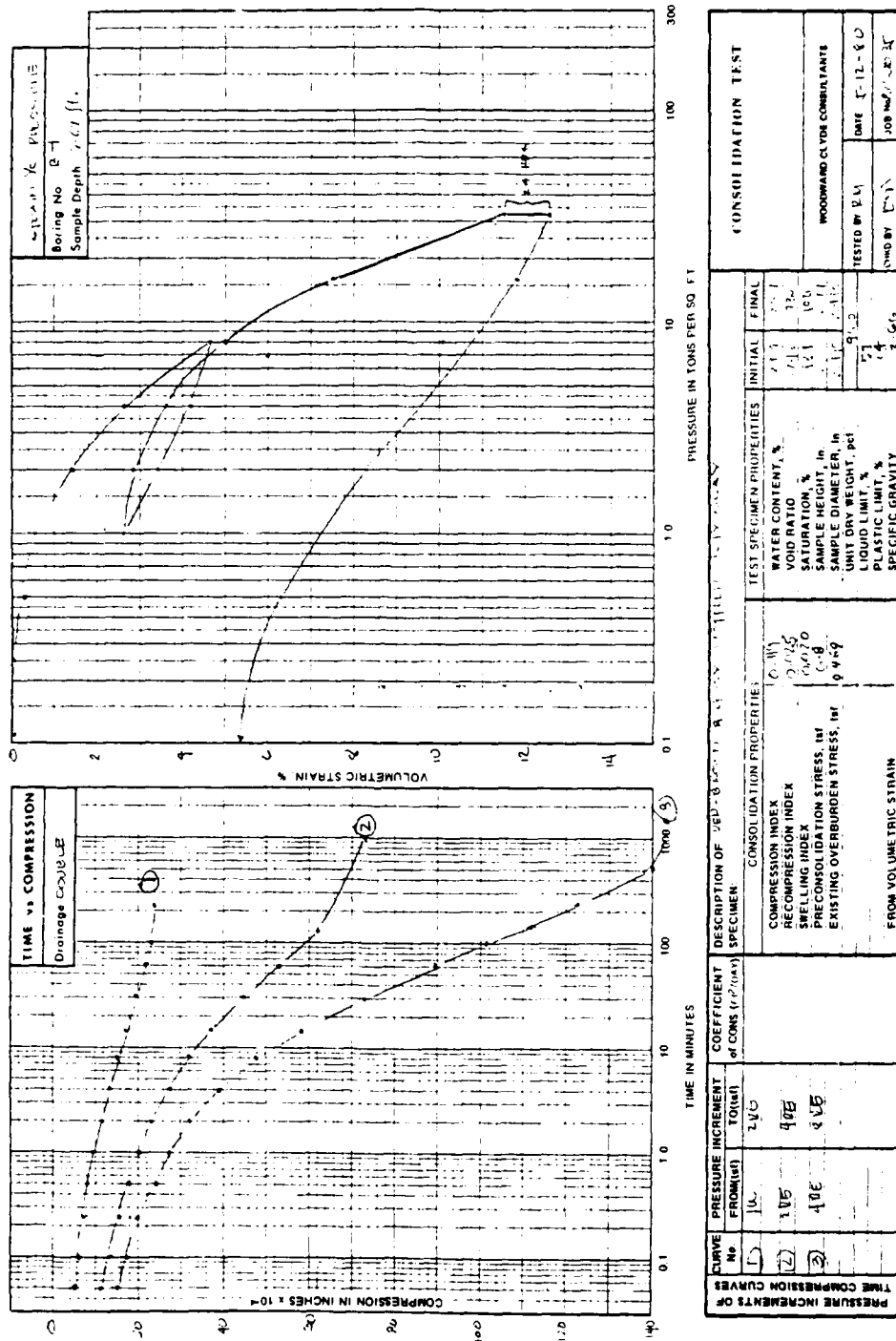
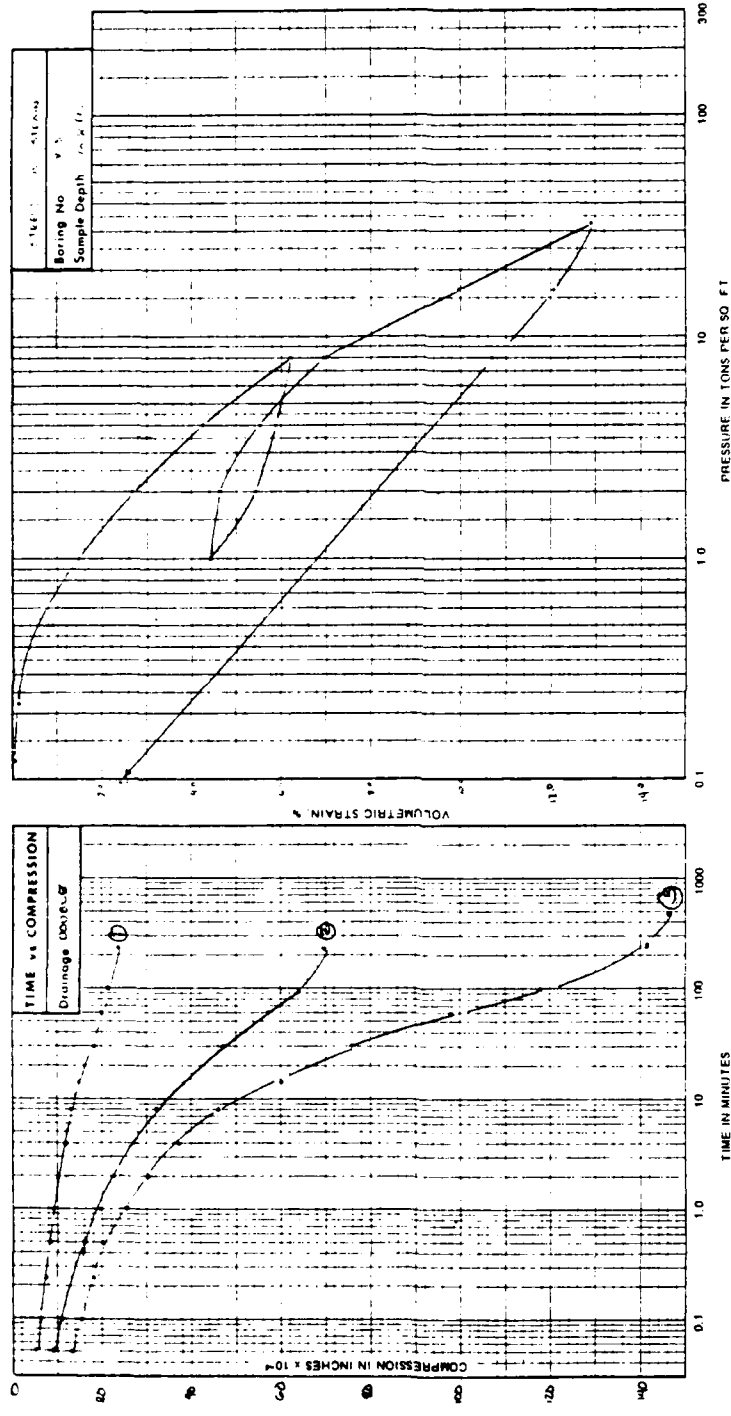


FIGURE A9

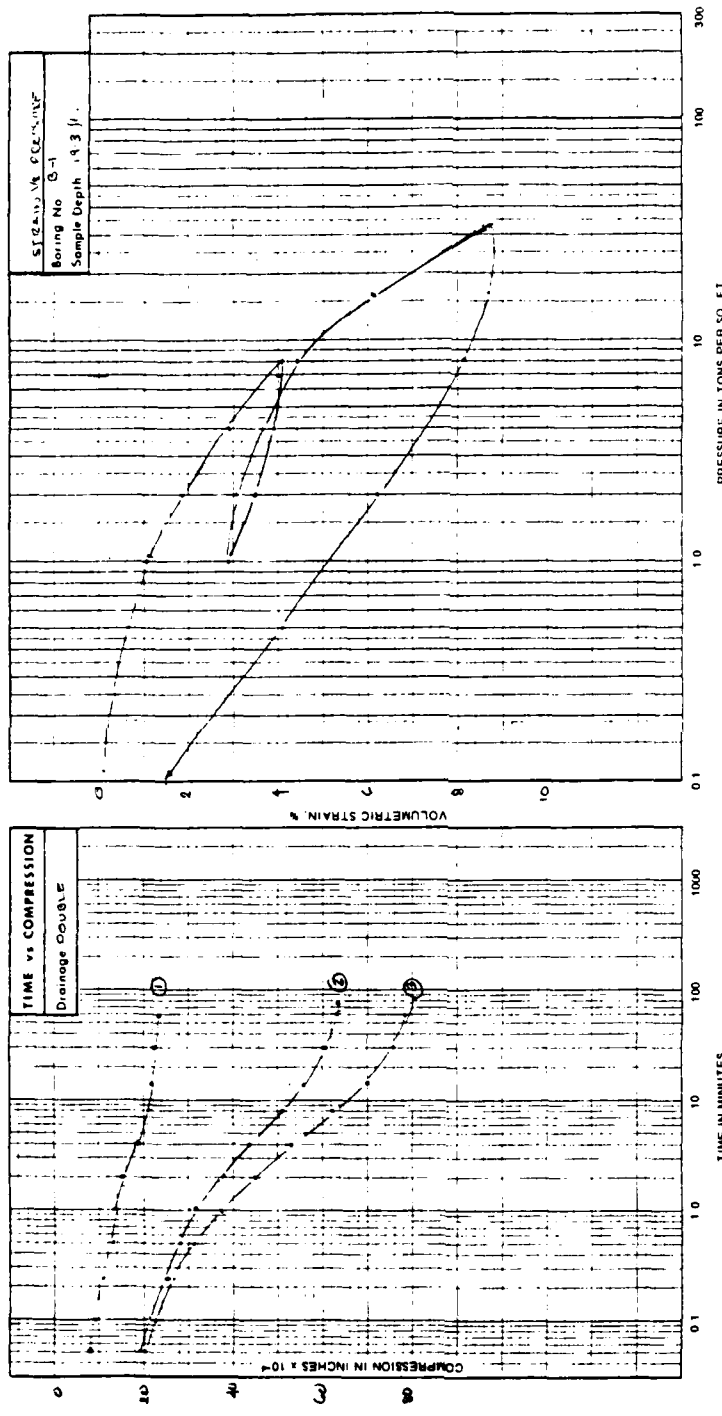




CURVE		PRESSURE INCREMENT		COEFFICIENT OF CONSOLIDATION	DESCRIPTION OF SPECIMEN	CONSOLIDATION PROPERTIES		TEST SPECIMEN PROPERTIES		FINAL	
No.	FROM (psi)	TO (psi)	TO (psi)			COMPRESSION INDEX	RECOMPRESSION INDEX	WATER CONTENT, %	VOID RATIO	INITIAL	FINAL
1	10	20	21.2		COMPRESSION INDEX	0.11	0.02	28.7	1.00	1.00	0.71
2	20	40	40.8		SWELLING INDEX	0.02	0.02	28.7	1.00	1.00	0.71
3	40	80	80.8		PRECONSOLIDATION STRESS, psi	5.40	5.40	28.7	1.00	1.00	0.71
					EXISTING OVERBURDEN STRESS, psi	5.40	5.40	28.7	1.00	1.00	0.71
					FROM VOLUMETRIC STRAIN			28.7	1.00	1.00	0.71

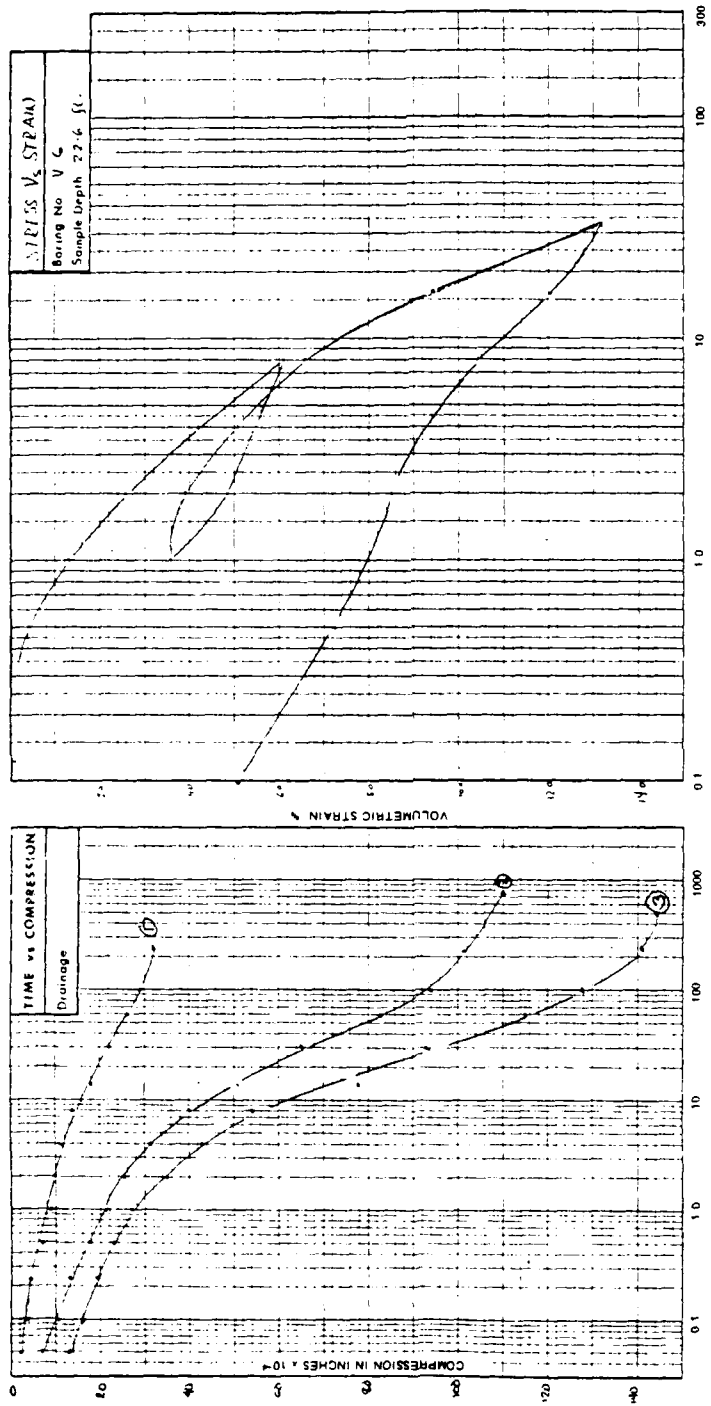
FIGURE A10





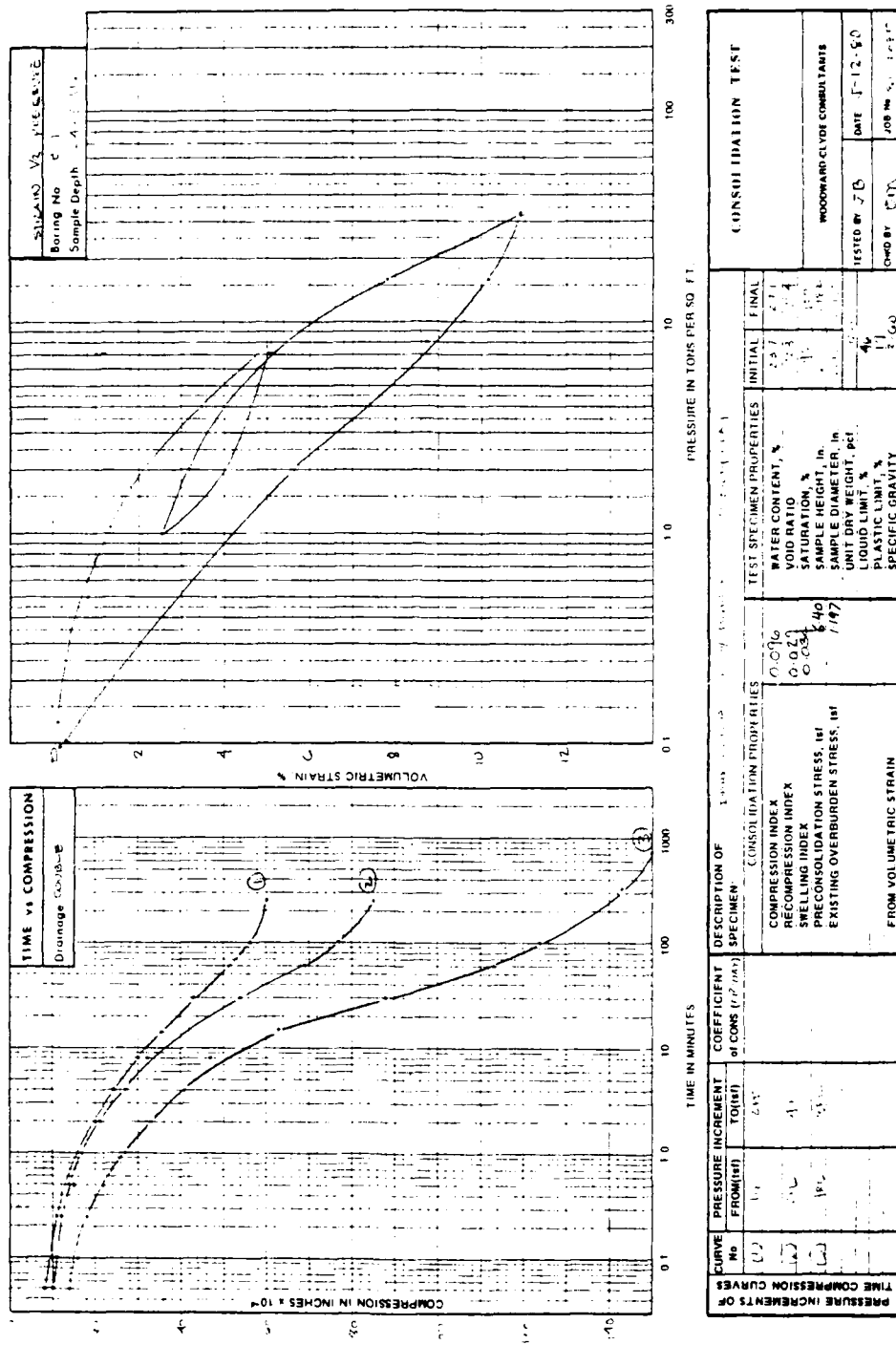
TIME COMPRESSION CURVES OR PRESSURE INCREMENTS OF		TIME IN MINUTES		COEFFICIENT OF CONS. (1/2 DATA)		DESCRIPTION OF SPECIMEN		CONSOLIDATION PROPERTIES		TEST SPECIMEN PROPERTIES		INITIAL		FINAL		CONSOLIDATION TEST	
Curve No.	Pressure Increment FROM (psi)	Pressure Increment TO (psi)	Time (min)	1/2 Time (min)	1/4 Time (min)	Compression Index	Swelling Index	Preconsolidation Stress, psi	Existing Overburden Stress, psi	Water Content, %	Void Ratio	Sample Height, in.	Sample Diameter, in.	Unit Dry Weight, pcf	Liquid Limit, %	Plastic Limit, %	Specific Gravity
1	1.0	1.5	1.0	0.5	0.25	0.090	0.017	0.001	0.001	22.7	22.3	1.0	1.0	1.0	1.0	1.0	1.0
2	1.5	2.0	1.0	0.5	0.25	0.090	0.017	0.001	0.001	22.7	22.3	1.0	1.0	1.0	1.0	1.0	1.0
3	2.0	2.5	1.0	0.5	0.25	0.090	0.017	0.001	0.001	22.7	22.3	1.0	1.0	1.0	1.0	1.0	1.0

FIGURE A12



TIME COMPRESSION CURVES		TIME IN MINUTES		COEFFICIENT OF CONS. ( $C_v$ )		DESCRIPTION OF SPECIMEN		CONSOLIDATION PROPERTIES		TEST SPECIMEN PROPERTIES		CONSOLIDATION TEST	
CURVE No.	PRESSURE INCREMENT FROM (psi)	TO (psi)	TIME (min)	COEFF. OF CONS. ( $C_v$ )	DESCRIPTION OF SPECIMEN	COMPRESSION INDEX	RECOMPRESSION INDEX	PRECONSOLIDATION STRESS, psi	EXISTING OVERBURDEN STRESS, psi	WATER CONTENT, %	VOID RATIO	INITIAL	FINAL
1	10	20	148		COMPRESSION INDEX	0.15		6.30	1.146	91.7	78.1	91.7	78.1
2	20	40	476		RECOMPRESSION INDEX	0.25		6.30	1.146	91.7	78.1	91.7	78.1
3	40	80	825		PRECONSOLIDATION STRESS, psi			6.30	1.146	91.7	78.1	91.7	78.1
FROM VOLUMETRIC STRAIN													
WATER CONTENT, %													
VOID RATIO													
SATURATION, %													
SAMPLE HEIGHT, in													
SAMPLE DIAMETER, in													
UNIT DRY WEIGHT, pcf													
LIQUID LIMIT, %													
PLASTIC LIMIT, %													
SPECIFIC GRAVITY													
TESTED BY V.A.													
DATE 8-11-60													
JOB NO. 800,203													
WOODWARD-CLYDE CONSULTANTS													

FIGURE A13



VOLUME III

ASSESSMENT AND PREDICTION  
OF SKIN FRICTION OF SHAFTS  
IN BEAUMONT CLAY

By

W. Gardner, G. Baker, and P. Sircar

## TABLE OF CONTENTS

	Page
PART I: INTRODUCTION .....	3
PART II: SCOPE OF INVESTIGATION .....	5
PART III: ANALYSIS OF LOAD TEST RESULTS .....	6
Shaft and Load-Test Data .....	6
Top Deformation-Total Shaft Load Behavior .....	6
Load-Transfer Behavior of Test Shaft S-1 .....	7
PART IV: SHAFT FRICTION PREDICTION FROM BASIC SOIL PROPERTIES....	10
Effective Stress Analysis .....	11
Analyses Using Undrained Shear Strength .....	19
PART V: SHAFT FRICTION ANALYSIS BY SIMILITUDE OR INDIRECT CORRELATION .....	25
Mortar-Soil Interface Shear Tests .....	25
Borehole Shear Tests .....	26
Moisture Migration Analysis .....	26
PART VI: LOAD-DEFORMATION ANALYSIS .....	29
Numerical Load-Transfer Analysis .....	30
Characterization of Load-Transfer Curves .....	30
Analyses Performed .....	36
PART VII: RESULTS OF THE LOAD-DEFORMATION ANALYSES .....	40
Results for Shaft S-1 .....	40
Results for Shaft S-3 .....	41
PART VIII: SUMMARY OF CONCLUSIONS AND RECOMMENDATIONS FOR FURTHER STUDY .....	42
Soil Classification and Stratigraphy .....	42
Space and Time Dependent Variations in Soil Properties .....	43
Undrained Shear Strength .....	44
Drained Shear Strength .....	46
State of Stress .....	49
Prediction of Ultimate Skin Friction .....	52
Load-Deformation Prediction .....	57
Areas of Needed Research .....	59

TABLE OF CONTENTS  
(Continued)

PART IX: LITERATURE CITED .....	63
7 TABLES	
21 FIGURES	
APPENDIX A: FIELD AND LABORATORY TEST RESULTS	
APPENDIX B: LOAD DEFORMATION ANALYSES - RAW DATA	



STUDY TO INVESTIGATE THE EFFECTS OF SKIN FRICTION ON THE  
PERFORMANCE OF DRILLED SHAFTS IN COHESIVE SOILS

VOLUME III - ASSESSMENT AND PREDICTION OF  
SKIN FRICTION OF SHAFTS IN BEAUMONT CLAY

PART I: INTRODUCTION

Presented herein is the third and final report in a series prepared by Woodward-Clyde Consultants for the U. S. Army Engineer Waterways Experiment Station under contract DACA 39-80-C-0001 entitled "Study to Investigate the Effects of Skin Friction on the Performance of Drilled Shafts in Cohesive Soils." This study has been conducted in three stages including (1) field investigations, (2) laboratory testing, and (3) geotechnical engineering analyses. This report presents a description of the assessment of techniques relevant to the prediction of the ultimate skin (shaft) friction of shafts drilled in cohesive soils as well as to prediction of the load-settlement relationship of such shafts.

As described in Volume I entitled "Field Investigations," the area of study is situated on the right-of-way at the intersection of State Highway 225 and Interstate Highway 610 in southeastern Houston, Texas. At this location, subsurface investigations and in-situ testing were conducted in proximity to four drilled shafts constructed and load tested in 1969 under the auspices of the Center for Highway Research at the University of Texas at Austin. Geologically, the test site lies within the Beaumont clays, a deposit of Pleistocene age soils extending over much of south-central Texas.

Parts II and III of the following text describe the scope of analyses conducted, and a detailed interpretation of the load test results reported for Test Shaft, S-1, respectively. An assessment of the various methods of evaluating the ultimate shaft friction of drilled

shafts is described in Parts IV and V. Load-settlement predictions are assessed and compared to the observed behavior of the test shafts in the area of study in Parts VI and VII, respectively. Tabulations and graphical data supporting the text are presented in Appendixes A and B.

## PART II: SCOPE OF INVESTIGATION

The analytic investigations were subdivided into (1) a detailed interpretation of the load test results on Test Shaft, S-1, (2) an evaluation of the ultimate shaft resistance in comparison with the existing load test data, and (3) evaluation of the conformance of load-settlement predictions with the observed behavior of the test shafts. Test Shaft S-1 was selected for detailed interpretation of the measured shaft-load transfer relationships. This dry-cast straight shaft is the most common type of installation in stiff to hard clays. This work involved an independent interpretation of the shaft load distribution measurements reported by O'Neill and Reese (1970).

Evaluation of ultimate shaft friction was first made by theoretically based techniques which utilized basic soil properties to predict shaft friction. Subsequently, other techniques were investigated including application of laboratory soil-mortar interface shear measurement, and in-situ borehole shear tests. In addition, the application of moisture migration concepts to the prediction of shaft friction was also investigated.

Evaluation of the load-settlement analyses focused on a numerical load-transfer technique first proposed by Seed and Reese (1957). This work included derivation of load-transfer curves from load test results and prediction of the load-settlement behavior of Test Shaft S-1. Wherever possible, conclusions and recommendations are presented for generic use of the various procedures developed to predict ultimate shaft friction and load-settlement behavior.

### PART III: ANALYSIS OF LOAD TEST RESULTS

The shaft load transfer reflecting the mean deformation of the shaft versus total shaft load was first analyzed using the interpretation of the instrumented load tests provided by O'Neill and Reese for each of the four shaft types employed. An interpretation of the load distribution data for each instrumentation location as provided by O'Neill and Reese was subsequently used to conduct an independent interpretation of the load-transfer curves at each level of instrumentation. The results of these analyses are summarized in the following sections.

#### Shaft and Load-Test Data

As noted earlier, Test Shaft S-1 was selected for detailed analysis. For interpretation of the load-transfer curves, the diameter of S-1 was assumed to be 2.5 ft and the shaft length 23.1 ft. Note that upon a subsequent removal of the shaft, an average diameter of 2.56 ft was measured.

The first loading of the shaft was conducted by applying loads in increments of 5 or 10 tons every 2.5 minutes. Loading continued until plunging of the shaft was observed. Subsequent to unloading, a second load test was immediately conducted to investigate reloading effects. Finally, 3.5 months after the initial testing, a third load test was conducted to investigate the effects of setup on the shaft capacity.

#### Top Deformation-Total Shaft Load Behavior

The total shaft (skin friction) and base load curve versus top deformation curves reported by O'Neill and Reese for each of the test shafts are reproduced in Appendix B as Figures B1 through B4. The peak and minimum post-peak ultimate shaft load and the associated mean deformation shaft at the top of the shaft are tabulated in Table 1 for all four shafts tested.

The data contained in Table 1 have been analyzed and used to calculate the average shaft friction,  $(\tau_f)_{ave}$ , for each of the test shafts. Values of  $(\tau_f)_{ave}$  normalized by both the average effective overburden and average undrained shear strength,  $(S_u)_{ave}$ , are presented in Table 2 for peak and residual ultimate shaft loads.

The  $(\tau_f)_{ave} / (S_u)_{ave}$  calculations were made using the  $S_u$  measurements summarized in Figure A5 of Appendix A. In these evaluations, the embedded area of the shaft was calculated using the shaft length shown to be effective in transferring load to the soil (as discussed in Part V), and not the total length of the shaft.

#### Load-Transfer Behavior of Test Shaft S-1

Load-transfer curves from the dry-cast, straight shaft S-1 were independently interpreted from the load distribution data reported by O'Neill and Reese (1970). In this interpretation, a fourth-degree polynomial least squares regression curve was selected to represent the load (Q) - depth (x) data. The form of this expression is shown as Equation 1:

$$Q = a + bx + cx^2 + dx^3 + ex^4 \quad (1)$$

In curve fitting, special boundary conditions were imposed at the ground surface. In this regard, it was assumed that the measured butt load is correct and that the slope of the load-depth curve is zero at the ground surface. This boundary condition also assumes zero load transfer at the surface which is believed to be a reasonable assumption considering the lack of confinement, desiccation effects, etc. The load versus depth curves developed on this basis for Shaft S-1 at various total butt loads are included in Appendix B as Figures B5 through B16.

### Load-Transfer Curves

From the regression curves relating shaft load and depth, the load-transfer curves were developed for each instrumentation level. This was accomplished for various depths by differentiations of the load distribution curve as expressed by Equation 2:

$$\frac{dQ}{dx} = b + 2cx + 3dx^2 + 4ex^3 \quad (2)$$

The load transfer at any particular depth was then calculated as:

$$\tau_x = \frac{1}{\pi d} \frac{dQ}{dx} \quad (3)$$

The load-transfer curve was then developed for each load increment to produce the load-transfer curves shown in Appendix B as Figures B17 through B24. The pile is assumed rigid, and thus, the pile settlements indicated in the figures represent both the butt settlement and also the settlement at the point where the load is measured.

### Load-Transfer Curve Characterization

The load-transfer curves were simulated by a hyperbolic representation described by Chang and Duncan (1970) after Kondner (1963). By this means the load-transfer curve is represented by an initial tangent modulus ( $E_i$ ) and the ultimate shear strength ( $\tau_f$ ). These parameters are obtained by plotting pile settlement ( $\rho$ ) versus  $\rho/\tau$ . As shown by Figure 1, this transformation provides a straight line for a substantial portion of the data. The y-axis intercept with this line represents  $1/E_i$ ; whereas the slope of the line represents  $1/\tau_{fh}$ . The results of these analyses are summarized in Table 3. Note that the reported  $R_f$  represents the ratio between the observed ( $\tau_f$ ) and the predicted ( $\tau_{fh}$ ) shearing resistances.

Figure 2, based on the foregoing interpretation, demonstrates the parabolic distribution of  $\tau_f$  along the drilled shaft. The distribution of  $\tau_f$  for Shafts S-2 and S-3, based on O'Neill and Reese (1970) data are also shown in Figure 2. Figure 3 shows  $\tau_f/\sigma'_{vo}$  (the Beta Factor) as a function of measurement depth for all three dry-cast shafts.

Shafts S-2 and S-3 exhibit a significantly higher load transfer than S-1 in the upper 10 ft of the shaft. This is reflected by the  $\beta$  factors interpreted in this interval, e.g.,  $\beta_{\max}$  of approximately 1.6 at 2.3 ft (S-1), 2.7 (S-2) and 2.5 (S-3) at 4.1 ft. The maximum unit skin friction along the shaft shown by Figure 2 approaches 1.0 tsf for all the dry-cast shafts. Except for S-3 (void below base), the test shafts exhibit the marked reduction in load transfer at and just above the base usually observed for both drilled shafts and driven piles.

#### PART IV: SHAFT FRICTION PREDICTION FROM BASIC SOIL PROPERTIES

Current state-of-the-practice static capacity predictions for piles and drilled shafts in cohesive soils are usually empirically related to the undrained shear strength ( $S_u$ ) of the bearing soils via an  $S_u$  reduction or "Adhesion" factor (Tomlinson, 1957; Skempton, 1959). However, the prediction of the ultimate shaft friction ( $Q_s$ ) by rational effective stress techniques, as first suggested by Chandler (1963), is gaining increased interest. This technique is thought by many investigators to provide the basis for future developments in deep foundation design methodology (Vesic, 1975).

Other  $Q_s$  predictive techniques of interest to this study include laboratory and in-situ tests conducted to attempt to simulate the shaft soil interface shear mechanism. One approach, incorporated as part of this study, has been to determine the shearing resistance between simulated shaft materials and soil by direct shear testing (Potyondy, 1961; O'Neill and Reese, 1970). In addition, model pile (rod shear) tests have been run in specially designed triaxial cells as described by Bea and Doyle (1975). O'Neill and Reese have also conducted laboratory moisture migration studies to attempt to relate the moisture change of the soil in contact with a drilled shaft to the Adhesion Factor ( $\alpha$ ).

In-situ testing to investigate shaft friction has been conducted using a pressuremeter-type probe as a model pile. In-situ tests utilizing the Iowa borehole shear device have also been conducted as part of this study to investigate the shearing resistance between mortar-faced shear plates and the in-situ soil. The results of these and other relevant field and laboratory tests are described in Part XI of the preceding Volume II, entitled "Laboratory Testing."

The following sections present a summary of investigations into the capability of the various types of shaft friction analysis to predict the peak and post-peak capacity of the drilled shafts which have been loaded at the test site. Analyses of the load test results from the four test shafts are summarized in the Tables 1 through 3.



### Effective Stress Analysis

Two basic effective stress formulations have been applied to the prediction of the shaft friction ( $\tau_f$ ) of both driven piles and drilled piers. These approaches are described and evaluated herein with respect to the observed versus predicted behavior of the drilled shafts of the test site.

#### Effective Stress Formulations

The earliest and most common formulation (Chandler, 1968) is based on the Mohr-Coulomb failure state and is described by Equation 4 as a function of the ambient effective horizontal stress ( $\sigma'_{ho}$ )\* and the shaft-soil interface friction angle ( $\delta$ ):

$$\tau_f = K_o \sigma'_{vo} \tan \delta \quad (4)$$

This expression implicitly assumes that the soil in contact with the shaft has been altered by installation so that the effective stress cohesion ( $c'$ ) is obscured. It also assumes that the ambient geostatic stress system which existed before construction and loading is restored at the shaft-soil interface, and that drained interface shear occurs during loading, e.g., no significant excess porewater pressures are generated. Chandler (1968) and, subsequently, Burland (1973) suggested that  $\delta$  is equivalent to the effective friction angle of the soil ( $\phi'$ ). Alternatively,  $\delta$  has been assumed to be less than  $\phi'$  in some design procedures (for example, the American Petroleum Institute Standards, 1981 proposed that  $\delta = \phi' - 5^\circ$ ).

In addition to Equation 4, a number of other Mohr-Coulomb failure state solutions can be derived. For example, if it is assumed that the effective stress in the vertical direction remains constant at its

---

\*  $\sigma'_{ho}$  is equivalent to the product of the effective overburden pressure ( $\sigma'_{vo}$ ) and the coefficient of earth pressure-at-rest ( $K_o$ ).

initial (pre-shaft installation) value during shear along a vertical shearing plane, and that shear resistance is fully mobilized, then:

$$\tau_f = \frac{\sigma'_{vo} \cos \delta \sin \delta}{1 + \sin^2 \delta} \quad (5)$$

Equation 5 is applicable only to normally consolidated soils and for this state would produce slightly higher values of  $\tau_f$  when compared to Equation 4 (Parry and Swain, 1977; Vesić, 1975).

A more rational effective stress solution (Esrig, et al., 1979) can be derived from Critical State Soil Mechanics as shown by Figure 4. As indicated, all stress parameters are given in terms of the effective mean normal (octahedral) stress  $(p'_o)^*$ , including the slope of the virgin compression line (VCL) and of the recompression line in the  $e(\text{void ratio}) - \log p'$  space, i.e.,  $C'_c$  and  $C'_r$ . The critical state failure condition can be expressed from Figure 4 as:

$$\tau_f = p'_{cs} \frac{M_1}{2} \cos \delta \quad (6)$$

The parameter  $M_1$  is  $(6 \sin \delta)/(3 - \sin \delta)$  and represents the slope of the critical state line (CSL) in  $p$ - $q$ , where  $q$  is the deviator stress  $(\sigma_1 - \sigma_3)$ . The parameter  $p'_{cs}$  represents the mean normal stress at failure as defined by the critical state criteria. (See Fig. 4.)

For normally consolidated soils,  $p'_{cs}$  can be solved from the relative positions of the VCL and the CSL and the fact that these lines are parallel when expressed in terms of  $\log p'$ . Based primarily on direct simple shear tests,  $p'_{cs}/p'_{nc}$  has been characterized by Esrig, et al. (1979) as

$$p'_{cs}/p'_{nc} = 0.11 + 0.0063 \text{ LL} \quad (7)$$

---


$$* p'_o = \frac{\sigma'_1 + \sigma'_2 + \sigma'_3}{3} = \frac{\sigma'_{vo} (1 + 2K_o)}{3}$$

with LL in Equation 7 representing the liquid limit of the soil expressed as a percentage. The value of  $p'_{cs}/p'_{nc}$  is limited to a value of 0.62

For the general case of an overconsolidated soil, the ultimate skin friction can then be expressed in terms of the maximum past mean normal effective stress ( $p'_m$ ) and the in-situ mean normal effective stress ( $p'_o$ ) as (Esrig, et al., 1979):

$$\tau_f = p'_o \frac{3 \sin \delta \cos \delta}{3 - \sin \delta} \left[ \frac{p'_m}{p'_o} \right]^{1-R} \frac{p'_{cs}}{p'_{nc}} \quad (8)$$

The exponent R represents  $C'_r/C'_c$  and  $p'_{nc}$  is the mean normal effective stress in virgin compression which has the same void ratio as  $p'_{cs}$ . The expression for  $p'_{cs}$  given in Equation 8 can be readily derived from the triangle defined in Figure 5 by points 1, 2, 3 and 4.

It is of interest to note in Figure 5 that the effect of shaft drilling is to rebound Point 2 to Point 2a and that the subsequent effect of concrete placement is to recompress the soil near the side-walls of the open shaft at least to the initial Point 2 and probably somewhat beyond this point. As the difference in weight of the excavated soil and the concrete fill is not great, it is reasonable to assume that shearing upon load application starts from near Point 2, e.g., the ambient geostatic stress is essentially restored before loading.

In reality, it is likely that the relaxation of a thin zone of soil around the shaft and the possible opening of small fissures in this zone will somewhat change the stress path during shear even with the restoration of the ambient geostatic stresses at the shaft-soil interface. It is postulated that the effect of this condition plus disturbance of the soil during the drilling process is to reduce the skin friction which would be realized if the effective cohesion and friction angle of the soil in contact with the shaft were unchanged from the in-situ state. This strength degradation effect is modeled in Equation 8 by assuming the effective cohesion is zero and the interface friction angle is less than  $\phi'$ .

### Comparison of Alternate Solutions

The locus of  $\tau_f/\sigma'_{vo}$  as predicted by Equations 4 and 8 are shown by Figure 6 for a range of shaft-soil interface friction angles. Note that  $\tau_f/\sigma'_{vo}$  is a useful parameter for evaluation and design application and is termed the Beta ( $\beta$ ) Factor. It is evident from Figure 6 that Equation 4 predicts significantly lower  $\beta$  values when OCR's are greater than about 3 and larger  $\beta$  values at smaller OCR's.

Recent studies by Esrig, et al. (1979) for driven piles have shown that Equation 8 modified so as to consider the increase in effective mean normal stresses due to pile displacement effects is a relatively sensitive predictor of skin friction for both low and high displacement piles. Alternatively, Equation 4 has been applied by Burland (1973) to predict the skin friction of shafts drilled in the overconsolidated fissured London clays at Wembley. The results reported by Burland indicate Equation 4 to give a reasonably good representation of skin friction for the Wembley test site as shown by Figure 7. Consequently, both Equations 4 and 8 were considered for the effective stress prediction or evaluation.

### Evaluation of Effective Stress Formulations

To evaluate the applicability of shaft friction evaluated by Equations 4 and 8, an analysis of the peak value of  $Q_s$  was conducted for Test Shaft S-1. The soil parameters adopted for this study are listed in Table 4.

The upper bound OCR shown in Figure A1 is predicated on Equation 9. The undrained shear strength ( $S_u$ ) used is from those unconsolidated undrained triaxial shear tests judged to be reasonably representative of the unfissured elements of the Beaumont clay:

$$OCR = \frac{1}{K} \left[ \frac{S_u}{\tau_{vo}} \right]^{1/n} \quad (9)$$

Note that in the absence of special tests to define the normalized shear strength parameters  $K$  and  $n$  (Ladd and Foott, 1974), these parameters have been conservatively characterized as 0.35 and 0.75, respectively, from available data on soils with similar characteristics (Gardner, 1977). The postulated variation of  $S_u$  versus depth at the test site is shown by Figure A5 of Appendix A.

As the first step in this evaluation, the  $\beta$  factor calculated from the load test curves of Test Shaft S-1 (see Table 3) were plotted on Figure 8(a) against the most probable OCR range of the soil at depths corresponding to the test data. Similar plots for Test Shafts S-2 and S-3 are provided in Figure 8(b). Equations 4 and 8 were solved for the interface friction angle range shown in Figures 8(a) and 8(b) (e.g.,  $\phi' = 21.9^\circ$  and  $\phi = \phi' - 4^\circ = 17.9^\circ$ ) using various OCR values. These generic solutions were then superimposed on the load test data as a measure of the degree of conformance of the observed and predicted variation of  $\beta$  factor with depth. Equation 4 appears as a poor predictor of ultimate skin friction, at least within the Beaumont clay; whereas Equation 8 appears more promising for these soils. Some other observations from Figures 8(a) and 8(b) are particularly worthy of note. They are:

- a. The interpreted  $\tau_f$  and  $\beta$  values must not be considered to be precise representations of true behavior considering the approximations associated with the instrumentation positioning and function, as well as with the load versus depth curve fitting procedure used in the interpretation process.
- b. The trend of  $\beta$  versus depth in the upper 15 ft of the shaft appears to be a reasonable approximation of the trend predicted by Equation 8.
- c. Below 15 ft, there appears to be no correlation of the observed versus predicted  $\beta$  trend. This is consistent with the significant reduction in shaft load transfer noted at and just above the base of the test shafts.

The above observations reflect the parabolic distribution of  $\tau_f$  along the test shafts (see Figs. 2 and 3). This phenomenon has, in part, been attributed to a reduction in the effective stresses normal to the shaft surface in a zone immediately above the base. O'Neill and Reese

(1970) and others have postulated that this reduction is a result of the orientation of base load generated stresses which act to reduce the ambient normal stress in the zone immediately above the base. Note that the formulations such as given by Equations 4 and 8 do not attempt to model this shaft-soil interaction response.

The next step in the effective stress evaluation was to more closely evaluate Equation 8 as a predictor of the peak and residual skin friction of all the shafts which have been load tested in the area of study. To accomplish this, it was necessary to establish techniques to model the elements of field behavior which significantly depart from the theoretical predictions. In this regard, the "tip effect" of dry-cast straight shafts was modeled by using a reduced shaft length. For example, no load transfer was assumed below a depth of 19 ft for Shaft S-1 (approximately 1.6 shaft diameters above the base). This essentially follows the recommendations of Reese (1978) who suggests that the lower two shaft diameters be ignored in calculation of shaft capacity of dry-cast straight shafts.

The slurry-cast straight shaft, S-4, did not exhibit load shedding near the base possibly because of encountering more competent soils in the lower portion of the shaft.\* Consequently, no tip effect was assumed for this pier. A similar situation was noted for Test Shaft S-3, no doubt as a result of the prepared void existing below the base of the shaft. The dry-cast belled shaft, S-2, did exhibit some load shedding characteristics near the top of the bell. Consequently, an effective shaft length of 17.8 ft is assumed in the analysis of this shaft.

The observed near-surface  $\beta$  factors for all test shafts depart somewhat from the theoretical predictions of Equation 8. A limiting  $\beta$  ( $\beta_{max}$ ) of about 1.6 is suggested for all the piers, based primarily on data from Shaft S-1. It is likely that the theoretical predictions by Equation 8 become invalid for overconsolidation ratios greater than about 15. This limitation was also expressed by Esrig, et al. (1979) in

---

\* Note that the last 5 ft of this shaft were drilled without slurry.

their evaluation of driven piles using the critical state effective stress formulation.

Table 5 presents an evaluation of the average  $\beta$  factor at the peak ( $\beta_p$ ) and at the residual shaft load ( $\beta_r$ ) for each of the four test shafts. Table 5 also summarizes the effective shaft lengths and average diameters used in these analyses. The tabulated residual shaft loads are based on the lowest shaft loads recorded during either constant rate of penetration or repeated load tests.

Note on Table 5 that the average  $\beta$  factors represent the tabulated shaft loads divided by the average effective overburden pressure acting along the effective shaft length.

The average  $\beta$  factors for both peak and residual shaft loads are plotted on Figure 9 as a function of the average normalized undrained shear strength ( $S_u/\sigma'_{vo}$ ) of the soils in contact with the shaft. Note that the conversion from OCR to  $S_u/\sigma'_{vo}$  can be expressed by Equation 9. The value of  $S_u/\sigma'_{vo}$  can be readily obtained from Figure A5 for any of the test shafts. Direct use of  $S_u/\sigma'_{vo}$  also provides a more convenient measurement than OCR, provided a sufficient number of UU tests can be obtained to define the upper bound (essentially unfissured) undrained shear strength of the Beaumont clay.

Theoretical predictions of the average  $\beta$  factor, using Equations 6 and 9, have been superimposed on Figure 9 for a range of average interface friction angles. The solutions assume a limiting  $\beta$  factor of 1.6 as is noted from the test data, and a limiting ( $S_u/\sigma'_{vo}$ ) factor of 2.45. These limits correspond to a value of OCR ranging from 14 to 16. Comparison of the theoretical predictions with the load test results indicate a grouping of the dry-cast shafts S-1 and S-2 for the peak shaft loads. These data suggest that the average interface friction angle can be represented as  $\phi' - 4$  degrees. The dry-cast "void" shaft (S-3) results suggest a larger reduction in  $\phi'$ , i.e., about six degrees, although problems with the field measurements provide some uncertainty.

The average  $\delta$  of the slurry-cast straight shaft, S-4, is significantly lower than the dry-cast shafts. The interpretation also indicates that  $\delta$  is well within the range of the residual friction angle of the soils ( $\phi'_r = 9$  to  $15^\circ$ ) and that there is little difference between the peak and residual shaft friction. Similarly, the average  $\delta$  for the residual shaft friction of all shafts are generally within the range of the stress-dependent residual friction angle of the soil.

#### Effective Stress Predictions

The foregoing assessment indicates that Equation 8 is a reasonable predictor of the peak and ultimate shaft friction at failure and that  $\tau_f$  is a function of the average OCR or average  $S_u/\sigma'_{vo}$  of the soils in contact with the shaft. In addition, the effective stress analysis requires characterization of a limiting  $\beta$  value and of the length of the shaft which is effective in load transfer. The  $\beta_{max}$  of 1.6 adopted in the analysis corresponds to limiting values of OCR and  $S_u/\sigma'_{vo}$  of 14 to 16 and 2.45, respectively. To characterize the shaft length effective in load transfer, the embedded shaft length has been reduced by 1.6 shaft diameters, consistent with the behavior of Test Shaft S-1. This assessment has also proven to be quite conservative for application to the dry-cast belled shaft, S-2.

To test the sensitivity of the foregoing "average layer" analysis of shaft friction, a "discrete layer" analysis was developed using the following procedure:

- a. Characterize the  $S_u$  profile from UU tests where  $S_u$  is not appreciably influenced by the fissured structure of the clay (see Fig. A5).
- b. Divide the effective shaft length into equal segments and calculate  $S_u/\sigma'_{vo}$  for the mid-point of each segment.
- c. Select the effective friction angle as a function of plasticity index for each segment (see Fig. A3 for  $\phi'$ , and Fig. A6 for PI).
- d. For the peak and residual (large strain) ultimate shaft load at failure, assume  $\delta = \phi' - A$  degrees and  $\phi' = \phi'_L$ , respectively, and vary A to bracket the  $\phi'$  reductions predicted by the "Average Layer" analysis.



e. Calculate  $\beta$  from Equations 8 and 9 for the  $S_u/\sigma'_{vo}$  appropriate for each segment.

f. Compute the shaft load ( $Q_s$ ) as:

$$Q_s = \frac{\pi d L_e}{n} \sum_{i=1}^n \beta (\sigma'_{vo}) \quad (10)$$

where  $n$  is the number of shaft segments.

The discrete layer procedure has been programmed to enable calculation of  $Q_s$  given the characteristics of a straight shaft pier, the soil friction angle reduction factor and the  $S_u$  data. A program listing and printouts of solutions relevant to the test site are enclosed in Appendix B. Table 6 summarizes the average effective friction angle required to reproduce the measured peak, post-peak and residual shaft loads at failure for all the shafts, for both the "discrete layer" and "average layer" analyses.

The discrete layer analysis results indicate slightly higher interface friction angles than the average layer procedure. Note that sensitivity studies relative to the  $\beta_{max}$  parameter using a discrete layer analysis, demonstrate that  $Q_s$  differences for  $\beta_{max}$  between 1.7 and 2.5 are within five percent. The results of the analyses are included in Appendix B.

The fundamental parameters of OCR or  $S_u/\sigma'_{vo}$  must also be carefully considered for use in either the average or discrete layer procedures. It should be clearly understood that these parameters are interrelated only if normal soil behavior can be assumed, in that  $S_u$  can be characterized by samples whose strength is not unduly influenced by the presence of fissures or other structural anomalies.

#### Analyses Using Undrained Shear Strength

Conventional methods of relating shaft resistance to undrained shear strength ( $S_u$ ) involve a transfer function termed the Adhesion or Alpha Factor ( $\alpha$ ). Consequently, shaft friction ( $\tau_f$ ) is simply expressed as:

$$\tau_f = \alpha S_u \quad (11)$$

The Alpha Factor as conventionally used in design has been determined from load test results by several investigators as a ratio of the average  $\tau_f$  to the average shear strength ( $S_u$ ) of the soil in contact with the frictional area of the shaft. Figure 10 presents a synopsis of  $\alpha$  versus  $S_u$  as derived from tests on drilled shafts. The limitations of this method, the derivation of an alternate rational approach, and the observed versus predicted ultimate shaft friction of the test shafts are described as follows.

#### Limitation of Current Procedure

A primary drawback to the use of most of the published  $\alpha$  versus  $S_u$  criteria is that the associated data bases may be either site (soil type) dependent or involve significant inconsistencies in the measurement of  $S_u$ . The application of these criteria to layered profiles is also uncertain at best, and this problem is unlikely to be completely resolved by analytic techniques which do not rigorously model constitutive soil behavior and shaft-soil interaction. Another drawback to the conventional techniques is that they do not account for the effects of shaft length even though field observations indicate that this may be an important consideration.

Measurement of  $S_u$  in the various  $\alpha$  derivations has involved a variety of shear tests including in-situ vane shear, direct shear, unconfined compression, unconsolidated undrained and consolidated undrained triaxial tests. Unfortunately, none of these methods would be expected to produce the same  $S_u$  on identical samples. This is a result of sample anisotropy combined with the different induced failure modes\*

---

\* Each different type of shear test produces a different rotation ( $\theta$ ) of the direction of the principal stress at failure. For example,  $\theta$  is zero degrees, 90 degrees and approximately 45 degrees for triaxial compression, triaxial extension and direct simple shear, respectively. Note that  $\theta$  is measured from the vertical axis of the sample.

or water content changes during consolidation. Even with a single test type, sample disturbance can be a significant variable as described by Lambe and Ladd (1963) and Noorany and Seed (1965).

More recent  $\alpha$  derivations (O'Neill and Reese, 1970), have been based on UU test results. This currently appears to be the most practical approach, particularly in stiff to hard clays where sample disturbance is minimized. However, as described in the preceding report (Volume II), the use of average UU test results in fissured clays introduces another variable. This is related to the sensitivity of the average  $S_u$  value to the number of tests conducted, the sample size, as well as the time of testing after sample recovery.

It is widely acknowledged that  $S_u$  is a function of stress history and soil type (Ladd and Foott, 1974). In this regard, the  $S_u$  of a deep normally consolidated clay could be identical to a shallow overconsolidated clay, although each of these clays would produce a quite different shaft friction contribution. For example,  $S_u$  of a typical normally consolidated clay of medium plasticity consolidated under an effective overburden pressure of 1.5 tsf and the same clay with an OCR of 4 under an overburden pressure of 0.5 tsf would be about equivalent. However, the ratio of the mobilized skin friction of the normally consolidated to the overconsolidated clay as predicted by Equation 8 is about 0.3. Consequently, even though both clays have the same  $S_u$ , they have quite different stress states and, therefore, different Alpha Factors, a behavior not reflected by any of the current  $S_u$  versus  $\alpha$  design criteria.

#### Rational Alpha Derivations

A theoretical derivation of the Alpha Factor can be obtained by equating  $\alpha S_u$  to  $\tau_f$  as expressed in Equation 8. Consequently,  $\alpha$  becomes a function of the stress history of the soil (as represented by OCR) and of the soil type (as represented by plasticity index). Note that  $\phi'$  can be correlated to plasticity index (PI) as shown on Figure

A3 and that  $K_o$  can be correlated to both  $\phi'$  and PI.\* A simple relationship exists between the effective stress  $\beta$  factor and  $\alpha$ . This relationship is shown as a function of the normalized shear strength ( $S_u/\sigma'_{vo}$ ) in accordance with Equation 12:

$$\alpha = \frac{\beta}{S_u/\sigma'_{vo}} \quad (12)$$

This procedure then provides a rational method to predict either  $\alpha$  or  $\beta$  from normalized shear strength or alternatively from OCR. The use of ( $S_u/\sigma'_{vo}$ ) rather than  $S_u$  as a correlative parameter is proposed to significantly reduce the data scatter inherent in  $S_u$  measurements whose quality is not readily assessed, e.g.,  $S_u/\sigma'_{vo}$  measurements can usually be readily compared with published Normalized Soil Property (NSP) data for similar soils and stress histories.

Figure 11 presents  $S_u/\sigma'_{vo}$  versus  $\alpha$  solutions for plasticity indices of 20, 35, 40 and 60 percent. Note that Equation 13 has been used to express the relationship between  $\phi'$  and PI shown for the Beaumont clay on Figure A3:

$$\sin \phi' = 0.789 - 0.265 \log PI \quad (13)$$

Equation 13 could be replaced by a more general expression (NAVDOKS DM-7, 1971) to provide similar solutions for generic use. However, without field calibration such solutions must be used with caution. The real advantage of this approach is to provide a more rational framework for the correlation of properly documented load test data which will, hopefully, lead to an improved deep foundation design methodology.

---

\* Note that if independent test data are not available, the  $K_o$  can be related to OCR and to PI after Gardner (1977) as follows:

$$K_o = (1 - \sin \phi') (OCR)^m; \quad m = 0.58 PI^{-0.12}$$

### Measurement of Normalized Shear Strength

As concluded in the preceding text and in the preceding soil property characterization study (Volume II), development of  $S_u/\sigma'_{vo}$  from good quality UU tests is believed to be a convenient and satisfactory approach. The primary drawbacks previously cited are sample disturbance and  $S_u$  measurements which are affected by sample discontinuities such as fissures. For fissured soils, such as the Beaumont clays, it has been concluded that characterization of  $S_u$  is best based on test specimens whose strength is essentially unaffected by the presence of fissures. It has been noted that smaller samples are less likely to contain unfavorably oriented fissures. Consequently, the testing of 1.4-inch-diameter samples is recommended.

For soil specimens which are not subject to structural change under elevated consolidation pressure, i.e., are not highly structured, cemented or unduly sensitive, it is possible to measure rather than estimate the NSP parameters  $K$  and  $n$  contained in Equation 9. These measurements can also be used to investigate the effects of sample disturbance on  $S_u/\sigma'_{vo}$  as determined by UU tests. This determination is made with  $\overline{CIU}$  tests which are consolidated under pressures at least one and one-half times the maximum past pressure imposed on the sample. Subsequent to consolidation, the sample can be rebounded, if required, so as to simulate the in-situ OCR. Thus, for a given soil type, the normalized shear strength measured is independent of water content and the magnitude of the consolidation pressure, being dependent only upon OCR and the type of shear test employed.

The foregoing NSP procedure is identified by Ladd and Foott (1974) as the Stress History and Normalized Soil Engineering Properties (SHANSEP) technique. It is significant to note that a growing normalized soil parameter data base provides relatively good estimates of  $S_u/\sigma'_{vo}$  as a function of only the plasticity and OCR of a soil deposit for a particular type of shear test. It is likely that there will be an ever increasing confidence level in such predictions as this data base is expanded.

Although  $S_u/\sigma'_{vo}$  measurements along with plasticity indices are sufficient to provide predictions of OCR relevant to the development of  $\alpha$  or  $\beta$  factors for deep foundation design, it is always advisable to make independent determination of OCR from interpretation of one-dimensional consolidation tests on good quality samples.

## PART V: SHAFT FRICTION ANALYSIS BY SIMILITUDE OR INDIRECT CORRELATION

In addition to  $\tau_f$  assessment from basic soil properties, an evaluation of other techniques which attempt to simulate the shaft-soil load-transfer mechanism or provide indirect correlations have been made as a part of this investigation. These techniques include mortar-soil interface shear investigations utilizing direct shear tests, borehole shear tests employing mortar-faced shear plates, and moisture migration studies as suggested by O'Neill and Reese (1970). An assessment of the application of each of these techniques is described in the following sections.

### Mortar-Soil Interface Shear Tests

Mortar-soil interface shear tests were conducted as described in the Volume II report entitled, "Laboratory Testing." As indicated in this report, the average results incorporating all test data indicated that the direct shear resistance of mortar-soil specimens and companion soil specimens is identical although there are specific differences for individual companion sample tests. The relationship between shearing resistance and the normal effective stress for both types of direct shear tests is reproduced as Equation 14:

$$\tau_f = 0.3 + \sigma'_n \tan (18.2^\circ) \quad (14)$$

It was concluded that this relationship probably represents a condition of partial drainage during shear, although it may also reflect the anisotropy of the soil when compared to the triaxial compression tests (see Figure A3 of Appendix A). However, if the cohesion term is ignored, an interface friction angle of 18.2 degrees compares well with that interpreted for dry-cast, straight shafts using the effective stress methodology. Considering that the mortar-soil and conventional

direct shear soil test results are identical, however, significant uncertainties exist as to the relevance of this method for prediction of the ultimate shaft resistance of shafts drilled in cohesive soils.

#### Borehole Shear Tests

The results of borehole shear tests drilled above the groundwater level produce results very similar to that derived from the consolidated undrained triaxial tests employing pore water pressure measurements. It was, therefore, concluded that the scale effects of shear plates preclude development of true interface shear failure. However, these results do indicate that the test method is promising for determination of the friction angle of the soil.

The substantially reduced friction angle measured by the borehole shear tests conducted below water level, suggests partial drainage during shear. Therefore, to investigate the effective friction angle in medium to highly plastic soils, it appears necessary to conduct the test at a much slower rate of strain and to prevent significant buildup of pore pressures during shear. It is likely that substantial modifications in the shear plates would be necessary to use the borehole shear tests to investigate mortar-soil interface shear behavior. One possible modification would be to conduct a pressuremeter-type of test where a cylinder is expanded against the sidewalls of the borehole and subsequently pulled while maintaining the expansion pressure constant.

#### Moisture Migration Analysis

The results of moisture migration studies conducted as part of the mortar-soil interface shear tests are summarized by Figures A7 and A8 of Appendix A. From these results, it was judged that the reliability of shaft friction predictions based on Alpha Factor correlations with soil moisture content changes at the shaft-soil interface, is comparatively low, particularly when applied to a complex structured clay such as the



Beaumont formation. Nevertheless, it is of interest to apply the moisture-migration test results to the prediction of Alpha Factors for the dry-cast shaft identified as S-1.

#### Water Content Correlations

For design applications, the most practical Alpha Factor correlation parameter derived from moisture migration studies would be the natural water content as shown by Figure A7. However, the correlation shown in Figure A7 is quite uncertain considering the large data scatter and the limited number of tests conducted for this investigation. For this reason, an attempt was made to correlate the natural water content with the water content on the failure plane to take advantage of the reduced data scatter exhibited by the failure water content-Alpha relationships shown by Figure A8. By eliminating a test associated with an abnormal natural water content and the tests conducted at the lowest normal stress consolidation pressures (0.54 tsf), the remaining data support the approximate relationship between the failure plane and water content ( $w_f$ ) and the natural water content ( $w_n$ ) described by Equation 15:

$$w_f = 1.49 + 0.92 w_n \quad (15)$$

Note that this equation is valid only for a  $w_n$  range between 24 and 28 percent.

#### Alpha-Water Content Correlation

After converting  $w_n$  to  $w_f$ , Alpha Factors were calculated from Figure A8 for each of the generalized strata identified in Figure A9 of Appendix A. This interpretation was made using the median of the range of data shown in Figure A8. The results of  $\alpha$  predicted directly from  $w_n$  ( $\alpha_1$ ) and from  $w_f$  via Equation 15 ( $\alpha_2$ ) are summarized in Table 7.

It is noted that the last column of Table 7 represents the average Alpha Factor as interpreted from the load test results on Shaft No. S-1 (see Table 2). For this interpretation, the shear strength profile shown as Figure A5 was utilized.

By comparing  $\alpha_1$  and  $\alpha_2$  with the average  $\alpha$  interpreted from the S-1 load test, it is readily seen that the moisture migration data from this study would significantly overpredict field values. This was recognized by O'Neill and Reese (1970) who proposed further reductions in  $\alpha$  to compensate for the soil remolding, the opening of surface fissures during installation and for the load shedding effects noted near the ground surface and just above the base of the drilled shafts. These investigators concluded that the Alpha Factors interpreted from moisture migration tests in the Beaumont clay are about 0.8.

## PART VI: LOAD-DEFORMATION ANALYSIS

Several methods have been proposed to conduct load-deformation analysis of deep foundation elements. These can be categorized into two classifications--one which is basically empirical and the other which has some basis in theory. Examples of empirical applications, primarily based on load test results, are described by Skempton (1959), Burland, et al. (1966), and O'Neill and Reese (1970). The theoretically based methods include elastic and elasto-plastic techniques (Mattes and Poulos, 1969), numerical solutions incorporating load-transfer relationships (Seed and Reese, 1957; Meyer, et al., 1975), and finite element analyses (Ellison, et al. 1971).

The numerical load-transfer technique has been selected for this study primarily because of its simplicity and ability to simulate non-linear load-deformation behavior discussed in earlier sections. The key element of this analysis is the simulation of the load transfer (T-Z) curves along the shaft and at the base. In current practice T-Z curves are primarily empirically derived from numerical curve fitting of field observations, or from data published in literature.

In this investigation, primary emphasis is placed on correlation of T-Z relationships with basic soil parameters as discussed in the previous sections. The following sections address the method of analysis, characterization of the load-transfer curves for shafts drilled at the test site, the prediction of the load-settlement response of these shafts, and their comparison to the actual measured data.

As the only conventional dry-cast straight shaft, Test Shaft S-1 has been featured in the analyses and formed the basis of subsequent conclusions. An additional analysis was performed for Shaft S-3 (void below base) to test the applicability of the method of analysis adopted. The primary emphasis is placed on the peak-load behavior for the shafts. Some analyses, however, have also been made to investigate the effects of the drop-off of the resistance capacity of the shafts at displacements beyond the peak (post-peak behavior).

### Numerical Load-Transfer Analysis

In the present investigation, the load-deformation behavior of the pile has been analyzed using the technique described by Meyer, et al. (1975). The technique was implemented using the AXCOL program, which is also discussed by Meyer, et al. A brief discussion of the technique and the associated computer program follows.

In the analytic model, the pile is modeled as a column consisting of a series of equal discrete elements. Each element has an axial stiffness and may accommodate specified loads and supports acting on it. The pile elements are considered to be linearly elastic. The support conditions may, however, be either or nonlinear, thus the nonlinear (hyperbolic) soil-shaft interaction curves discussed in the previous sections may be incorporated in the analyses. A schematic of the AXCOL model is shown in Figure 12.

The analytic technique essentially consists of the solution of a set of simultaneous finite-difference equations depicting the axial displacements for each element and the force equilibrium relations at the nodes between the elements. The equations are solved for the unknown displacements at each node, using a direct elimination procedure described by Holmquist, et al. (1975). It should be recognized that the solution technique is based on a linear elastic system. The nonlinear soil-pile interaction effects are incorporated by iterative techniques. The AXCOL program, which was used in this investigation, is also described by Holmquist, et al. The program is the axial solution counterpart for BMCOL28, the program for the lateral solution of beam-column for nonlinear supports (Matlock and Halliburton, 1964).

### Characterization of Load-Transfer Curves

There have been a variety of load-transfer curve formulations (T-2 curves) proposed for cohesive soils. Perhaps the most widely used of

these formulations are those proposed by Reese, et al. (1969), who define the load transfer curves in terms of the ultimate resistance of the shaft or the tip ( $T_u$ ) and the relative soil-pile movement at which the ultimate resistance occurs ( $Z_c$ ). As per present state of practice, the load-transfer curves are bilinear, with the shaft or tip resistance ( $T$ ) increasing linearly with the relative soil-pile movement ( $Z$ ), until the ultimate soil-pile resistance reaches its ultimate value ( $T_u$ ) at a relative movement of  $Z_c$ . The soil-pile resistance remains at a constant value of  $T_u$  for values of movement greater than  $Z_c$ . The actual shape of the curve is, therefore, disregarded. In addition, no consideration is given to decreasing resistance with increasing soil-pile movement beyond the peak (post peak behavior).

The standard state of practice applies to a wide variety of cases where the pile is relatively flexible, compared to the load-transfer curves, such as in long steel pipe piles in normally consolidated to moderately overconsolidated clays. For the very stiff piers studied here, however, the actual shape of the pre-peak portion of the load-transfer curves has a major influence on the load-deformation behavior of the pile. In addition, the significant drop-off of resistance with increasing soil-pile movement evident in the highly overconsolidated soils, make Reese, et al.'s formulation inappropriate for the present study.

Analyses of the load deformation behavior of the shafts, as described in Part III, indicated that the load-transfer curves for the Shaft S-1 can be fairly well simulated by hyperbolic curves as functions of the ultimate shaft resistance ( $\tau_f$ ) and the initial slope of the T-Z curve,  $E_i$ . Similar formulations have also been noted by Woodward, et al. (1972) and Holloway, et al. (1975). This general approach of hyperbolic transformation has been used for the assessment of the observed load-transfer curves derived for S-1 as subsequently described.

### Load-Transfer Curve Parameters

The load-transfer interpretations made for Test Shaft S-1 are presented in Part III of this text (Analysis of Load Test Results). In this interpretation, the shaft friction at any depth ( $\tau$ ) has been expressed by Equation 16 as a function of the shaft deformation ( $\rho$ ) in the form of a hyperbolic transformation after Kondner (1963):

$$\tau = \frac{R_1 \rho}{\frac{1}{E_i} + \frac{\rho}{\tau_f}} \quad (16)$$

$$\text{and } \tau \leq \tau_f$$

In this equation,  $\tau_f$  represents the theoretical skin friction prediction by Equation 8, and  $E_i$  the initial tangent to the load-transfer curve.

A correction factor ( $R_1$ ) is also necessary to provide for the compatibility of  $\tau_f$  with the associated shaft deformation ( $\rho_f$ ). This factor is expressed by Equation 17:

$$R_1 = \frac{\tau_f}{\rho_f E_i} + 1 \quad (17)$$

A hyperbolic T-Z curve can thus be defined as a function of  $\tau_f$ ,  $E_i$ , and  $\rho_f$ .

If there is a post-peak drop-off in  $\tau_f$ , Equations 16 and 17 are no longer valid for  $\rho > \rho_f$ . An examination of the computed load-transfer curves suggests that the post-peak strength,  $\tau_{fpp}$ , may be defined as the resistance at the point beyond which the rate of drop-off decreases dramatically. The shaft friction,  $\tau$ , can then be empirically modeled by Equation 18 as a cosine function in terms of the shaft segment deformation ( $\rho_{pp}$ ) required to develop  $\tau_{fpp}$  at deformation greater than  $\rho_f$ :

$$\tau = \left[ \cos \left\{ \frac{(\rho - \rho_f) \pi}{\rho_{pp} - \rho_f} \right\} - 1 \right] \frac{\tau_f - \tau_{fpp}}{2} + \tau_f \quad (18)$$

Note that this solution requires estimates of both  $\rho_{pp}$  and  $\tau_{fpp}$ .

The residual resistance ( $\tau_{fr}$ ) occurs after a considerably greater pile movement, and the rate of drop off is rather mild.

#### Ultimate Shaft Friction

The ultimate shearing resistance ( $\tau_f$ ) for any segment of the shaft can be predicted by the effective stress Equation 8 using the discrete layer method of analysis given by Equation 10. Note that this prediction does not inherently incorporate shaft-tip-soil interaction effects as described in the section of Part IV entitled "Effective Stress Analyses." Consequently, "tip effects" are modeled by assuming the effective shaft length to be less than the actual length. The "free surface effects" are also empirically modeled as a limiting normalized shearing resistance, i.e., a limiting Beta Factor ( $\beta_{max}$ ) of 1.6. Modeling the peak and post peak  $\tau_f$  by Equation 8 requires selection of the proper interface friction angle ( $\delta$ ). For example, for the first load peak and post peak  $\tau_f$  of dry-cast, straight shafts,  $\delta$  is approximately  $\phi - 3$  degrees and  $\phi - 6$  degrees, respectively. For slurry-cast shafts and for dry-cast shafts failed by very large single or cumulative (repetitive loading) movements,  $\delta$  is assumed to be equivalent to the residual friction angle of the soil ( $\phi_r$ ).

#### Initial Slope Parameter

The  $E_i$  parameter, normalized with respect to the effective overburden pressure ( $E_i/\sigma'_{vo}$ ), as derived from the S-1 load test is shown in Figures 13 and 14 as a function of both the OCR and  $S_u/\sigma'_{vo}$ . The equations of these functions are given as:

$$E_i/\sigma'_{vo} = 47.5 (\text{OCR})^{0.91} \quad (19)$$

$$E_i/\sigma'_{vo} = 170 (S_u/\sigma'_{vo})^{1.21} \quad (20)$$

Note that equations (19) and (20) are valid only for the load transfer measurements which are not appreciably influenced by the tip effect of the S-1 shaft.

As  $S_u/\sigma'_{vo}$  and OCR are interrelated by Equation 9, the two correlations are essentially similar. Other correlations with undrained shear strength and such parameters as plasticity index either proved invalid or had more scatter. It may be noted that the OCR or  $S_u/\sigma'_{vo}$  versus  $E_i/\sigma'_{vo}$  relationships encompass the  $E_i$  interpretations for the entire shaft, deviating only somewhat near the base.

Although Equations 19 and 20 expressing  $E_i/\sigma'_{vo}$  cannot be theoretically derived, it is of interest to speculate on the relationship of  $E_i$  to fundamental soil properties. Basically, this parameter would be expected to be most directly related to the small strain shear modulus ( $G_{max}$ ) of the soil.  $G_{max}$  has been expressed by Hardin and Drnevich (1970) as:

$$G_{max} = 14760 \frac{(2.973-e)^2}{1+e} (OCR)^2 (\sigma'_m)^{0.5} \quad (21)$$

Note that  $e$  is void ratio and  $\sigma'_m$  is the mean normal effective stress, i.e.,  $\sigma'_{vo}(1+2K_o)/3$ . Seed and Idriss (1970) have also suggested that  $G_{max}$  can be expressed in terms of the undrained shear strength as:

$$G_{max} = 2300 S_u \quad (22)$$

In the case of a driven pile or drilled shaft, it has been postulated that  $\sigma'_m$  after installation is approximately restored to the initial stress state and, therefore, is related to stress history as represented by OCR. Thus,  $G_{max}$  and  $E_i/\sigma'_{vo}$  would be expected to be related to the same parameters in approximately the same way. Figure 15 presents  $G_{max}/E_i$  as a function of OCR where  $G_{max}$  has been estimated from the soil properties using Equations 21 and 22. The trend shown suggests that  $G_{max}$  is directly related to  $E_i$  where the shaft load transfer is not influenced by free-field and base load effects. Additional studies using measured  $G_{max}$  correlations are recommended to substantiate this easily applied relationship.



### Deformation at Failure

For simulation of the load-transfer curves, it is necessary to define the deformations ( $\rho_f$ ) at which the peak  $\tau_f$  is developed along the shaft. Independent interpretation of the S-1 load-transfer curves indicates that the deformation required to develop peak  $\tau_f$  increases with depth to about 15 ft below the ground surface. At greater depths there is a trend of decreasing deformation until just about the shaft base (see Fig. 16a).

For Shafts S-2 and S-3, however, there is a trend of decreasing deformation along the entire shaft length (see Fig. 17). The reasons for this difference in the observed  $\rho_f$  trend with depth are not readily apparent and should be investigated further.

The S-1 load test data suggest that for the portion of the drilled shaft not significantly influenced by "tip effects," the critical deformation increases with confining pressure. Further, comparing the shaft length to diameter ratios of the test shafts (excluding S-3) with the top deformation required to mobilize the average peak shearing resistance, there is a trend of increasing critical deformation with  $L/D$ . These observations are summarized on Fig. 16(b).

As a result of the foregoing observations, it appears as if  $\rho_f$  should be modeled as a function of both the depth ( $x$ ) of the load-transfer curve below the surface and the  $L/D$  of the shaft. Equation 23 approximately describes  $\rho_f$  (in inches) based on the observations at Test Shaft S-1.

$$\text{For } 0.125 < \frac{x}{L_e} < 0.680: \log \rho_f = \frac{x/L_e - 0.125}{0.975} - 1 \quad (23a)$$

$$\text{For } 1.0 > \frac{x}{L_e} > 0.68: \log \rho_f = \frac{1 - x/L_e}{0.575} - 1 \quad (23b)$$

Note that  $L_e$  represents the length of the shaft effective for load transfer. Based on the very limited site data, Equation 24 approximately describes the  $\rho_f$  ratios of various  $L/D$  values referenced the shortest shaft ( $L/D = 7.4$ ).

$$R = 0.75 + 1.95 \log \frac{L/D}{7.4} \quad (24)$$

Thus, the product of Equations 23 and 24 provide an estimate of  $\rho_f$  which factors both shaft geometry and depth.

Since no tip effects were expected for Shaft S-3, it is likely that the pattern for the deformation at peak,  $\rho_f$ , along Shaft S-3 will be different. A cursory examination was made of the pattern for  $\rho_f$  along the shaft, based on the load-transfer curves derived by O'Neill and Reese (1970). The examination revealed a monotonic decrease of the value of  $\rho_f$  with depth, as shown in Fig. 17. The trend may be approximately represented by Equation 25:

$$\log \rho_f = \frac{0.82 - x/L}{0.595} e^{-1} \quad (25)$$

It is noted that Equation 25 is very similar to Equation 23b which represents the bottom part of Shaft S-1.

#### Analyses Performed

The analyses performed by the AXCOL3 program (Holmquist and Meyer, 1975) are discussed in the following paragraphs. The results of the analyses are discussed in Part VII.

#### Analyses for Shaft S-1

Analyses were performed for Shaft S-1 using two types of T-Z curves: (1) assuming no drop-off of resistance after the peak value was reached (peak load behavior), and (2) assuming a drop-off in strength using Equation 18 (post-peak behavior).

Peak Load Behavior. Peak load behavior was analyzed using four load levels at the head of the shaft: 40k (20 tons), 140k (70 tons), 220k (110 tons), and 280k (140 tons). These four loads were among those actually used in the field. The values of peak resistance  $\tau_f$  were computed using Equation 8 with the aid of Figure 8. For these analyses,

a value of  $\delta = 19.9$  degrees ( $\phi' - 2^\circ$ ) was used, and the value of  $\beta$  limited to 1.6 ( $\beta_{\max}$ ). Note that other combinations of  $\delta$  and  $\beta_{\max}$  will change the amplitude of the computed load-settlement curve. The degree of such changes can be readily evaluated from the results of the  $\beta_{\max}$  sensitivity analyses included in Appendix B.

The parameter  $E_i$  for the hyperbolic T-Z curve was based on Equation 19 (Fig. 13). The values of  $\rho_f$  were based on Equations 23a and 23b. In summary, all data obtained from the field were used for the analysis of Shaft S-1.

The shaft was modeled only for its effective length,  $L_e$ , of 19 ft. Nineteen 1-ft segments were used for the computations. A twentieth increment of one foot was added at the bottom of the shaft. This bottom increment was not associated with any shaft resistance, but only the tip resistance. The tip resistance was modeled identically to what has been presented by O'Neill and Reese (1970).

Post-Peak Behavior. The T-Z curves used for the analysis of post-peak behavior were identical to those used up to the displacement value  $\rho_f$  required to develop  $\tau_f$ . For displacements greater than  $\rho_f$ , the curve was assumed to follow the cosine function given as Equation 18. The values of  $\rho_f$  and  $E_i$ , as well as the analytic model of 20 segments were identical to the one used to calculate peak load behavior.

The first load post-peak resistance,  $\tau_{fpp}$ , is based on a value of  $\delta = 16.9$  degrees ( $\phi' - 5^\circ$ ) and a  $\beta_{\max}$  of 1.6. The corresponding value of displacement,  $\rho_{pp}$ , was assumed to be 0.5 in., based on the field test data. For displacements greater than  $\rho_{pp}$ , the resistance was assumed to remain constant at  $\tau_{fpp}$ .

Displacement, rather than loads, at the head of the shaft were input in order to facilitate the analysis of the drop-off of load. The first four displacements input were those computed for the four loads in the peak load behavior analysis. These were followed by four additional specifications of head displacement to a maximum of 0.6 in.

### Analyses for Shaft S-3

Analyses were performed for Shaft S-3 using two types of T-Z curves: (1) assuming no drop-off of resistance after the peak value  $\tau_f$  was reached (peak load behavior), and (2) assuming a drop-off of resistance to a value corresponding to the residual value, at a very large displacement (residual load behavior).

Peak Load Behavior. For peak load behavior, the values of peak resistance,  $\tau_f$ , used were identical to those used for Shaft S-1. The values for the initial slope of the T-Z curves were also similar to those used for the analyses for S-1, being based on Equation 19. The distribution of  $\rho_f$  values with depth were based on Equation 25, which was specifically derived for S-3.

Because of the void below the shaft, tip effects were assumed to be absent, and the entire 23 ft of the shaft were used in the model as 23 1-ft increments. Loads of 40k, 80k, 180k and 220k were specified at the head of the shaft.

Residual Load Behavior. For the residual load behavior, the T-Z curves used were identical to those used earlier in the peak load behavior analysis up to the displacement value of  $\rho_f$ , corresponding to the peak resistance value,  $\tau_f$ . For displacements greater than  $\rho_f$ , up to a value of  $\rho_{pp}$ , corresponding to the post peak resistance,  $\tau_{fpp}$ , the cosine curve defined in Equation 18 was used. For displacements greater than  $\rho_{pp}$ , the resistance was assumed to decrease linearly to the residual value,  $\tau_r$ , at a displacement,  $\rho_r$ . The resistance was assumed constant at  $\tau_r$ , for values of displacement greater than  $\rho_r$ .

The values of  $\tau_{fpp}$  were computed based on a value of  $\delta$  equal to 16.9 degrees ( $\phi' - 5^\circ$ ). The corresponding values of  $\rho_{pp}$  were assumed as two times  $\rho_f$ . This assumption was based on a cursory examination of the load-transfer curves for S-3 presented by O'Neill and Reese (1970).

The values of  $\tau_r$  were based on a value of  $\delta$  equal to 9 degrees, the minimum residual friction angle ( $\phi'_r$ ) of the soil. The corresponding displacement,  $\rho_r$ , was taken as nine inches.

Displacements, rather than loads, at the head of the shaft were input in order to facilitate the analysis of the drop-off of load. The first four displacements input were those computed for the four loads in the peak load behavior analysis. These were followed by four additional specifications of head displacement to a maximum of 10 in.

## PART VII: RESULTS OF THE LOAD-DEFORMATION ANALYSES

The results of the load-deformation analyses using the AXCOL computer program are presented on Figures 18 through 21. Figures 18 and 19 show the load take-out along the shaft and the load-deformation behavior at the head of the pile, respectively, for Shaft S-1. Figures 20 and 21 show the corresponding figures for S-3. The results and their comparisons with actual field behavior are discussed in the following paragraphs.

### Results for Shaft S-1

As noted in Part VI, Shaft S-1 was analyzed for the peak load behavior and also for post-peak behavior.

The peak load behavior results for both the load takeout and the load displacement (Figures 18 and 19) agree well with the field load test results. There appears to be some divergence from the field test at higher loads, where the influence of the tip effect assumes greater significance.

The post-peak behavior was identical to the peak behavior for loads up to 220 kips, and fell only slightly below the peak curve for higher load levels. To illustrate better the post-peak behavior, only the load taken up by the shaft is plotted against the shaft head displacement, similar to the one presented for the corresponding test case by O'Neill and Reese (1970). The displacement for peak shaft resistance occurs at a higher value than that for the field test results, i.e., 0.3 versus 0.2 in. This departure may partially be attributed to the use of a constant value of 0.5 in. for  $\rho_{pp}$ , the displacement corresponding to post-peak resistance  $\tau_{fpp}$ . It appears that using a value of two times  $\rho_f$ , such as used for Shaft S-3, would have yielded results closer to those measured in the field.

### Results for Shaft S-3

Comparison of the computed versus observed shaft load-settlement response (Figs. 20 and 21) of Shaft S-3 indicates that the peak  $\tau_f$  of about 113 tons underpredicts the observed 121 tons by between 6 and 7 percent. However, if  $\beta_{\max}$  is taken as 2.5 (a more appropriate  $\beta_{\max}$  factor for Shaft S-3) and  $\delta$  as  $\phi' - 3$  degrees, the predicted total resistance is 122 tons, a rather remarkable correlation. The shape of the load-deformation curve, as well as the residual load on the shaft head are also found to produce a satisfactory match between the field test results and the computed data.

PART VIII: SUMMARY OF CONCLUSIONS AND  
RECOMMENDATIONS FOR FURTHER STUDY

The following summary presents highlights of the findings and conclusions of each of the three phases of investigation conducted for this study, i.e., Field Investigation (Volume I), Laboratory Testing (Volume II), and Assessment and Prediction of Skin Friction of Shafts in Beaumont Clay (Volume III). Based on these results, recommendations are also presented for further study of the behavior of drilled shafts in cohesive soils.

Soil Classification and Stratigraphy

Conventional thin-wall tube sampling and visual classification, together with pocket penetrometer and torvane tests immediately upon sample recovery, gave a good definition of stratigraphy, particularly when supplemented by water content, liquid limit and plastic limit laboratory tests. The soil classification trends of these properties with depth were also found to be similar to those reported by O'Neill and Reese at the time of their 1969 investigations. This is evidenced by an almost exact correlation of the regression line through the two liquid limit, plasticity index data sets as plotted on a plasticity chart. Although not as exact, these data sets plus water content, when plotted versus depth, were also in substantial agreement.

Profile Enhancement

A significant enhancement of soil profile variations by recording the variations in quasi-static penetration resistance was also obtained from results of the cone penetrometer tests. In particular, thin lenses or strata of cohesionless soils and soils with very low plasticity were readily identified from the cone records. Cone resistance also appeared to be a sensitive indicator of the variation in the consistency of cohesive soils with depth.



### Groundwater Regime

Piezometers were installed in selected borings to monitor groundwater levels at the test site. These measurements conducted over a period of approximately one month indicated a stabilized water level at about 11 ft below the existing ground surface. Similar observations made by O'Neill and Reese during their field investigations indicated a stabilized groundwater level at about 15 ft. This indicates a rise in groundwater level since 1969, although seasonal variations could account for such difference.

### Space and Time Dependent Variations in Soil Properties

During this study, the variation in the natural water content and consistency of the subsoils at the test site were investigated using thin-wall tube samples. These samples were obtained at various depths by horizontally jacking 4-1/2-in.-OD thin-wall tubes from a vertical access shaft. Determination of the water content from tubes taken at different depths below the ground surface were made at 1-in. intervals. The results of these tests indicated differences in water contents as much as four percentage points over distances as little as two inches. This variation was also observed on a macro-scale as evidenced by standard deviations of water content within generalized soil strata of as much as 4.9 percent.

### Data Comparisons

Comparison with the O'Neill and Reese (1970) data indicates a general conformance in water content variation. Only at a test depth of 15 ft were the O'Neill and Reese data significantly different (lower) than any of the other data in the two data bases. It was concluded that this is either due to a rise in water level or tests on a sample having an anomalously low plasticity index. The postulation by O'Neill and Reese that the water content is highest nearest to the shaft was not substantiated by this study. If such a trend does exist, it is obscured by the significant natural variations in the free-field water content.

Physical properties, such as unit weight, specific gravity and grain-size distribution as measured during this study, were found to be in substantial agreement with the O'Neill and Reese 1970 data base. Some variations in the plasticity index with depth were noted, but were not substantial within the maximum depth of investigation for this study (35 ft).

#### Consistency Variation

As a follow-up to the investigation of property variations with space and time, horizontal test specimens used for the water content variation analysis were also subject to pocket penetrometer tests to investigate the variation in consistency. Similar to the water content results, this study indicated variations in pocket penetrometer readings of as much as 1 tsf over distances as small as 5 in. No trend of consistency variation with proximity to the shaft was noted. Pocket penetrometer readings taken on vertically oriented thin-wall tube samples during the test boring operations generally fell within a data band of such measurements made by O'Neill and Reese during their field studies.

#### Undrained Shear Strength

The undrained shear strength of the subsoils at the site was investigated by both in-situ and laboratory testing. The field testing consisted of pressuremeter (PMT) and quasi-static cone penetration (CPT) tests. Undrained shear strength was measured in the laboratory by unconsolidated undrained triaxial compression (UU) tests. In addition to these tests, torvane measurements were made in the field immediately upon recovery of selected undisturbed samples.

#### Test Results

As indicated by Figure A5, there is a surprisingly close correlation between the undrained shear strength as measured by the torvane and pressuremeter tests using the Gibson and Anderson (1961) interpretation. The results of unconsolidated undrained triaxial tests on samples whose failures do not appear to be substantially influenced by fissures

also demonstrate the same trend with depth, but are somewhat lower than the torvane/PMT results. Below a depth of about 15 ft, the undrained shear strength as interpreted from the CPT test for a cone factor of 20 also appears to be in reasonable agreement with the torvane/PMT results. Above this depth the CPT interpretation indicates significantly higher undrained shear strength and appeared to be sensitive to the change in overconsolidation ratio with depth.

#### Interpretation of UU Tests

In practice, the undrained shear strength of cohesive soils is conventionally determined by unconsolidated undrained triaxial tests, if at all possible on good quality samples. For fissured cohesive soils such as the Beaumont clays, however, the results of UU tests are often influenced by premature failures due to the orientation of fissures within the sample. This effect is observed in this study and in the previous study by a significant scatter in the undrained shear strength data.

Conventional interpretations of UU test data for design purposes are to determine a "mean value" strength profile by judgement or by regression analysis. As the position of this "mean line" is affected by the number of tests conducted, the sample size, and the test sample distribution with depth, this representation becomes a somewhat arbitrary plane of reference. Further, the vertically oriented direction of the failure plane along the shaft would be expected to be much less influenced by the presence of fissures than during UU tests.

As a consequence, it was concluded that the undrained shear strength of samples whose failure stress is not significantly influenced by the presence of fissures is a more rational plane of reference to be used for pile and drilled shaft design analyses. Testing procedures to define the "unfissured" undrained strength should utilize smaller test specimens (1.4-in.-diameter is suggested) and a sufficient number of tests should be run to define the unfissured strength variation with depth.

### Conclusions

The normalized undrained shear strength of saturated cohesive soils has been shown to be a key parameter in the use of effective stress methodology for analysis of the load-carrying capacity of drilled shafts. For routine application, UU tests on good quality samples can be used to characterize the undrained strength and stress history provided the clay exhibits "normal behavior" under elevated consolidation pressures, i.e., no significant changes in soil structure or discontinuities (fissures, etc.) influencing failure modes are observed. As a supplement to UU tests, torvane tests should also be routinely run immediately upon sample recovery so that these data may be used to help assess the unfissured, undrained shear strength profile as developed from UU tests.

Extension of the proposed concept of undrained shear strength characterization to fissured soils other than the Beaumont clays must first consider the fissure frequency within the soil mass. For example, should a fissure spacing much closer than is observed in the Beaumont clay be encountered, it may not be practical to define an unfissured strength using UU tests. The application of UU tests for the prediction of OCR is also dependent on characterization of the  $S_u$  versus OCR relationship. As indicated, this relationship can be estimated within reasonable bounds. However, it is always prudent to reduce the degree of uncertainty by establishing this relationship by SHANSEP CIU testing of representative samples whenever possible.

### Drained Shear Strength

The drained shear strength of representative samples of the subsoils was measured for both peak and residual strength conditions. The drained strength (effective stress) parameters of the soil were developed from isotropically consolidated triaxial tests with porewater pressure measurements; whereas residual strength was determined primarily by direct shear testing of specimens with pre-cut failure planes.

An isotropically consolidated drained triaxial test employing a pre-cut failure plane and stage loading techniques was also conducted to supplement the direct shear test results.

#### Peak Strength Parameters

The effective friction angle,  $\phi'$ , was determined from the  $\overline{\text{CIU}}$  tests for three basic groups of soil specimens to represent the subsoils on the basis of their classification and plasticity index PI. For the average PI values of 17, 31 and 35,  $\phi'$  was found to be 28.5, 23.1 and 22.6 degrees, respectively. These data were supplemented from the  $K_o$  triaxial tests by interpreting  $\phi'$  from  $K_o$  values measured in the normally consolidated range. The  $\phi'$  values determined from these tests for plasticity indices of 34, 43 and 48, were 27.4, 21.1 and 19.9 degrees, respectively. As indicated by Figure 25 (Volume II), all but one of the combined data sets can be used to predict  $\phi'$  from PI with good confidence. This is quite useful for predicting the skin friction of shafts drilled in Beaumont clay by means of effective stress analyses.

Other effective stress parameters interpreted in this study included the effective cohesion and the pore pressure response at the maximum deviator stress (failure). Although these parameters are not relevant to the analyses reported herein, they are useful in comparing response of the Beaumont clay with other similar materials. For example, within the OCR range of interest, the measured  $A_f$  versus OCR trend appears to be quite similar to that of the London clays.

#### Residual Friction Angle

The results of slow (drained) loading of triaxial and direct shear specimens with pre-cut failure planes define a residual friction angle of nine degrees for effective normal stresses ( $\sigma'_n$ ) on the failure plane above about 1.7 tsf. Three tests within a  $\sigma'_n$  range of about 0.7 to 1.2 tsf indicated an average  $\phi'_r$  of 15 degrees. It was concluded that  $\phi'_r$  of the Beaumont clays is stress-dependent as has been reported for numerous other clays. From the work of many investigators, it has also been established that  $\phi'_r$  is dependent on the plasticity index of the soil.

Thus,  $\phi'_r$  of the Beaumont clay was found to be dependent upon both the plasticity index and the effective stress normal to the plane of shear.

The variation of the trend of  $\phi'_r$  with PI was assumed to follow that recommended by Kanji and Wolle (1977). This relationship, summarizing the work of a number of investigators, was adjusted to fit the data points developed during this study. A further adjustment was made to reflect the influence of effective normal stress. The combined adjustments were incorporated as a single influence factor to be used with the Kanji and Wolle (1977) data as described by Equation 4 (Volume II).

#### Borehole Shear Tests

Borehole shear tests were conducted at five locations at average depths ranging from 6.8 to 18.9 ft below the ground surface. For these tests, the grooved metal shear plates were faced with mortar to simulate shaft-soil interaction. Above the water table (approximately 11 ft) the shear tests were judged to be essentially drained; whereas below the water table, drainage conditions during shear are quite uncertain. Within the unsaturated soil zone, three stage test series yielded friction angles of 22.3, 24.4 and 24.1 degrees. There was some evidence that longer consolidation periods prior to shear yielded slightly higher values of  $\phi'$ . Below the water table the same type of test yielded remarkably similar friction angles of 10.4, 10.8 and 10.7 degrees. An additional single test series was run in the unsaturated soil zone (6.8 ft) after filling the hole with water. This test yielded a friction angle of 13.3 degrees, intermediate between the unsaturated and saturated zone test results.

Comparison of the unsaturated zone tests indicates excellent correlation with  $\phi'$  as determined by laboratory triaxial tests. It was concluded that tests below the water table which yielded  $\phi$  values on the order of 10.5 degrees probably represent undrained shear, although these values are similar to the residual friction angle measured at very large strains.

### Conclusions

The effective angle of internal friction,  $\phi'$ , of the Beaumont clay has been found to be related to plasticity and ranges from as much as 28.5 degrees at an PI of 15 percent to as little as 20 degrees at an PI of 48 percent. Within the ranges of stresses used during testing, no significant curvature of the Mohr-Coulomb envelope was apparent. Thus, for purposes of drilled shaft analysis,  $\phi'$  can be expressed as a function of PI with relatively good confidence.

The residual friction angle was found to be dependent on both the plasticity of the test sample and the effective normal stress on the plane of failure. Within the effective normal stress range tested (0.7 to 5.0 tsf),  $\phi'_r$  ranged between 15 and 9 degrees, the minimum value being developed at effective normal stresses greater than about 1.75 tsf. To estimate  $\phi'_r$ , a simple relationship is presented as Figure 27 (Volume II) which considers both plasticity and effective normal stress levels.

### State of Stress

As the effective stress approach to the prediction of the load-carrying capacity of piles or drilled shafts is dependent upon the characterization of the in-situ state of stress of the subsoils, the relevant parameters must be very carefully evaluated. Specifically, it is necessary to characterize the maximum past pressure ( $\sigma'_{vm}$ ), the overconsolidation ratio (OCR) and the coefficient of earth pressure-at-rest ( $K_0$ ). This study has focused upon characterization of these parameters by both laboratory and field testing, as well as by correlation with other soil properties/parameters.

### Maximum Past Consolidation Pressures

Assessment of the  $\sigma'_{vm}$  and OCR (the ratio of  $\sigma'_{vm}$  to overburden pressure,  $\sigma'_{vo}$ ) is made by direct interpretation of the results of consolidation and pressuremeter tests and is estimated from correlations between the normalized shear strength  $S_u/\sigma'_{vo}$  and OCR. Of the various methods used to interpret the consolidation tests, the method proposed by

Burmister (1951) was judged to produce the most consistent variation of  $\sigma'_{vm}$  with depth and values which were somewhat higher than interpreted from the other procedures. As typically observed,  $\sigma'_{vm}$  is underpredicted from consolidation test interpretations (primarily as a result of unavoidable sample disturbance); the Burmister predictions were taken as the most realistic of those derived from consolidation tests.

Prediction of OCR from Equation 9 is derived from  $S_u/\sigma'_{vo}$  data. These data are based on UU tests where the failure of the sample did not appear to be significantly influenced by the presence of fissures. The bounds of the OCR versus depth predictions were made assuming the exponent  $n$  of Equation 9 to vary from two-thirds to three-fourths and the coefficient  $K$  to be a constant, 0.35. The lower bound OCR profile defined by this method was found to be somewhat higher than that derived from the upper bound consolidation tests. Subsequently, these bounds were concluded to be a conservative representation of the probable in-situ OCR variation with depth.

Comparison of the above  $\sigma'_{vm}$  bound predictions from the pressure-meter tests with those from the consolidation tests indicated reasonable conformance below a depth of about 15 ft, but with increasingly smaller PMT predictions at shallower depths. Further, the trend of PMT predictions, becoming less with decreasing depth, did not reflect the zone of apparent desiccation clearly defined by the consolidation tests, the quasi-static cone resistance profiles and by near-surface liquidity indices. It was concluded that interpretation of  $\sigma'_{vm}$  from the PMT is basically an empirical procedure. Further, the postulated  $\sigma'_{ho}$  PMT measurement is not directly related to the vertical preconsolidation pressure, particularly where the soils have been subject to desiccation.

#### Coefficient of Earth Pressure-At-Rest

Measurement of  $K_o$  in the laboratory was performed by "no lateral strain" triaxial tests and was interpreted from the results of pressure-meter tests. This parameter was also predicted as a function of the measured plasticity and interpreted OCR of the subsoils.



The  $K_o$  laboratory tests conducted at depths of 4.3, 11.0 and 22.3, produced  $K_o$  values of 0.80, 0.84, and 0.78, respectively. Based on past experience with heavily overconsolidated clays, these values were judged to be well below those which would be expected in-situ. It is generally accepted that this phenomenon is the result of the unavoidable sampling disturbance, which is realized even with good quality samples, coupled with the extreme sensitivity of  $K_o$  to sample disturbance.

The value of  $K_o$  as interpreted from pressuremeter tests ranges between 1.1 and 1.8 and is somewhat erratic with depth. All the measurements were not considered to be of equal quality. By eliminating a questionable near-surface measurement and the maximum value measured, the trend below a depth of approximately 9 ft is reasonably consistent with the OCR versus depth trend predicted by the laboratory tests.

Values of  $K_o$  have been predicted from the profiles of OCR, effective friction angle and plasticity index in accordance with Equation 3 of Volume II. The OCR bounds are those defined by the upper limit from consolidation test interpretations and the lower limit from shear strength interpretations. As shown by Figure 20 (Volume II), the predicted upper bound of the  $K_o$  versus depth envelope (with one exception) is just below the envelope predicted by the most credible PMT measurements. In this analysis, the effective friction angle used was that determined from the laboratory testing of representative specimens, as previously described.

#### Summary

It is concluded that carefully conducted consolidation tests on good quality soil specimens can be used to predict a lower bound of the most probable maximum past consolidation pressures within the soil deposit. The investigators' experience with this and other studies indicate that the Burmister (1951) technique often provides what appears to be a somewhat more representative interpretation. In this interpretation, care must also be taken to conduct laboratory tests so as to preclude reduction of  $\sigma'_{vm}$  due to secondary compression effects. Should samples of questionable quality be interpreted,  $\sigma'_{vm}$  should also be

interpreted as recommended by Schmertmann (1955) and the largest values taken as being most probable.

It has been concluded that laboratory  $K_o$  measurements are likely to predict values which are too low, primarily a result of sample disturbance. Although not always applicable, it is recommended that SHANSEP testing techniques be employed in conjunction with  $K_o$  triaxial tests to attempt to mitigate the effects of sampling disturbance.

Pressuremeter interpretations of  $K_o$  show promise, although the interpretation procedure is essentially empirical. The interpretation of  $\sigma'_{vm}$  from PMT records appears to be less promising and could be completely invalid should  $\sigma'_{vm}$  be evolved primarily due to desiccation effects. Should the stress history be dominated by unloading effects, it is more likely that measured  $\sigma'_{ho}$  values (if such can be measured) may be related to  $\sigma'_{vo}$ . In all cases, there remain uncertainties connected with drainage conditions existing within the soil zone stressed by the pressuremeter probe.

#### Prediction of Ultimate Skin Friction

Methodology for the prediction of the ultimate skin friction of drilled shafts has been assessed incorporating the field and laboratory studies performed as part of this investigation, together with the results of the instrumented load tests conducted at the site in 1969. The focus of this assessment has been to attempt to predict the observed peak and post-peak skin friction using methods based on fundamental soil properties and parameters. Predictions from laboratory and/or field tests conducted so as to simulate soil-shaft load transfer and thereby directly measure ultimate skin friction were also investigated.

#### Analysis from Soil Properties

Two effective stress formulations for prediction of skin friction were evaluated by comparing theoretical predictions to observed behavior. The method based on critical state soil mechanics (see Equation 8 of Part IV, Volume III) was found to yield a reasonable prediction of

skin friction provided the surface and tip effects on shaft capacity were considered. To predict skin friction, Equation 8 was applied in the form of both an "average layer" and a discrete layer solution. The discrete layer solution, by being sensitive to the variation of soil properties with depth, is a more rational approach and is recommended if justified by the available data base.

#### Soil Properties/Parameters

It has been proposed that Equations 8 and 10 of Volume III be solved in terms of either OCR or, for "normal" clays, in terms of  $S_u/\sigma'_{vo}$ . It has been concluded that  $S_u/\sigma'_{vo}$  is usually more convenient for routine applications, and with high quality samples, may produce a better representation of OCR. This is particularly true should the  $S_u/\sigma'_{vo}$  versus OCR relationship be developed by SHANSEP testing procedures. For fissured clays, such as the Beaumont formation, it is noted that  $S_u/\sigma'_{vo}$  must represent the normalized shear strength of samples which are not significantly influenced by fissures. It has also been shown that the relationship between  $S_u/\sigma'_{vo}$  and OCR can usually be conservatively estimated from published information.

The remaining soil parameters of interest to the proposed effective stress analyses consist of the  $\phi'$  and  $K_o$ . The effective friction angle,  $\phi'$ , has been characterized for the Beaumont clay from laboratory test data as described in an earlier subsection of Part VIII entitled "Peak Strength Parameters." More generic representatives of  $\phi'$  could be incorporated if generalized solutions are generated similar to the Alpha Factor -  $S_u/\sigma'_{vo}$  relationship shown as Figure 11 of Volume III.

The coefficient of earth pressure-at-rest has been characterized as a function of the plasticity index and OCR of the subsoils in contact with the shaft in accordance with Equation 3 (Volume II). It is noted that the parameters in this equation were originally derived from special oedometer tests on reconstituted soils and that similar tests on undisturbed samples usually indicate somewhat higher  $K_o$  values. It is concluded that this conservatism is appropriate for the proposed method of ultimate skin friction evaluation.

### Empirical Correlation Factors

To recognize the free-surface effects on the ultimate shaft friction, the recommended method of analysis limits the ratio of calculated shear strength to the effective vertical stress (the Beta Factor) to a maximum of 1.6 at any location along the shaft. The effect of base loading on the shaft load transfer above the base is recognized by reducing the shaft length to that length which is effective in transferring load to the soil. This reduction was about 4 ft (1.6 diameters) for the single conventional dry-cast, straight shaft tested (S-1). A somewhat smaller reduction was noted for the dry-cast belled shaft (S-2). Reese and Wright (1977) suggest that both straight and belled shafts which are dry-cast should be shortened by one diameter; whereas O'Neill and Reese (1972) recommend a 5-ft reduction of shaft lengths in the Beaumont clays. As the base shaft-load interaction is a function not only of the bearing diameter, but also the stiffness of the bearing soils, this phenomenon clearly needs additional research.

In the proposed methodology for the prediction of skin friction, the shaft-soil friction angle ( $\delta$ ) has been characterized as a reduced  $\phi'$  by correlating the predictions with load test data for the Beaumont (O'Neill and Reese, 1970) and the London (Whitaker and Cooke, 1966) clays. The derived  $\delta$  is expressed by applying a constant reduction factor (in degrees) to  $\phi'$  as a function of the method of drilling and the amount of deformation beyond that required to develop the peak shearing resistance. For shaft deformations sufficiently large enough to define the residual shearing resistance,  $\delta$  is assumed to equal  $\phi'_r$  and no further reduction in  $\delta$  is assumed with greater deformations.

Close correlation of the average peak  $\tau_f$  (as predicted by the discrete layer analysis) was obtained with the S-1 and S-2 load test results by characterizing  $\delta$  for the dry-cast shafts as  $\phi' - 3$  degrees. For simulation of the minimum post-peak average  $\tau_f$  during the first loading of Shaft S-1,  $\delta$  was found to be  $\phi' - 5$  degrees. For those shafts failed with large deformations,  $\delta$  was found to range from 8.0 to 12.4 degrees, which suggested that  $\delta$  can be approximated

by  $\phi'_r$ . The application of  $\phi'_r$  to the prediction of  $\tau_f$  for slurry drilled shafts is also suggested by the results of the analysis of test shaft S-4, i.e., average  $\delta$  is approximately 13.5 degrees without considering the last 5 ft of the shaft being drilled dry.

#### Skin Friction Similitude Methods

Test methods were assessed to investigate the possibility of simulation of shaft-soil interaction and direct interpretation of peak skin friction from the test results. The methods considered were soil-mortar interface shear tests, borehole shear tests and moisture migration correlations.

Soil-mortar interface shear was investigated by direct shear tests on specimens prepared to simulate in-situ soil-shaft interface conditions. The test specimens were sheared under various effective normal pressures at rates approximating the rate of field loading. The Mohr-Coulomb envelope derived from these tests was found to be identical to the envelope derived from direct shear tests on companion soil samples, although the strength ratios of individual sample pairs usually ranged between 0.81 and 1.18. It was, therefore, concluded that this technique shows little promise as a method for direct simulation of the skin friction mobilized during the loading of drilled shafts.

In-situ borehole shear tests were conducted at various effective normal stresses by stage-loading techniques. To simulate soil-shaft interface conditions, the shear plates engaging the soil within the borehole were faced with a mortar mix identical to that used in the laboratory interface shear tests. Various rates of loading were investigated to evaluate the effects of shear rate.

The results of the borehole shear tests above groundwater level yielded friction angles slightly higher than  $\phi'$  as measured by triaxial compression tests in the laboratory. Below the groundwater level, friction angles on the order of 10.5 degrees suggested that the soil was not being sheared under fully drained conditions. The shearing resistance-deformation curves derived from the tests indicated that peak shearing resistance was obtained at movements significantly less than

that observed from shaft load-transfer curves. Their configuration also usually demonstrated a significant post-peak reduction in shear strength. From these results, it was concluded that the borehole shear test as configured in this study is not appropriate for simulation of drilled shaft interface shear. However, this test does appear promising for the in-situ evaluation of  $\phi'$  for the subsoils.

The moisture migration studies were conducted in conjunction with the laboratory interface shear tests. These studies related the difference in the post-shear water contents of the soil in the proximity of the mortar and the natural water content to the strength ratio of the companion test samples. A correlation was developed between the strength ratio and the maximum water content of the soil in proximity to the plane of failure. This somewhat tenuous relationship indicated average stress ratios for three generalized strata ranging from 0.83 to 0.92 as compared with the 0.8 factor reported by O'Neill and Reese (1970) for similar tests in Beaumont clay. These investigators recognized that water content changes are only partially responsible for degradation of the undisturbed strength of the subsoils produced by shaft installation and loading. In any event, it was concluded that the large moisture content variation existing over short distances within the Beaumont clays would preclude effective use of the moisture migration concept for evaluation of the shearing resistance of shafts drilled at the site.

#### Summary

The application of effective stress concepts using critical state methodology appears to be, by far, the most promising technique investigated for the prediction of the peak shearing resistance of drilled shafts in cohesive soils. The soil parameters for the proposed formulation (Equation 8) can be readily obtained from routine triaxial shear and consolidation tests in laboratory, as well as by correlation with parameters such as plasticity index and overconsolidation ratio. Analyses conducted to predict the results of load tests conducted at the site employed both "average layer" and "discrete layer" analyses. The latter

method was recommended because of its sensitivity to changes in soil property with depth.

Generic solutions for shafts drilled in Beaumont clay was generated in terms of both the Beta Factor ( $\tau_f/\sigma'_{vo}$ ) and the conventional Alpha Factor ( $\tau_f/S_u$ ) as a function of either the overconsolidation ratio or the normalized shear strength. For application of this technique in routine practice, it is suggested that unconsolidated undrained triaxial tests on good quality undisturbed samples, together with plasticity indices are all that are required to provide a reasonably accurate solution of Equation 8. However, the clays tested must exhibit "normal behavior," i.e., exhibit no structural changes under elevated consolidation pressures. Finally, it is concluded that the proposed methodology should not be used as a sole technique for prediction of the drilled shaft skin friction pending additional correlation of the method with available load test data representing a variety of relevant subsurface conditions.

Investigation of laboratory interface shear tests, specially adapted borehole shear tests and moisture migration techniques fail to identify any promising rational correlation between the test results and the shaft friction derived from the load tests. The borehole shear test did show significant promise for the in-situ evaluation of the  $\mu'$  of the soils. An evaluation of the configuration of the shear plates considering the scale and end constraint during shear may be appropriate upon a re-evaluation of this test approach for skin friction prediction. Further, a review of critical deformation as determined from laboratory rod shear tests, the borehole shear tests and the full-scale test piers may provide information to evaluate the shaft diameter scale effects on the amount of deformation required to develop peak shearing resistance.

#### Load-Deformation Prediction

Prediction of the load-settlement response of the test shafts has been approached by an accredited method of load-deformation compatibil-

AD-A114 305

WOODWARD-CLYDE CONSULTANTS HOUSTON TX

F/S 8/13

STUDY TO INVESTIGATE THE EFFECTS OF SKIN FRICTION ON THE PERFOR--ETC(U)

MAR 82 J AUDIBERT, D AGGARWAL, W GARDNER

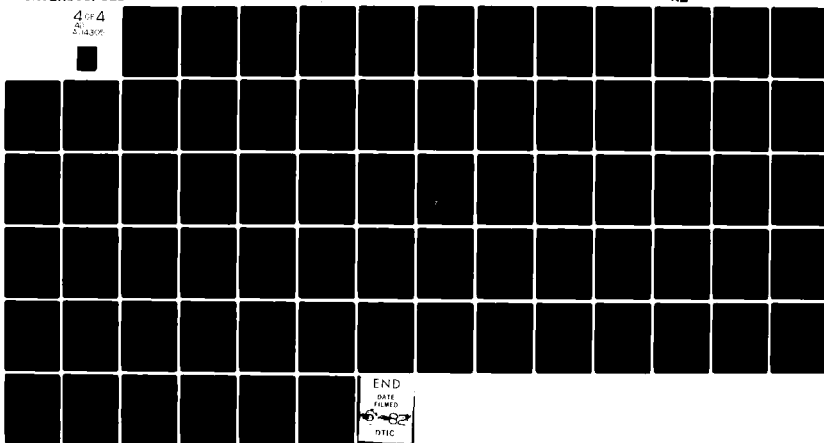
DACA39-80-C-0001

UNCLASSIFIED

TR-6L-82-1

NL

4 OF 4  
AD-A114 305



END  
DATE  
FILMED  
DTIC



ity analysis (AXCOL) employing load-transfer curves. Consequently, emphasis has been given to the development of a rational method of load-transfer curve simulation as a function of relevant soil properties and shaft geometry.

#### Initial Tangent to Load-Transfer Curve

Independent evaluation and analysis of the strain gage measurements for Test Shaft S-1 indicated that the interpreted load-transfer curves can be mathematically simulated with good confidence up to peak stress using the hyperbolic transformation technique. With this approach, the initial tangent to the load deformation curve, the maximum shearing resistance and the critical deformation need to be predicted. It was found that the initial tangent could be predicted as a function of OCR, except where the shaft load transfer was influenced by surface and tip effects. As  $S_u/\sigma'_{vo}$  can be directly related to OCR for most soils, an alternate relationship was also derived. A limited investigation to relate the initial tangent slope to the maximum (small strain) shear modulus also proved to be extremely promising in that  $G_{max}/E_i$  appears to be a constant, except at the zones of surface and tip influence.

#### Critical Deformation

As the effective stress technique appears to be a rational method of predicting the peak and residual shearing resistance along the shaft, it remained to characterize the relative shaft-soil movement required to mobilize  $\tau_f$ , i.e., the critical and if appropriate, post-peak deformations. Although the average critical deformation of drilled shaft in stiff clay is generally accepted to be on the order of 1/4 inches, the critical deformation of various depths along the shaft was found to be variable.

Review of the critical deformations,  $\rho_f$ , at various depths along the shafts for Test Shafts S-1 and S-3 indicated the critical deformation decreased either along the entire length of the shaft (S-3) or along the lower one-third of the shaft (S-1). It is not known whether a

reversal of this trend in the upper part of the S-1 shaft is anomalous or representative behavior, remembering that S-3 is also a dry-cast shaft of similar length and diameter and differs only by the presence of a void beneath the base of the shaft. There is, however, a promising correlation between the  $\log \rho_f$  and the depth shaft-length ratio. There is also some evidence that  $\rho_f$  is influenced by the length-diameter ratio of the shaft.

Reduction in shear strength upon deformations greater than the critical deformation required to develop peak shearing resistance was modeled after a cosine function restrained to meet the peak shearing resistance at a rotation of zero degrees and the prescribed post-peak shearing resistance at a rotation of 180 degrees. Consequently, it is necessary to predict the residual or an intermediate post-peak shearing resistance and the associated deformation required to develop this resistance. Unfortunately, there is insufficient data available from the load test results to provide any rational correlations with post-peak load-deformation behavior.

#### Summary

The load-settlement curves of selected test shafts were successfully predicted using the established AXCOL program and incorporating load-transfer curves simulated primarily from the soil properties and stress history of representative samples of the Beaumont clay. The greatest uncertainties of the method are associated with the critical and post-peak deformation predictions as a function of depth along the shaft. The sensitivity of these parameters (average versus variable values) should be investigated, as well as the applicability of the technique to shafts with different lengths and sites with other subsurface conditions.

#### Areas of Needed Research

Some of the concepts and methodologies identified by this study are believed to be sufficiently promising to justify additional inves-

tigation. Some of the more significant of these findings are discussed as follows.

#### Ultimate Skin Friction Prediction

Further investigation of the effective stress approach proposed to predict ultimate skin friction (Equation 8) is believed to be appropriate. This investigation would focus on confirming the applicability of the critical state methodology to drilled shafts at sites with soil types and stress histories which are different than the Beaumont clays. Equally important is to evaluate shafts with larger length-to-diameter ratios than have been considered in this study. This investigation should include an extension of the preliminary analysis included in this study of the London clay load tests reported by Whitaker and Cooke (1966).

#### Effect of Base Load on Skin Friction

Currently a reduction in shaft load transfer usually observed just above the base is accommodated by arbitrarily assuming that the last one diameter or four feet of the shaft does not transfer any load in skin friction. Investigation of this behavior is needed to develop a less arbitrary approach. This proposed study would likely include analysis of available instrumented load test data and mathematical simulations considering possible influencing parameters such as the stiffness of the bearing soils, the bearing stress and the geometry of the shaft. The object of this investigation would be to develop a rational, but simplified, design procedure to model tip effects on skin friction under both working and ultimate loads.

#### Soil-Shaft Friction Angle

As the proposed skin friction solution incorporates an empirically derived  $\delta$ , it is important to attempt to provide a more rational approach to the determination of this parameter. For example, Randolph and Wroth (1981) have suggested that the direct simple shear (DSS) test may approximate the failure mode at the soil-shaft interface. This is significant as the effective friction angle determined by triaxial tests ( $\phi'_{tx}$ ) can be as much as five degrees greater than would be mea-

measured by the DSS test. The work of these investigators also provides a theoretical basis for the reduction of  $\phi'_{tx}$  to  $\phi'_{dss}$ .

The foregoing concepts may provide a basis to characterize  $\delta$  from  $\phi'_{tx}$  of either the undisturbed or remolded soil by two and possibly three reduction parameters. The primary reduction parameter ( $\Delta_1$ ) accounts for the rotation of the principal stress direction during shear as previously described. The next reduction parameter ( $\Delta_2$ ) represents the influence of soil disturbance and softening caused by the construction process. This is probably not as significant as  $\Delta_1$ . The third potential reduction parameter ( $\Delta_3$ ) is associated with the curvature of the Mohr-Coulomb envelope. However, this reduction parameter may be significant only for relatively long shafts and possibly for shafts in heavily overconsolidated soils.

#### Load-Transfer Curve Simulation

The primary deficiency in the approach to simulation of the shaft load-transfer curves employed in this study is the uncertainty related to the prediction of the distribution of critical deformation along the shaft. There is a similar uncertainty in characterizing the amount of relative soil-shaft movement required to predict residual strengths. These parameters, therefore, need additional study.

Although a promising approach has been identified for derivation of the initial tangent to the load-transfer curve, this approach also needs to demonstrate correlations which are applicable to instrumented load tests from more than one source. For the Beaumont clays, the correlation of  $E_i$  with calculated  $G_{max}$  values also needs to be confirmed by laboratory  $G_{max}$  tests such as cyclic torsion (resonant column).

#### Pressuremeter Tests

There is some evidence that pressuremeter tests may be used to provide in-situ measurement of  $\sigma'_{ho}$  provided soil disturbance is minimized during creation of the probe access hole and that drained conditions are achieved before each new load increment is applied. Further, a one-to-one correlation of  $\sigma'_{vm}$  with the yield pressure as defined by the pressuremeter test has been suggested, although there is apparently no clear basis in theory for this contention.

As in-situ measurement of  $\sigma'_{ho}$  and  $\sigma'_{vm}$  would be of great utility for a number of applications; research of the pressuremeter test with an emphasis on stress history determination in cohesive soil would be a significant contribution. It is envisioned that an appropriate method of investigation would be tests conducted under controlled laboratory conditions in soils prepared to simulate different stress histories. Sedimented and subsequently preloaded soils could be tested by implanting the pressuremeter probe prior to sedimentation or by inserting the probe after sedimentation, but prior to preloading; thus, simulating the field application condition.

#### PART IX: LITERATURE CITED

American Petroleum Institute. 1981. API recommended practice for planning, designing, and constructing fixed offshore platforms, Twelfth Edition. Washington, D. C.

Bea, R. G. and Doyle, E. H. 1975. "Parameters Affecting Axial Capacity of Piles in Clay," Proceedings of the Offshore Technology Conference, Vol II, Paper OTC 2307, pp. 611-623.

Bureau of Yards and Docks, Department of the Navy. 1971. Design manual: soil mechanics, foundations, and earth structures, NAV DOCKS DM-7. Washington, D. C.

Burland, J. F. 1973. Shaft friction of piles in clay - a simple fundamental approach. Ground Engineering. Vol 6 (3): 30-42.

Burland, J. B., Butler, F. G. and Dunican, P. 1966. "The Behavior and Design of Large Diameter Bored Piles in Stiff Clay," Proceedings of the Symposium on Large Bored Piles, Institution of Civil Engineers, London.

Burmister, D. M. 1951. The application of controlled test methods in consolidation testing, ASTM Special Technical Publication No. 126, p 83, ASTM, Philadelphia. PA.

Chandler, R. J. 1968. The shaft friction of piles in cohesive soils in terms of effective stress. Civil Engineering and Public Works Review. London.

Chang, C-Y and Duncan, J. M. 1970. Analysis of soil movements around deep excavation. Journal of the Soil Mechanics and Foundations Division, ASCE. Vol 96 (SM5).

Chuang, J. W. and Reese, L. C. 1969. Studies of shearing resistance between cement mortar and soil, Research Report 89-3, Center for Highway Research, University of Texas at Austin, Austin, Texas.

Ellison, R. D., D'Appolonia, E. and Thiers, G. R. 1971. Load-deformation mechanism for bored piles. Journal of the Soil Mechanics and Foundations Division, ASCE, Vol 97 (SM4): 661-678.

Esrig, M. I., Kirby, R. C. and Murphy, B. S. 1979. "Advances in General Effective Stress Method for the Prediction of Axial Capacity for Driven Piles in Clay," Proceedings of the Offshore Technology Conference, Vol I, Paper OTC 3406, pp 437-448.

Gardner, W. S. 1977. Soil property characteristics in geotechnical engineering practice. Geotechnical/Environmental Bulletin. Woodward-Clyde Consultants. Vol 10 (2).

Gibson, R. E. and Anderson, W. F. 1961. In situ measurement of soil properties with the pressuremeter. Civil Engineering. Vol 56: 615-620.

Hardin, B. O. and Drnevich, V. P. 1970. Shear modulus and damping in sands, 1. Measurement and parameter effects, Technical Report No. UKY 26-70-CE2. University of Kentucky, College of Engineering, Soil Mechanics Series No. 1. Lexington, Kentucky.

Holloway, D. M., Clough, G. W. and Vesic, A. S. 1975. The mechanics of pile-soil interaction in cohesionless soils, Final Contract Report S-75-5. U. S. Army Engineer Waterways Experiment Station, Vicksburg, Mississippi.

Holmquist, D. V. and Meyer, P. L. 1975. A program for discrete-element solution of axial-columns with non-linear supports, Report to the American Petroleum Institute. Austin, Texas.

Kanji, M. A. and Wolle, C. M. 1977. "Residual Strength - New Testing and Microstructure," Proceedings of the 9th International Conference on Soil Mechanics and Foundation Engineering, Tokyo, Japan, Vol I: 153-154.

Kondner, R. L. 1963. Hyperbolic stress-strain response: cohesive soils. Journal of the Soil Mechanics and Foundations Division, ASCE. Vol 89 (SM1): 115-143.

Ladd, C. C. and Foott, R. 1974. New design procedure for stability of soft clays. Journal of the Soil Mechanics and Foundations Division, ASCE. Vol 100 (GT7): 763-785.

Ladd, C. C. and Lambe, T. W. 1963. "The Strength of 'Undisturbed' Clay Determined from Undrained Tests," ASTM-NRC Symposium, Ottawa, Canada.

Matlock, H. and Haliburton, T. A. 1964. "BMXOL 28, A Program for Finite-Element Solution of Beam-Columns on Non-Linear Supports." Austin, Texas.

Mattes, N. S. and Poulos, H. G. 1969. Settlement of single compressible piles. Journal of the Soil Mechanics and Foundations Division, ASCE. Vol 95 (SM1).

Meyer, P. L., Holmquist, D. V. and Matlock, H. 1975. "Computer Predictions for Axially-Loaded Piles with Nonlinear Supports," Proceedings of the Offshore Technology Conference, Vol I, Paper OTC 2186, pp 375-389.

Noorany, I. and Seed, H. B. 1965. In-situ strength characteristics of soft clays. Journal of Soil Mechanics and Foundations Division, ASCE. Vol 91 (SM2): 49-80.

O'Neill, M. W. and Reese, L. C. 1970. Behavior of axially loaded drilled shafts in Beaumont clay, Research Report No. 89-8. Center for Highway Research, the University of Texas at Austin.

O'Neill, M. W. and Reese, L. C. 1972. "Behavior of Bored Piles in Beaumont Clay," Journal of the Soil Mechanics and Foundation Division, ASCE, Vol 98, No. SM2, pp 195-213.

Parry, R. H. G. and Swain, C. W. 1977. Effective stress methods of calculating skin friction on driven piles in soft clay. Ground Engineering. pp 24-26.

Potyondy, J. G. 1961. Skin friction between various soils and construction materials. Geotechnique. Vol XI (4), London.

Randolph, M. F. and Wroth, C. P. 1981. Application of the failure state in undrained simple shear to the shaft capacity of driven piles. Geotechnique. Vol 31, No. 1.

Reese, L. C. 1978. Design and construction of drilled shafts. Journal of the Geotechnical Engineering Division, ASCE. Vol 104 (GT1): 95-116.

Reese, L. C., Hudson, W. R. and Vijayvergiya, V. N. 1969. "An Investigation of the Interaction Between Bored Piles and Soil," Proceedings of the Seventh International Conference on Soil Mechanics and Foundation Engineering.

Reese, L. C. and Wright, S. J. 1977. Construction procedure and design for axial loading, Drilled Shaft Manual, Vol 1. U. S. Dept. of Transportation, Office of Records and Development.

Schmertmann, J. M. 1955. "The Undisturbed Consolidation of Clay," Transaction, American Society of Civil Engineers, Vol 120, p 1201.

Seed, H. B. and Idriss, I. M. 1970. "Analysis of Ground Motions at Union Bay, Seattle During Earthquakes and Distant Nuclear Blasts," Bulletin, Seismological Society of America, Vol 60, No. 1, pp 125-136.

Seed, H. B. and Reese, L. C. 1957. "The Action of Soft Clay Along Friction Piles," Transactions, American Society of Civil Engineers, Vol 122.

Skempton, A. W. 1959. Cast-in-situ bored piles in London clay. Geotechnique. Vol IX (4), London.

Sowa, V. A. 1970. Pulling capacity of concrete cast in situ bored piles. Canadian Geotechnical Journal. Vol 7.

Tomlinson, M. J. 1957. "The Adhesion of Piles in Clay Soils," Proceedings of the International Conference on Soil Mechanics and Foundation Engineering, Vol 2, pp 66-71.



Vesic, A. S. 1975. "Principles of Pile Foundation Design," Proceedings of Boston ASCE Lecture Series on Deep Foundations, American Society of Civil Engineers, 1975.

Whitaker, T. and Cooke, R. W. 1966. An investigation of the shaft and base resistances of large bored piles in London clay, Proceedings of Symposium on Large Bored Piles, London.

Woodward, R. J., Gardner, W. S. and Greer, D. M. 1972. "Drilled Pier Foundations", McGraw-Hill Book Company, New York.

Table 1

Mean Deformation and Ultimate Shaft Load

<u>Shaft No.</u>	<u>Shaft Load (tons)</u>		<u>Deformation* (inches)</u>	
	<u>Peak</u>	<u>Residual**</u>	<u>Peak</u>	<u>Residual</u>
S-1	96.7	74.6	0.20	0.25
S-2	91.6	42.9	0.15	0.10
S-3	120.7	52.4	0.45	5.5
S-4	194.0	165.0	0.30	0.25

\* Represents the mean shaft deformation.

\*\* Minimum shaft load recorded on reloading or for large deformation on first load.

Table 2

Average Alpha and Beta Factors

<u>Shaft No.</u>	<u>S<sub>u</sub></u>	<u><math>\sigma'_{vo}</math></u>	<u>Peak <math>\tau_f</math></u>		<u>Residual <math>\tau_{fr}</math></u>	
	<u>(tsf)</u>	<u>(tsf)</u>	<u><math>\alpha</math></u>	<u><math>\beta</math></u>	<u><math>\alpha_r</math></u>	<u><math>\beta_r</math></u>
S-1	1.23	0.58	0.51	1.09	0.39	0.84
S-2	1.20	0.55	0.52	1.15	0.32	0.54
S-3	1.30	0.67	0.50	0.96	0.27	0.51
S-4	1.53	1.09	0.36	0.47	0.31	0.40

Note that Alpha ( $\alpha$ ) is defined as  $\tau_f/S_u$  and that Beta ( $\beta$ ) is defined as  $\tau_f/\sigma'_{vo}$ .

Table 3

Load-Transfer Curve Parameters

Measured	$\tau_f$	$\tau_f/\sigma'_{vo}$	$E_i$	$E_i/\sigma'_{vo}$	$R_f^{**}$	$\rho_f$
Depth (ft)	(tsf)	( $\beta$ )	(tsf/ft)	(ft-l)		(in.)
2.08	0.206	1.585	247	1900	0.89	0.093
4.17	0.357	1.370	219	840	0.77	0.125
8.33	0.726	1.394	257	494	0.78	0.187
12.50	0.950	1.216	279	357	0.85	0.347
14.58	0.940	1.032	300	329	0.96	0.552
16.67	0.719	0.726	227	229	0.85	0.187
18.75	0.379	0.359	166	157	0.81	0.130
20.83	0.610*	0.345*	50*	45*	-	1.75*

\* Data near tip may not be valid.

\*\*  $R_f$  is defined in Figure 1.

Table 4

Soil Parameters for Effective Stress Analysis

<u>Parameter</u>	<u>Reference</u>	<u>Remarks</u>
OCR	Fig. A-1	Upper Bound Prediction
$K_o$	Fig. A-2	$K_o = (1 - \sin \phi') (OCR)^m$
$\phi'$	Fig. A-3	Assumes average $\phi' = 21.9^\circ$
$\delta$	Fig. A-3	$\delta = \phi'$ and $\phi' - 4^\circ$
$\sigma'_{vo}$	Fig. A-4	Groundwater Level @ 15 ft consistent with 1969 data and conditions

Table 5

Test Pier Analysis Summary

Shaft	Dia.	L	$L_e^*$	$(Q_s)_p$	$(Q_s)_r^{**}$	$\sigma'_{vo}$	$\beta_p$	$\beta_r$
No.	(ft)	(ft)	(ft)	(tons)	(tons)	(tsf)	—	—
S-1	2.56	23.1	19.0	96.7	74.6	0.56	1.09	0.84
S-2	2.59	23.0	17.8	91.6	42.9	0.67	1.15	0.54
S-3	2.58	23.0	23.0	120.7	63.7	0.67	0.96	0.51
S-4	2.67	45.0	45.0	194.0	165.0	1.09	0.47	0.40

\* Shaft length transferring load to soil.

\*\* Lowest  $Q_s$  upon reloading or upon CRS test to large deformation.

Table 6

Calculated Average Friction Angles

Shaft No.	Average Friction Angle (Deg.)*					
	<u>Peak</u>		<u>Post-Peak**</u>		<u>Residual</u>	
	Discrete	Average	Discrete	Average	Discrete	Average
S-1	19.7	17.0	17.5	13.5	12.4	12.4
S-2	19.8	18.5			8.0	7.5
S-3	19.7	16.0			8.0	7.5
S-4	13.5 <sup>+</sup>	9.7			11.2 <sup>+</sup>	8.0

\*  $\beta_{max} = 1.7$ .

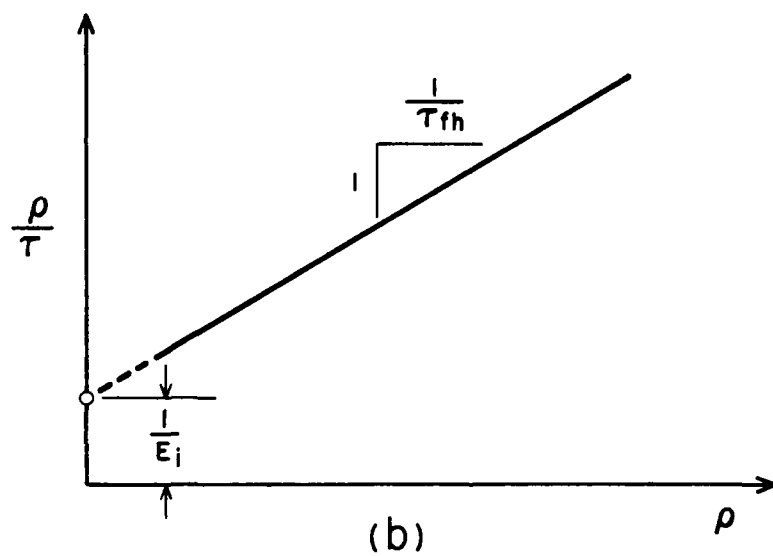
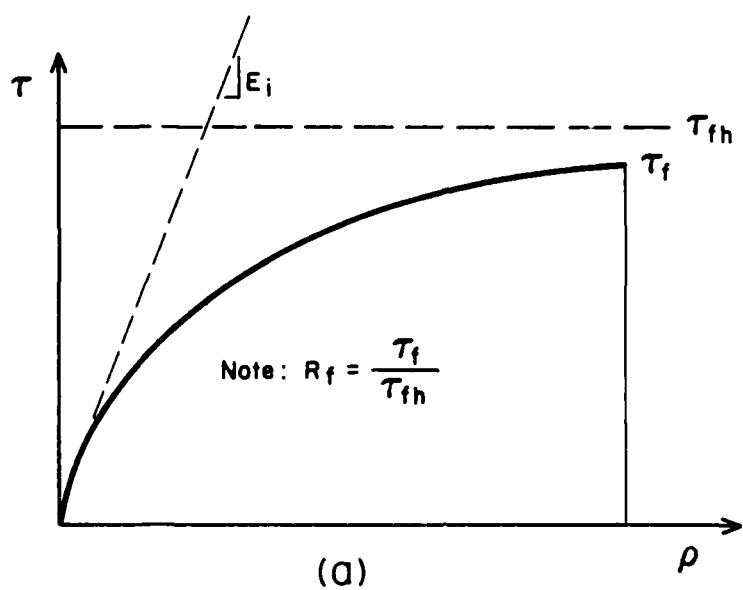
\*\* Minimum first load post-peak  $\tau_f$ .

+ Includes 15 ton reduction for shaft wedging effects.

Table 7

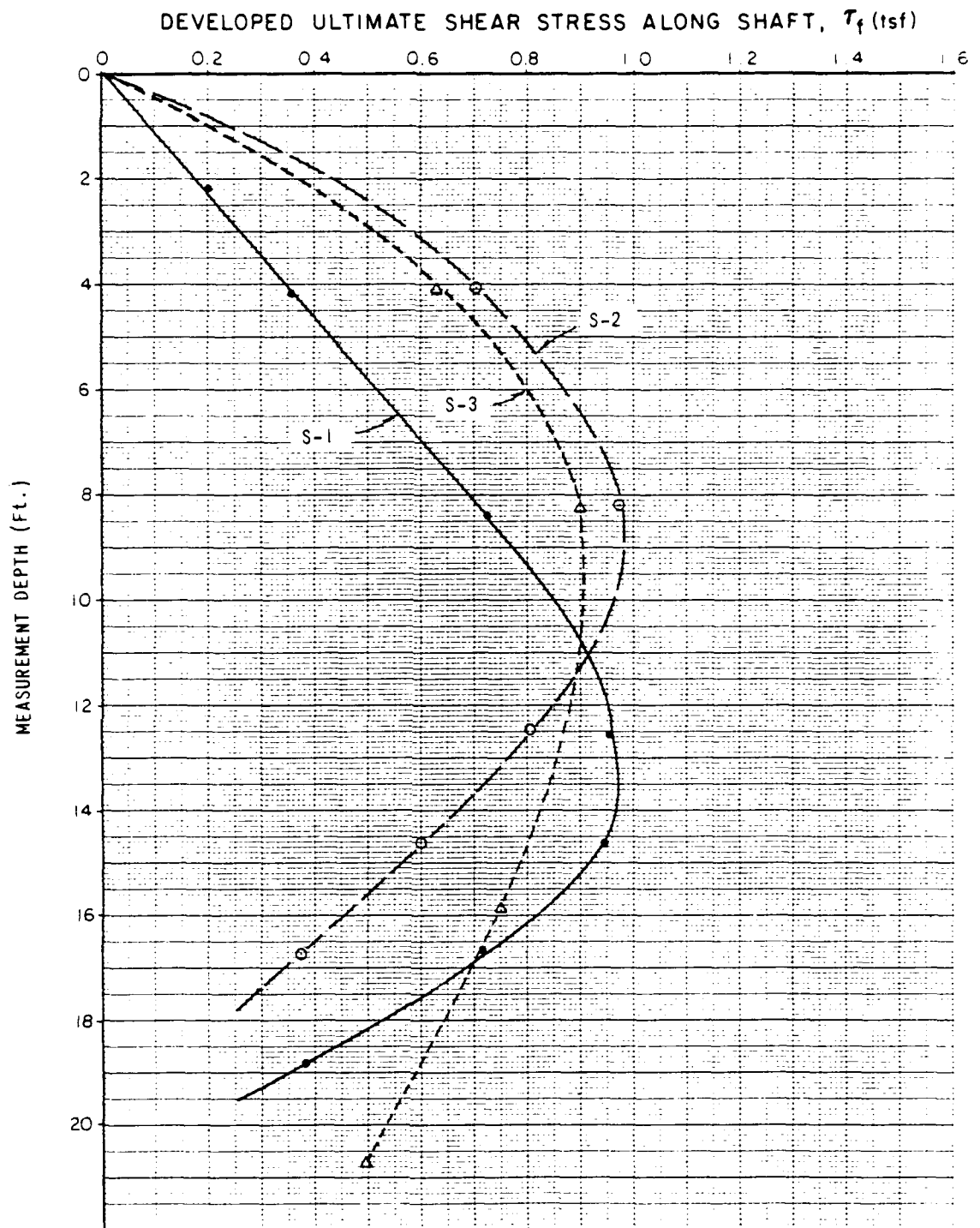
Alpha Factor From Moisture Migration Tests

Stratum No.	Depth (ft)	$w_n$ (%)	$w_f$ (%)	$\alpha_1$	$\alpha_2$	$\alpha$
1	0-17	24.5	24.0	1.01	0.92	
2	17-20	23.5	23.1	0.96	0.83	0.51
3	20-26.5	23.7	23.3	0.98	0.85	



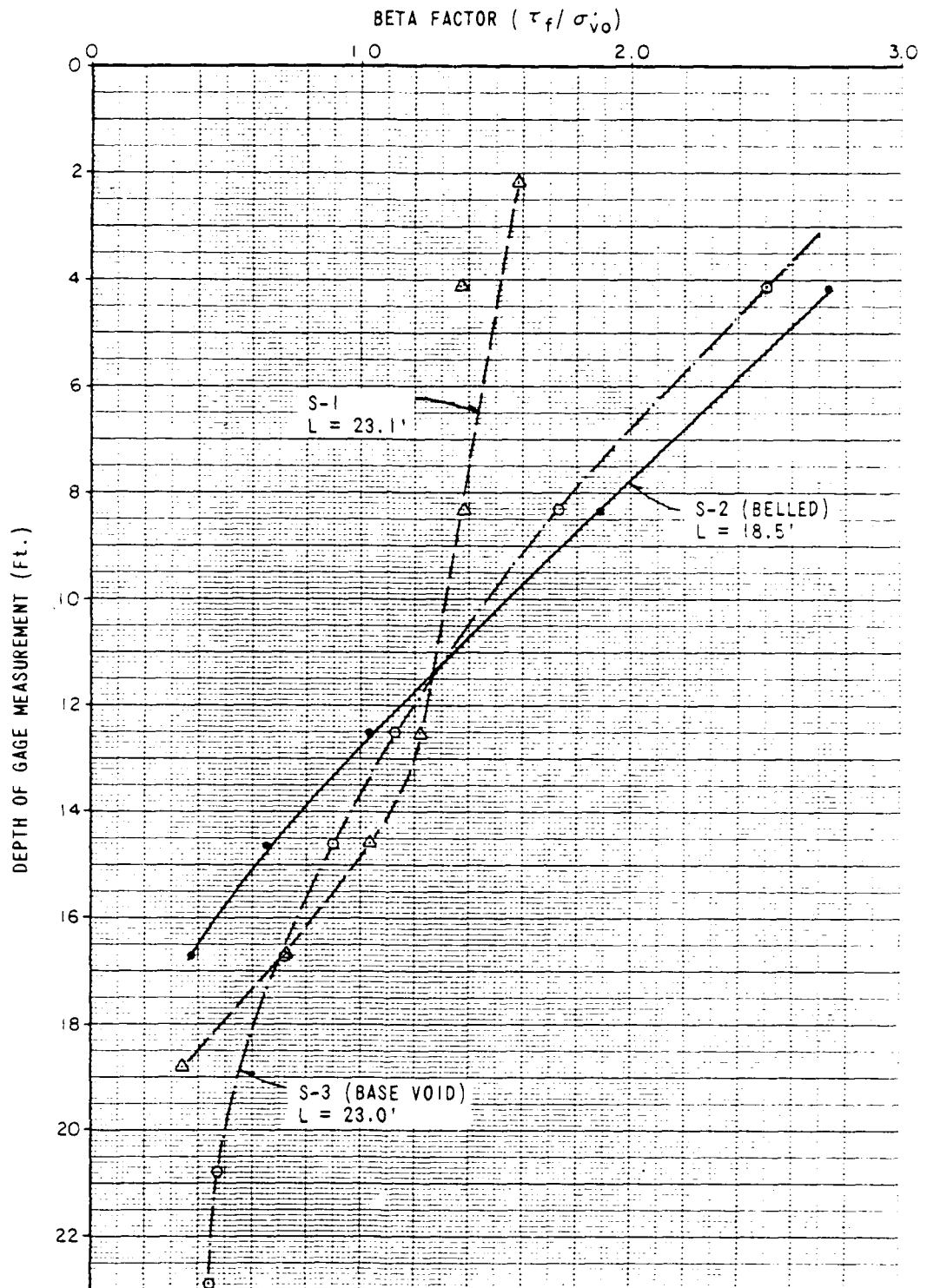
Hyperbolic Transformation  
of  
Shaft Load-Transfer Curve

Fig. 1



PEAK SHAFT RESISTANCE  
VS.  
DEPTH OF MEASUREMENT  
DRY CAST SHAFTS - FIRST LOAD

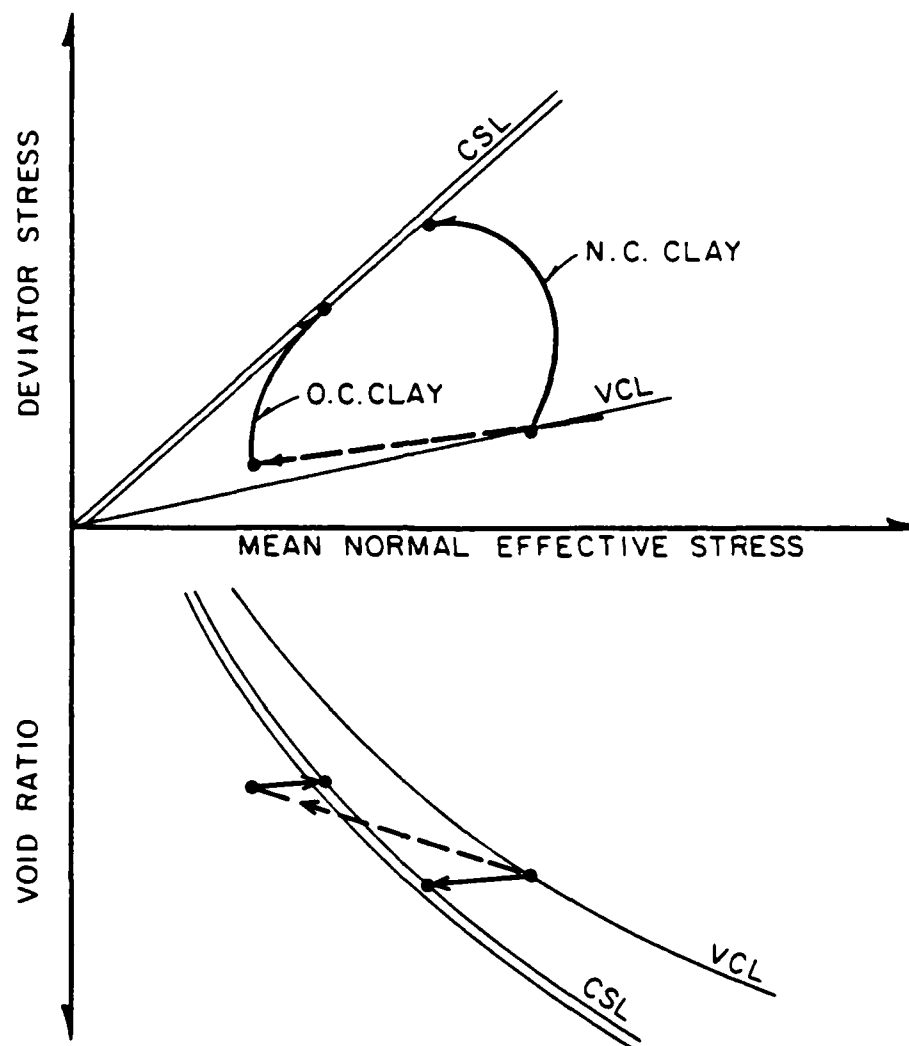
Fig. 2



BETA FACTOR VS.  
DEPTH OF MEASUREMENT  
FOR DRY-CAST TEST SHAFTS

Fig. 3

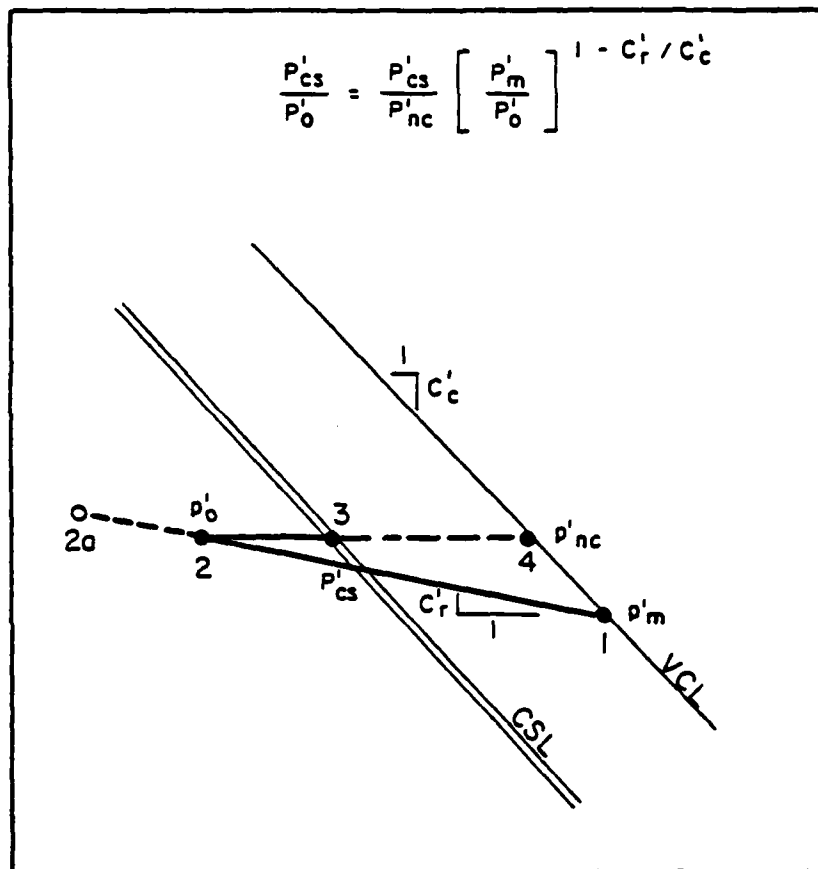




CRITICAL STATE REPRESENTATION OF  
EFFECTIVE STRESS PATHS  
DURING SHAFT LOADING

Fig. 4

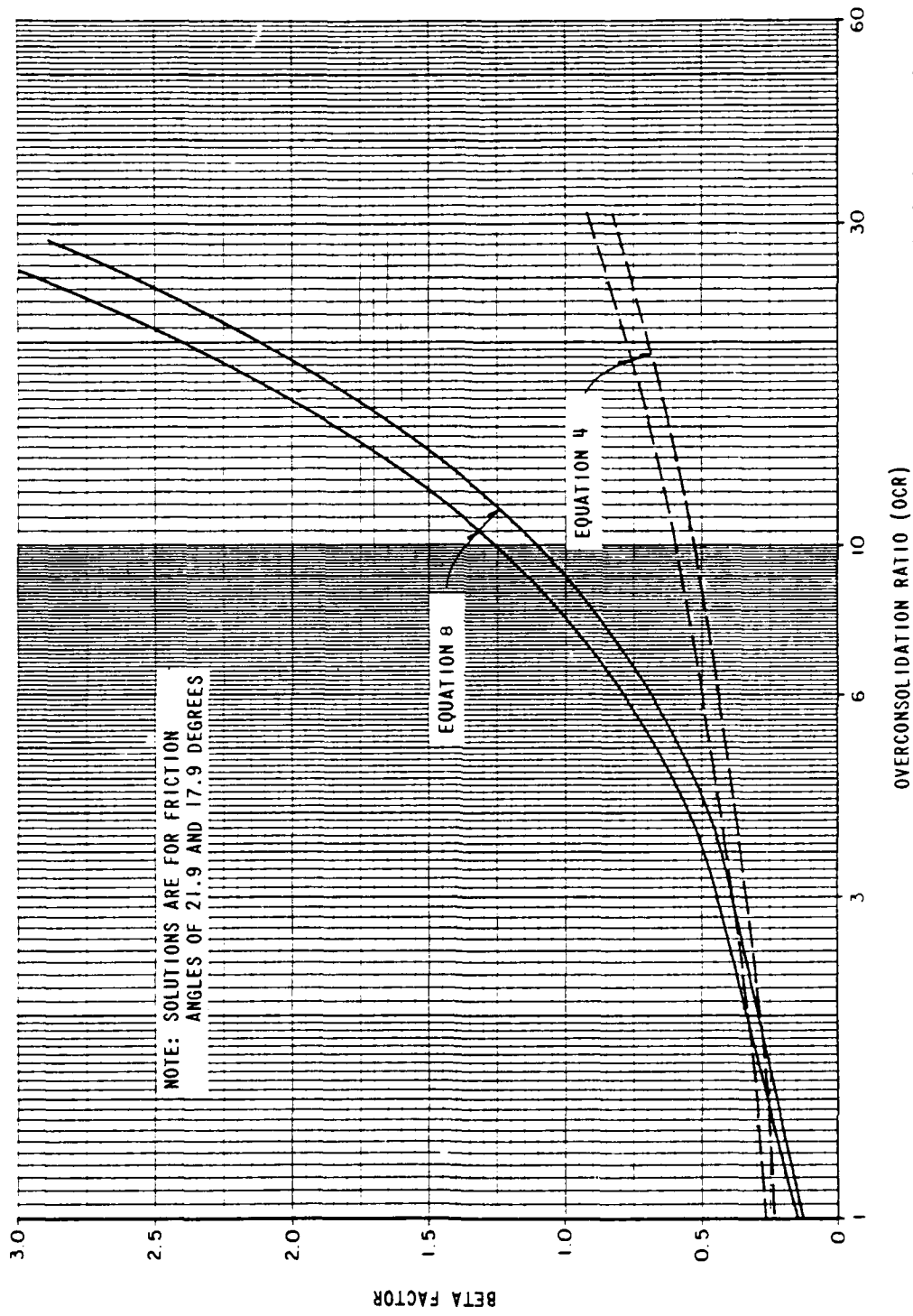
VOID RATIO



LOG MEAN NORMAL EFFECTIVE STRESS

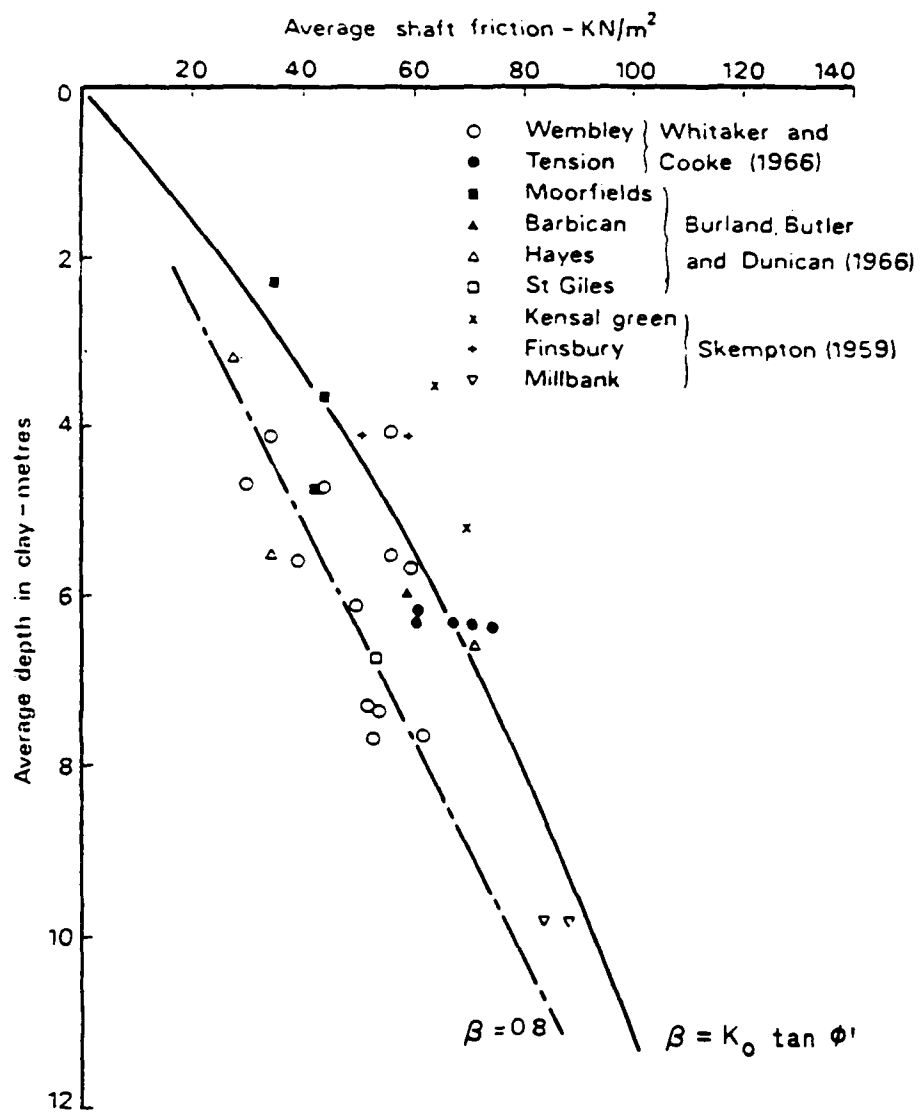
CRITICAL STATE FAILURE REPRESENTATION  
FOR SHAFTS IN OVERCONSOLIDATION CLAY

Fig. 5



BETA FACTOR SOLUTIONS  
FOR  
EQUATIONS 4 AND 8

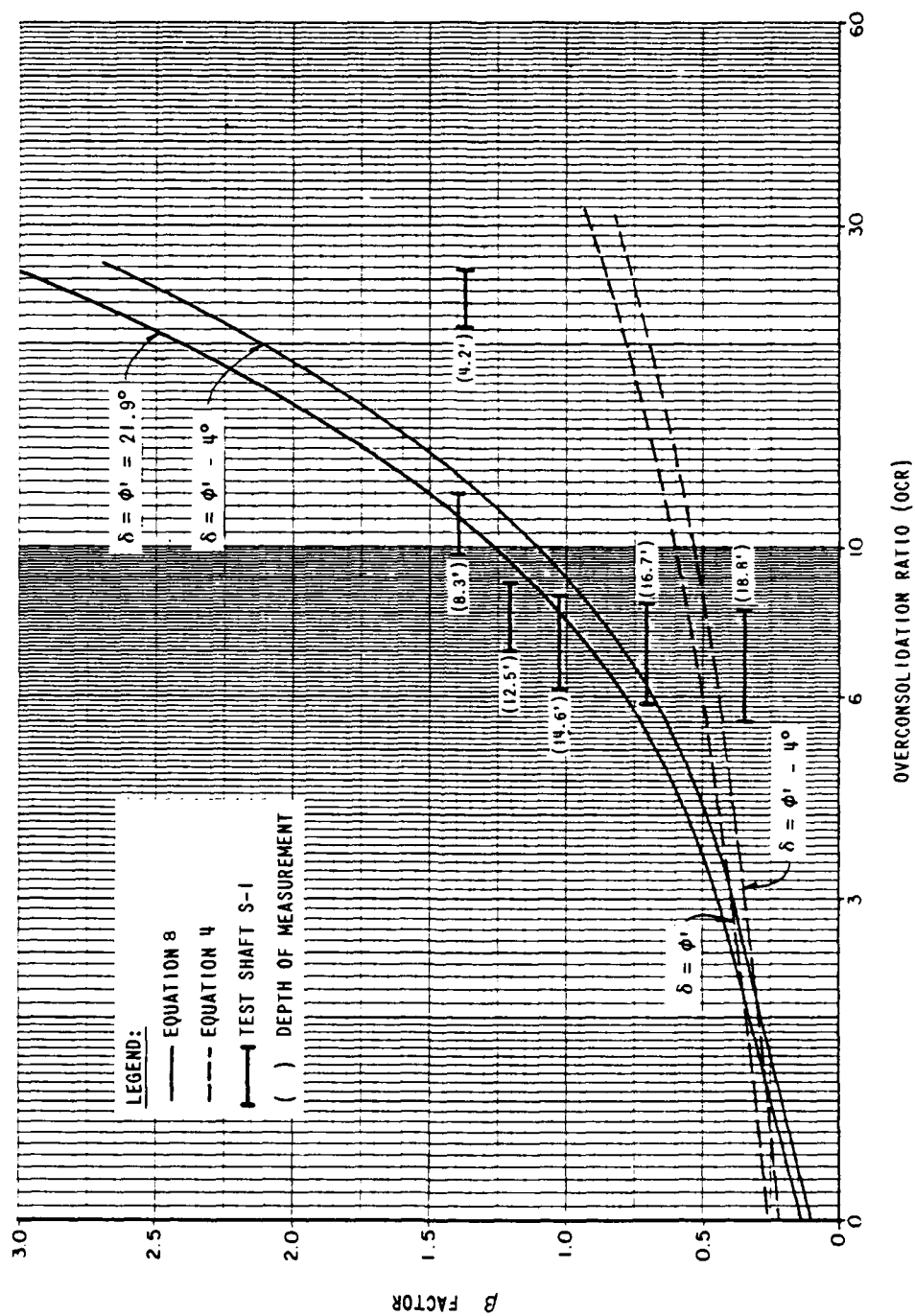
Fig. 6



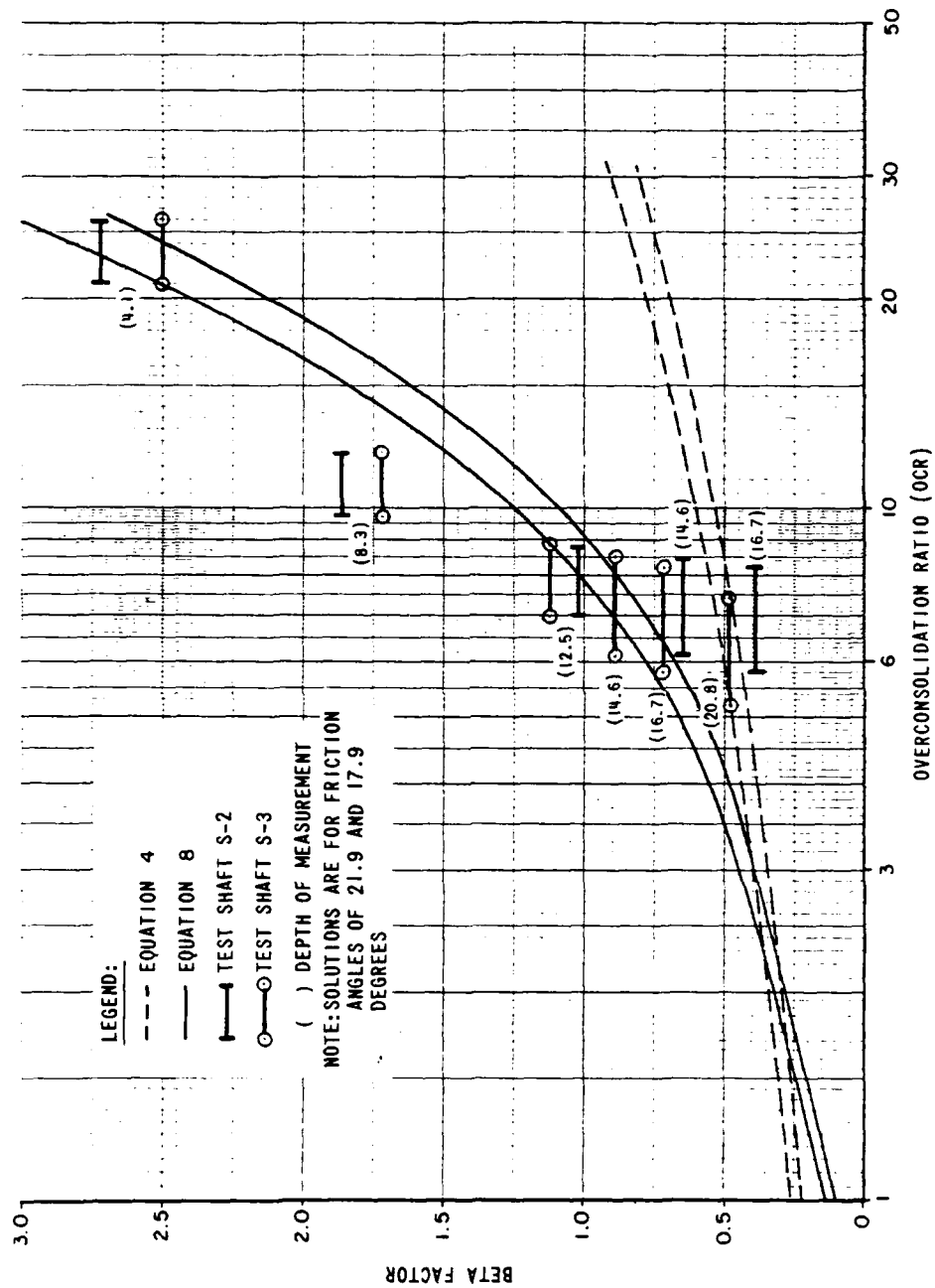
Adapted from Burland (1973)

APPLICATION OF EQUATION 4  
SHAFTS DRILLED IN LONDON CLAY

Fig. 7

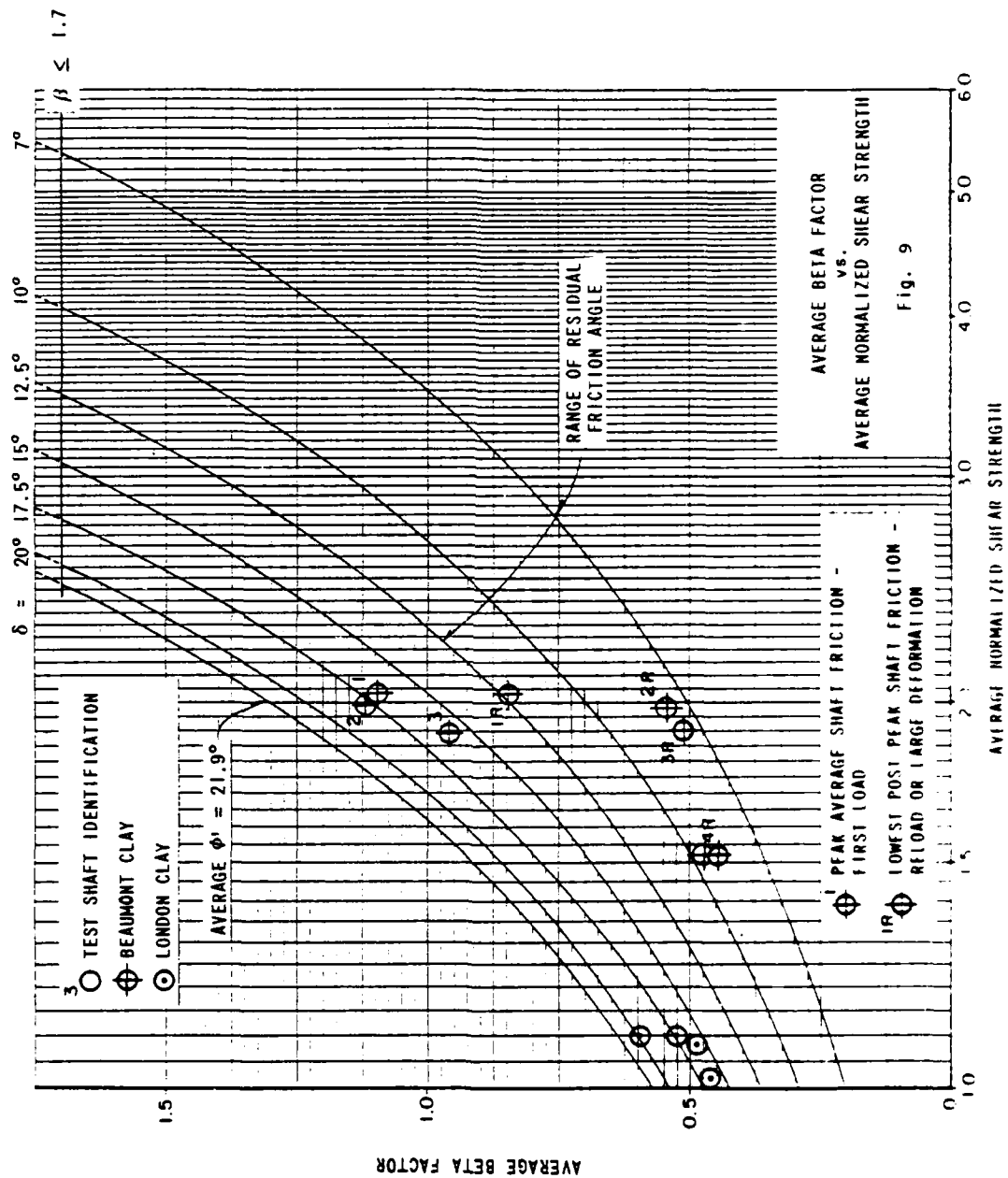


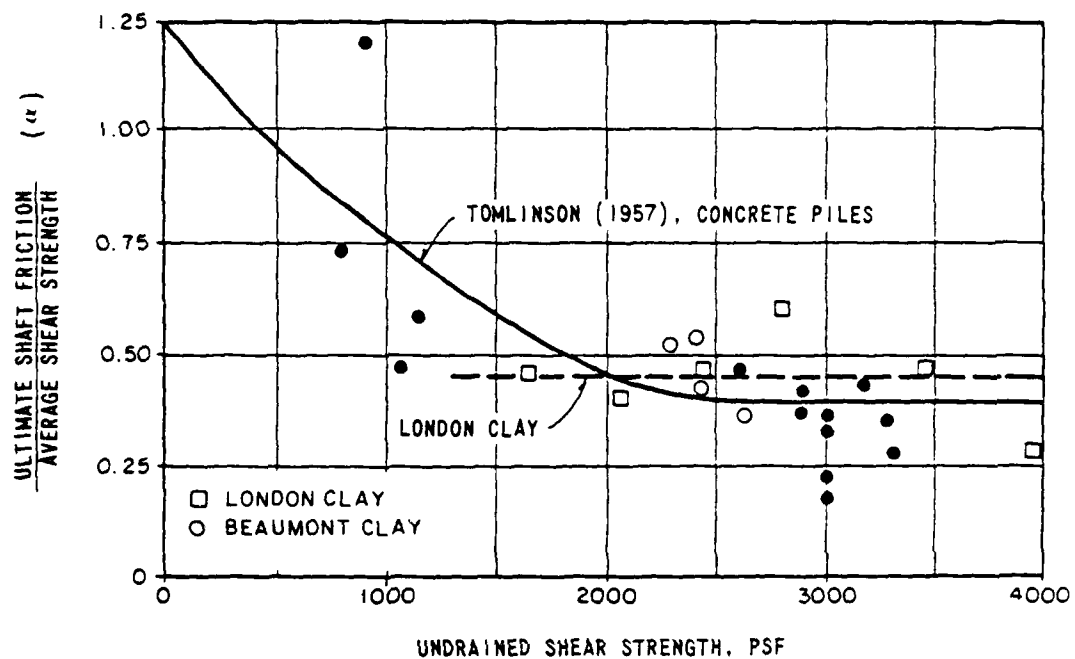
SOIL OCR vs.  $\beta$  FACTOR  
TEST SHAFT S-1  
Fig. 8(a)



SOIL OCR vs.  $\beta$  FACTOR  
TEST SHAFTS S-2 AND S-3

Fig. 8(b)



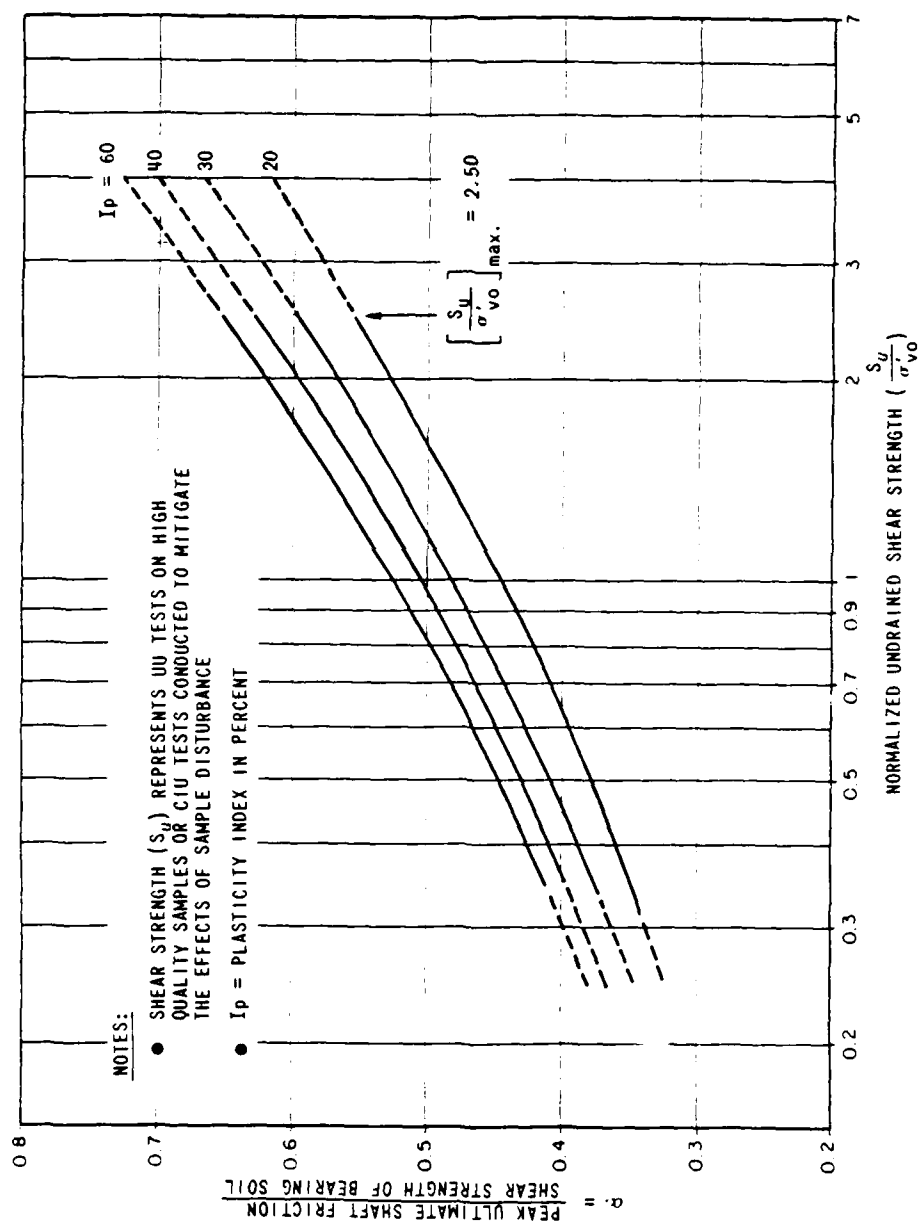


Adapted from Sowa (1970)

ALPHA FACTOR vs. UNDRAINED SHEAR STRENGTH  
DRILLED SHAFTS IN COHESIVE SOILS

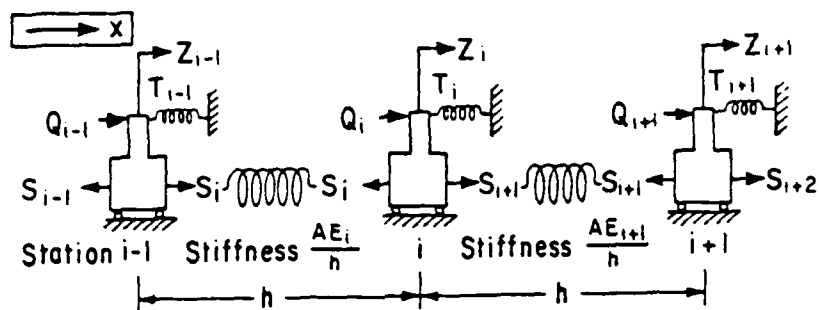
Fig. 10





ALPHA FACTOR ( $\alpha$ ) vs. NORMALIZED SHEAR STRENGTH  
 DRY-CAST STRAIGHT SHAFTS  
 DRILLED IN COHESIVE SOILS

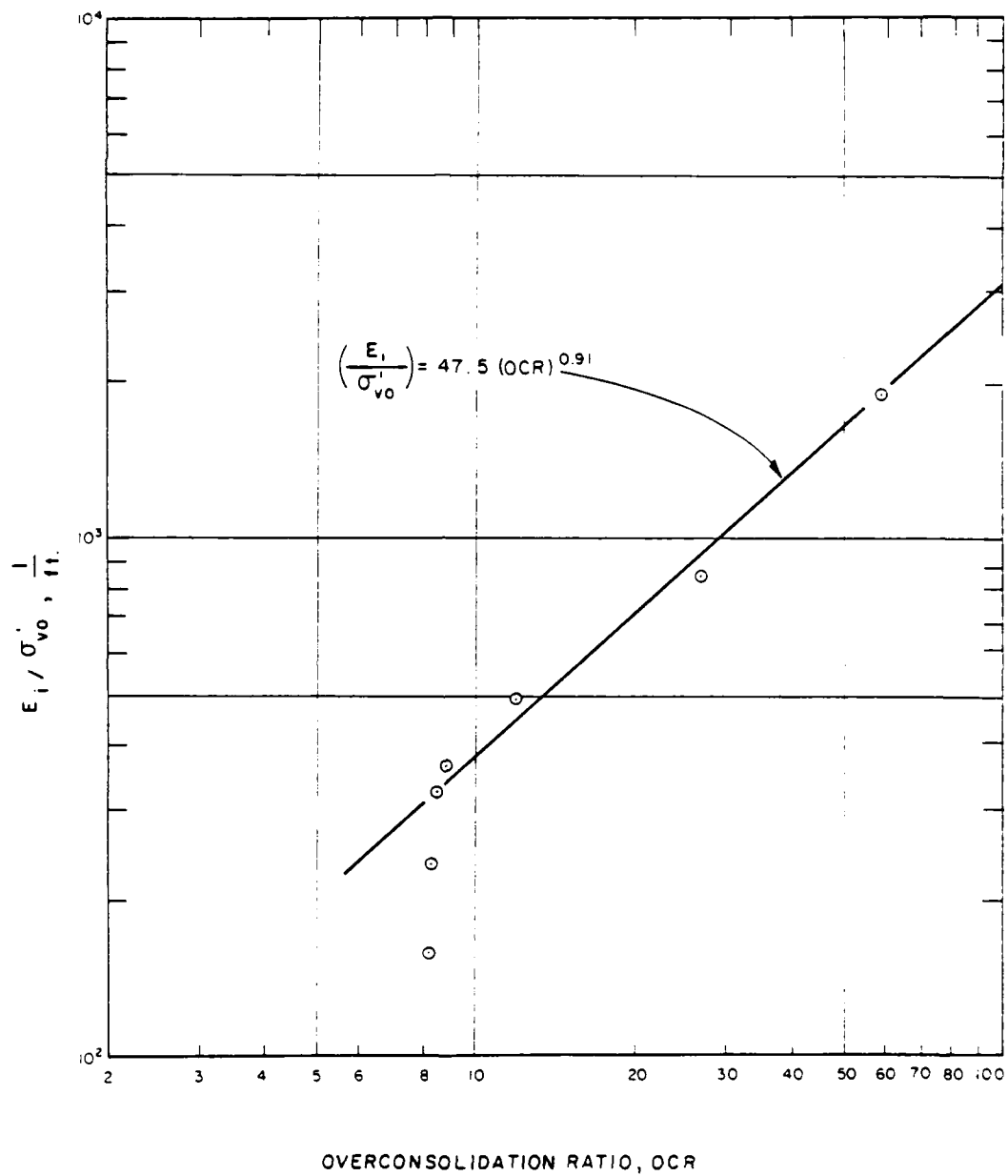
Fig. 11



- $i$  = external station number
- $x$  = length along column from station zero (top)
- $Z_i$  = displacement at station  $i$
- $h_i$  = length of one increment
- $AE_i$  = product of area and modulus of elasticity for the bar between station  $i$  and  $i-1$ .
- $T_i$  = load carried by the restraint at station  $i$
- $S_i$  = load carried by the column at station  $i$
- $Q_i$  = external load at station  $i$

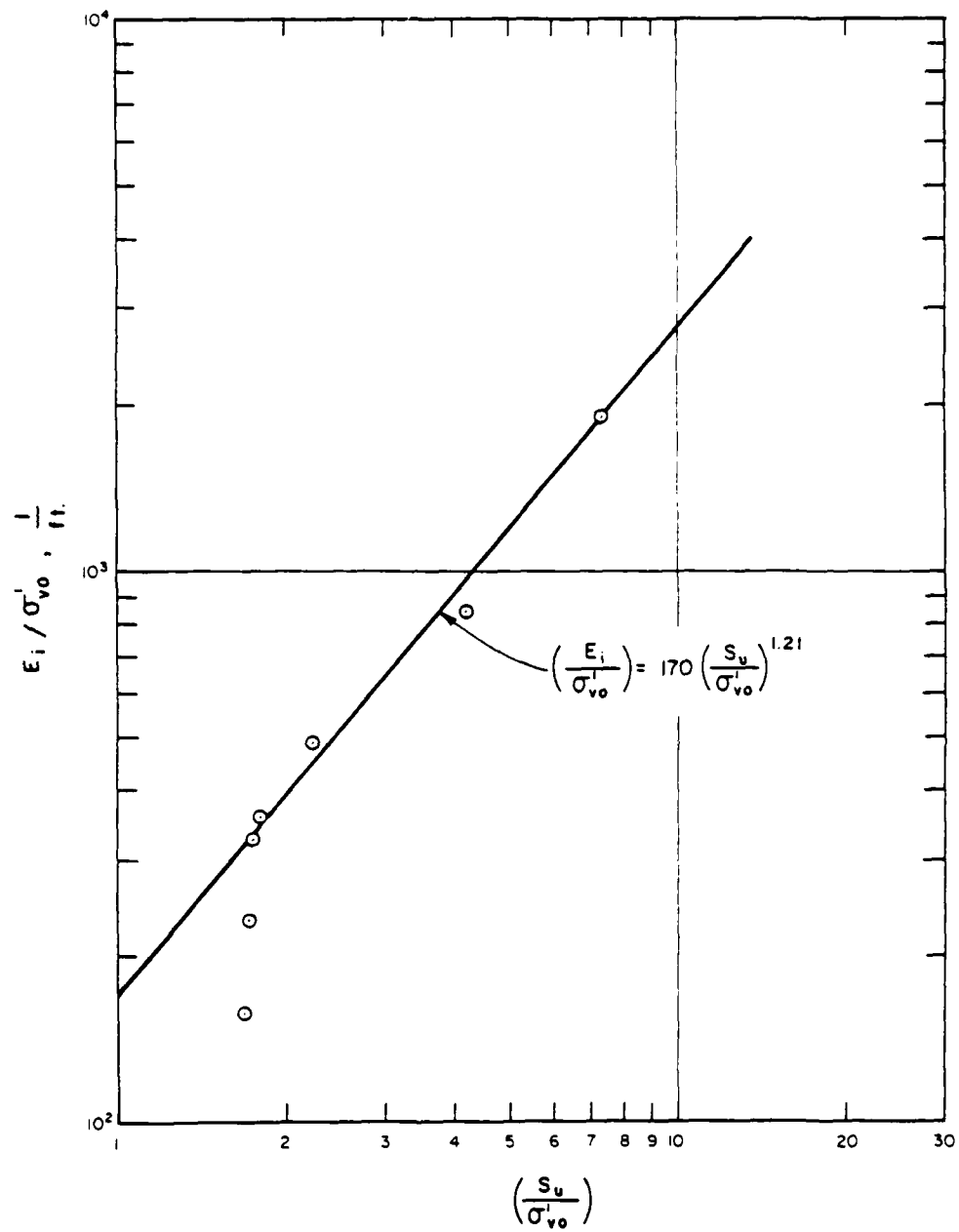
Axial-Column Model

Fig. 12



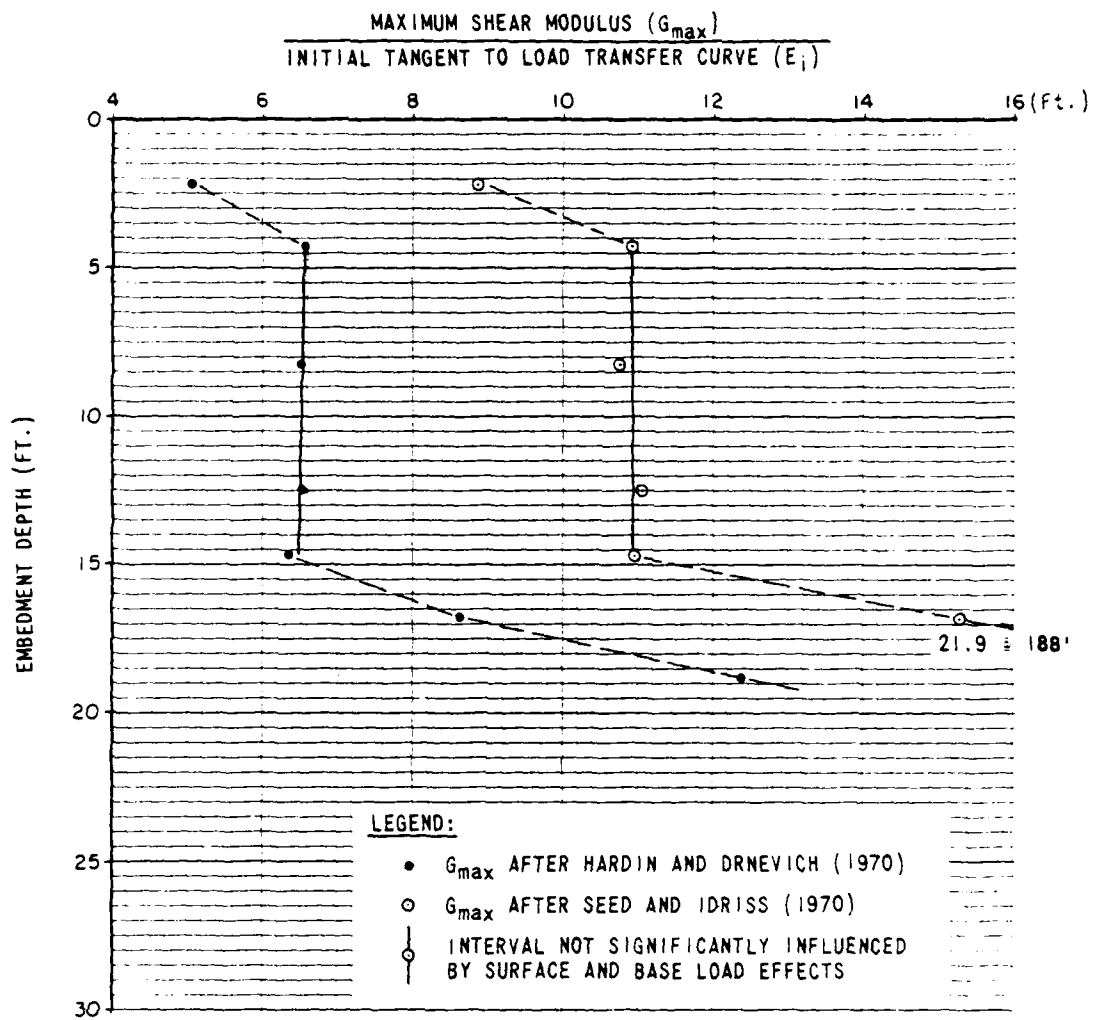
Normalized Initial  
Tangent Modulus vs. OCR

Fig. 13



Normalized Initial Tangent Modulus  
vs. Normalized Shear Strength

Fig. 14



$G_{max}/E_i$  VS EMBEDMENT DEPTH  
TEST SHAFT S-1

Fig. 15

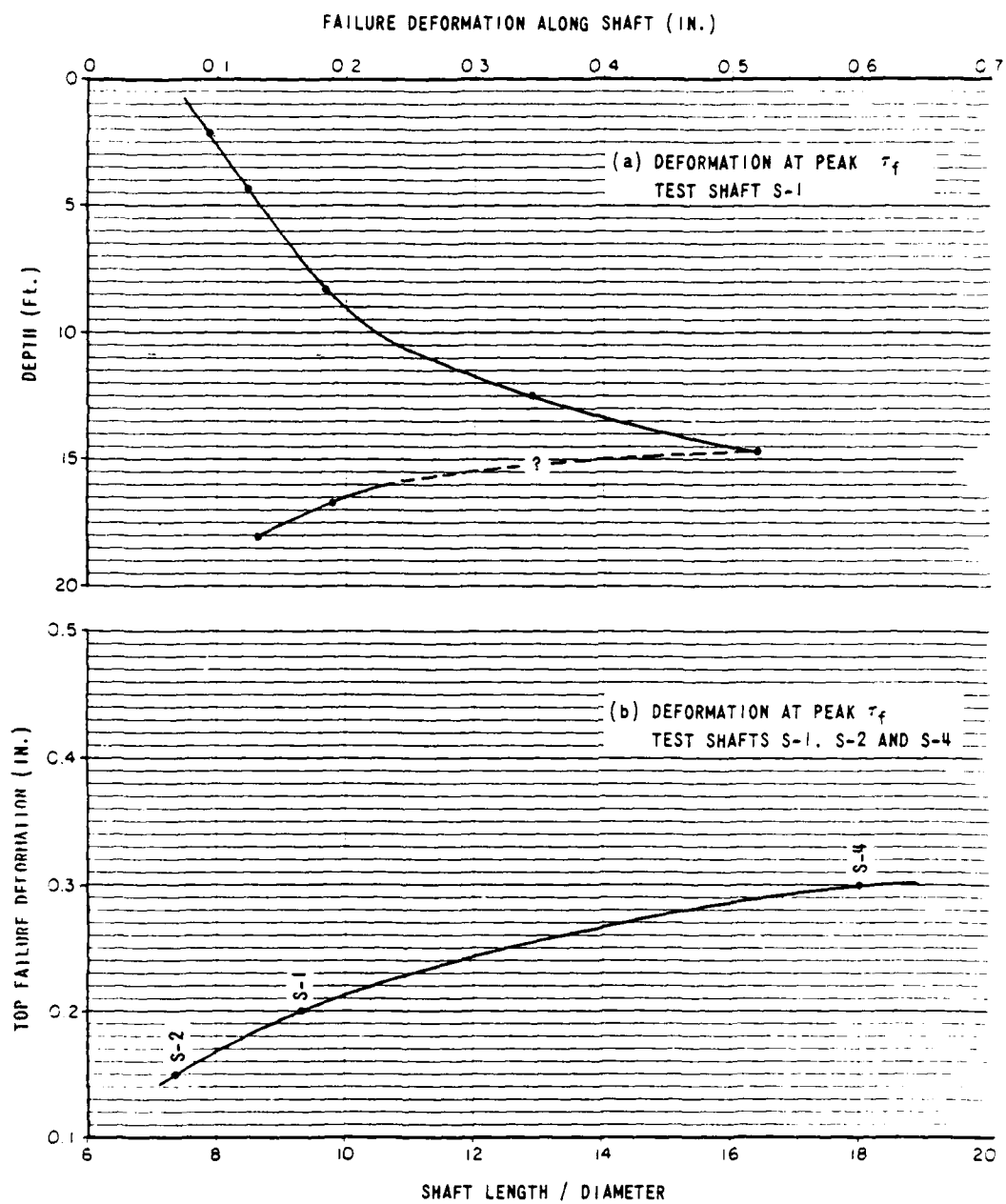
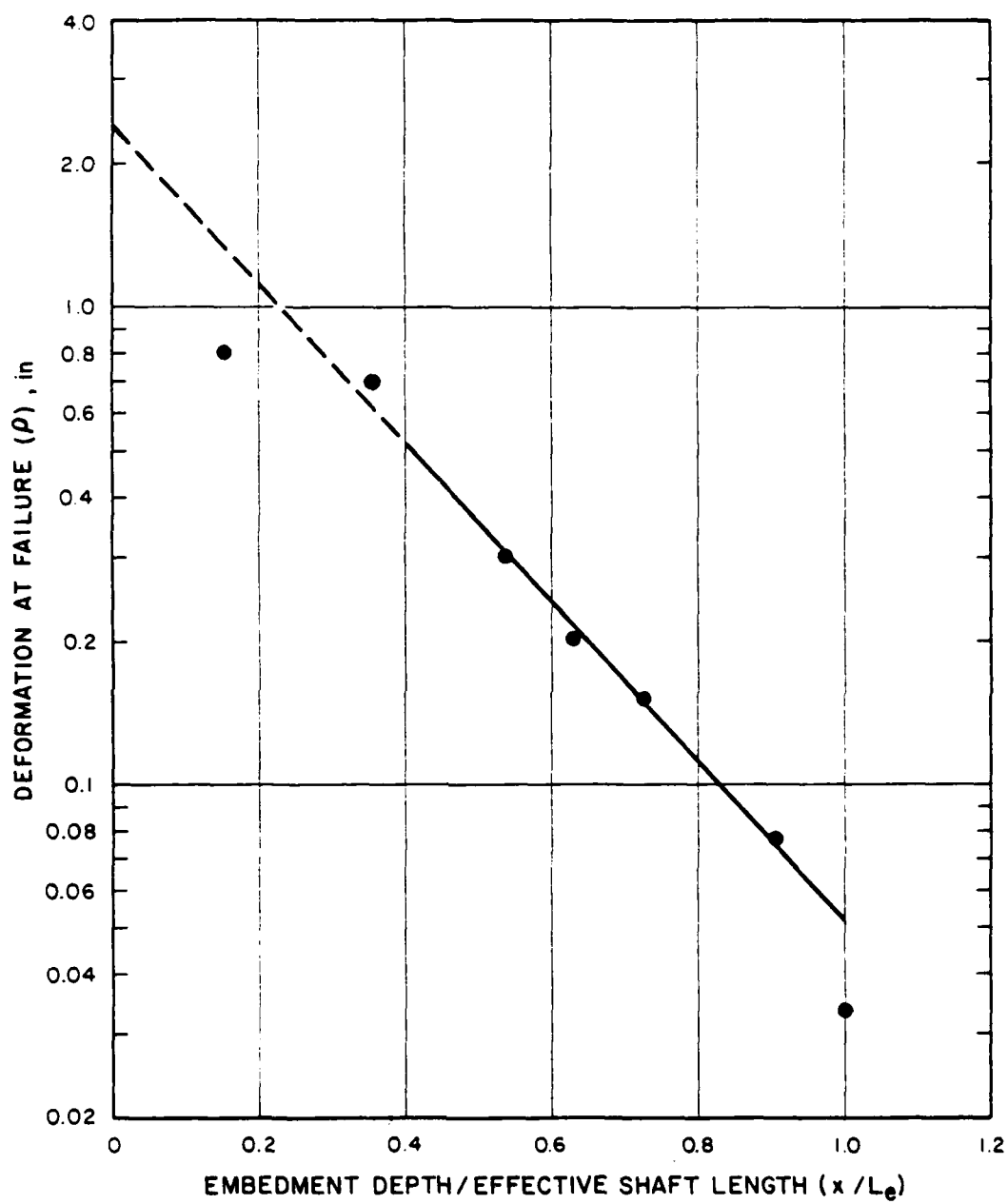
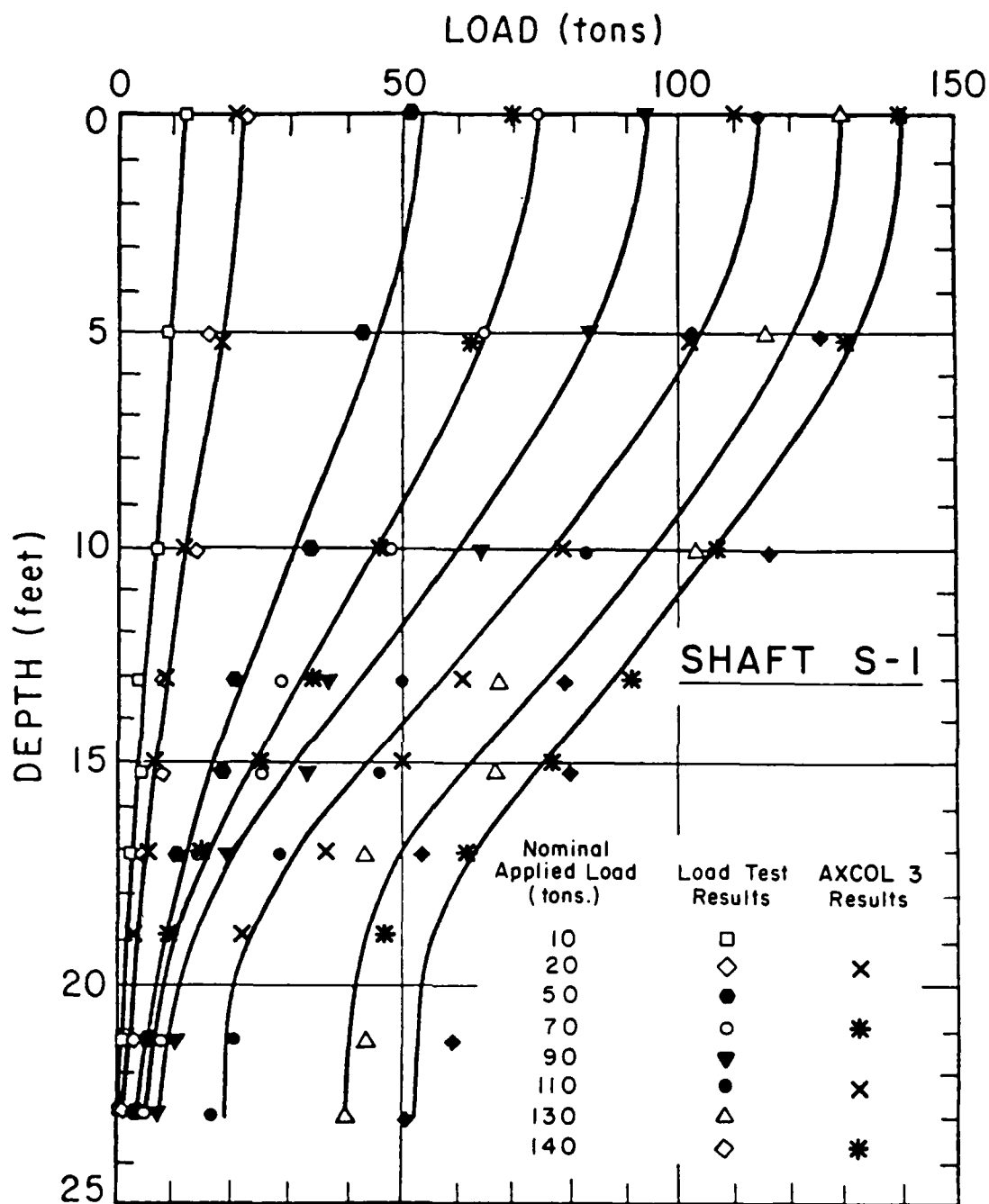


FIG. 16



Log  $\rho$  vs.  $x/L_e$   
Test Shaft S-3

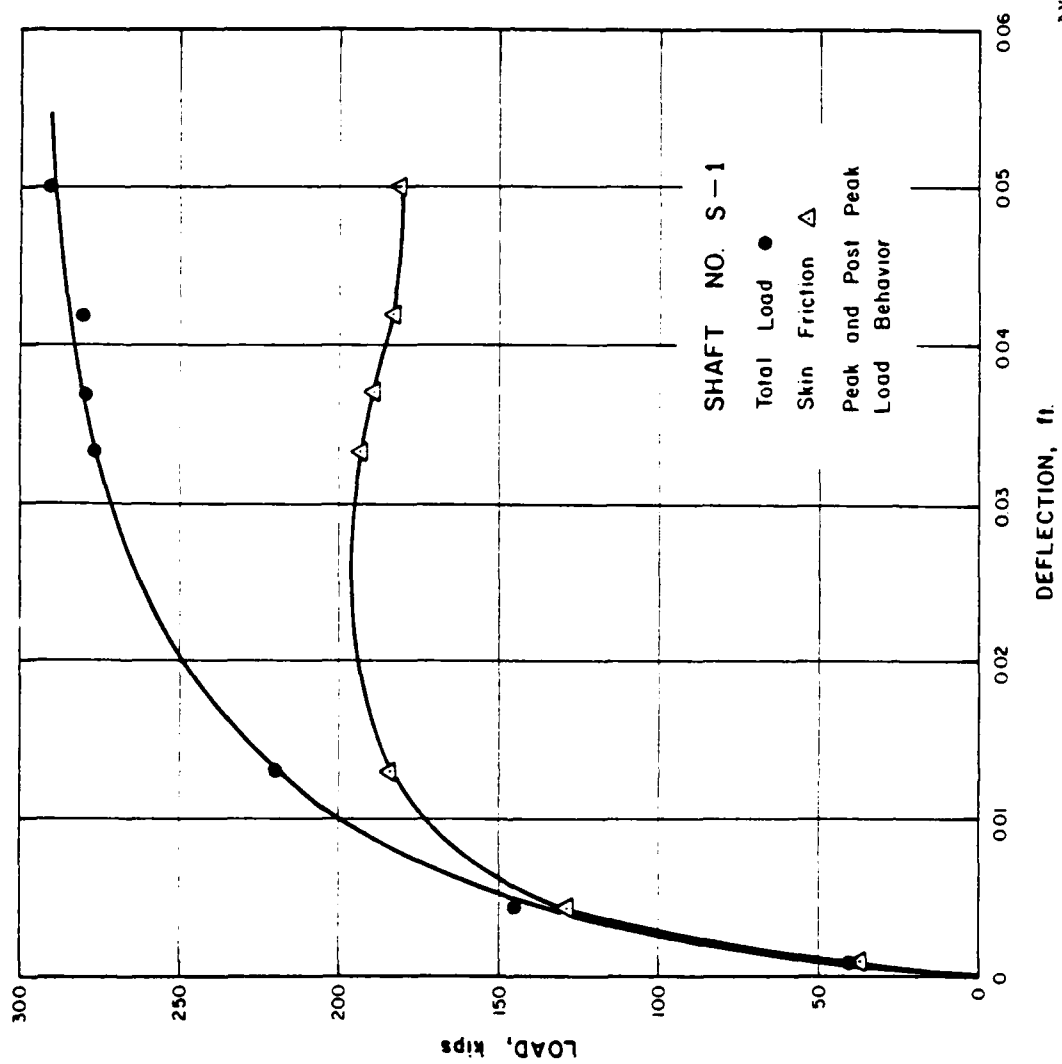
Fig. 17



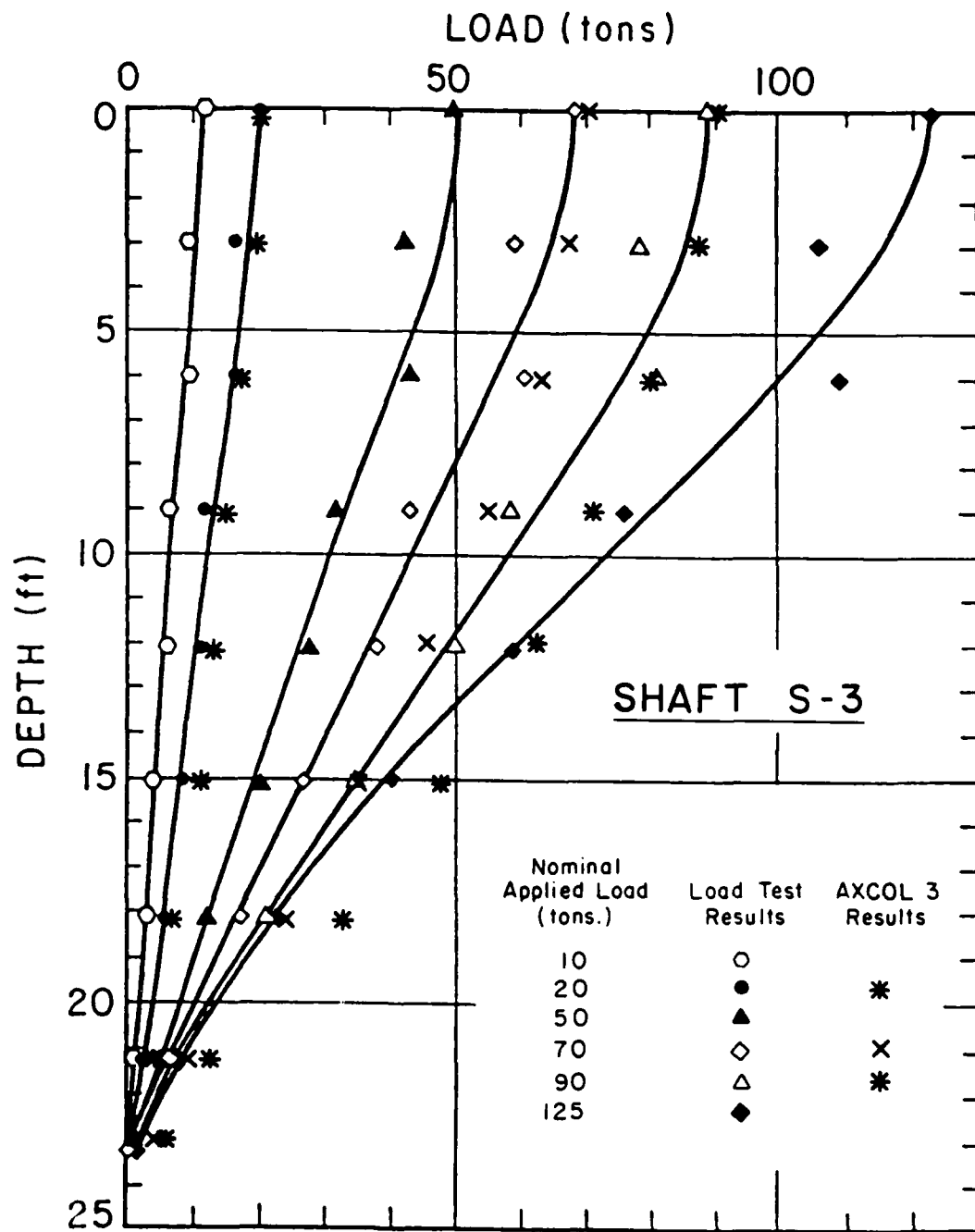
Load Distribution Curves  
for S1T1 with AXCOL 3  
Results

Fig. 18

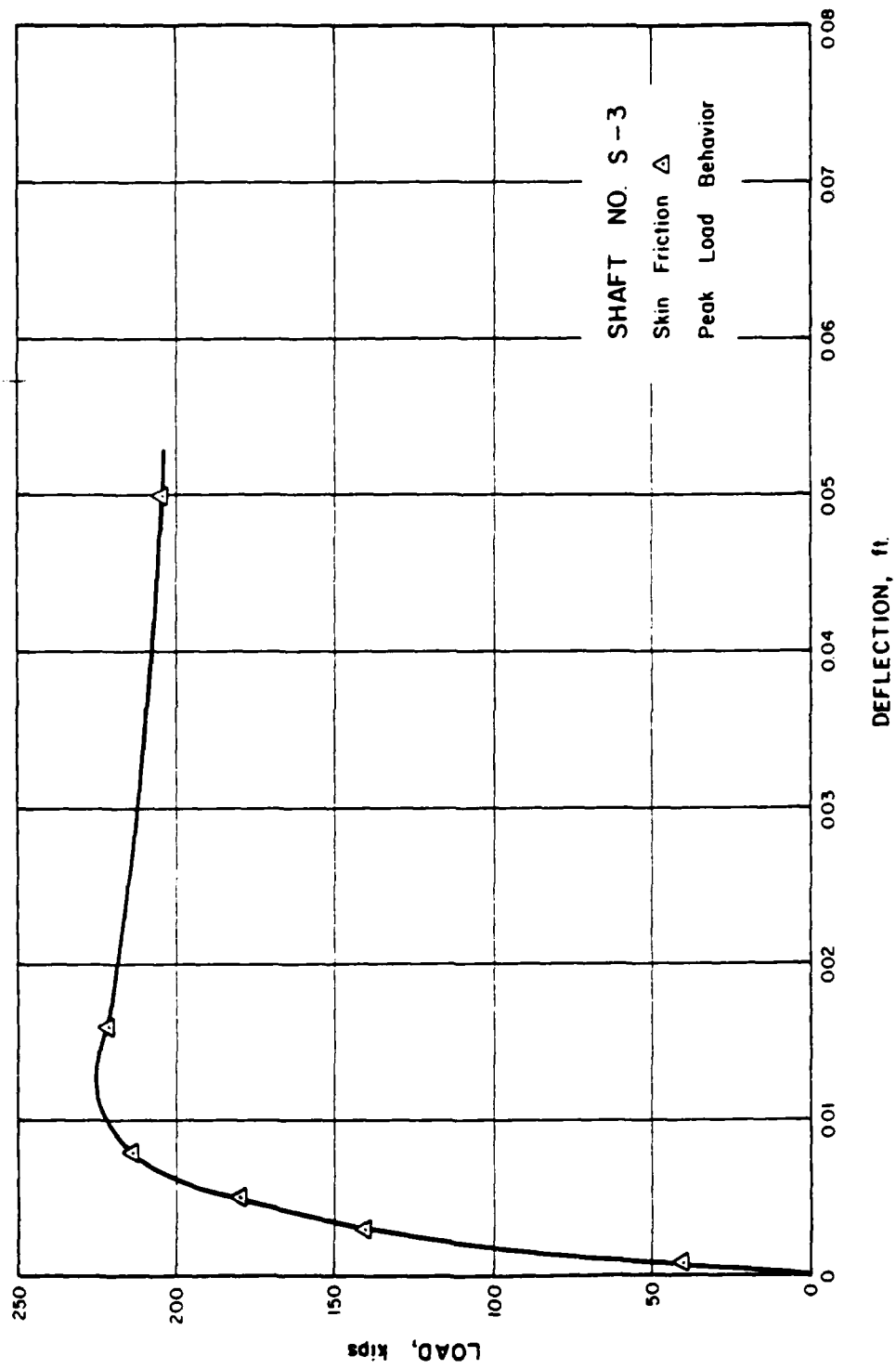




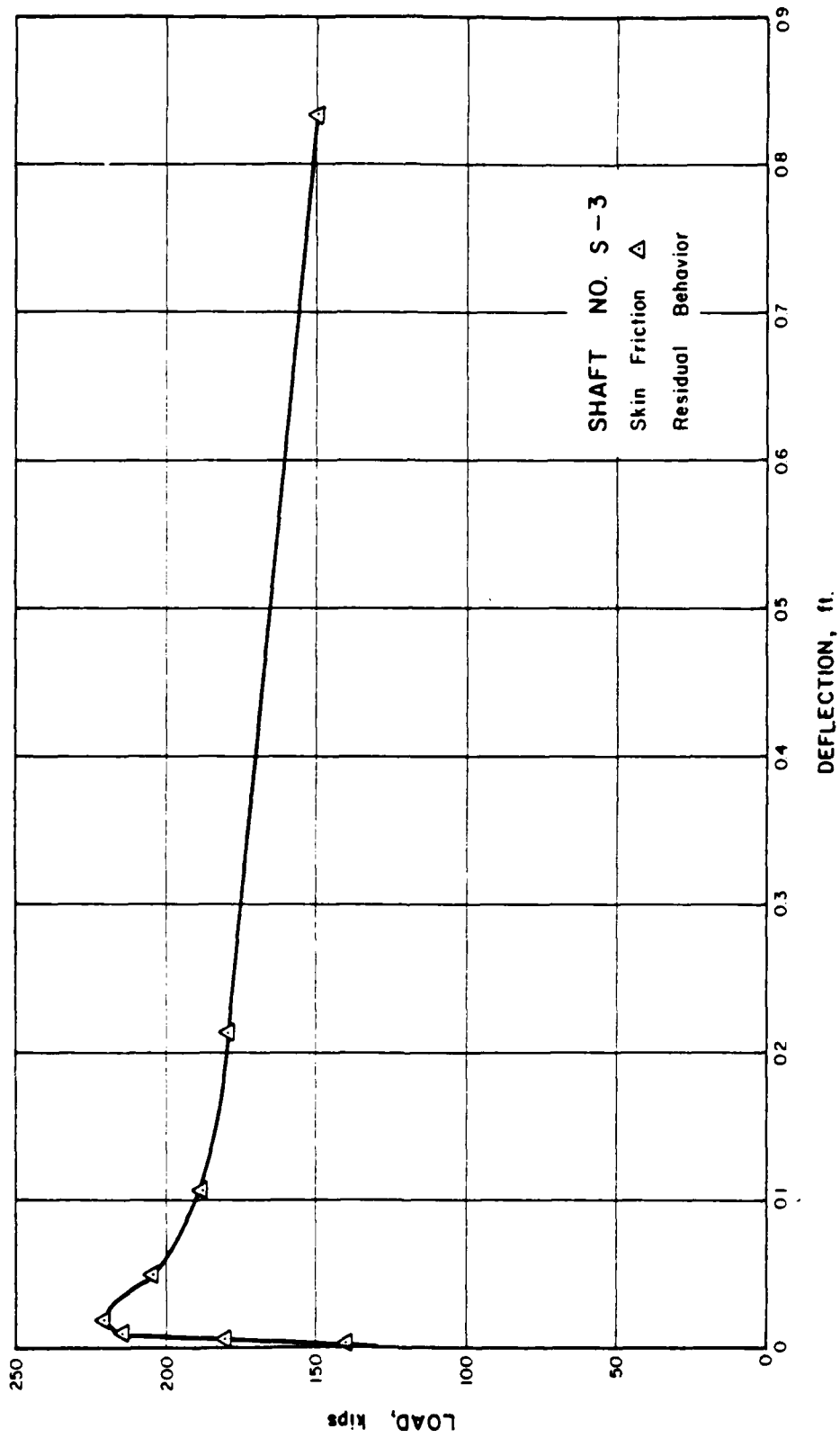
AXCOL Analyses for S-1  
FIG. 19



Load Distribution Curves for  
Quick Load Phase of S3T1L1  
with AXCOL 3 Results  
Fig. 20



AXCOL Analyses for S-3  
(Peak Load Behavior)  
FIG. 21(a)



AXCOL Analyses for S-3  
(Residual Behavior)  
FIG. 21(b)

APPENDIX A  
FIELD AND LABORATORY TEST RESULTS

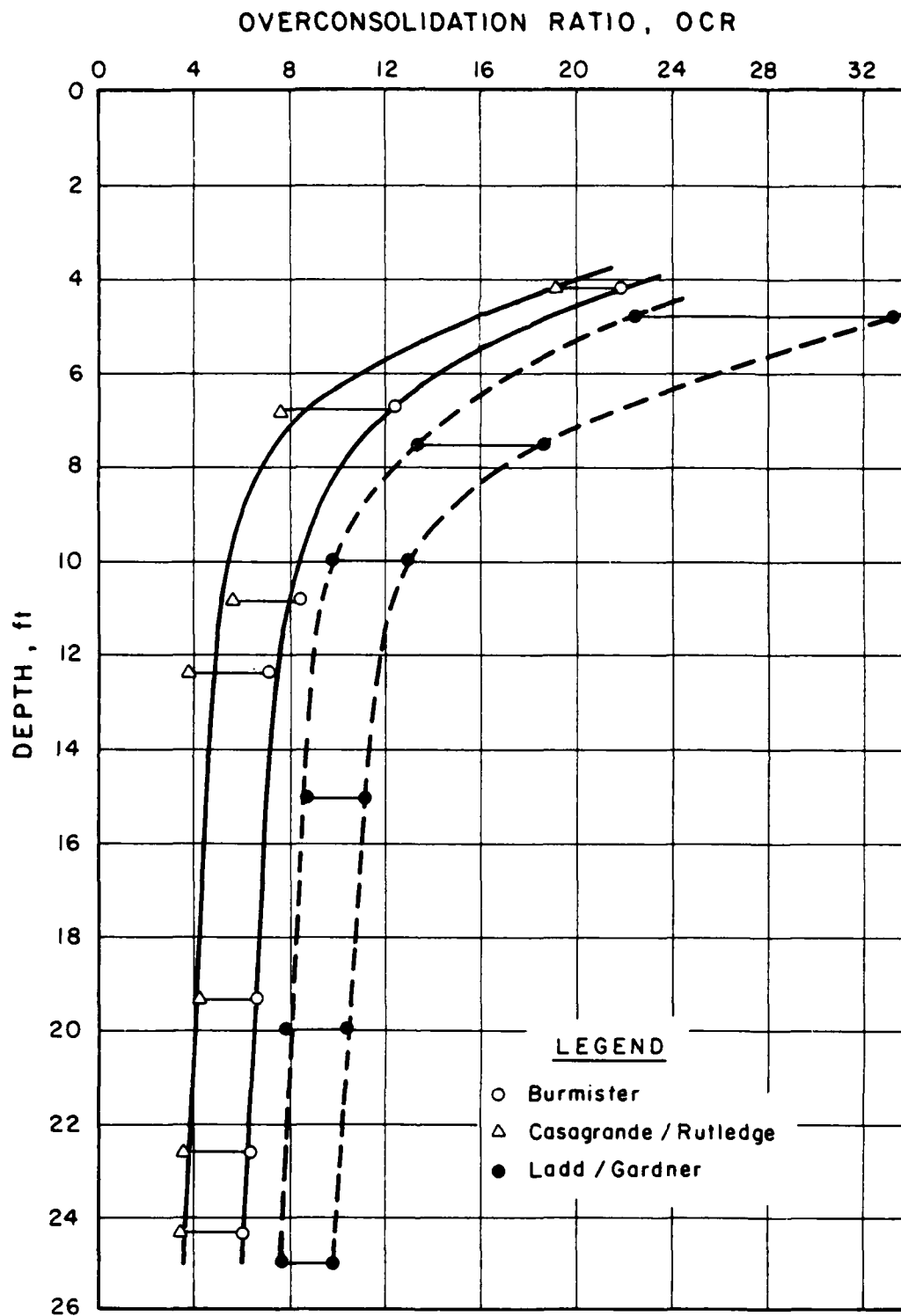


FIGURE A-1. OVERCONSOLIDATION RATIO INTERPRETATION FROM CONSOLIDATION AND UU TESTS

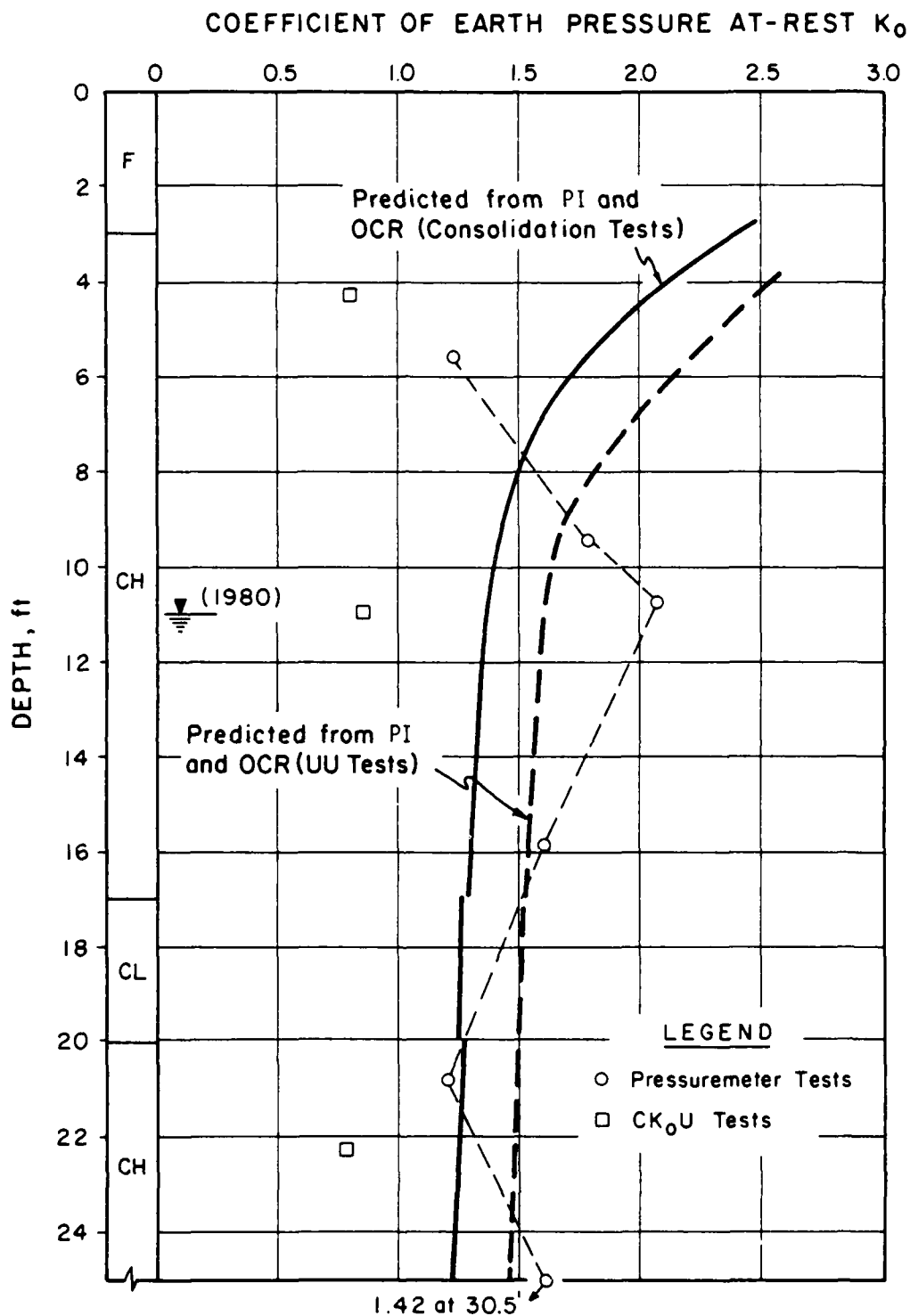


FIGURE A-2. COEFFICIENT OF EARTH PRESSURE AT-REST  
INTERPRETATION FROM  
LABORATORY AND PRESSUREMETER TESTS

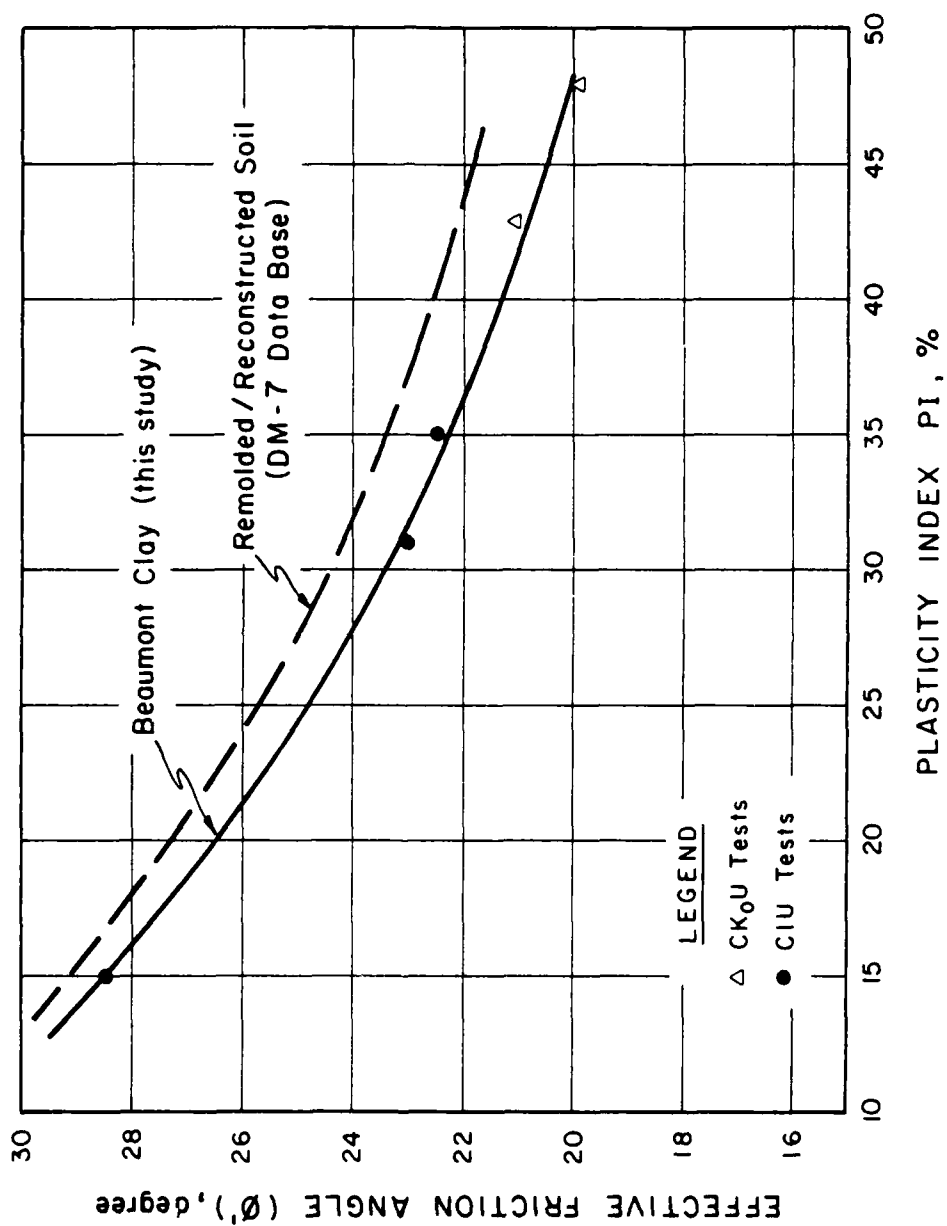


FIGURE A-3. EFFECTIVE FRICTION ANGLE VS. PLASTICITY INDEX



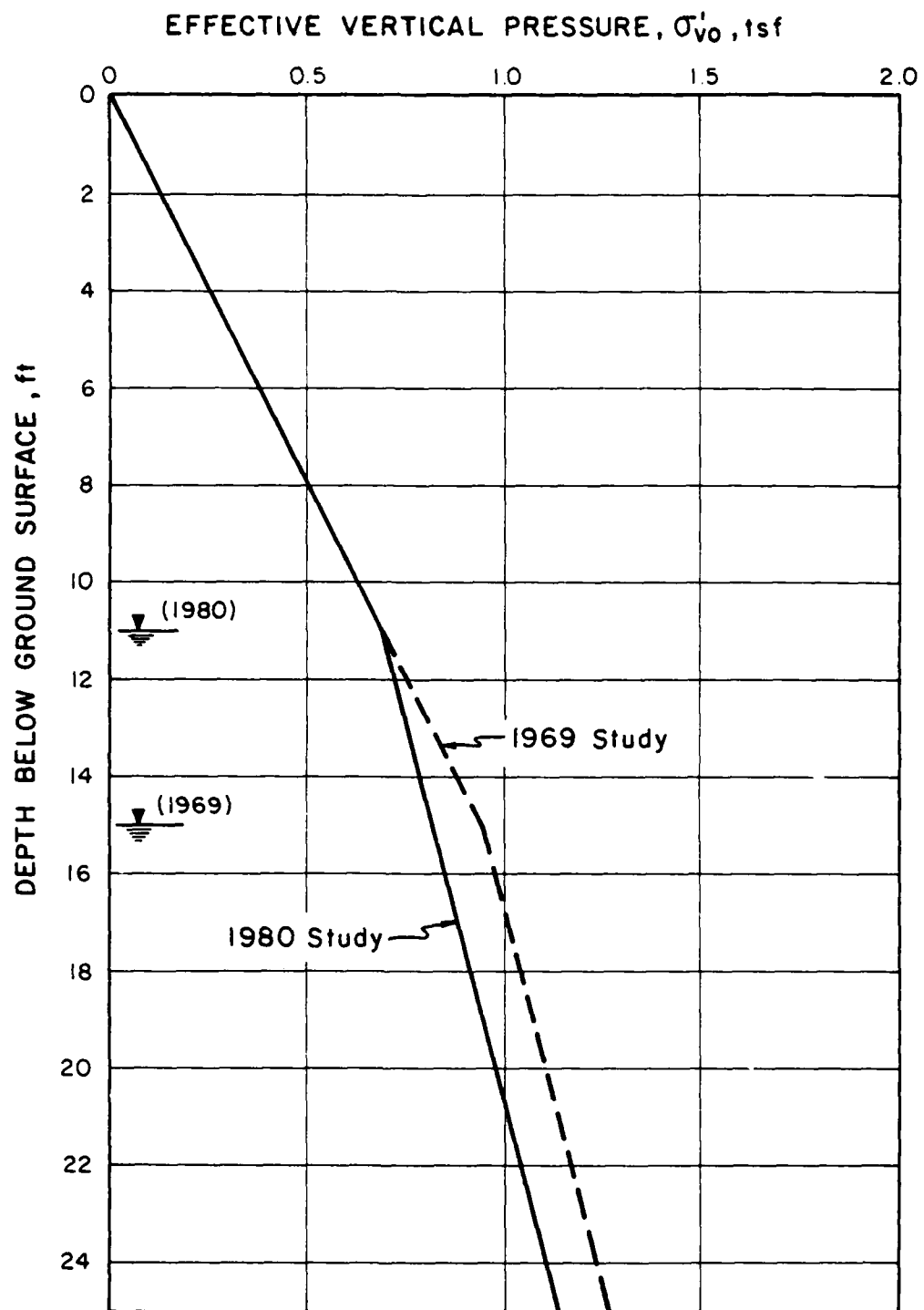


FIGURE A-4. EFFECTIVE VERTICAL PRESSURE FOR  
GROUNDWATER LEVELS  
DURING 1969 AND 1980 STUDIES

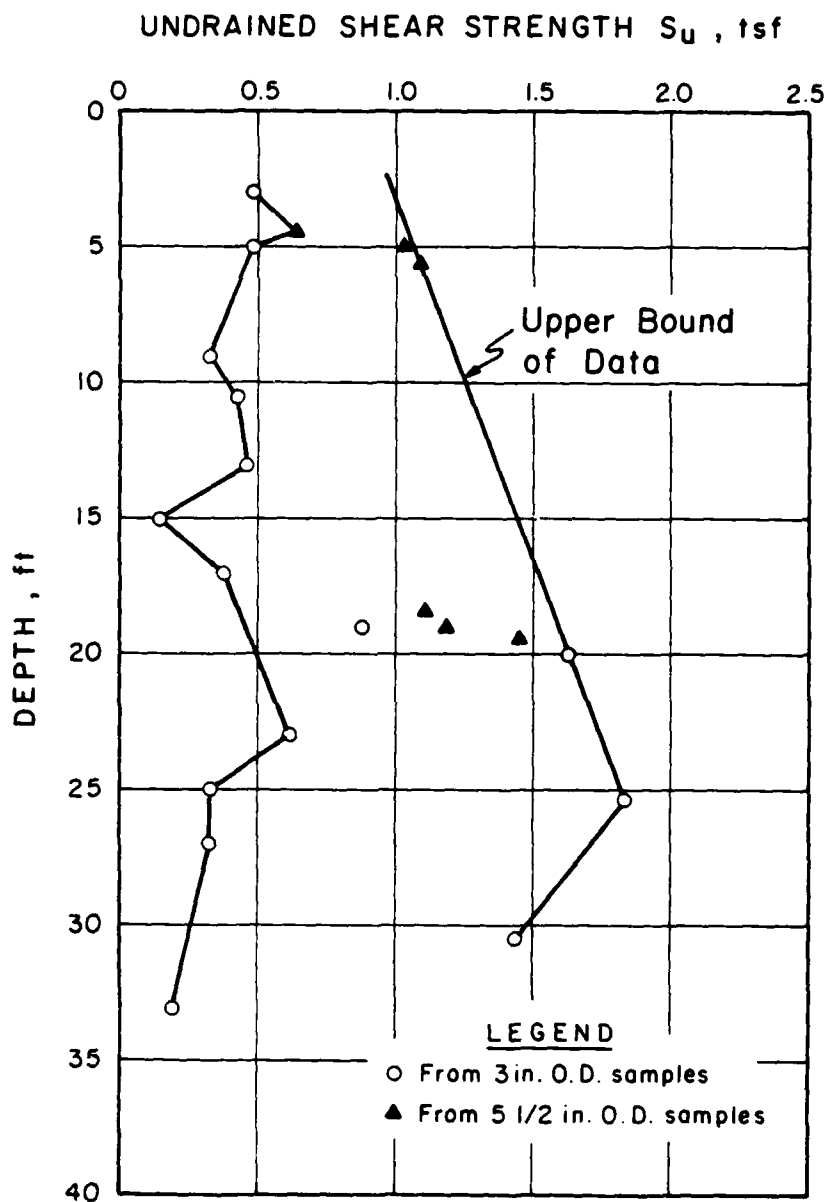


FIGURE A-5. UNCONSOLIDATED UNDRAINED TRIAXIAL STRENGTH TEST RESULTS

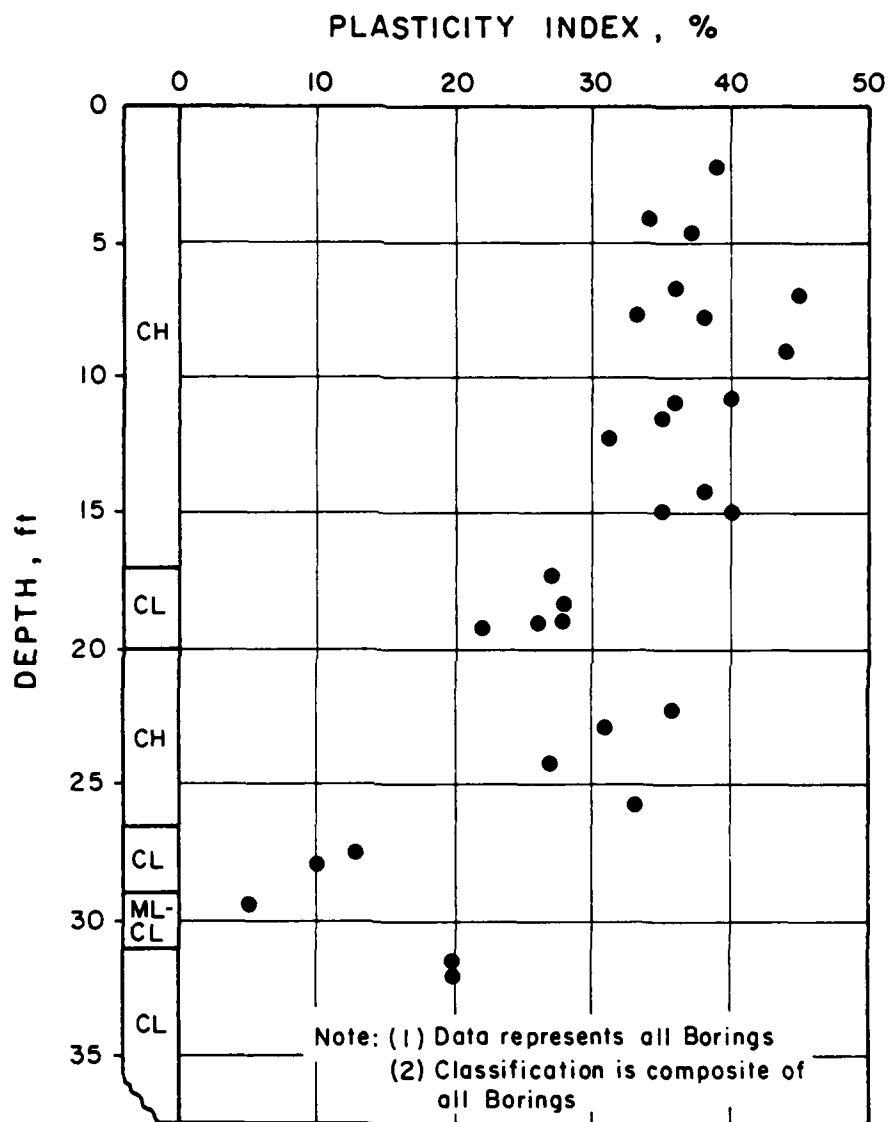


FIGURE A-6. PLASTICITY INDEX AND CLASSIFICATION VS. DEPTH BELOW GROUND SURFACE

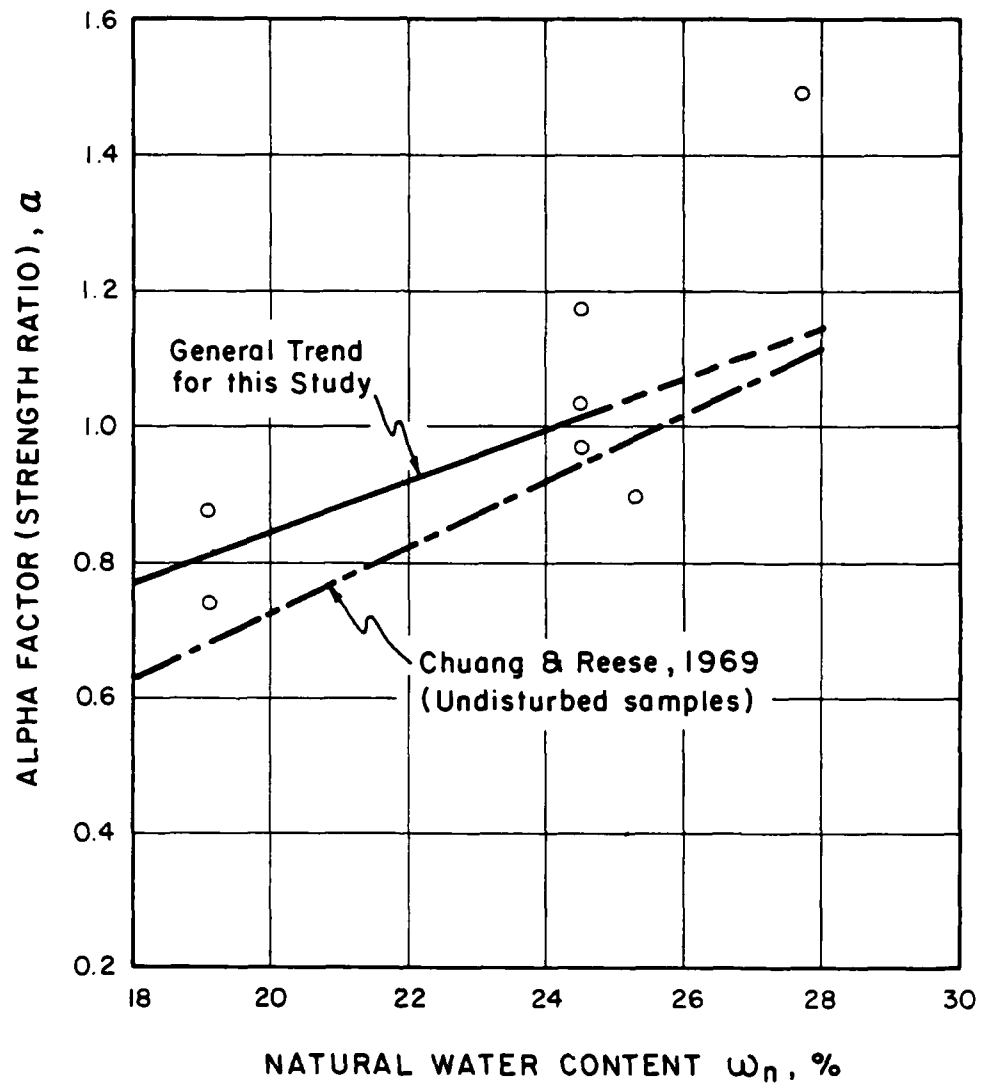


FIGURE A-7. NATURAL WATER CONTENT FROM INTERFACE  
SHEAR TESTS VS. STRENGTH RATIO  
(ALPHA FACTOR)

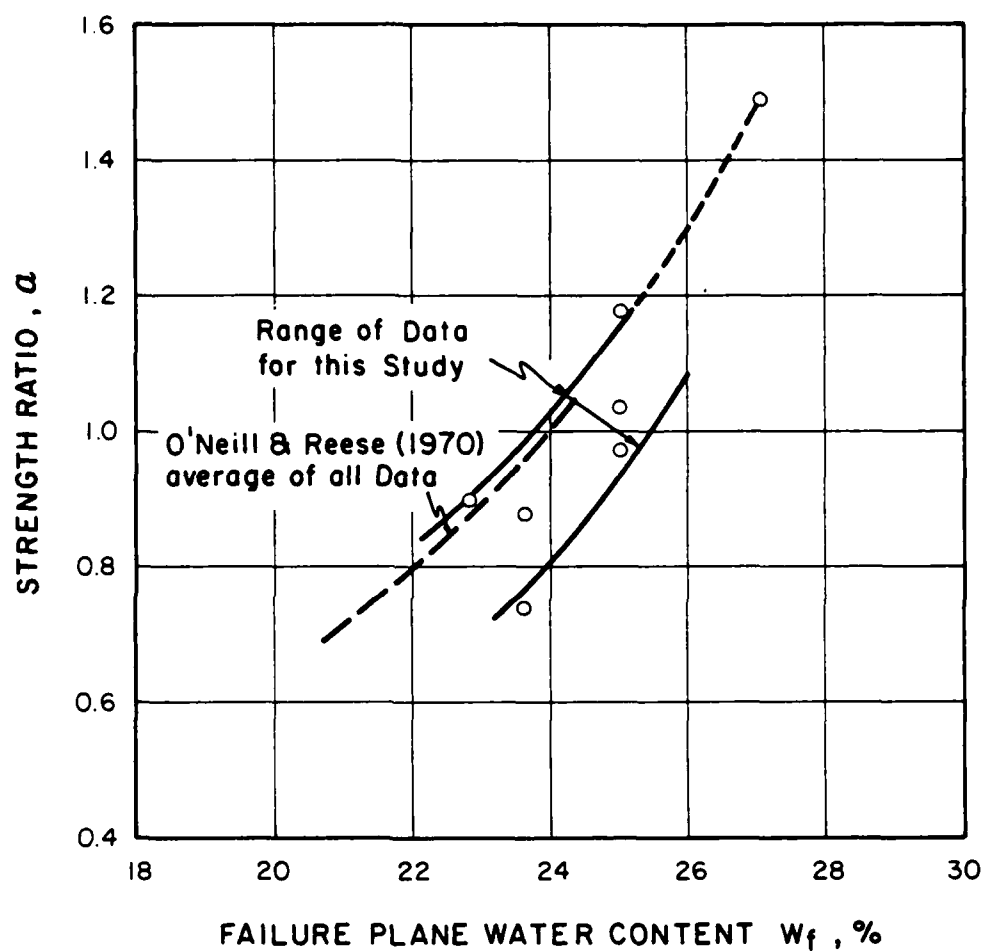


FIGURE A-8. FAILURE PLANE WATER CONTENT INTERFACE  
SHEAR TEST VS. STRENGTH RATIO  
(ALPHA FACTOR)

DEPTH, FT	STRATUM NO. & SOIL CLASSIFI.	W %		PI %		LL %		$\gamma_d$ pcf	
		$\bar{x}$	$\sigma$	$\bar{x}$	$\sigma$	$\bar{x}$	$\sigma$	$\bar{x}$	$\sigma$
5									
10	(1) CH	25.4	2.3	37	4	60	5	99.9 (125)	4.1
(1980)									
15									
(1969)									
20	(2) CL	23.5	1.3	26	3	47	6	102.9* (127)	2.2
25	(3) CH	23.7	4.9	32	4	58	8	101.0 (125)	7.3
30	(4) CL	23.2	2.6	12*	-	25*	-	99.9 (123)	6.7
	(5) CL-ML	19.5	2.6	5*	-	21*	-	102.1* (122)	4.5
35	(6) CL	15.2*	-	20*	-	33*	-	108.1* (125)	-

\* REPRESENTS ONLY TWO TESTS

( ) REPRESENTS ASSUMED AVERAGE TOTAL UNIT WEIGHT OF SOIL

FIGURE A-9. IDEALIZED STRATIGRAPHY AND  
SELECTED SOIL PROPERTIES

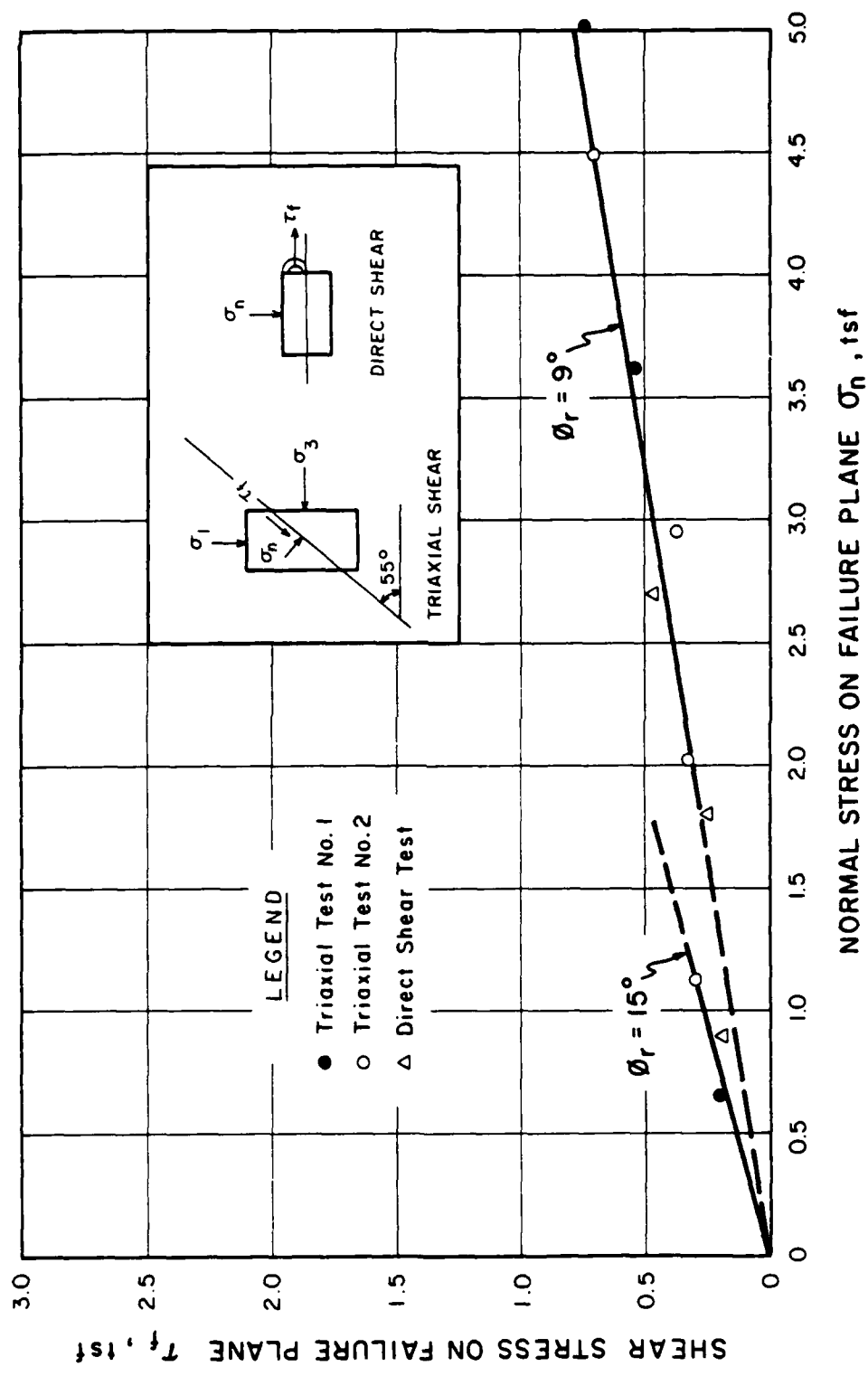


FIGURE A-10. NORMAL STRESS VS. SHEAR STRESS FROM RESIDUAL STRENGTH TESTS

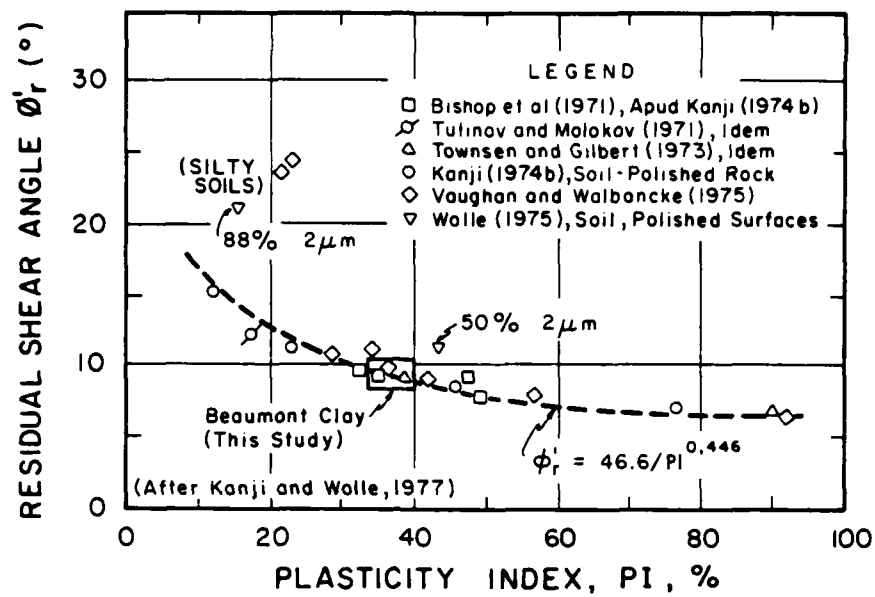


FIGURE A-11(a). DRAINED RESIDUAL SHEAR ANGLE VS. PLASTICITY INDEX

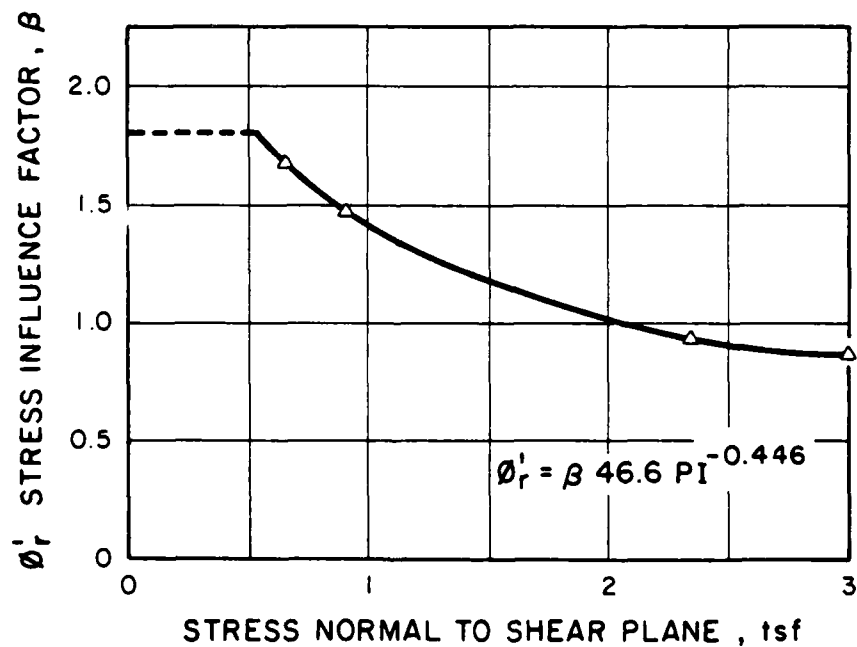


FIGURE A-11(b). INFLUENCE OF NORMAL STRESS ON RESIDUAL STRENGTH



APPENDIX B  
LOAD DEFORMATION ANALYSES - RAW DATA

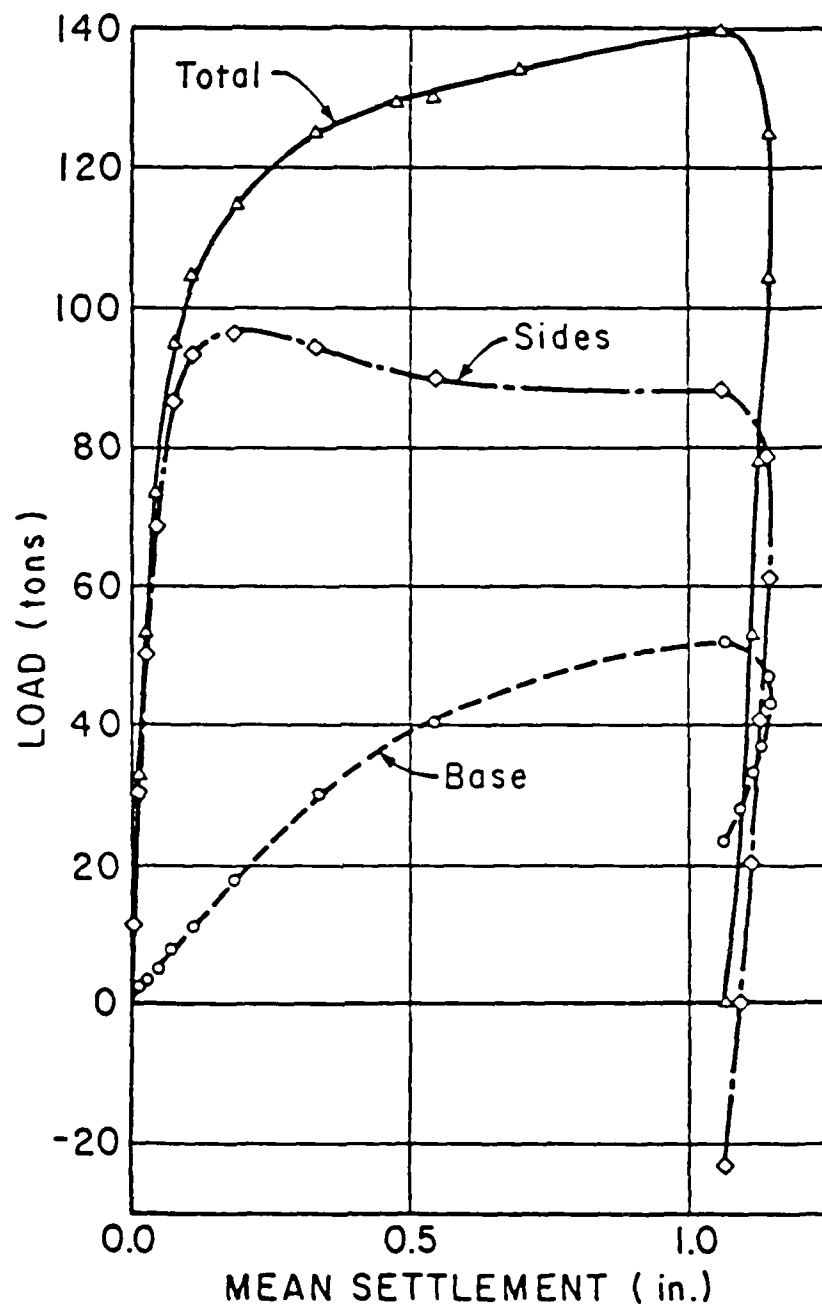


Fig. B-1: Load-Settlement Curves for S1T1  
(From O'Neill and Reese, 1970)

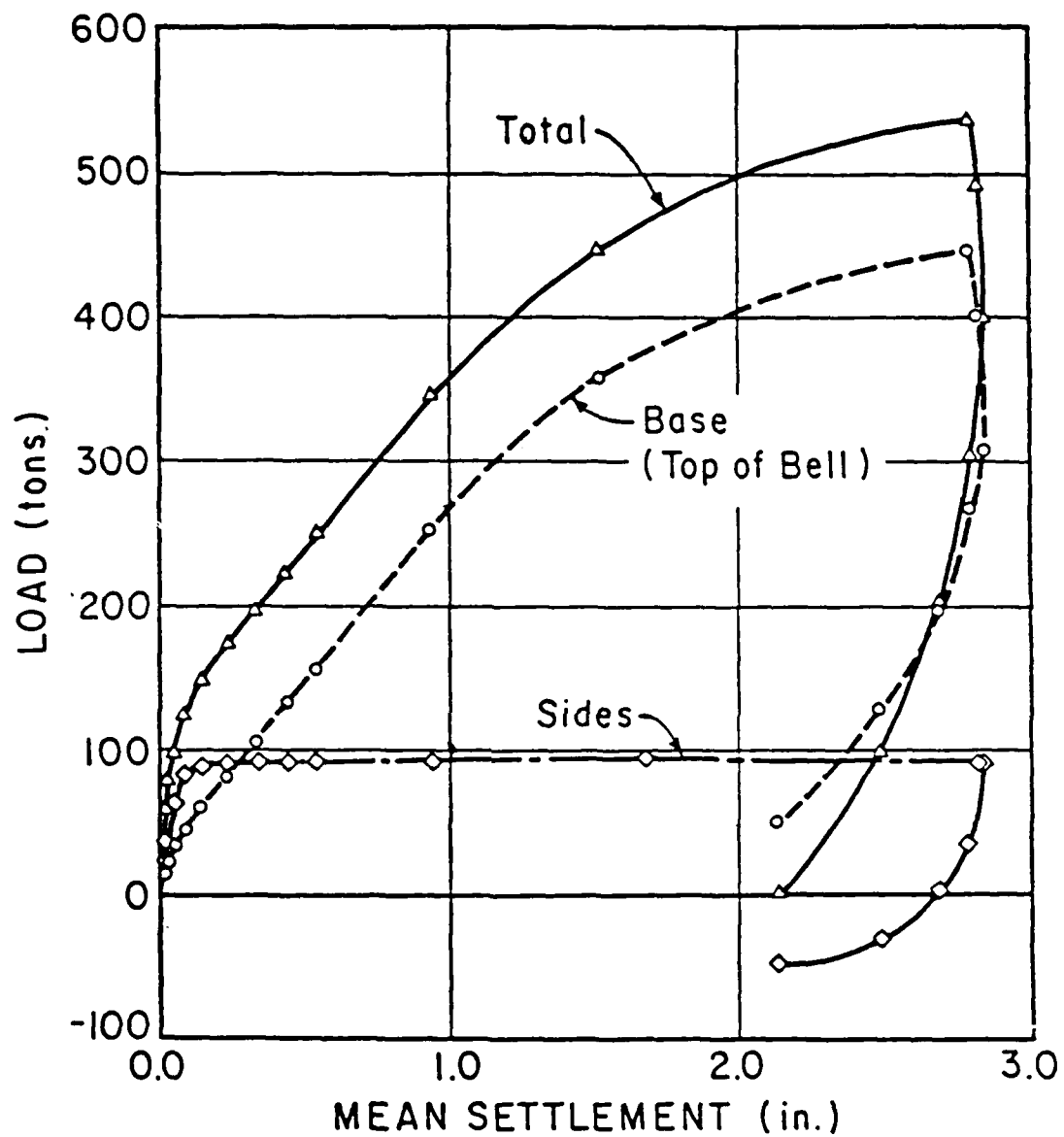


Fig. B-2: Load-Settlement Curves for S2T1  
(From O'Neill and Reese, 1970)

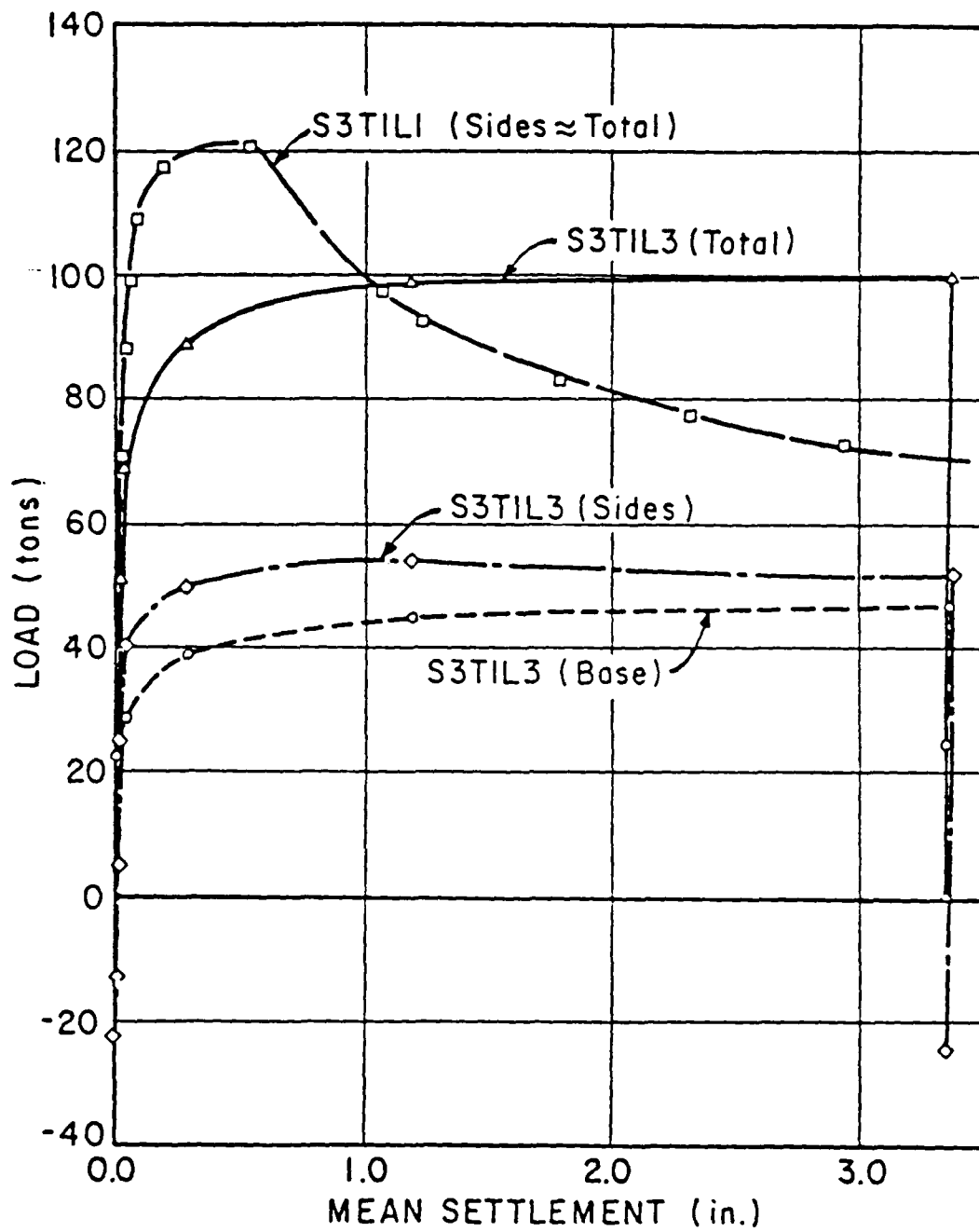


Fig. B-3: Load-Settlement Curves for S3T1  
(From O'Neill and Reese, 1970)

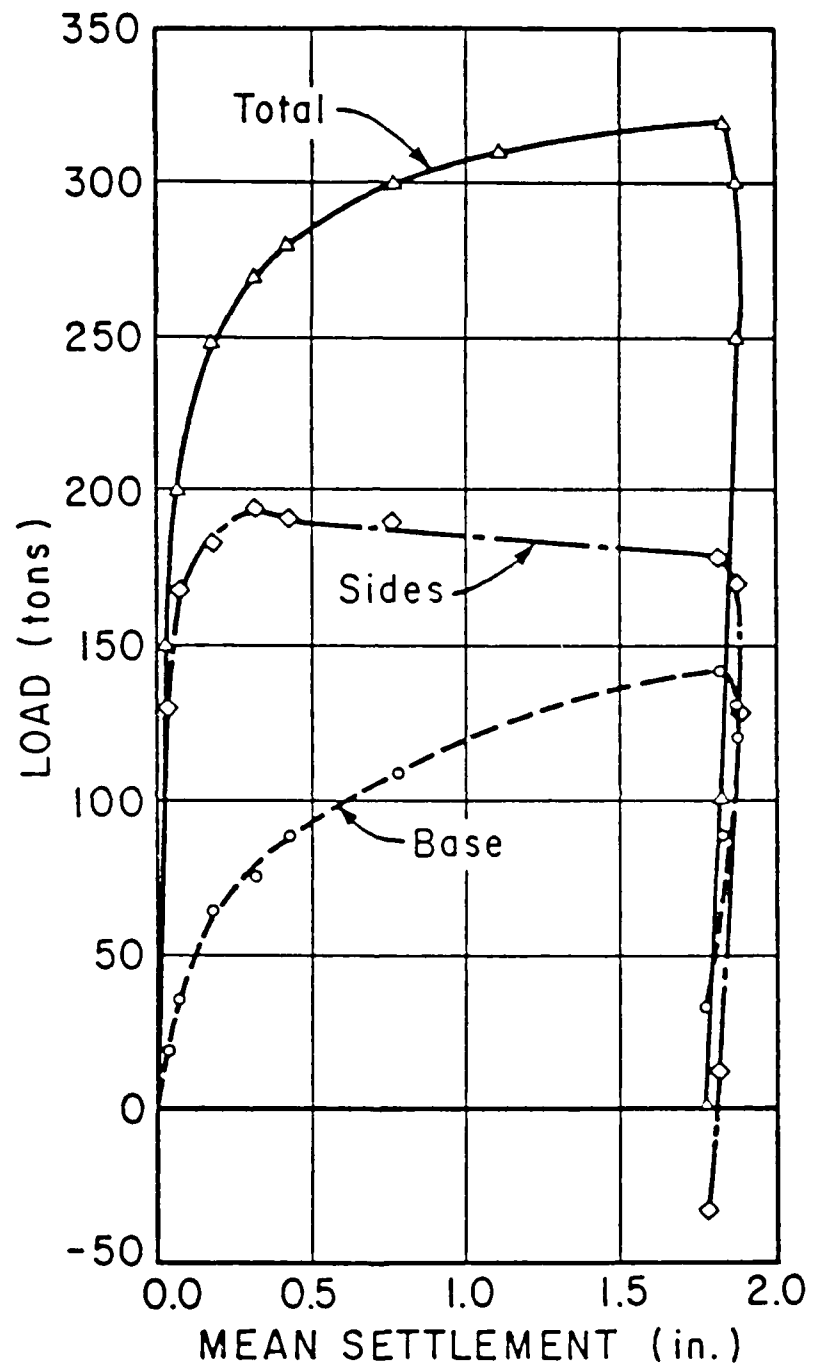


Fig. B-4: Load-Settlement Curves for S4T1  
(From O'Neill and Reese, 1970)

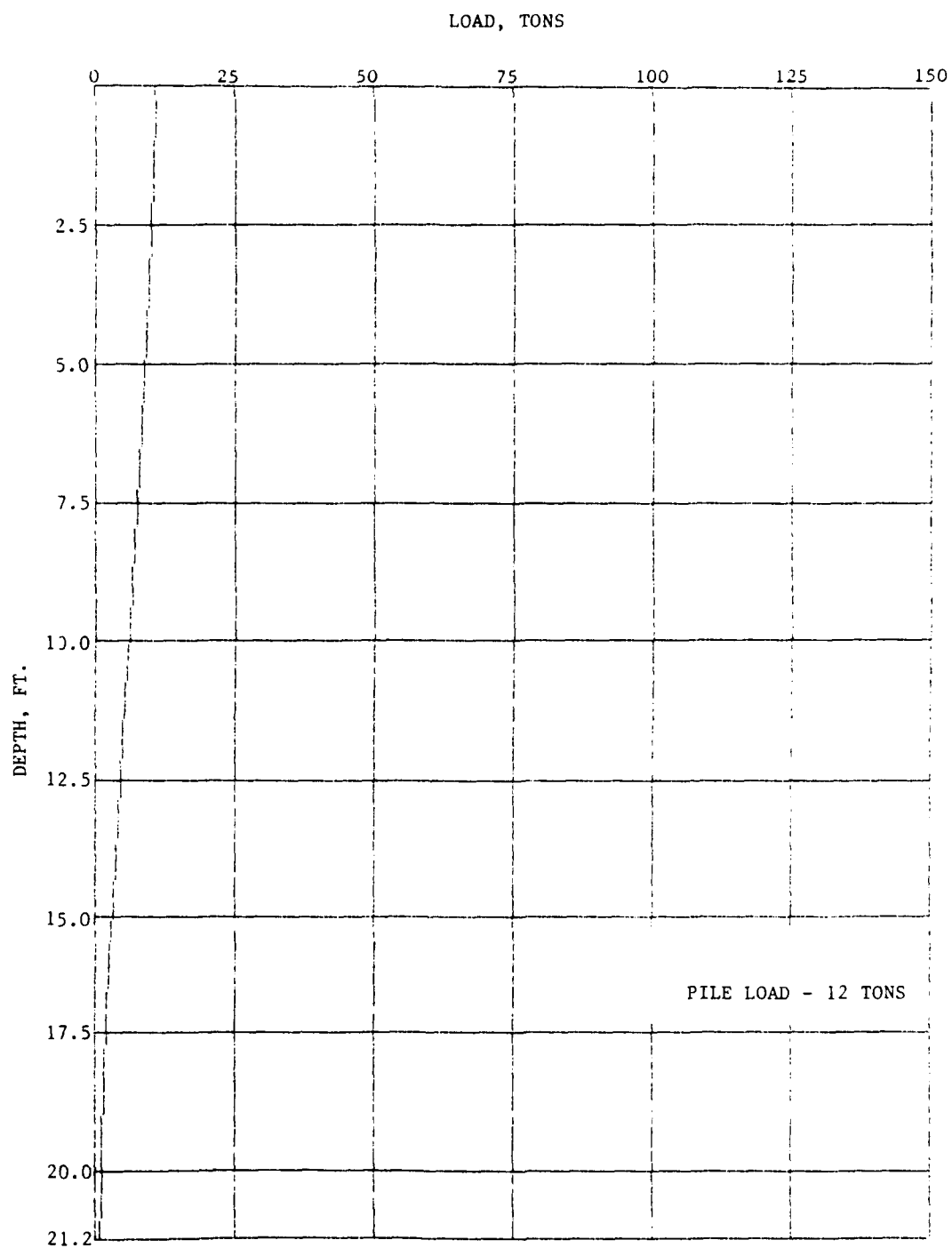


Fig. B-5 LOAD DISTRIBUTION CURVE SHAFT TEST - S1T1

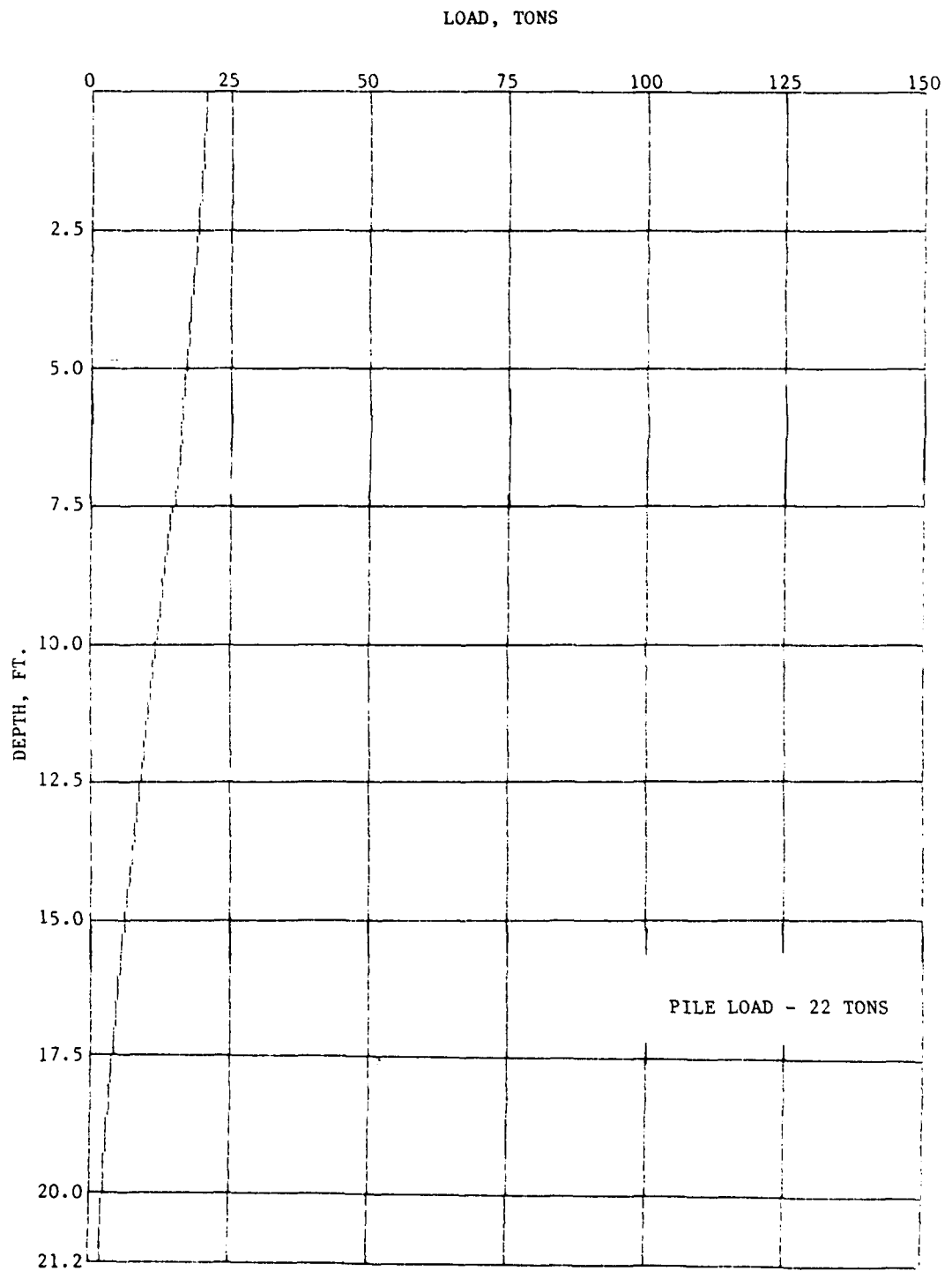


Fig. B-6      LOAD DISTRIBUTION CURVE SHAFT TEST - SJ71

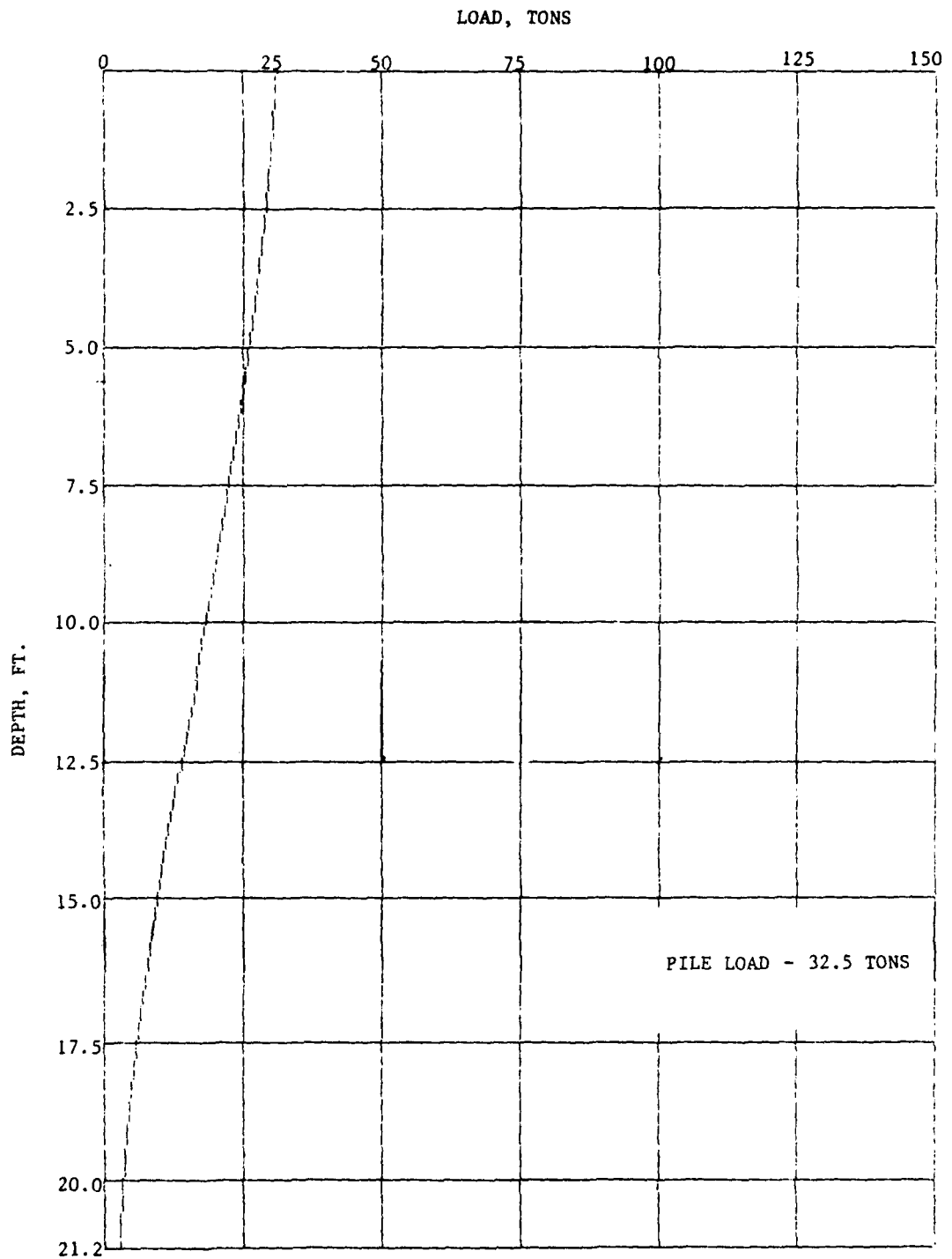


Fig. B-7 LOAD DISTRIBUTION CURVE SHAFT TEST - S1T1



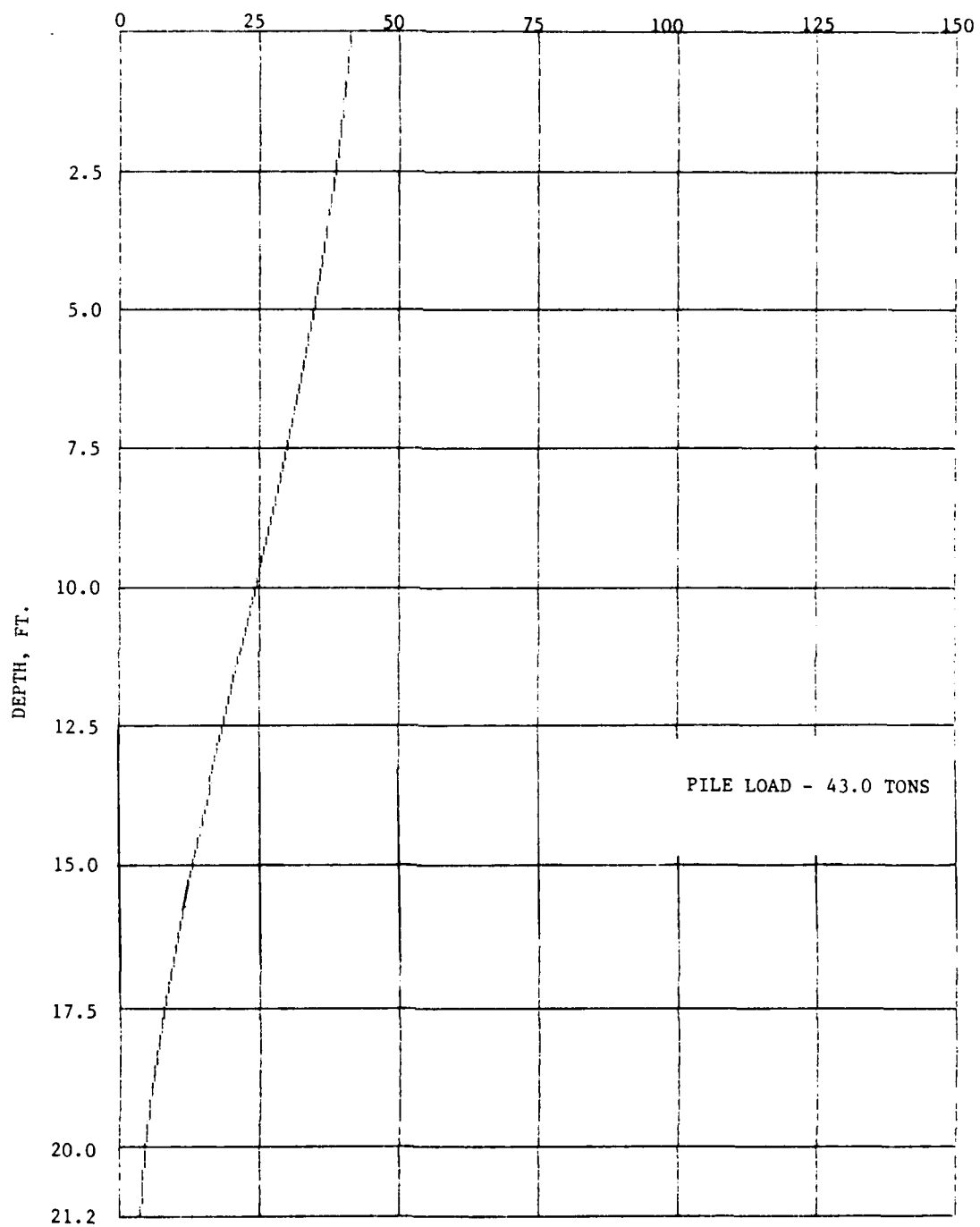


Fig. B-8 LOAD DISTRIBUTION CURVE SHAFT TEST - SIT1

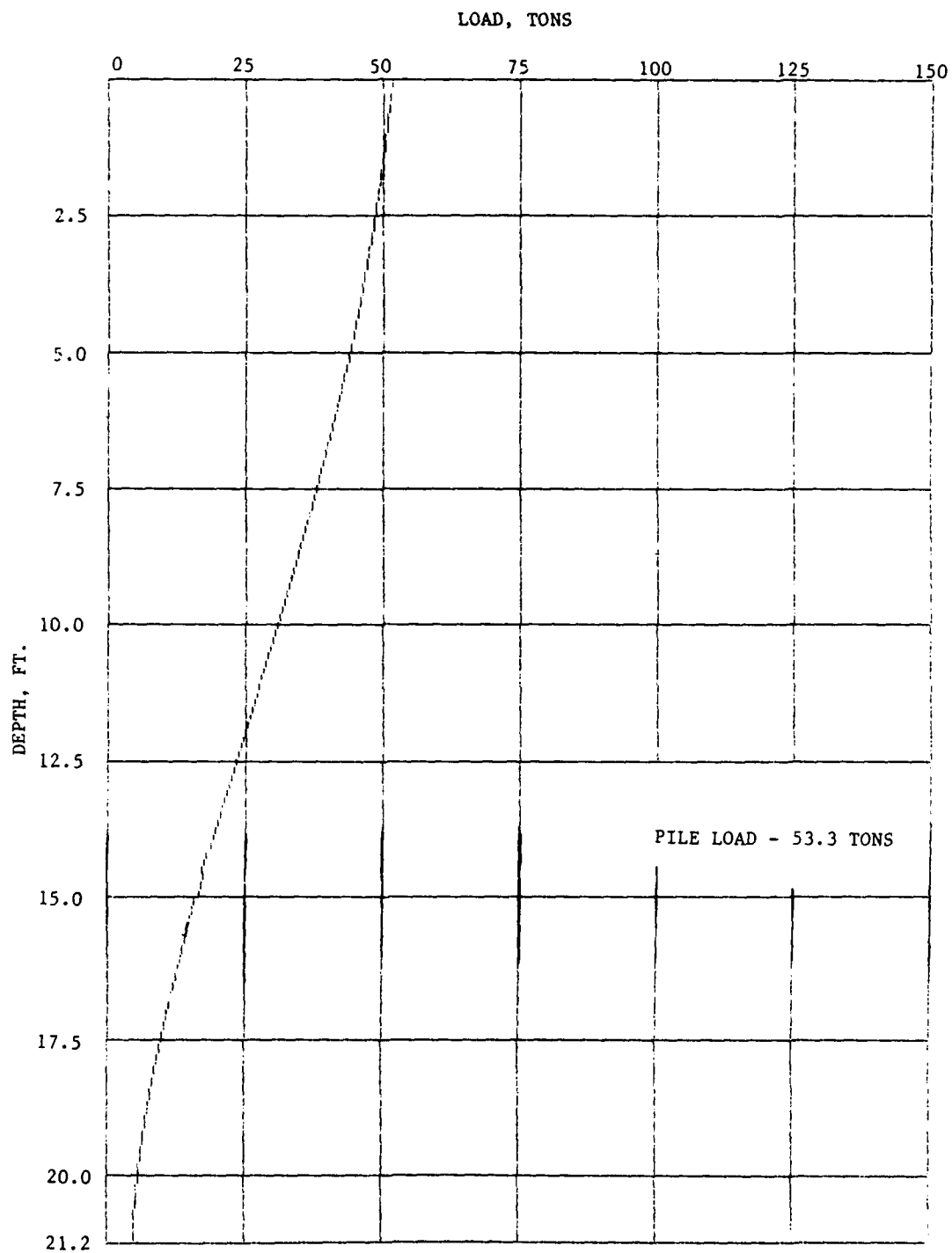


Fig. B-9 LOAD DISTRIBUTION CURVE SHAFT TEST - S1T1

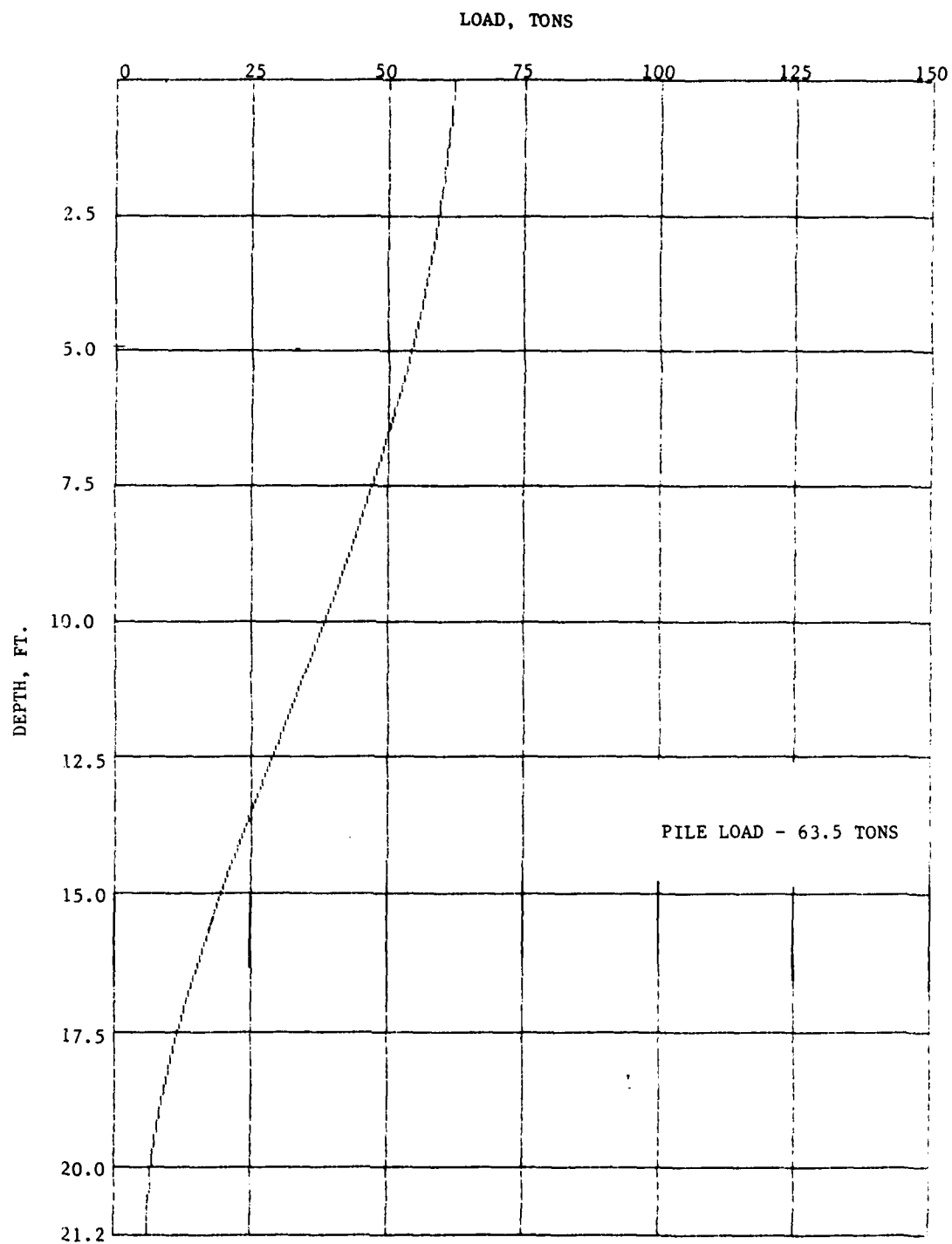


Fig. B- 10 LOAD DISTRIBUTION CURVE SHAFT TEST - S1T1

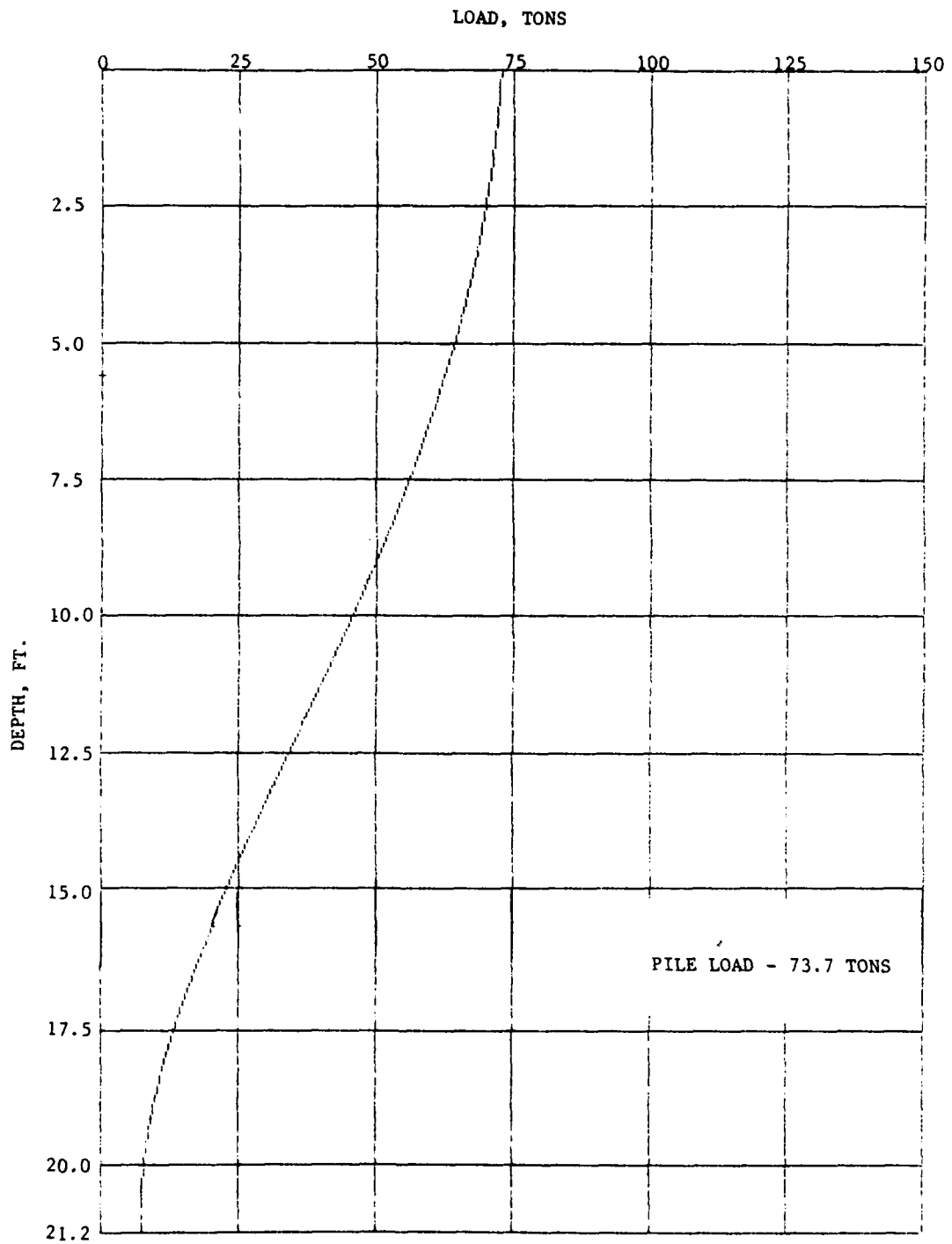


Fig. B-11 LOAD DISTRIBUTION CURVE SHAFT TEST - S1T1

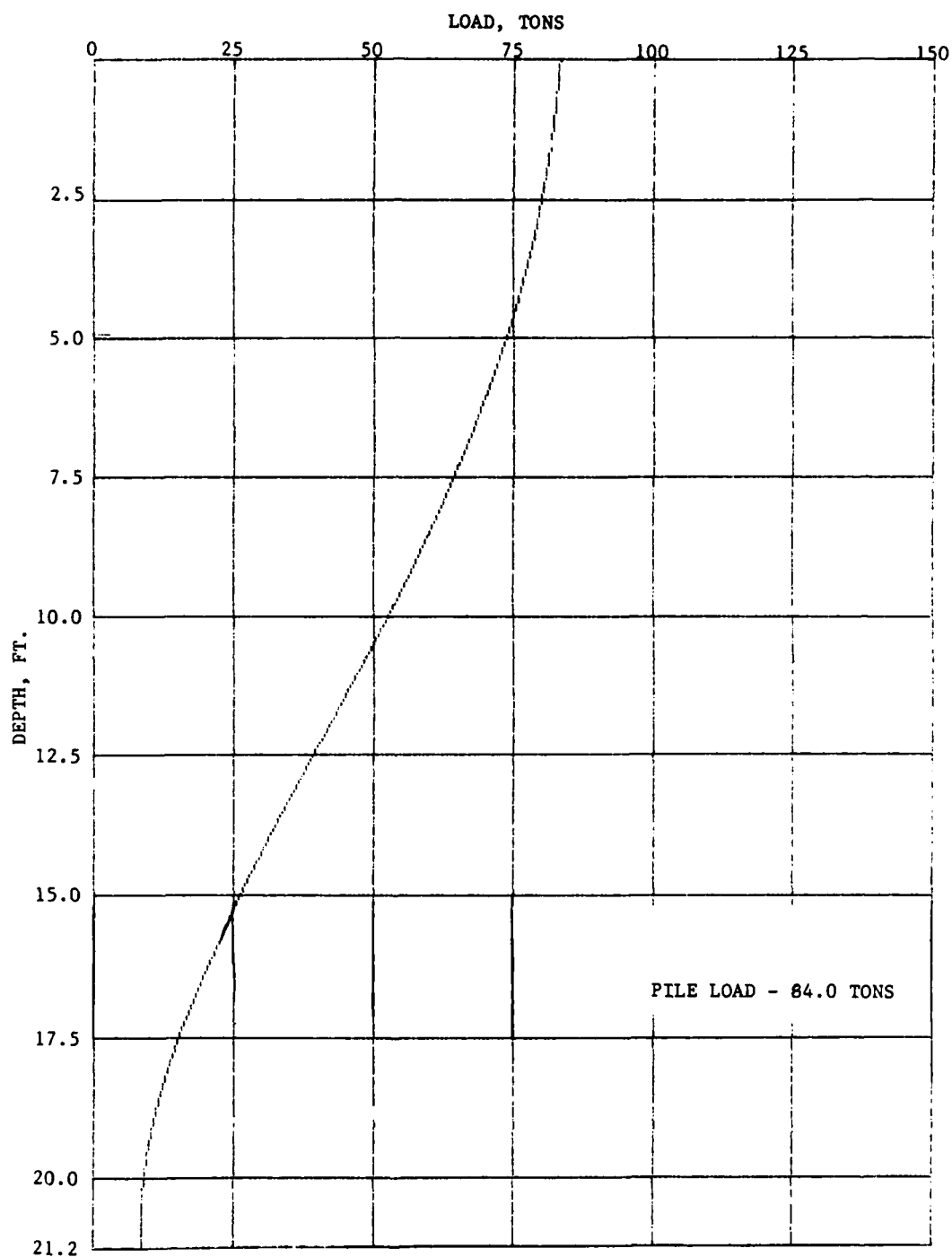


Fig. B-12 LOAD DISTRIBUTION CURVE SHAFT TEST - S1T1

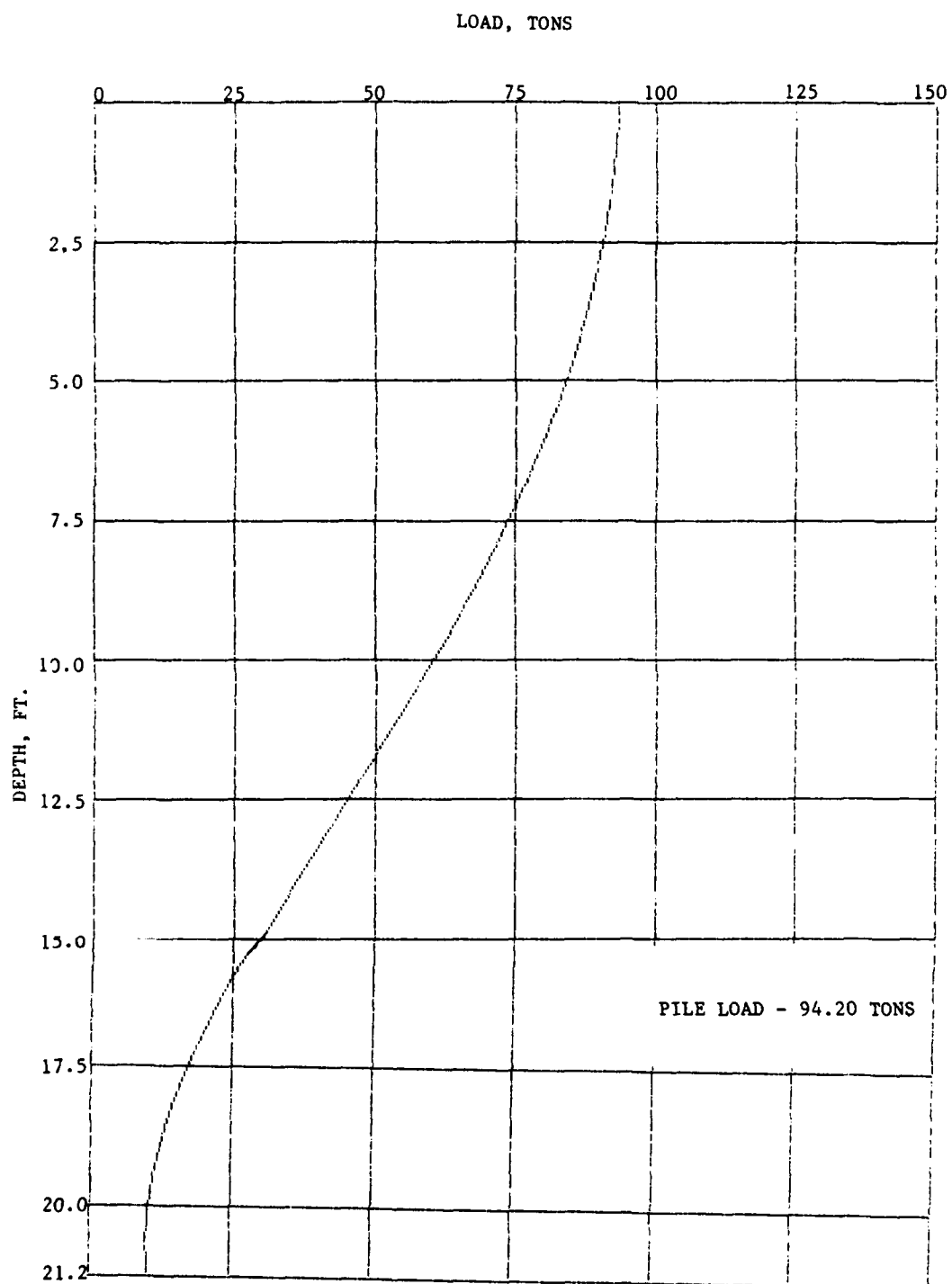


Fig. B-13 LOAD DISTRIBUTION CURVE SHAFT TEST - S1T1

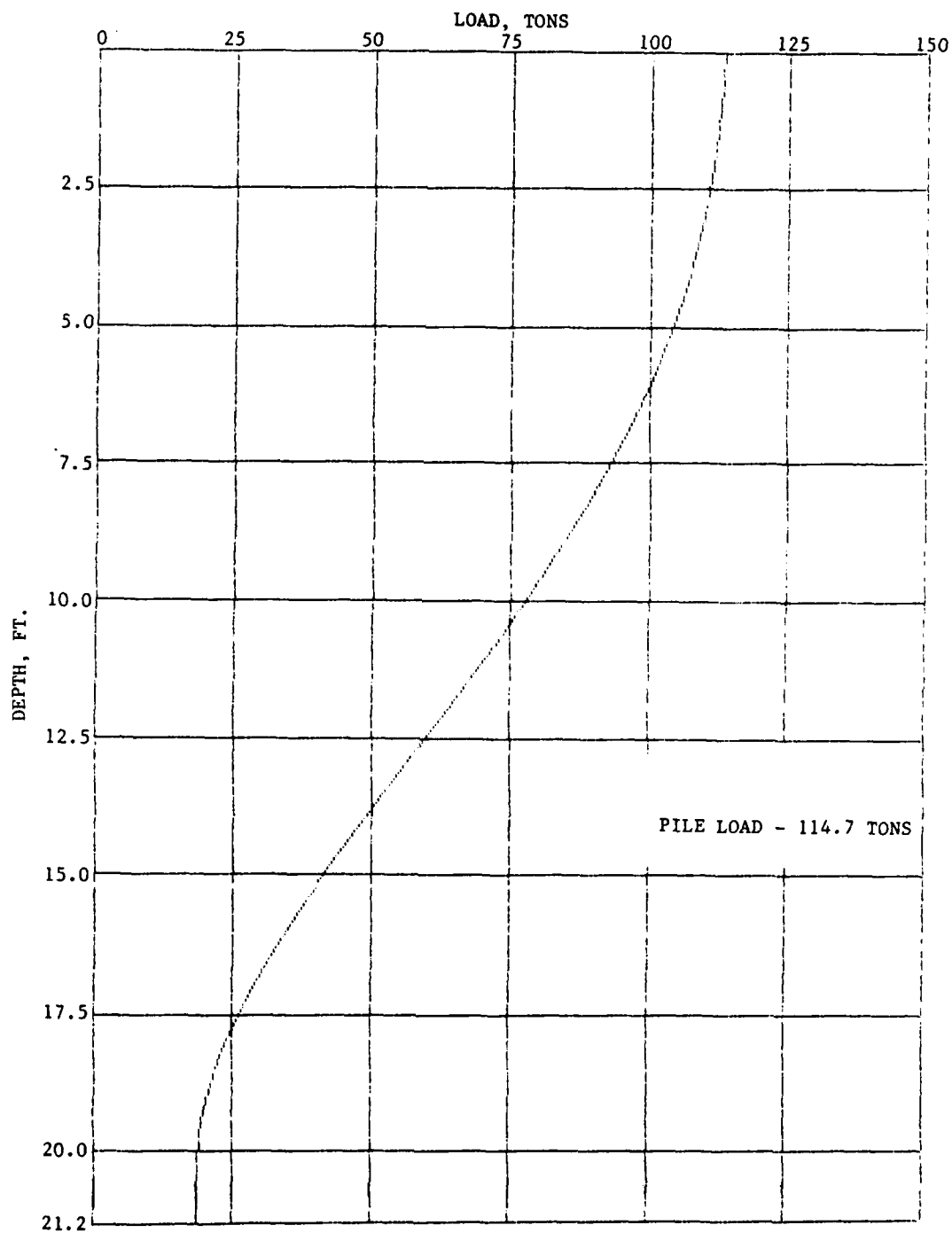


Fig. B-14 LOAD DISTRIBUTION CURVE SHAFT TEST S1T1

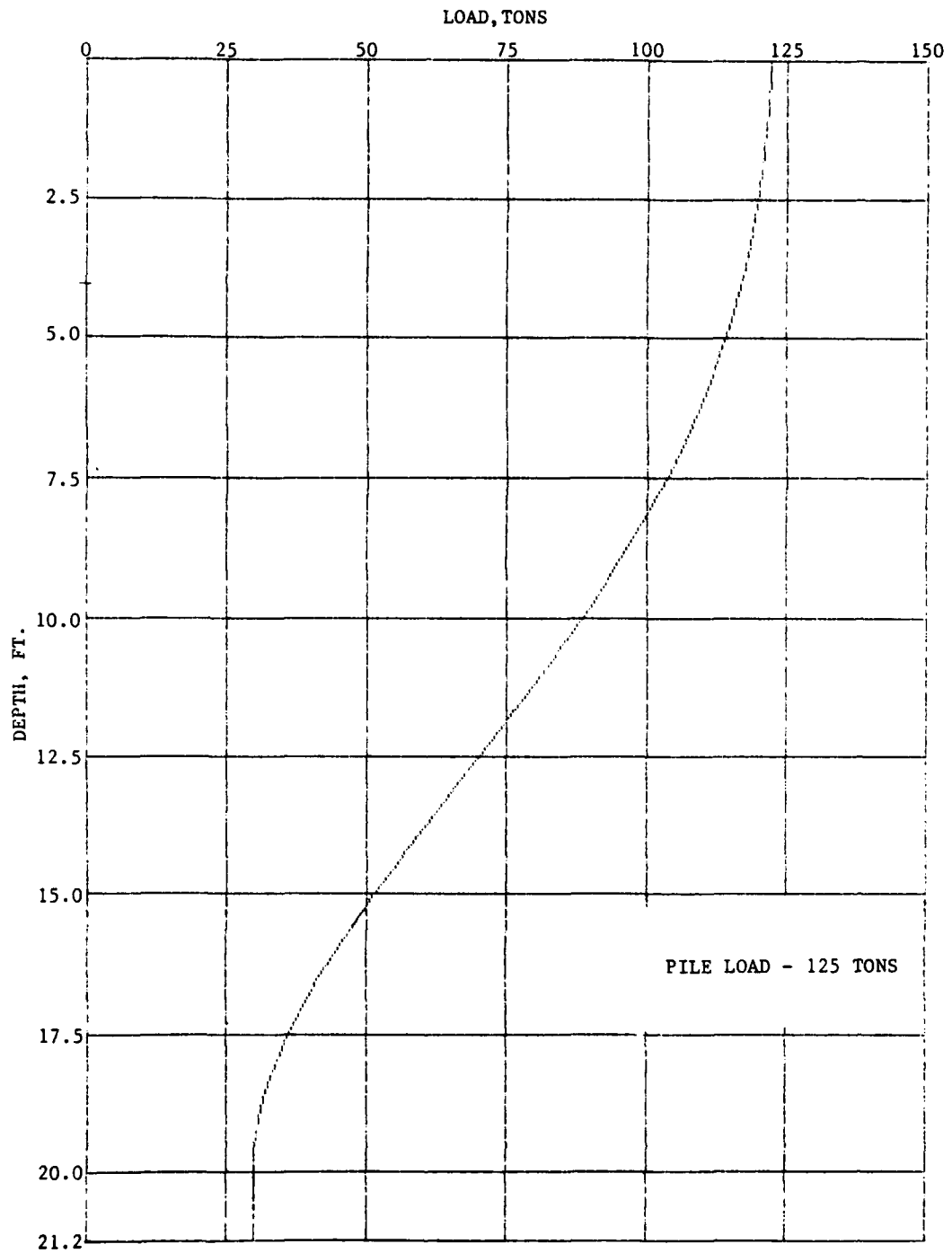


Fig. B-15 LOAD DISTRIBUTION CURVE SHAFT TEST - S1T1



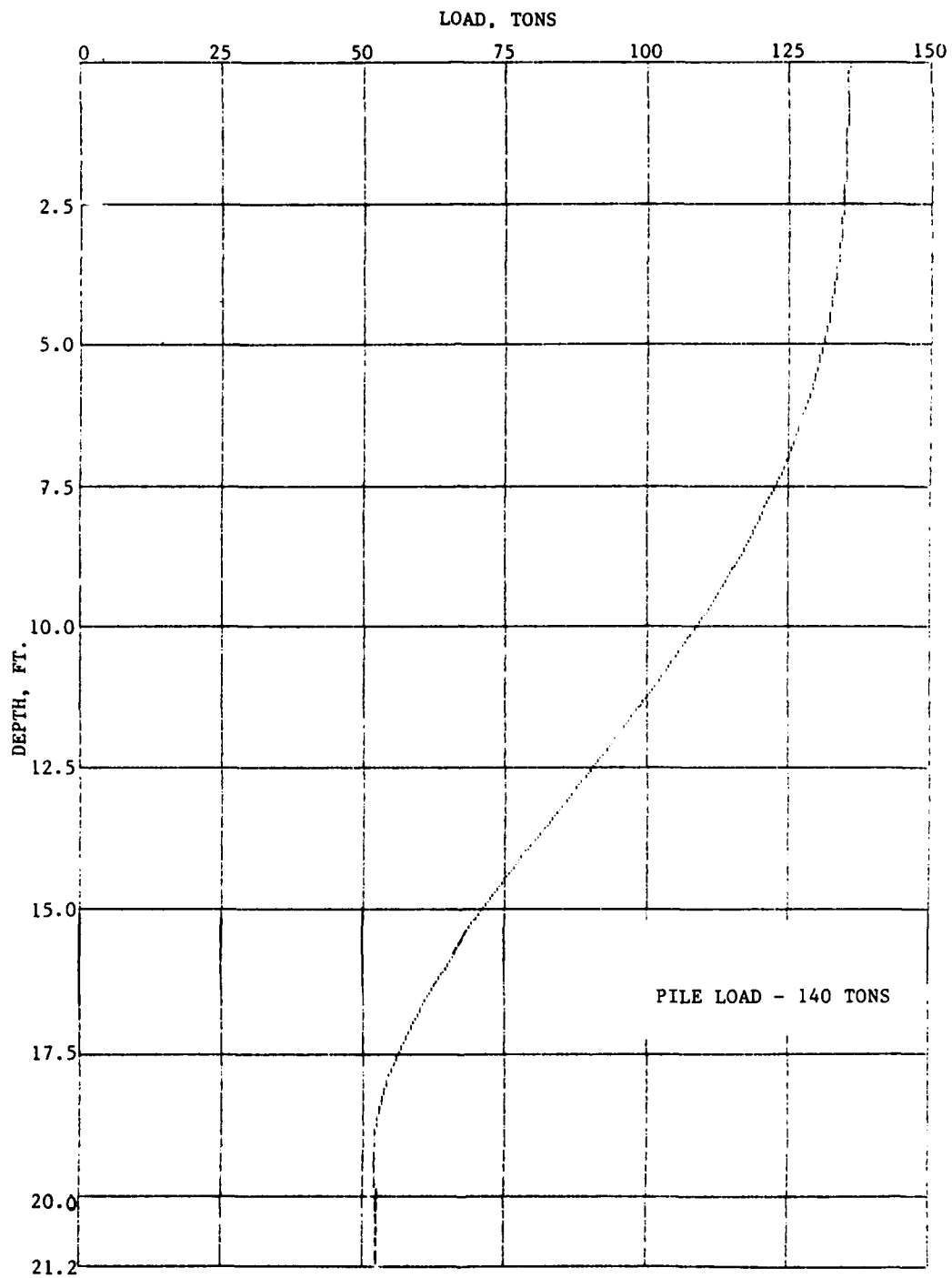


Fig. B-16 LOAD DISTRIBUTION CURVE SHAFT TEST - S1T1

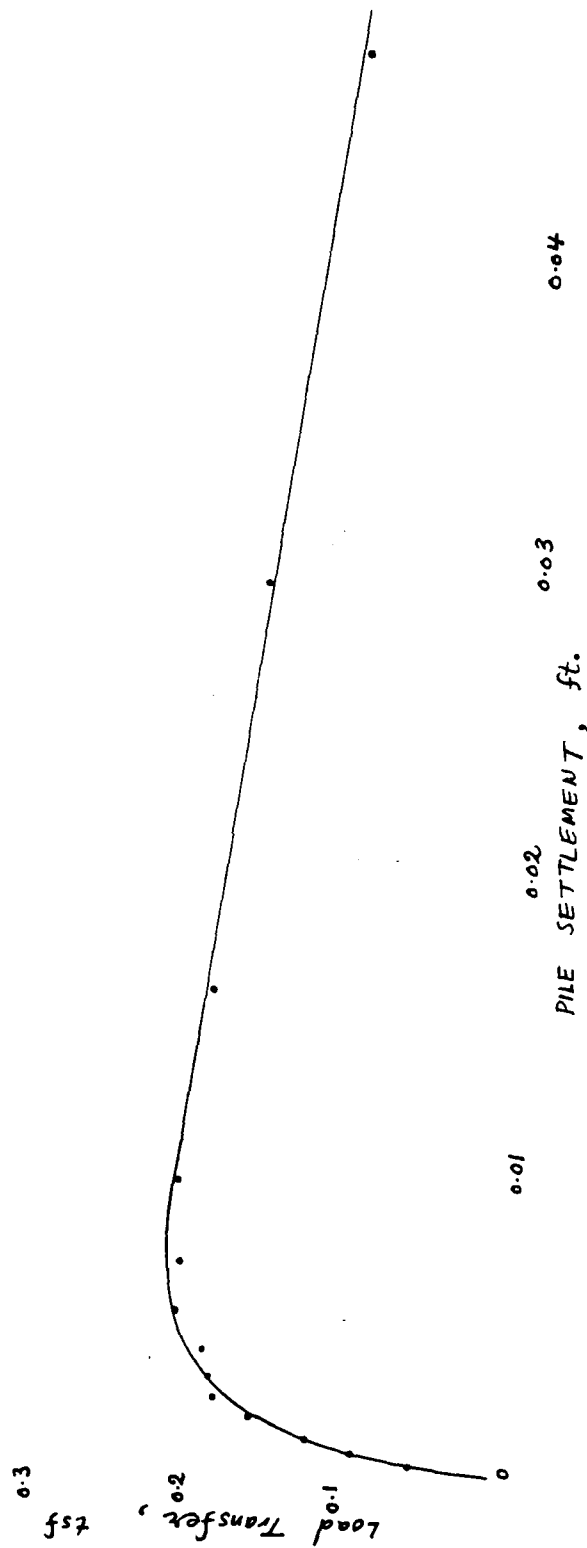


FIG. B-17 LOAD TRANSFER CURVE SHAFT TEST SITE AT DEPTH 2.08 FT.

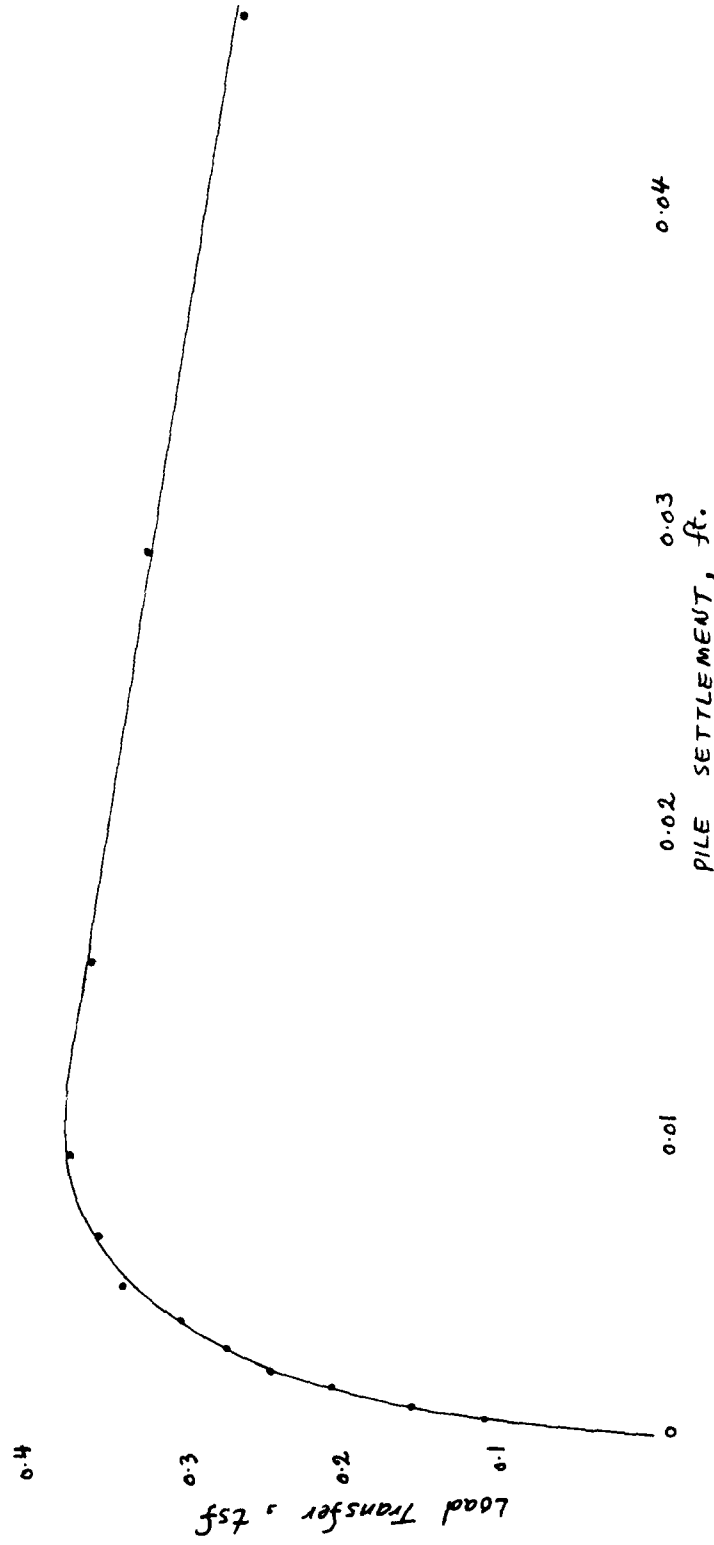


FIG. B-18 LOAD TRANSFER CURVE SHAFT TEST S1T1 AT DEPTH 4.17 FT.

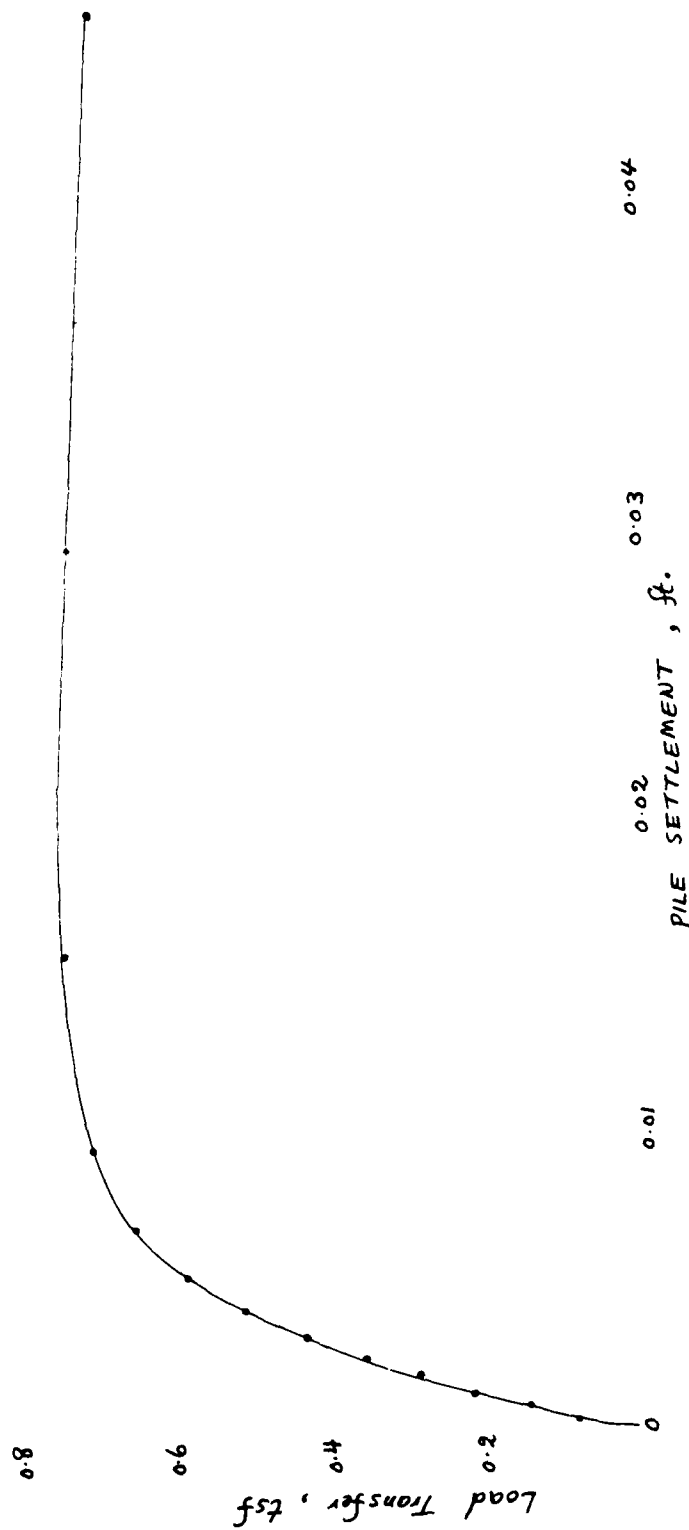


FIG. B-19 LOAD TRANSFER CURVE SHAFT TEST SITI AT DEPTH 8.33 FT.

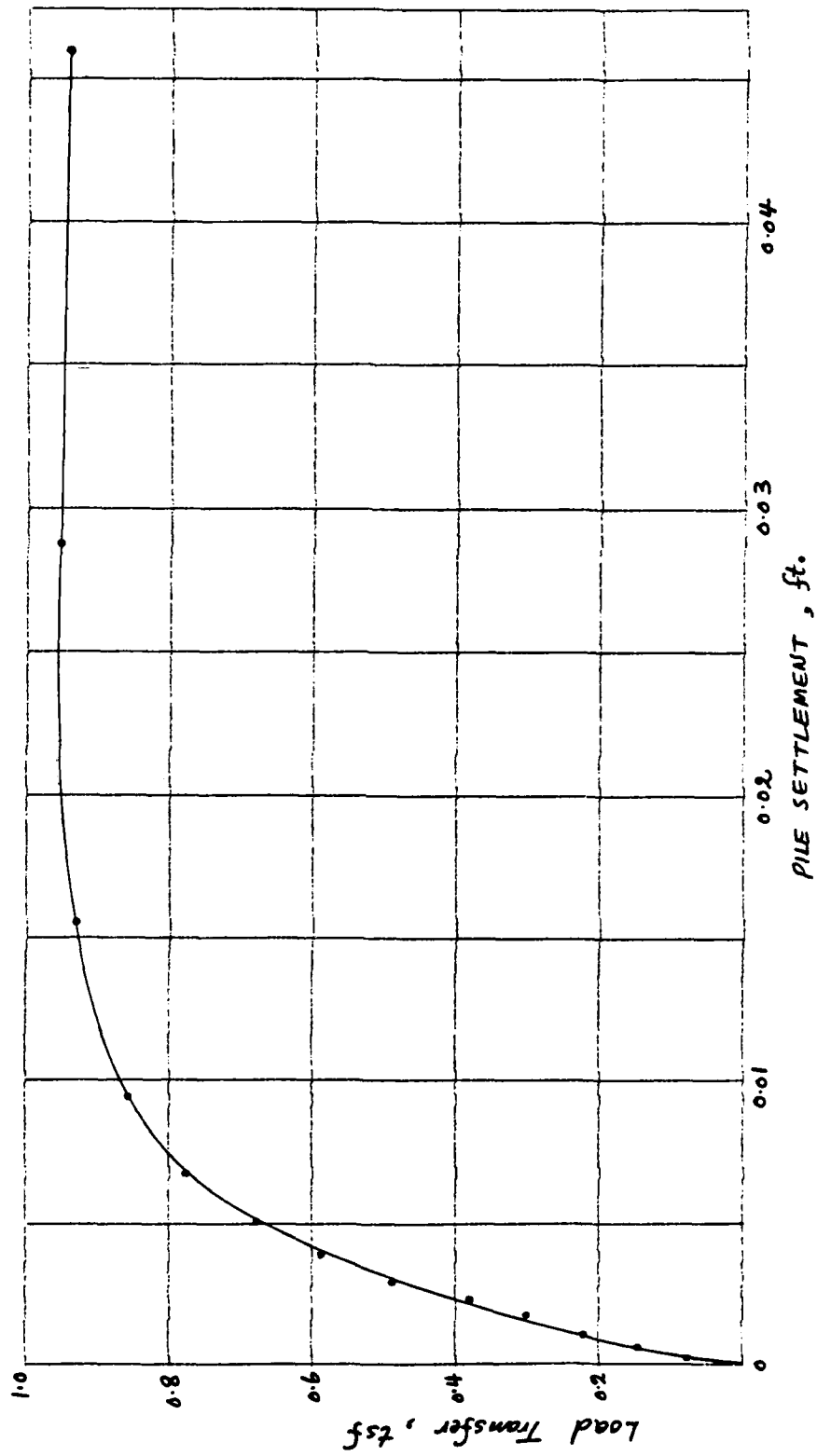


FIG. B- 20 LOAD TRANSFER CURVE SHAFT TEST S111 AT DEPTH 12.50 FT.

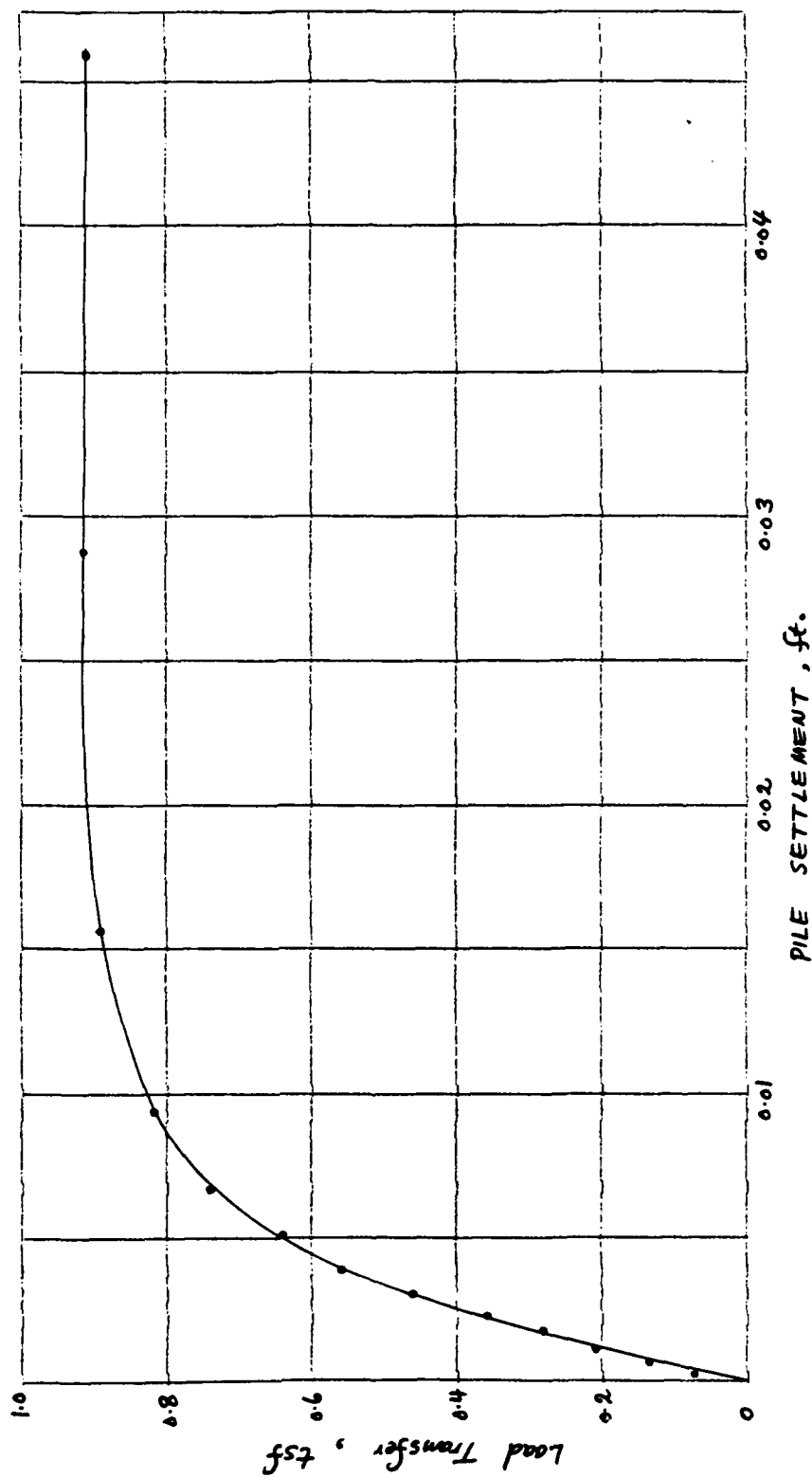


FIG. B - 21 LOAD TRANSFER CURVE SHAFT TEST SITE 1 AT DEPTH 14.58 FT.

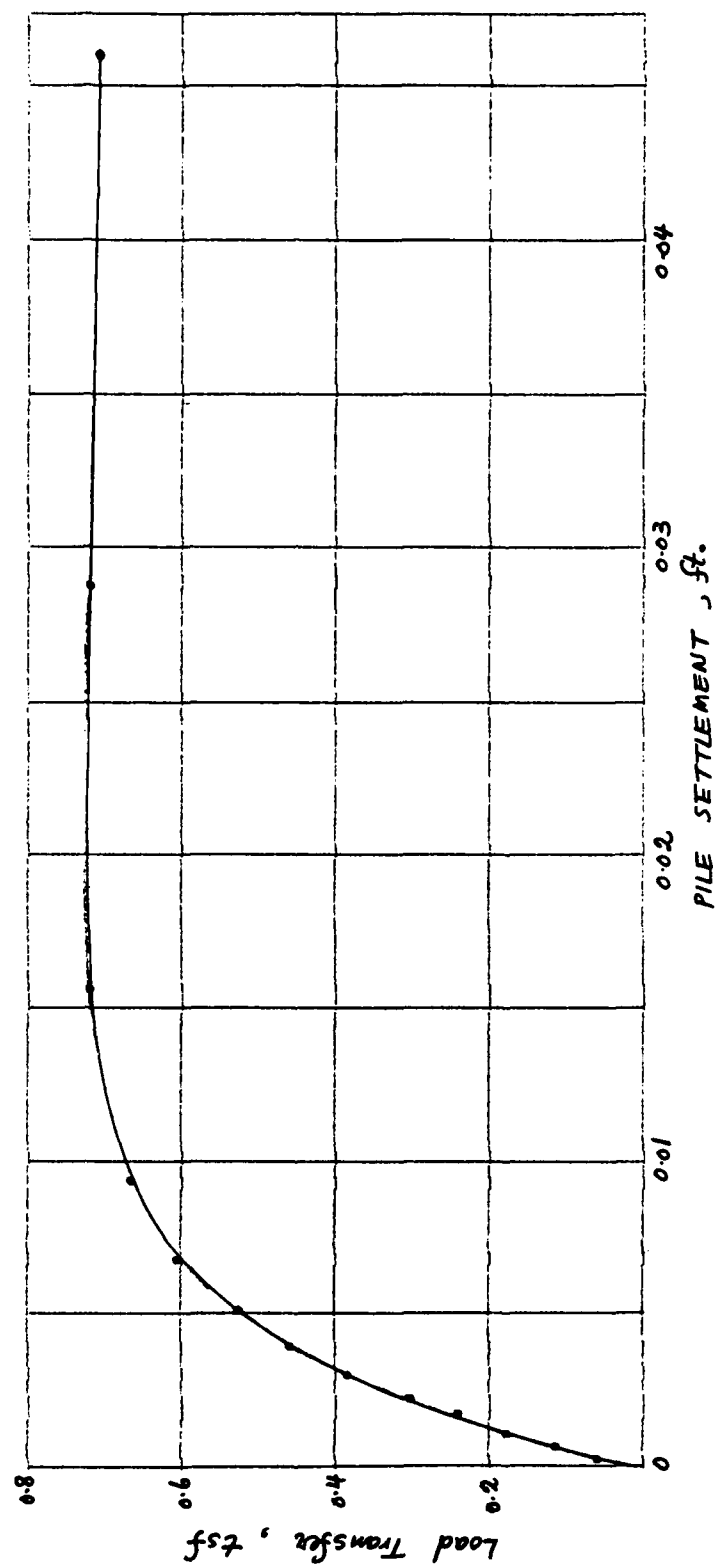


FIG. B - 22 LOAD TRANSFER CURVE SHAFT TEST S1T1 AT DEPTH 16.67 FT.

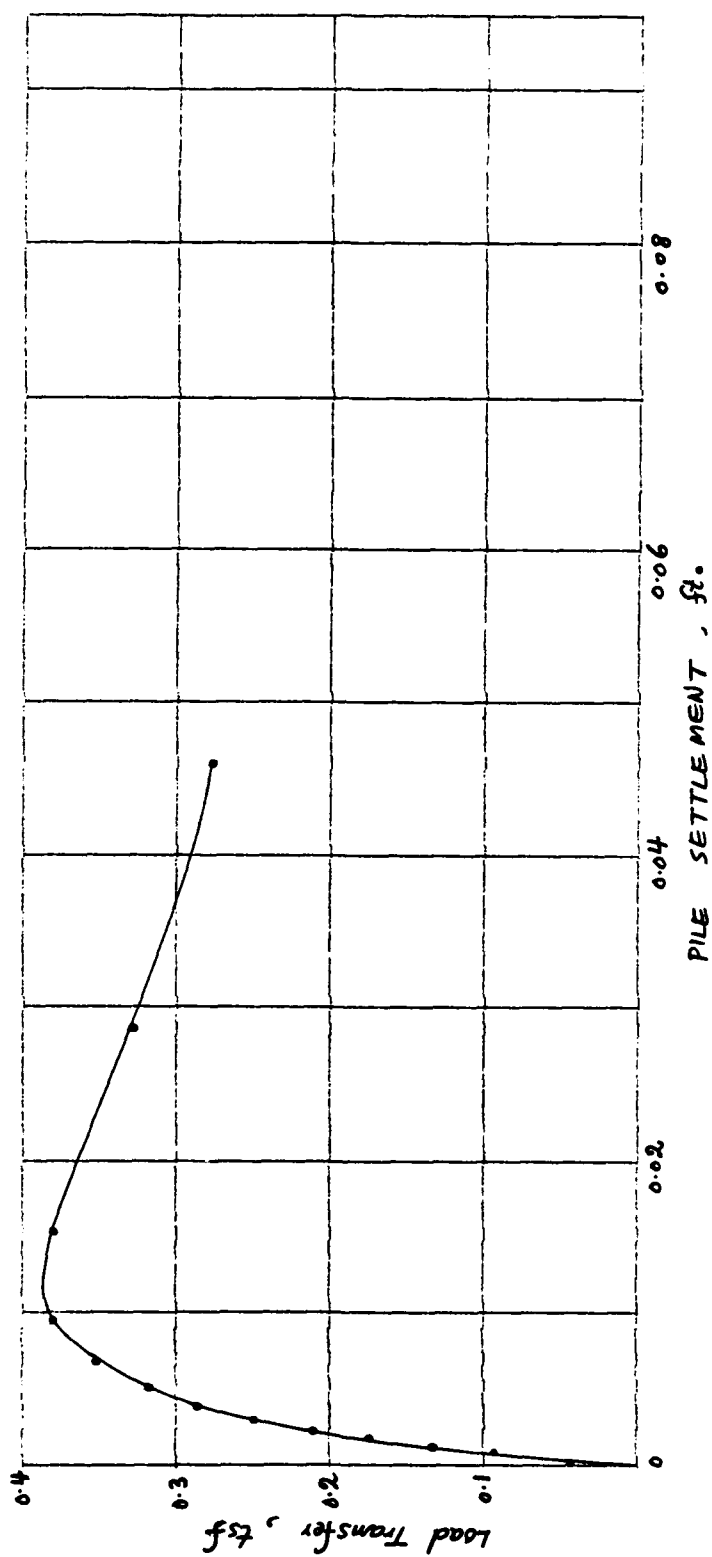
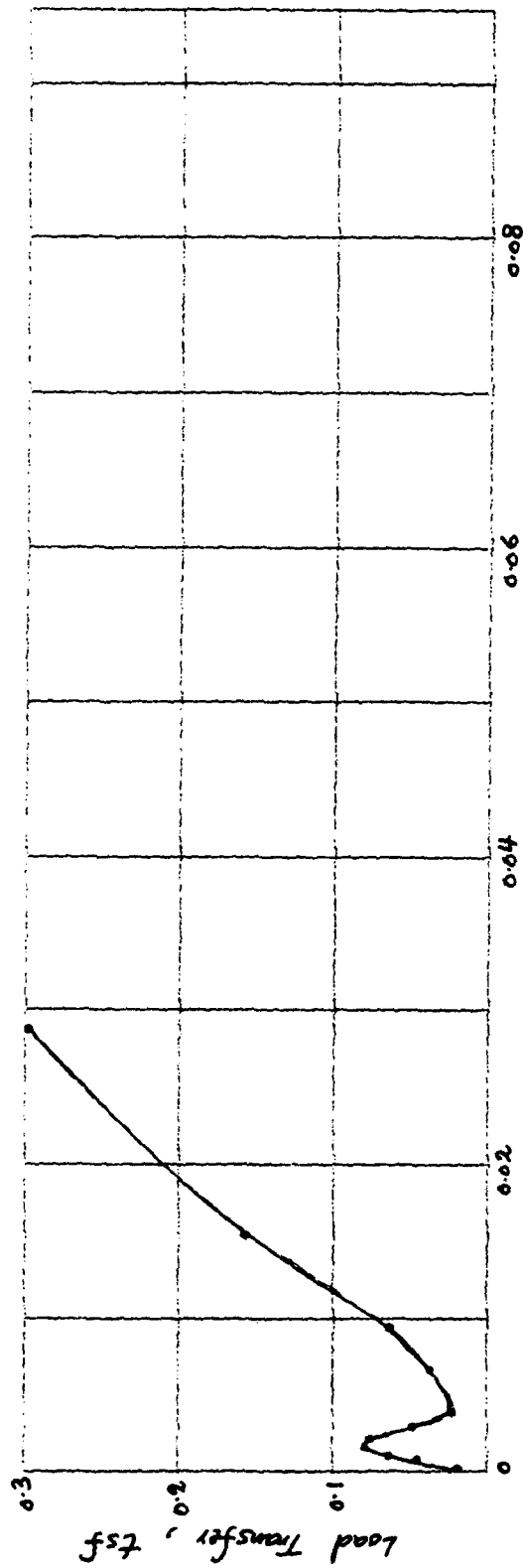


FIG. B - 23 LOAD TRANSFER CURVE SHAFT TEST S1T1 AT DEPTH 18.75 FT.





PILE SETTLEMENT, ft.

FIG. B - 24 LOAD TRANSFER CURVE SHAFT TEST SITE AT DEPTH 20.83 FT.

In accordance with letter from DAEN-RDC, DAEN-ASI dated 22 July 1977, Subject: Facsimile Catalog Cards for Laboratory Technical Publications, a facsimile catalog card in Library of Congress MARC format is reproduced below.

Study to investigate the effects of skin friction on the performance of drilled shafts in cohesive soils / by Woodward-Clyde Consultants, Houston, Texas. -- Vicksburg, Miss. : U.S. Army Engineer Waterways Experiment Station ; Springfield, Va. : available from NTIS, 1982.

3 v. in 1 ; ill. ; 27 cm. -- (Technical report ; GL-82-1)

Cover title.

"March 1982."

Final report.

"Prepared for Office, Chief of Engineers, U.S. Army."

"Monitored by Geotechnical Laboratory, U.S. Army Engineer Waterways Experiment Station under Work Unit AT40/E0/006."

Bibliography: p. 28-29.

1. Friction. 2. Shafts (Excavations). 3. Soils-- Testing. I. Woodward-Clyde Consultants. II. United

Study to investigate the effects of skin friction : ... 1982.  
(Card 2)

States. Army. Corps of Engineers. Office of the Chief of Engineers. III. U.S. Army Engineer Waterways Experiment Station. Geotechnical Laboratory. IV. Title V. Series: Technical report (U.S. Army Engineer Waterways Experiment Station) ; GL-82-1.  
TA7.W34 no.GL-82-1

